Investigation of mixture preparation for natural gas engines

Tang, Wei

Award date:
1995

Awarding institution:
University of Bath

INVESTIGATION OF MIXTURE PREPARATION

FOR NATURAL GAS ENGINES

Submitted by

Wei TANG

for the degree of PhD
of the University of Bath

1995

ProQuest LLC
789 East Eisenhower Parkway
P.O. Box 1346
Ann Arbor, MI 48106-1346

To my wife

and

my parents

SUMMARY

With increasing concern for the environment and energy resources, natural gas has regained world-wide interest. However, natural gas fuelled engines are not yet mature and much development work remains to be done. For example, the existing mixture preparation system does not always produce a satisfactory mixture and the knowledge available on the mixture preparation in natural gas engines is very limited. Therefore a research project was initiated with the focus of the study concentrated on the mixture formation in venturi type natural gas engine carburettors and the influence of the mixture prepared on the engine performance and emissions. The research not only contributes to the fundamental understanding of the dynamic mixing mechanisms of the natural gas engine carburation system, but also provides expertise and knowledge of the application of the newly emerged computational fluid dynamics technique and the novel flame ionisation detector technique.

The state-of-the-art of natural gas engine technology and of the applications of the newly emerged computational fluid dynamics (CFD) technique to engines were firstly reviewed. These produced a clear picture about the features of natural gas engines and of the problems which remained to be resolved. The review also evaluated the current application status, the capability and uncertainty of the CFD technique, and in so doing the necessary background knowledge was acquired.

The CFD code validations on some of the flow variables were then carried out by using both BS1042 and duct flow experiments. The results showed that the code could reliably predict flow behaviours quickly and at low cost compared with experimental methods. By using the validated CFD package, the fluid dynamics and mixture formation in a venturi type gas-air mixer was simulated. The computational studies revealed, for the first time, the effect of flow patterns on the mixture formation. As a result of these findings, the mechanism governing the performance of venturi type mixers was better understood. The effects of a few key mixer design parameters on the mixture formation were also studied in the research, which provided useful guidelines for venturi type mixer designs.

Next, the computational results and the findings were experimentally confirmed on the mixture concentration distributions and some other flow variables by using a well calibrated flame ionisation detector and other pertinent equipment. The work demonstrated that the CFD technique could be reliably used as a new approach to the study of the mixture formation in natural gas engines. The validation of the general purpose CFD package on mixture concentration distributions in a curved flow domain is another feature which has not yet been considered in other published work.

Experimental studies were also performed on the comparison of the mixers performance between the newly designed mixer and three proprietary mixers. The comparative study showed that the newly designed gas air mixer exhibited similar or superior performance to the three proprietary mixers tested. The simplicity of the new design could result in potentially lower manufacturing costs.

To examine the influence of the mixture produced by different mixers, engine performance and emissions comparison between the newly designed mixer and two of the proprietary mixers was carried out. In terms of the engine power output and brake mean effective pressure (BMEP), the engine with the new mixer produced the highest power and maximum BMEP over most of the engine operating speeds at wide open throttle (WOT). With regard to engine brake specific energy consumption, brake thermal efficiency and to engine emissions of CO, HC and NOx, there was not much difference amongst the three mixers when the air fuel ratio produced was the same irrespective of the engine operating speed and load. But the advantage of having a lower air flow restriction did produce superior engine power output and BMEP. However, the engine emissions variation from cylinder to cylinder with the three gas mixers did not give the results which might have been expected from the mixture homogeneity obtained from the mixers. To clarify the influence of the throttle valve and the intake manifold, mixture distributions inside the intake manifold were then studied. Measurement was also made on the transient pressure in the intake manifold in order to examine the steady pressure assumption made during the CFD simulations.

After this, the attention of the project was directed towards the CFD aided gas-air mixers scaling-up design with the aim of widening the product operation range and enlarging the potential market of the newly designed mixer. Due to the fact that the CFD simulations were successfully applied to replace the test rig evaluations which used to be the main method of developing a new product design, many comparisons were made on different design options in a short time and at low cost. More detailed information about the mixing behaviour within the whole mixer flow domain of each design concept resulted in a better understanding, which speeded up the design optimisation procedure. The work has highlighted the capability of integrating the CFD technique into some of the engine components design processes, which will promote the industrial applications of the new technique. As a result of the project, the mixers designed have been patented in countries world-wide and suitable manufacturers are being sought.

The final chapter of the thesis gives the conclusions which were drawn from the extensive computational and experimental studies carried out in the project. Recommendations for future work in the field are also proposed at the end of the thesis.

Acknowledgements

The author is indebted to his supervisor, Mr. John Slowley, for his advice, encouragement and supervision received during the course of this study.

He would like to express his grateful thanks to Dr. Stephen J. Charlton for his guidance and support at the beginning of this study.

Thanks also go to Dr. Dennis J. Jager, Mr. Graham Roberts, and Mr. Jeremy S. Doyle for their assistance at various stages of the project and many invaluable discussions.

The help and technical assistance with the test facilities from Mr. Don Blake, Mr. Vijay Rajput and many other individuals are greatly appreciated.

The study is under the Sino-British Friendship Scholarship Scheme which is jointly sponsored by the Chinese State Education Commission, Yue-Kong Pao Foundation and the British Council. The support from British Gas plc at various stages is also greatly acknowledged.

Nomenclature

Symbols which are frequently used in the text are listed below. Those locally employed are defined when required.

C	Coefficient of discharge	-
$\bar{c}_p$	Mean constant pressure specific heat at temperature T	J/kg K
$\bar{c}_v$	Mean constant volume specific heat at temperature T	J/kg K
c_p^0	Reference specific heat at temperature T_0	J/kg K
$C_{\varepsilon,j}$	Empirical coefficients (j=1,2,3,4)	-
C_μ	An empirical coefficient, usually taken as a constant	-
d	Diameter of throat of the venturi tube	m
D_c	The molecular diffusivity of component c	m^2/s
e	Specific internal energy	J/kg
$F_{c,j}$	Diffusional species flux component	kg/s m^2
$F_{h,j}$	Diffusional energy flux in direction x_j	J/s m^2
f_μ	Empirical coefficient	-
h	Static enthalpy	J/kg
H_m	Heat of formation of constituent m	J/s
I	Turbulence intensity	-
k	Turbulent kinetic energy	m^2/s^2
l	Turbulence length scale	m
m_c^0	A reference concentration	-
m_m	Mass fraction of mixture constituent m (local concentration)	-
M_k	Molecular mass of a constituent k	kg/kmol
p	Static pressure of fluid	N/m^2
q_m	Mass flow rate of the incompressible fluid	kg/s
s_c	Species production or consumption due to chemical reaction	kg/s m^3
s_i	Momentum source components	N/m^3
s_h	Energy source	W/m^3
s_m	Mass source	kg/m^3
t	Time	s
T	Temperature of fluid	K
u_i	Fluid velocity component in direction x_i	m/s
$\tilde{u}_j$	u_j-u_{cj}; relative velocity between fluid and local moving co-ordinate frame that moves with velocity u_{cj}	m/s
v	Fluid velocity component in direction y	m/s
w	Fluid velocity component in direction z	m/s
x_i	Cartesian co-ordinate (i = 1,2,3)	m

Δp	Differential pressure	N/m^2
β	The thermal volumetric expansion coefficient	1/K
β_c	The expansion coefficient for constituent c	1/K
δ_{ij}	Kronecker delta, is unity when i=j and zero otherwise	-
ε	Turbulence dissipation rate	m^2/s^3
γ	Ratio of the specific heats at constant pressure and volume	-
η	Expandability (expansion) factor	-
κ	The Von-Karman constant	-
λ	The mixture relative air fuel ratio	-
μ	Fluid viscosity	Pa s
ρ	Mass density of fluid	kg/m^3
ρ_c	Density of constituent c	kg/m^3
$\sigma_{c,t}$	The turbulent Schmidt number	-
$\sigma_{h,t}$	The turbulent Prandtl number	-
σ_k	An empirical coefficient	-
σ_ε	An empirical coefficient	-
τ_{ij}	Stress tensor components	
ω	The swirl added to the velocity	rev/min
$\sqrt{g}$	Determinant of metric tensor	-

Subscript

0	Refers to an initial state of the variable;
t	Refers to a turbulent value of the variable.

Superscript

'	Refers to fluctuations of a variable about the ensemble average value i.e. the turbulent value;
-	Refers to an ensemble averaging process of a value.

Abbreviations

ANG	Adsorbed Natural Gas
BMEP	Brake Mean Effective Pressure
BSEC	Brake Specific Energy Consumption
BSFC	Brake Specific Fuel Consumption

CAD	Computer Aided Design
CAE	Computer Aided Engineering
CAM	Computer Aided Manufacture
CARB	California Air Resources Board
CFD	Computational Fluid Dynamics
CHP	Combined Heat and Power
CNG	Compressed Natural Gas
CoV	Coefficient of Variation
CP	Constant Pressure
DI	Direct Injection
EEC	European Economic Community
ECE-R49	Economic Commission for Europe, Regulation No. 49
EGR	Exhaust Gas Recirculation
EPA	Environmental Protection Agency
EUDC	Extra Urban Drive Cycle
FID	Flame Ionisation Detector
FTP	Federal Test Procedure
FV	Finite Volume
HC	Hydrocarbons
HWA	Hot Wire Anemometry
IDI	In-Direct Injection
LDA	Laser Doppler Anemometry
LEV	Low Emissions Vehicle
LNG	Liquefied Natural Gas
MBT	Minimum Ignition Advance for Best Torque
NDIR	Non-Dispersive InfraRed
NGV	Natural Gas Vehicle
NMHC	Non-Methane Hydrocarbons
NMOG	Non-Methane Organic Gas
NOx	Nitrogen oxides
RON	Research Octane Number
SI	Spark Ignition
ULEV	Ultra Low Emissions Vehicle
WOT	Wide Open Throttle

Contents

1. Introduction and literature review

1.1 Introduction

The evolution of internal combustion engines has brought about so much benefit to the world that the engines have become essential prime movers for mankind. However, with the increase of fossil fuel burning engines, people are not only the beneficiaries, but also the sufferers due to the emissions released from the engines. The severe problems of plant damage, eye and throat irritation, cracking of stressed rubber and poor visibility have been experienced by people living in industrial cities where cars using petrol and diesel fuels are identified as the main emissions source. The control of engine emissions has come to the top of the agenda of engine researchers and manufacturers, especially now that legislation to control emissions has been implemented by most countries.

To meet the standards of the engine emissions, many aspects have been looked at so far. With respect to evaporative emissions, crankcase blowby devices were invented to control the emissions from the original crankcase ventilation systems. Since then, emissions from the fuel system such as the carburettor and fuel tank have been significantly reduced. In relation to the exhaust emissions, much research and development have been carried out and consequently, technologies of the lean burn system, exhaust gas recirculation, closed loop mixture strength control, and after treatments such as the 3-way catalyst system and particulate trap have been innovated and proved to be very effective at reducing the emissions from petrol and diesel engines under most engine operating conditions. However, due to increased public awareness, the emission standards have become more and more stringent. The currently required and proposed standards for various kinds of engines have made it very difficult for traditional petrol and diesel engines to meet these limits, even with the very advanced and effective emissions controlling technologies. For example the newly proposed Californian emission standards (Appendix I) are extremely difficult to be met by current passenger car engines fuelled with diesel or petrol [1]. While making efforts to pursue new technologies to reduce the emissions from the engines fuelled with either petrol or diesel, researchers and manufacturers are also considering using the so called clean fuels for both stationary and automotive engines to meet these challenging requirements.

1.1.1 Alternative fuels and their comparison

Many alternative fuels for reducing emissions have been tested by researchers and manufacturers during the past two decades. They are natural gas, alcohol, liquefied

petroleum gas and hydrogen. Sometimes reformulated petrol, low sulphur diesel and even electricity are also allocated into the alternative category in order to distinguish them from the conventional petrol and diesel fuels. Most of them can act as substitutes and reduce the emissions to a much lower level than that proposed by emissions standards.

The liquefied petroleum gas often used is liquefied propane or butane. Countries like Canada use it as automotive fuel because of its low cost, but the NOx emissions are higher than that of petrol fuelled engines [2]. Even with the advantage of having a higher energy density (the amount of heat energy able to be released per unit volume) [3], the liquefied petroleum gas will not be widely accepted as an alternative fuel where natural gas is also available because its cost is higher than that of natural gas (the price is doubled in the USA [1]). In addition, its lower octane number 112 (RON) compared to natural gas makes the thermal efficiency of a propane fuelled engine lower than that of a comparable natural gas fuelled engine.

Hydrogen has long been believed to be one of the most promising alternative fuels for internal combustion engines [4]. It has been used as an engine fuel in space vehicles for a long time [5]. In land vehicles or ordinary engines, attempt has been made to use hydrogen as a fuel. In a strategic view, the non-fossil production of hydrogen from water is, in the long run, a unique way for human beings to be independent from the limited fossil energy resources. Hydrogen totally eliminates the HC emissions and emits no CO_2 or CO at all. In addition, hydrogen has a very fast flame speed and broad flammability limits. To make use of these features, studies were conducted on using the hydrogen as part of the fuel supplied to an engine. The main portion of the fuel was natural gas. The hydrogen supplementation to natural gas engines resulted in a reduction of regulated exhaust emissions and an increase of the engine efficiency [6]. Hydrogen was used, in some other study, to extend the lean limit of the natural gas air mixture in an effort to achieve ultra-low levels of NOx emissions [7]. Even used as supplement, however, the benefit gained was hardly enough to justify the added expense of hydrogen. Presently, hydrogen is mainly produced from fossil fuel processing such as methane steam reforming, which consumes vast amount of fossil fuel energy and produces large amount of emissions as well. Water-splitting reactions such as water electrolysis carried out by using solar energy or nuclear energy can be a feasible way, but it is too expensive at present. Only when the price of hydrogen production is competitive to that of fossil fuels by using certain kind of innovative technology, can hydrogen be a practical fuel for engines used for ordinary purposes provided that hydrogen fuelling and onboard storage problems, engine induction system backfiring problems, engine mixture preparation and combustion related problems can be resolved.

Similar to hydrogen, electricity has been used to drive machines such as light duty vehicles for quite a long time. Strictly speaking, electricity is not a fuel. It is only a secondary form of energy. Although many primary fuels such as coal and oil can be used to produce this secondary energy, the cost of the electric vehicle is still too expensive to be used for ordinary commercial applications. Even with nuclear power as the primary source of the electricity, the cost is still excessive. Needless to say the current battery recharging process is too slow to be commercially accepted. Another impediment of the electric vehicle is the battery capacity which is not great enough to drive its vehicle over a satisfactory operating range. Break through in battery design which can replace current electrolyte method is necessary in order to develop a novel type of battery with ultra capacity. Even so the emissions that come out of the exhaust pipe have not been eliminated. They have only been shifted from tail pipes to power station's smokestacks.

As a liquid fuel, alcohol has its engineering and cost advantages in vehicle applications. A comprehensive comparative analysis of methanol and natural gas was made by DeLuchi, M. A., et al. [8] on the aspects of resource supply, performance, emissions, fuel storage, safety, costs and transitions. Their analysis showed that methanol was easier to store than natural gas, but had a slightly higher life cycle cost. In terms of efficiency, engines fuelled with the two fuels were similar to each other. The emissions from the engines fuelled with the two fuels caused different effects on the environment. Natural gas engine emissions were more active as greenhouse gases than the methanol engines, whilst methanol caused more ozone formation than natural gas. Generally, natural gas engines emit slightly lower emissions. The recent developments on both methanol and natural gas engines has made the differences on engine performance and emissions become small [9] [10]. The optimised methanol engine has also achieved a high brake thermal efficiency comparable to diesel engines [11] [12] and with very low emissions as well. However, the availability of the methanol or ethanol which belong to the same family of alcohols is quite limited except in some areas like Brazil where it was the predominant automobile fuel in the eighties due to its relatively low price owing to the glut of cane sugar in world-wide markets at the time.

Compared to other alternatives, natural gas not only has an inherent potential for low emissions, but also has high availability as a world wide energy resource. Natural gas is a primary fuel and not necessarily tied to petroleum production [1]. In some areas natural gas is readily available at very low cost. In these areas it appears that natural gas is the most viable clean fuel of the alternatives tested. Therefore natural gas fuelled engines have attracted great attention world-wide since 1980s.

1.1.2 Features of natural gas engines

Natural gas fuelled engines offer a number of significant environmental and technical benefits compared to the diesel and petrol fuelled engines [13]. As a gaseous fuel, natural gas can mix readily with air in any proportion under normal ambient conditions. It gives nearly no evaporative emissions from the fuel supply system due to the pressure tight fuel supply system and it produces nearly no cold start and low temperature emissions because of the elimination of cold choking enrichment as natural gas remains in a gaseous state even at very low temperatures. With the lowest carbon atoms and the simplest molecular structure, natural gas engines emit a negligible amount of particulates which have been suspected to be the cause of certain diseases like asthma and emit a negligible amount of non-methane hydrocarbons as well. The carbon monoxide produced from natural gas engines is also very low if a proper air-fuel ratio is used. The low sulphur content of natural gas compared to petrol or diesel results in very low SO_2 and sulphate particle emissions. With respect to unregulated emissions, in particular benzene and 1,3-butadiene, the level is very low for natural gas engines while formaldehyde is roughly the same as for petrol engines [10]. Methane exhibits almost no ozone formation potential but it is a powerful greenhouse gas because of its large absorption of infrared radiation which is over 20 times higher than the CO_2 [10] [14]. This can be compensated by the fact that the natural gas engines emit about 20% less carbon dioxides than petrol or diesel engines due to the lowest C/H ratio. Recent compressed natural gas (CNG) fuelled buses in mass operation experiences showed that the CNG engines had met the CARB's tough new heavy duty emission standards whilst no diesel engine had been able to come close to the standards [15].

Natural gas has a high ignition temperature which is about 640 °C and a high equivalent research octane number which is about 120~130, the highest of any commonly used fuel. The high octane ignition quality of natural gas makes it an excellent fuel for spark ignition engine application. Compared to the engine compression ratios 6:1~11:1 for petrol, the natural gas engine can use as high as 15:1 without knocking for a well designed combustion system [16]. The high compression ratio used certainly results in high thermal efficiency of the engine well beyond the level that normal petrol engines can obtain. For a lean burn natural gas engine, the thermal efficiency achieved can be as high a value as that of a diesel engine and with a lower engine noise. However, the natural gas and air mixture has a lower laminar flame speed (the speed at which a flame proceeds through a combustible mixture at steady state) than any other hydrocarbon fuels mixture and has a very low energy density. The low energy density will cause severe storage problems when natural gas engines are used for vehicles. Recent research carried out jointly by Nissan Motor Co. and the University of Toronto showed that some

of the disadvantages normally associated with the use of natural gas can be minimised with a suitable engine design [17].

1.1.3 The objectives of the project

Revived interest in natural gas engines during the last few years has led to considerable research and development activities. However, natural gas fuelled engines are not yet mature and much development work is needed. Similar to the engines fuelled with petrol and diesel, the performance and emissions of natural gas engines are very sensitive to the mixture prepared. Without a good mixture preparation system, the advantages of using natural gas as engine fuel will disappear. The mixture required by natural gas engines, as engines fuelled with any other fuels, have two main characteristics. One is the quantity of air and fuel supplied under different engine operating conditions. The other is the quality of the mixture, which refers to the mixture concentration distribution after the mixture preparation system.

Main objectives of this project are to investigate the mixture formation in a venturi type natural gas engine carburettor by using the newly emerged computational fluid dynamics (CFD) technique; to optimise the design parameters of the carburettor in order to achieve a satisfactory mixture preparation system for the engines considered; to validate the numerical results and conclusions against experimental data obtained from carburettor performance tests using flame ionisation detector technique; to evaluate the effect of mixture preparation systems on the engine performance and emissions; and to attempt to design and develop a series of mixture preparation units which have a market potential.

In order to produce a required mixture, natural gas engine carburettors are normally composed of two parts, a mixing unit or mixer and a mixture air fuel ratio control unit. The task of the mixing unit is to mix the air and fuel together and produce a homogeneous mixture for each of the individual cylinders of a multi-cylinder engine under all of the engine operating conditions. The function of the control unit is to meter the fuel supplied to the mixing unit at the right amount as required under different engine operating conditions. In British Gas plc, an electronic control unit has been developed, which has been proved to be a very good control system for CHP natural gas engine mixture preparation systems during their development of natural gas engine powered combined heat and power co-generation systems [18]. Therefore the current study will only focus on the mixing unit and its effect on mixture preparation of natural gas engines for CHP applications. The findings will mostly be appropriate to the gas engines used for other purposes.

1.2 Literature review

To be aware of the progress which has been made and to get a clear view of the state of the art about the current technological situation of natural gas engines, a comprehensive literature search was made at the beginning of the study. Due to the limited publications on stationary natural gas engines, the up to date information associated with gas engines used for automobile purpose was also traced and collected in this review. Work reported on the applications of the CFD technique to engines was later reviewed in order to assess the capabilities of the novel technique for the complex mixing problem in question and to acquire knowledge in the discipline of concern. Another novel technique used in this study, the high speed flame ionisation detector (FID), will be reviewed on its applications to engines in chapter four, where it is used to measure the mixture concentration distributions.

1.2.1 Natural gas engines

Since 1986, natural gas fuelled engines have been exploited in various aspects because of the renewed world-wide interest, especially after the first international conference and exhibition on natural gas vehicles held in Australia. At the early stage, much attention was paid to how to convert parent diesel or petrol engines into natural gas engines properly, effectively and economically. With the evolution of technologies and accumulated experience, the conversion is no longer a problem for the engine researchers and manufacturers [19] [20]. To meet the increasing demands on natural gas engines, not only more and more purpose designed four stroke stationary and automobile natural gas engines are being put into production, but also the two stroke and the Wankel natural gas engines are being considered by some researchers and manufacturers [21]~[23]. The current research activities for all types of the natural gas engines are mainly being focused on how to reduce the exhaust emissions from natural gas engines while trying not to impair their efficiency or reduce their maximum power output. In addition, the engine operating reliability is another main concern when the natural gas engine is used for stationary application such as the combined heat and power plant [24] [25]. For vehicular applications, however, the gas on board storage and the transient characteristics of the engine are extra concerns. Details of the research and development work will be discussed in the following section.

1.2.1.1 Engine emissions control

As mentioned above, it is the inherent low emission level and the huge reserves that makes the natural gas engine gain the interest of the world. However, simply converted engines can not reduce exhaust emissions dramatically irrespective of the baseline

engine types, as have been experienced in the research conducted by Fritz, S. G. and Egbuonu, R. I., [26]. To meet the stringent emission standards, technologies tackling emissions have to be implemented. The research activities performed so far on natural gas engine emission control have been following in the same steps as that of the diesel and petrol engines because of the similarity in emissions formation mechanisms amongst the engines. The technologies adopted from engines using other fuels were mainly the lean burn system, catalyst conversion system, exhaust gas recirculation (EGR) and computer control [13] [27]. Each of them has its own constraints or drawbacks and each of them has its own scope of application. Usually, the combination of some of these technologies is used to tackle the emission problems of natural gas engines.

1.2.1.1.1 Lean burn system

The lean burn system is a method which supplies excessive air in the combustion chamber in order to burn the fuel completely. The product of incomplete burning CO and the unburned hydrocarbons HC in a lean burn system can be significantly reduced. The other benefits of the lean burn are its high thermal efficiency, low throttling loss, low exhaust gas temperature and consequently the high durability. Further more, the lean burn system may operate without using the catalyst or EGR system to achieve the emissions level demanded, which will simplify the control system and save the capital cost [16]. The severe disadvantages of the lean burn are the low power capacity and poor combustion stability when extremely lean mixtures are used.

There are different approaches to implement lean burn technology in natural gas engines. It can be implemented by using either a pre-combustion chamber system or an open chamber combustion system [28] [29], as schematically shown in Figure 1.1. The former is often used for those natural gas engines converted from indirect injection (IDI) diesel engines and the latter is often used for natural gas engines converted from direct injection (DI) diesel engines or petrol engines [30] [31].

Lean burn with pre-combustion chamber

With the pre-combustion chamber system, an approximately stoichiometric air fuel mixture is supplied into the pre-combustion chamber by using a separate fuel supply unit, a weak air fuel mixture is supplied to the main chamber. The mixture supplied to the entire combustion system is still in the lean side of a stoichiometric mixture. The spark plug is placed in the pre-combustion chamber which is located in the cylinder head usually by replacing the diesel fuel injector. Combustion is initiated here and then the high temperature flame and the unburned mixture in the pre-combustion chamber

spread into the main chamber, which makes it easier for the extra lean mixture in the main chamber to be ignited as long as the mixture strength is within its firing limits. To get a satisfactory mixture stratification within the pre-combustion chamber over a wide range of engine loads and speeds is essential for this system. Much research work was concentrated on this aspect by different researchers [32]~[34] using different means including CFD modelling and FID measurement. The configuration and the volume of the pre-combustion chamber, the position and the electrode orientation of the spark plug, the dimension and the direction of the passage (the nozzle) between the pre-combustion chamber and main chamber all proved to have a profound effect on the engine performance, reliability, stability and emissions for this type of lean burn combustion system [16] [28] [32] [35]. The results from the research [28] and [36] showed that the mixture supplied to the pre-combustion chamber had a substantial influence on the natural gas engine NOx emissions. It sometimes became the main source of NOx emissions if the air fuel ratio of the mixture supplied to the pre-combustion chamber was not well controlled. This indicated that the pre-combustion chamber system would not produce a lower level NOx emissions than the open chamber system could. Charlton, S. J. and his co-workers' result [36] also showed that the ambient temperature or the temperature of the mixture in the intake manifold had a significant effect on the emissions of NOx, which was illustrated by other researchers as well [37]. The research conducted in both [28] and [36] demonstrated that extremely low NOx emissions of below 2 g/kW.h were possible under certain mixture preparation with the pre-combustion chamber lean burn system without any after treatment. However, the high thermal load in the pre-combustion chamber region and the difficulties in achieving good combustion and stability over a wide range of operations prevented this kind of lean burn system from being widely accepted for vehicular natural gas engines [27] [28] [38]. Currently this system is mainly used in large stationary natural gas engines and in small engines with limited operating ranges [27].

Lean burn with open combustion chamber

There are merits in using the open combustion chamber system for natural gas engines compared to the pre-combustion chamber system. It has been argued that the mixture control system is simpler because only one mixture supply system is needed. The modifications of the engine are easier [20]. The emission of unburned hydrocarbons are lower because of the smaller crevice volumes. So this combustion system is increasingly used in natural gas engines converted from DI diesel engines or petrol engines [39] [30]. After a series of discussions and comparisons between the pre-combustion chamber and the open combustion chamber system both using different emissions control strategies, Stone, C. R. and his colleagues [16] designed a fast burn spark ignition combustion system for a 6-cylinder lean burn natural gas engine with swept volume of 3.6 litres.

To obtain a short flame travel distance and improve flame speed, the engine compression ratio was 15:1 which was much higher than that normally used in petrol engines. The engine was tested at wide open throttle for a wide range of mixture fuel/air equivalence ratio (which is the ratio of the actual fuel/air ratio to the stoichiometric ratio) using natural gas and natural gas diluted with 30% and 40% carbon dioxide which were to simulate the bio-gas fuel operation. Their extensive experimental results showed that the maximum output of the engine occurred with a slightly rich mixture. The engine maximum efficiency was 33% and it was fairly insensitive to the equivalence ratio in the range of 0.75 to 0.85. With the fast burn combustion system and ignition timing, the first 10% mass fraction of fuel burned coincide with the top dead centre and the rest of the fuel was burned within 30 °ca for a wide range of mixture strengths. With an equivalence ratio of 0.6, the brake specific emissions of NO had been as low as 3 g/kW h. With their combustion system, a very low level cycle-by-cycle variation having a 2% imep coefficient of variation (CoV = standard deviation/mean) was achieved for all operating conditions. They later applied the system to another type of natural gas engine and obtained very promising results [40] [41]. A very low emissions level of NOx and HC and a very low fuel consumption compared to a conventional open chamber system had been achieved by using the fast burn combustion system. At weak mixtures, NOx emissions below 1 g/kW h became possible with the fast burn combustion system with retarding ignition timing, but with certain engine efficiency and power output penalties. With this fast burn combustion system a big engine operating margin could be achieved if the emission constraints were limited to the conditions of 5g CH_4/kW h. and 5g NO_2/kW h. The system also led to a reduction in the cycle-by-cycle variations in combustion which tended to cause a torque fluctuation of the engine. Their two zone combustion simulation results showed a similar trend of the performance and emissions to the experimental results.

In order to speed up the combustion rate and reduce the tendency to knocking in a lean burn system with an open combustion chamber, many researchers paid much attention to the appropriate in-cylinder turbulence and swirl arrangement, which gave rise to a number of combustion chamber configuration designs [19] [29] [38] [42] [43]. Chmela, F. G. and Kapus, P. [29] [44] designed a bowl shape combustion chamber on the top of the piston aiming at extending the mixture lean limit. With the aid of CFD analysis, the overall flow patterns and turbulence distributions generated in the combustion system were obtained and optimised by directing and combining the intake swirl and the piston squish flow. With the new bowl shape symmetrical combustion chamber, a very low mean flow velocity and a very high turbulence level at the time of ignition was obtained, which increased the ignition quality and required low ignition energy. To cope with the ignition difficulty incurred by the lean mixture, the spark plug was positioned at a place where the mixture had a very low mean velocity and high turbulence. Thus

the initial flame volume could grow without disturbance. This design guaranteed the ignition stability and the high turbulence generated throughout the combustion chamber. The results showed that the emissions of NOx, CO and particulates according to the ECE R49 13-mode test were well below the emission standards of Euro III 1999. At lean mixture, an NOx level of 1 g/kW h. was achieved at a reasonable combustion stability (the CoV of imep was less than 5%) [29]. A similar kind of study was also performed in Ricardo [27] [38] for their fast burn "Nebula" combustion system which generated high charge turbulence at the time of ignition and during combustion without the high bulk velocities which could extinguish a flame kernel or distort a developing flame front. The chamber was applied to a 7.3 litre turbocharged natural gas engine converted from a swirling DI diesel engine with a compression ratio of 11.5:1. Their operating results indicated that the engine could be run over a wide range of air fuel ratio between λ 1.2 and 1.6 without detonation or lean misfire problem. Here the λ is called the relative air fuel ratio and is defined as the actual air fuel ratio over the stoichiometric air fuel ratio. The performance of the engine could match its base diesel engine. Transient cycle emissions of 1.7 g/bhp h. NOx+NMHC had been obtained from their de-rated engines used in a field trial test. With accurate mixture strength control and fresh charge cooling, the emissions could be further reduced [45].

In addition to the intake swirl related turbulence generation, Evans, R. L. and Blaszczyk, J. [42] designed a "squish-jet" combustion chamber which was based on the principle of using squish motion to generate a series of jets directed towards the centre of the chamber just prior to ignition. By controlling the dimensions of the detailed part of the chamber carefully, the generation of the turbulence intensity and the turbulence scale were able to be controlled. Comparison was made between the new chamber and its base case by using the same compression ratio 10.2:1. Their results showed that the fast burning rate resulted in an average 5% reduction in brake specific fuel consumption and an increase in the lean limit of combustion. Their lean burn system enabled the engine to met the US EPA heavy duty emissions regulations without using any of the after treatment methods. Shiells, W. and his colleagues in the University of Auckland [19] had also developed a series of combustion chambers by directing the significant swirl and squish, and their results showed that the deliberately generated turbulence and squish could lead to a highly desired faster combustion in the natural gas engine used.

To compare the difference between the two lean burn combustion systems, Beaty, K. D. [28] designed two systems for the same natural gas engine. Both combustion systems had the same piston design and approximately the same compression ratio which was 12:1. The tests were run by following the same test procedure for both systems. The results illustrated that the two combustion systems gave the similar engine emissions level. CO and HC emissions seemed to be insensitive to the combustion systems. At

part loads engine operating conditions, NOx emission level from the pre-combustion chamber system appeared to be lower than that from the open combustion system, but the tendency was the opposite for higher engine speeds and torque. Under most operation conditions the open chamber combustion system produced a higher efficiency than the pre-combustion chamber system because of the higher thermal loss in the pre-combustion chamber region. The difference was especially great for lower loads operation. It was the open chamber combustion system which was finally used for their conversion.

According to the size of the base engines and the development history, some engines like RK 270 spark ignition natural gas engine produced by Ruston Diesels having a bore of 270 mm and stroke of 305 mm combined the pre-combustion chamber system and the open chamber system together by using two spark plugs and a microprocessor based control system which controlled independently the amount of the gas and air supplied to the engines, the gas supply pressure to the pre-combustion chamber and the ignition timing [46] [47]. Their experience showed that the combined combustion chamber could give relatively low exhaust emissions and a good fuel economy as well provided that the control system working properly under different engine operating conditions. Their experience also showed that the nozzle configuration between the pre-combustion chamber and main chamber and the fresh charge temperature had a profound effect on the combustion in the main chamber and on the NOx emissions [48].

1.2.1.1.2 Catalyst converters

The lean burn system is a method of treating pollutants inside the combustion chamber. The catalytic converter is a unit which converts the pollutants into harmless materials just before they enter the air. A catalyst is a material that causes a chemical change without entering into the chemical reaction. In effect, the catalyst stands by and encourages two chemicals to react. There are two kinds of converters used for natural gas engines according to the mechanism of the chemical reaction. They are the non-selective converters and the selective converters.

Non-selective converters

The catalyst in a non-selective converter is in the form of different phases from the reaction medium (the heterogeneous catalysis [49]). The acceleration of the reactions takes place at the surface of the catalyst. Thus the large surface to volume ratio of the catalyst is required to increase the conversion rate of the exhaust emissions. To increase the surface of the catalyst, the material is often coated onto a ceramic or metallic

monolith support body which is either constructed into small spherical balls (pellets) or honeycomb shaped cylindrical channels. The latter construction prevails in Europe, and has as large a surface area as 20,000 square metres per litre of catalyst volume. The smaller the diameter of the channels, the bigger the surface area and the higher the flow resistance through the converter. Normally a density of about 60 channels per square centimetre is not too difficult to make. In order to improve the sintering stability and the catalytic activity, some rare earth metals are added into the oxide intermediate layer.

Many materials have been tested for the conversion of engine exhaust emissions. The precious metal platinum (Pt) is often used as the catalyst which oxidises with CO and HC to produce H_2O and CO_2. The precious metal rhodium (Rh) is often used in a non-selective catalytic converter to reduce NOx, which splits the nitrogen from the oxygen. The catalytic converter that can convert the three pollutants CO, HC and NOx at the same time in one compact unit is called as three-way catalyst converter. As for petrol and diesel engines, the catalytic converter is a very effective way to reduce the exhaust emissions from natural gas engines when they are running at a stoichiometric mixture. The air fuel ratio control is very critical for catalytic converters. If there is too much oxygen in the exhaust, there will be insufficient radicals of CO and H_2 to split the N_2 from the NOx in their predominant reactions. If the exhaust contains too little oxygen, the hydrocarbons and the carbon monoxide can not be completely oxidised to H_2O and CO_2. For natural gas, the λ window within which a high conversion rate can be achieved, see Figure 1.2, is very narrow compared with that of petrol fuel [10] [39]. Conventional Pt-Rh based three-way catalysts (at a Pt/Rh ratio of about 5) have shown a good performance for the conversion of CO and NOx at near stoichiometric mixture. But these catalysts are not effective at converting methane, which typically makes up 85%~99% of the total volume of the natural gas, due to its saturated molecular structure [13] [50] [51]. A high conversion rate for methane can be expected when the mixture is on its rich side (λ= 0.995), but the efficiency is not very satisfactory [10] [39] [50] [52]. Methods to improve methane oxidation in the catalytic converter are still required.

Engler, B. H., et al. [50] tried different catalyst formulations based on palladium (Pd) searching for a high conversion rate of methane and a wider λ window in CNG engines. Screening experiments were not only made on the formulation of the precious metals such as rhodium, iridium, palladium and platinum, but also made on the formulation of the wash-coat upon which the catalyst was precipitated. The wash-coat was the intermediate layer in a pore structure consisting mainly of alumina and some other additives. Their optimal Pd based converter not only showed a good performance at stoichiometric mixture, but also gave a good oxidation rate for CO and HC at lean mixtures. A methane conversion rate of more than 90% could be achieved at a temperature about 400 °C with mixtures between λ 0.98 and 1.02. For stoichiometric

mixture, both the Pt based and the Pd based catalysts could convert the pollutants effectively. But the former one was deactivated rapidly with ageing effects. The major cause of the ageing effect is believed to be related to phosphorous poisoning through oil consumption. For stationary engines the ageing problem of the catalyst is more serious because these engines often run thousands of hours continuously under full load condition [51]. Thus the Pd based catalyst should be chosen.

Because the catalyst only acts in a certain mixture strength range, which is slightly in the rich region close to the stoichiometric at about λ=0.98~1 [10] [14] [51], the mixture strength has to be controlled under all engine operating conditions to get a high conversion rate. Otherwise, the conversion efficiency can be below 50% [27] or even a negative NOx conversion [14] if the mixture air fuel ratio control accuracy is poor, or if the exhaust temperature is very low. An effective way to control the mixture strength is using λ-sensors (or oxygen sensors) in conjunction with an advanced control unit to adjust the air fuel ratio supplied to the engines via different means and control strategies [14] [18] [51] [53] [54].

To overcome the disadvantages such as higher thermal loads and lower efficiency brought about by the stoichiometric mixture with 3-way catalyst converter, two-way oxidation catalysts specifically formulated for lean burn natural gas engines have been tested. Beaty, K. D. [28] used two prototype lean burn oxidising catalysts for a Volvo natural gas engine. His results were very promising for both catalysts. The reduction of total HC and CO emissions were above 80% over a wide range of steady state engine operating conditions, where the catalyst temperatures were relatively stable. But when the oxidising catalyst was used for an ultra lean burn combustion natural gas engine, the low exhaust temperature did not activate the catalyst and the HC emission was still relatively high. Duggal, V. K. [1] also used a two way oxidation catalysts and his result exhibited a conversion of 85% on total HC with a significant reduction of CO at the rated air fuel ratio 26:1 in a Cummins L10 CNG urban bus natural gas engine.

Apart from the engine exhaust oxygen concentration and exhaust temperature, the construction of the converter, the formula of the catalysts and their purity also affect the emissions conversion rate and the life expectancy of the converter. Sakai, T., et al. [55] [56] evaluated eight types of catalytic converters on their purification characteristics for a liquefied natural gas (LNG) fuelled automobile engine under several engine operating conditions. These converters were Pt, Rh, Pd, Pd/Rh, Pd/Pt, Pt/Rh/Pd, Pt-Pd, and Pd-Cu. Their results showed that the dual-bed Pt-Pd catalyst converter offered the highest unburned methane oxidising rate at λ=1.2 in the range of 1.6 to 3.2 g/*l* Pd loading weight. The methane oxidation started at a temperature of about 300 °C. At about 400 °C the oxidation rate was above 97% and almost 100% oxidation could be

achieved when temperature rose to 550 °C. It was believed by the authors [56] that the Pt catalyst was high in catalytic activity for methane oxidation. Intermediate products of methane not oxidised by the Pt catalyst were easily oxidised at the subsequent Pd catalyst. The ageing effect for different catalysts and the emissions of formaldehyde under various engine operating conditions were also investigated in their study.

Selective converters

To deal with the problem of NOx emission, there was another kind of after treatment method called the selective NOx catalytic converter [49] [57] [58]. Instead of using the precious metal rhodium, ammonia was injected into the exhaust gas at a temperature of 300 ~ 400 °C and this mixture was allowed to flow through a catalyst where the NOx and the ammonia (NH_3) were converted into nitrogen and water. The conversion rate depended on the amount of ammonia added. A conversion rate of 90% or higher was achievable in certain applications. The larger the amount added, the higher the conversion efficiency. But there is a limit to the maximum amount of ammonia added, because the extra ammonia (the NH_3-slip) is also a kind of emission. To control the amount of ammonia to suit different engine operating conditions, a computerised control unit was shown to be a very effective means. There are advantages for the selective converter. One of them is that the excessive oxygen, such as is the case in the lean burn system, is allowed in the exhaust gas. Another one is that the poisoning possibility of the catalyst by those heavy metallic compounds such as lead, arsen, halogen, sulphur and phosphors coming from the fuel or from the lubrication oil is not as high as that in the non-selective converter. But the masking possibility by the dust and ashes is nearly the same. Because of the size required for the reactor with catalyst and ammonia storage system, it is very difficult to apply this kind of selective conversion system to automotive natural gas engines. It was mainly used for large stationary natural gas engines and those power plant units where the size and volume were not a problem.

1.2.1.1.3 The EGR system

Considering the mechanism of the NOx formation, efforts have been made at reducing the peak temperature and its duration of the combustion process via retardation of the ignition timing. It has been found that retarding the ignition timing is a very effective way to reduce the combustion peak temperature and hence the NOx emissions. But for the sake of fuel economy and power output, the scope for retarding the ignition timing is limited. Thus the EGR technique was used in conjunction with the ignition timing retardation without severe penalty of fuel economy and power output [27]. The EGR

technique is a method which introduces a portion of exhaust gas back into the cylinder during the induction process. The fresh charge is diluted by the recirculated exhaust gas and the heat capacity of the charge is increased. The highest temperature of the combustion is constrained. Consequently the amount of NOx formation is reduced. The limited combustion temperature also prevents overheating of engine components and the catalyst, which is problematic in turbocharged natural gas engines [16].

There are two types of EGR system developed for reduction of NOx emissions from engines, the external EGR system and the internal EGR system. The external EGR means that the exhaust gas is returned to the inlet manifold or carburettor from the exhaust manifold through some extra pipeline connections, while the internal one means that the exhaust gas is returned by the extended valves overlap or re-opened exhaust valve [59]~[61]. Both EGR systems had been proved to be an effective method to reduce NOx emissions without decreasing the fuel economy very much if the amount of the exhaust gas could be controlled accurately according to the varying engine operating conditions. For the engine combustion chamber designed [17], fuel consumption decreased with increasing EGR mole fraction from 0.03 to 0.13 because of the tolerability of the chamber to the low flame speed. The EGR mole fraction or EGR ratio was defined as the moles of recirculated exhaust gas divided by the total moles of EGR, and the fuel and air. Compared to no EGR use, the maximum EGR ratio of 0.13 used in their tests provided a 68% reduction in NOx emissions at the cost of a 58% increase in total HC emissions where the respective MBT (Minimum ignition advance for Best Torque) spark timing values were used in the external EGR system [17]. The increased HC emissions was because the EGR reduced the flame temperatures and diluted the mixture for stoichiometric operation. When EGR was used with the lean burn combustion system, a very low level of NOx was obtained without using a catalyst [27]. But HC emissions were quite high. Another advantage was that EGR could be used in conjunction with the catalyst system to control the emissions, the exhaust temperature and the knocking tendency in an effort to assure an acceptable engine durability [62]. To achieve this goal, a fast burn combustion chamber is critical for natural gas engines. Otherwise, a significant cyclic variation of the engine performance will be very difficult to tolerate. When the internal EGR technique was used in conjunction with the lean burn system, HC emission was offset by lessening the mixture short-circuit flow and also improving the warm up operation [60]. For EGR systems, however, the control of the amount of the exhaust gas recirculated under different engine operating conditions is very difficult and costly, which sometimes even incur a variation of the behaviour of the closed-loop natural gas fuel control system due to the influence of extracted EGR on the oxygen sensor, as claimed in reference [17].

1.2.1.2 Engine power capacity and efficiency improvement

As an engine fuel, natural gas has the inherent merit of possible low emissions. Unfortunately, it has the inherent disadvantage of low energy density, which leads to a low engine power capacity. In addition to the lower charge energy density, the loss of the positive effect of liquid fuel evaporation on the volumetric efficiency often further deteriorates natural gas engines power output. For stationary natural gas engines operating at stoichiometric mixture, the situation is acceptable. But for natural gas engines operating under lean mixtures, the problem becomes very severe. On certain applications, the engine brake mean effective pressure levels are often required to have the same level as their base diesel engines. In these cases compensations for the low energy density has to be made in order to meet the demands on the engine brake mean effective pressures and thermal efficiencies, especially when some emissions control technologies which may deteriorate the engine performance have been applied. There are two means to increase the engine specific power. One of them is turbocharging technology and the other is high compression ratio. Both of them can improve the brake power output and thermal efficiency of natural gas engines.

1.2.1.2.1 Turbocharging

The turbocharging technique has been used by many researchers [14] [29] [37] [38] to ensure the engine power output and driveability have the same level as their base diesel engines. Since the mechanical losses did not rise in proportion to the power output, the efficiency was improved as well [40]. A high BMEP level of more than 18 bar was claimed by researchers in [29] with a diesel-like thermal efficiency which was about 40% at WOT, but the high boost pressures required were constrained by the thermal loads limit and the detonation limit even with very retarded ignition timing. The higher thermal load was caused by the increased fuelling levels, the long burn period, the low expansion ratio and air fuel ratio, and the small valve overlap angle used. It was predicted that an effective engineering limit on the BMEP level for a stoichiometric turbocharged natural gas engine using diesel engine materials was around 9.5 bar [27]. It could be much higher for lean burn combustion system. But the BMEP was still limited by the difficulty in keeping the NOx emissions low enough when it exceeded 12 bar [37]. Apparently the stoichiometric mixture with catalyst converter will not be a good choice if the turbocharged natural gas engine with a BMEP of over 12 bar is required. In this case the lean burn system with oxidising catalyst and/or the EGR system will be a wise choice for the turbocharged natural gas engine [27]. Dealing with the detonation tendency, the intercooling technique is often used in order to extend the margin and to improve the engine volumetric efficiency [45]. The intercooler can reduce the temperature in the intake manifold and reduce the NOx emissions significantly [32]

[36] [37] [46]. To obtain good matching between the turbocharger and the engine over a wide range of engine operating conditions, wastegate control unit was used by many researchers and manufacturers [1] [14] [38]. In addition to the matching problem, some other matters need to be considered when turbocharging is used in conjunction with a stoichiometric mixture and catalytic converter. In this case some engine components such as spark plug, cylinder head, valves and valve seats will have extremely high thermal loads [1] [14] [19]. Materials like platinum and nimonic alloy were even used for the spark plug electrode by the researchers in [47] to withstand the severe condition. The condition is also severe for the spark plug in the lean burn operation due to the high ignition energy required and the low valve overlap angle used. To ensure the durability of the valve and valve seat, not only high thermal resistance but also high wear resistance materials have to be used because there are no combustion generated carbon deposits which have a lubricating effect, especially when landfill gas is used [14]. The compression ratio and the ignition timing have to be adjusted carefully to keep the catalyst from being overheated. To maintain the catalyst temperature below its limit and prevent the overheating of the components, a highly retarded ignition timing should be avoided in turbocharged natural gas engines. Sometimes the techniques such as the water cooled spark plug housing, the water cooled turbocharger bearing housing, the gallery cooled piston with particular profile and ring pack will be necessary to dealing with the high thermal load problem for turbocharged natural gas engines. Of course with the turbocharging technique, the valve guide oil sealing problem caused by the intake vacuum and the piston ring pack arrangement will be relieved compared to naturally aspired engines no matter whether the base engine is a diesel or a petrol engine [1] [14].

1.2.1.2.2 High compression ratio

The power output of an engine is proportional to the fuel total energy input and the efficiency of energy conversion. The higher the engine compression ratio, the higher the engine efficiency. Thus increase of the engine compression ratio will increase the natural gas engine power capacity. Many researchers have used this technique to maintain the natural gas engine efficiency at the same level as its base diesel engine. For a petrol engine based CNG engine, a 7% power gain and a 15% improvement in fuel economy was obtained when the engine compression ratio was increased from 8.9:1 to 14:1 at near stoichiometric mixture [39]. At lean operation, an additional 19% fuel consumption improvement was obtained but the catalytic conversion was very poor for all the three emissions. The high compression ratio is often accompanied with the compact combustion chamber which will overcome the low flame speed problem of natural gas [20]. However, there is a limitation on the compression ratio above which the engine performance will deteriorate. A high compression ratio will cause high engine components temperature and require a high ignition energy. The temperatures of

the exhaust valve, piston and cylinder head are similar to that of petrol engines when they are operated at the same load and are very sensitive to the mixture air fuel ratio and ignition timing [63]. Thus the design methods used for diesel and petrol engines to reduce the component thermal loads have to be adopted to natural gas engines with high compression ratios. Because of the high ignition temperature of natural gas, high energy spark ignition systems are often used especially for the lean burn or EGR diluted mixture. The high ignition energy required often causes a durability problem of the spark plug. To improve the performance and reliability of the ignition system for natural gas fuelled stationary engines, Klimstra, J. and Overmars, F. [64] conducted an investigation into the spark plug gap monitoring. With their monitor developed, the engine ignition system reliability could be guaranteed and the maintenance cost was reduced. The commonly used ignition distributing mechanism often causes problems in the event of entry of dust or humidity to a high tension distributor cap when it is used in the high compression or turbocharged engines which require high firing voltage. Natural gas engines like the Hercules in Italy adopted the idea from high performance petrol engines to solve this problem [43]. The distributor was replaced by using one coil for each cylinder. The idea of multiple coil Hall effect sensors triggered ignition system was also used by other researchers due to the consideration of reliability and durability of the ignition system [1] [15] [19].

It should be mentioned at this point that to raise the specific power capacity and shaft efficiency by raising the compression ratio or the boost pressure has a negative effect on emissions control [37]. If the mixture is lean, the ignition timing should be adjusted between the MBT and the timing for acceptable emission level. When the mixture is stoichiometric, the 3-way catalyst converter and the EGR system emissions control strategy should be applied for the turbocharged or high compression ratio natural gas engines with the accurate closed loop control. Due to the higher expansion ratio, exhaust temperature may be too low for the catalyst to be enactivated for the high compression ratio approach. In this case the ignition timing has to be adjusted. To obtain a high performance and low emissions with high reliability and good driveability, both the emissions control approaches and the performance improvement approaches discussed above have to be carefully considered and their combinations should be optimised according to each individual application.

1.2.1.3 Mixture preparation system and its control

The study carried out by Ask, T.ϕ., et al. [65] [66] on ignition and initial flame growth in a natural gas engine indicated that the initial flame growth and the flame propagation thereafter were very much dependent on the mixture quality besides the in-cylinder gas motion and turbulence. There are two kinds of mixture preparation systems for natural

gas engines [9] [13] [26] [54] [67]. One of them is the fuel injection system which is the analogous product of the fuel injection system used in petrol engines fuel systems [21] [25] [68]. The other one is the conventional mixing device which is also analogous to the carburettor used on petrol engines. Each of the preparation methods has its own advantages and application scope. Low pressure gas injection in the inlet ports may offer the possibility of high accuracy air fuel ratio control with the simpler type of closed loop control system. The high pressure cylinder direct injection can reduce the HC emissions and prevent the engine from knocking, but usually requires high gas pressures in an order of 200~1000 psi. The well-designed gas carburettor can provide more homogeneous mixture for the natural gas engine without the need for a pressurised unit. Comparisons of the engine performance with the two types of mixture preparation systems have been conducted under different conditions of assessment [69]~[71]. Each of them exhibited its own features.

1.2.1.3.1 Natural gas injection

Engines fuelled purely with natural gas can use either low pressure injection or high pressure injection techniques. The former was often applied for two stroke natural gas engines and four stroke engines with intake manifold injection or throttle body fuel injection [21] [56] [69] [72] [73]. The latter was mainly used for four stroke natural gas engines with direct cylinder injection and some dual fuel engines in order to cope with the original diesel fuel supply system [74]~[80]. Because of the high pressure needed, the in-cylinder injection was obviously suitable for a CNG engine where the fuel had already been compressed to the pressure desired [54].

In an effort to improve the engine thermal efficiency and HC emission, Goulburn et al. [21] developed a diaphragm type cam driven low pressure injector for a two stroke crankcase compression natural gas engine, see Figure 1.3. With the aid of CAD and CAM techniques, a cam/follower injection mechanism was optimised. Test rig operating speeds up to 3000 rpm had been achieved for the newly designed cam injector. Compared to the stratified charge crankcase compressed two stroke natural gas engine which they originally developed at their initial study [22], the injection system improved the engine efficiency. Green, C. J. and Wallace, J. S. [68] also designed a natural gas injector for a two stoke natural gas engine so as to prevent short-circuit of the gas directly to the exhaust system. Their injector was based on direct electromagnetic actuation using a high energy multipole solenoid, see Figure 1.4. After intensive study on different configurations of the solenoid actuator, different constructions and materials of the injector components such as pintle, seat and return spring, their prototype natural gas injector intended for metering the gas supplied at 2 MPa (300 psig) had achieved as short as 1.5 ms injection duration at up 2100

injections per minute on an engine test rig. The quantity of the fuel delivered could be well controlled using the appropriate solenoid trigger signal width. However many of the injector features were not cost effective in actual applications.

So far a few studies on the single point natural gas injection system have been reported. One of them was the GFI (Gaseous Fuel Injection) system which was developed in Ortech International [81]. A computer was used to adjust the fuel flow by turning on the proper combination of injectors according to the absolute pressure of the atmosphere, fuel and manifold and the absolute temperature of the fuel. The metered fuel was then routed into a fuel nozzle in the intake air stream. The GFI system could operate open loop or closed loop with lean or stoichiometric strategies and accommodate the presence or absence of EGR and catalyst systems. To deal with fuel leaking problems of the system, special connection units were developed for the joints of the gas delivery lines from fuel container to injection nozzle. However, the leakage from the injector seat and regulator side were still present sometimes although it was much lower than the leakage from conventional petrol engine injection systems. The GFI system had been tested for a number of natural gas engines [70] [71]. The results showed that the injection system worked properly and the emission of NOx was exceptionally low (1.16 g/kW h.). The GFI system was also put into trial for 30 natural gas fuelled cars in a joint project between the British Gas plc and the Ford Motor Company in the UK.

Geiss, R. O., et al. [82] developed a multi-point fuel injection system which consisted of a fuel rail assembly, electronic control module and separate injector driver module in their Chrysler Dodge NGV programme. A speed-density fuel control strategy was employed in the closed loop control unit, which needed input signals such as engine manifold absolute pressure, throttle position, exhaust oxygen concentration and gas pressure and temperature after its regulator. The injectors used were low impedance solenoid, pulse width modulated ball type units, which had a good linearity between fuel flow rate and pulse width. The engine performance and emissions test with 3-way catalytic converter showed that the emissions level was very low and the performance and driveability were very impressive. The researchers at Concordia University [83] also made an attempt to develop solenoid operated natural gas high pressure injectors which were converted from a diesel injector used for its base diesel engine. In order to avoid the application of the high pressure gas pump, a small powerful solenoid was introduced into the injector and a special switching circuit was developed to control the opening and closing of the injector. After a computer simulation of the solenoid controlled gas injection process, a multiobjective optimisation of the design variables was made to reduce the opening and closing time needed. The results of the work showed that the performance of the solenoid injector was close to the hydraulically operated injectors at moderated engine speed. Another multi-point gas injection case

was reported by Sierens, R. and Rosseel, E., [69] in the University of Gent, Belgium. An engine performance comparison was made between the injection and the carburation of natural gas, and the performance of the injector was examined. Even though the opening time and duration of the injectors were controlled by an accurate electronic circuit, the mass flow through each injector was different due to an uneven opening delay of each individual injector. This resulted in an unequal fuel distribution from cylinder to cylinder and poor combustion. Uniform fuel distribution should have been the advantage of the multi-point inlet injection. This study showed that reliable gas injectors have yet to be developed.

For natural gas engines with direct fuel injection, combustion chamber system matching amongst the injector configurations, the combustion chamber shape and the charge flow patterns within the chamber, are essential to the engine's performance and emissions. Jennings, M. J. and Jeske, F. R. [84] [85] conducted an investigation into the flow mechanism that governs the injection process in order to truly optimise both the combustion chamber and the injector configuration. In conjunction with an engine test, multi-dimensional CFD analysis was used, which provided fundamental insight to the problem. Their computational results showed that a fuel rich core of the natural gas plume formed near the nozzle exit where the high level turbulence energy was generated by the jet shear layer during the initial stages of injection. The core contained bulk of unmixed fuel mass and the mixing of this fuel with the air around was controlled by the turbulence generated. For a single hole nozzle, the smaller the hole was, the more efficient the mixing, even though the penetration of the plume and the turbulence energy were tending to offset this benefit of the reduced plume size. But if the size was too small and the holes exceeded certain number in the case of multiholes, the plume merging would inhibit the mixing. The optimal number of holes was that which produced the largest number of separate plumes or largest total plume surface area.

Because of the eliminated short-circuit losses, throttling losses and the lessened tendency to knock, the main benefits of the direct cylinder injection are the emissions reduction while retaining diesel levels of fuel economy and performance. Another potential benefit may come from charge stratification in a lean burn natural gas engine. However, natural gas is more difficult to inject than liquid fuels because the low density gas jet cannot easily penetrate and spread [80]. So far the homogeneity of the mixture from the injectors is still not as good as that from the gas air mixers. In addition to the poor mixture homogeneity, the sealing, wearing and pressurising difficulties are still problematic and remain to be solved. A higher cylinder pressure needs a higher injection pressure for a certain amount of gas demanded. The high pressure not only causes sealing problems, but also consumes a large amount of energy to compress the gas. Even with these problems resolved, a natural gas injection system is still more

expensive than its counterpart, the carburation system, because of the cost of more precise components and fuel filtration. As such, suitable high pressure gas injectors are still in the development stage [84]~[86].

1.2.1.3.2 Natural gas carburation

Majority of natural gas engines in service are using carburettors rather than the injection for mixture preparation. According to the operating principle, there are mainly four types of carburettor. They are the venturi type, vortex type, orifice type and variable restriction type, see Figure 1.5. Some of them have been widely used by different manufacturers [14] [53]. Although the natural gas should theoretically mix better with air because of its peculiar physical property [8], the experience from different researchers showed that none of them produced satisfactory mixture as required by the engines under different operating conditions [1] [87] [66].

Klimstra, J. [87] conducted an investigation into four carburettors. By using an adjustable speed motor driven fan, the performance of the carburettors were studied for their nominal flow rates. To measure the mixture homogeneity, the mixture out of each carburettor was divided into four segments with each segment representing the quarter part of the out let plane of the mixer. The mean mixture composition within the quarter segment was analysed by using a paramagnetic oxygen meter. In addition to the mixture homogeneity, the characteristic of air fuel ratio control and the flow restriction (or pressure loss) were also studied. With respect to the pressure loss across each carburettor, the results showed that the venturi type mixer was the best of those mixers tested and the variable restriction one was the worst. The pressure loss across the vortex type depended on the angle of the intake blades. With respect to the mixture air fuel ratio control, the variable restriction mixer offered the best inherent controllability and it was not sensitive to the pressure variation in the fuel supply system. But none of them could meet the increasing requirement on the mixture homogeneity. An uneven initial distribution of fuel over the air stream and an insufficient mixing length were believed to be the primary causes of the mixture inhomogeneity.

It should be noticed that the mixture homogeneity will not be a problem when the carburettor is located upstream of the compressor in a turbocharged natural gas engine because of the extra mixing time and the turbulent mixing enhancement within the compressor. In this case a low gas supply pressure will be allowed. That was why the majority of turbocharged natural gas engines using pipeline natural gas had the mixture compressed rather than air alone [37] [38]. For CNG or LNG engines, gas pressure was still high enough to cope with the boost pressure after one or two regulators were incorporated in the gas supply line. Thus the gas air mixer was sometimes placed

downstream of the compressor in order to reduce the shaft power required for turbocharging [1] [43]. The downstream installation of the mixing unit was also convenient for the placement of the intercooler if it needed but with the mixture homogeneity penalty [38] [53].

1.2.1.3.3 Air fuel ratio control

No matter which kind of mixture preparation system is used, the air fuel ratio control must meet the accuracy required in order to obtain a high performance and low emissions for natural gas engines [10] [71] [82] [88]. There are two kinds of control system used in the present gas engine market. One simply uses a mechanical system to regulate the gas flow area according to the gas signal or the air depression pressure in the mixer [27] [45] [53] [54] [89]. Another kind of the control unit is a more sophisticated electronic system which regulates the gas flow area according to the oxygen content in the engine exhaust manifold. Many newly converted natural gas engines used the latter kind of control unit to obtain a more accurate mixture air fuel ratio control [18] [53] [72] [73] [82] [90].

In the control unit designed by Franklin, M. L., et al. [72] [73], the injector driver and ignition system were controlled according to the measured manifold absolute pressure, measured manifold air temperature and the mapping obtained from extensive engine bench tests. The signals to the driver and the ignition unit were connected via fibre-optic cables in order to protect the computer and system against stray voltage and current spikes damage, and electro-magnetic noise disturbance. The control system was able to adjust the spark timing and the air fuel ratio of a lean burn natural gas engine simultaneously to its best thermal efficiency operating point considering the trade-offs between efficiency and emissions.

Tiedema, P. and Wolter, L. [53] presented a microprocessor air fuel ratio control system which picked up the actual mixture strength signals using an exhaust oxygen sensor and then adjusted the air fuel ratio through a stepper motor driven gas metering valve. Their field operation experience showed that the control system could get a satisfactory air fuel ratio correction for different ambient conditions and fuel compositions. Consequently the natural gas engine emissions were reduced to a very low level. The exhaust oxygen heated zirconia sensoring technique was also used by Roberts, G. R. and his colleagues [18] in their millivolt output digitally linearising control system. The control system was fitted to a variable geometry mixer which was retained to carry out the primary gas-air control and mixing function. The gas inlet pressure was controlled by the unit to trim the air fuel ratio to the required value. The bench test showed that the mixture could be controlled to a variation of λ value of 0.02 at a setpoint of 1.5 for a

lean burn combustion natural gas engine. For stoichiometric mixture, the control system could maintain the λ value to within 0.004 at a nominal setpoint of 1.000. The emissions level of the NOx and CO could be reduced to well below the current European limits with excellent reliability after 5000 hours test without adjustment. However, because of the high hydrogen content with natural gas fuelling, the accuracy of the oxygen sensor and its sensitivity is problematic no matter whether it is the zirconia heated oxygen sensor or the thick film titanium dioxide heated sensor. There resulted in a variation of mixture strength even in the steady state, which was much higher than the variations which occurred in conventional petrol engine control systems [17].

To meet the response requirement from automobile applications, some systems like the Impco mechanical control system have been recently developed [91] [54]. In ordinary venturi type mixers, the mass flow of fuel changes only according to the velocity of air at the throat, not the density of air. Thus with different ambient temperatures the density of air varies and this gives rise to a change in mixture relative air fuel ratio. To avoid this, the new Impco microprocessor based fuel management system incorporated an engine speed/density measuring unit and a fuel mass flow sensor by using hot wire anemometer technology. The system could measure the quantities of the gas and air directly and compensate for the air fuel ratio changes under different ambient conditions and gas properties. This fuel system could be used for both stationary and automobile natural gas engines [92]. Kittelson, D. P. and his colleagues [90] also developed a microprocessor based adaptive control system which could be used for both automobile and stationary natural gas engine MBT timing control. The test results showed that the system had good features. Because of the adaptability of the system, the compensation for the fuel compositions and other variables could be properly adjusted.

1.2.1.4 Gas compositions and on board gas storage

1.2.1.4.1 Effect of gas compositions on engine performance

Natural gas is comprised of 88%~96% methane, with other non-methane components such as ethane, propane, butane, nitrogen, carbon dioxides and water. The compositions of the natural gas supplied change from place to place and from time to time. This may cause problems to the air fuel ratio control, to the ignition quality and the exhaust gas catalyst conversion. The test results on conversion of different hydrocarbons [14] implied that the composition would influence the conversion rate of the unburned hydrocarbons from natural gas engines because the bond energy associated in those non-methane members in the paraffin group of hydrocarbons were lower and should be easier to be converted by the 3-way catalyst [10]. The heavier the hydrocarbons, the

higher the HC conversion rate. It had been experienced that the catalyst tended to selectively convert the more reactive hydrocarbons [39].

The effect of compositions on engine performance was thoroughly investigated by Charlton, S. J., et al. [93] and also by some other researchers [52] [89] [94]~[96]. Unlike the effect on the catalyst conversion rate, the composition of natural gas had only a small direct effect on flame initiation and propagation speed providing that the gaseous fuel was not the industrial gas, nor the bio-gas. With higher level of the higher hydrocarbons, the burning rate was slightly faster and consequently a higher cylinder pressure was expected. The extra addition of higher hydrocarbons such as ethane, propane and butane in a small quantities did not affect the result too much no matter whether it was at naturally aspirated test condition or at boosted condition. Because the composition had an effect on the octane number of the fuel, the knock sensitivity was different and the compression ratio which could be used was different for different gas compositions [13] [96] [97]. However for an engine with constant compression ratio and a reasonable knocking margin, the effect of composition on the octane number was difficult to obtain under normal operating conditions. For lean burn natural gas engines with open loop mixture air fuel ratio control systems, the engine flammability limit will be greatly influenced by the composition of the fuel because the metering performance of the mixer is affected by the composition [89]. If the non-hydrocarbon content contained is too high, as the case in bio-gas or industrial gas, the mixture ignition and flame propagation will be significantly influenced for this kind of diluted gas. Consequently, the engine performance will vary with changes of dilutent concentration irrespective of ignition principles used [98]. Generally, the engine brake power output, fuel economy and before catalyst emissions of the regulated pollutants will not be affected significantly by the variations in gas composition with effective closed-loop fuel control for stoichiometric engine mixture operations [52].

1.2.1.4.2 Gas storage technologies

For stationary natural gas engine, the gas is often fuelled directly from the national gas distribution pipe lines. The gas storage is not a problem of interest in this application. When a natural gas engine is designed for automobile use, however, the on board gas storage is a very serious impediment because of the low energy density of natural gas. There had been different ways to tackle the low energy density problem when the natural gas was used as the fuel for vehicular engines [1] [14] [28] [38]. One was to store the gas on the vehicle in a compressed form with a pressure of 3,000 psi (i.e. 20 MPa) at temperature of about 20 °C in a special steel gas cylinder to cover a reasonable vehicle range [10] [82] [99]. Even with this pressure, the cylinders still occupied about five times the volume of the diesel fuel tank and four times the volume of the petrol tank

having the same energy equivalent content [13]. In addition to the volume, the weight used to be another problem. Thus a number of new products, all aimed at reducing cost, weight and size of the CNG tanks, were developed. Composite materials such as glass fibre, carbon fibre and aluminium graphite have been tested as wrappings for metal or thermoplastic liners [70]. The applications of these lighter materials effected lower cylinder weight but with higher cost. The ability of a composite gas container to withstand tough standard durability and safety test such as bonfire, gunfire, drop and impact did not inherently come from the use of the material itself. The container design methodology, manufacturing methods, and construction of the material also played a very important part [100]. Due to the pressure used in CNG application, proper sealing at all connections of the fuel system, such as pressure relieve devices, gauges, and regulators was also very important [82]. Due to the existence of water content in gas containers, corrosion problems, water condensation and even freezing problems have to be considered to ensure the required container design life. Sometimes dehydration of the natural gas has to be carried out should the water content exceed a certain level.

Another method was to store the gas as a cryogenic liquid at about -160 °C (113 K). At this liquefied state, the volume is much less than with the compressed gas storage. Compared to the CNG, the LNG offers definite advantages in energy storage density and reduced vehicle weight. In liquid form methane has a density of 422 g/*l* at its normal boiling point, compared to 160 g/*l* for the CNG at 3,000 psi and ambient temperature [8]. Thus in some usage such as heavy duty trucks and locomotives [97], the LNG is often used prior to the CNG. But the LNG container, as schematically shown in Figure 1.6, is more complicated and more expensive than the CNG container because of the heat insulation problem. Without proper design of the LNG container, its supply piping and vapouring system, LNG can not be stored for extended periods and may cause serious venting pollution [101]. Research conducted by Tummala, M. and his co-workers showed that the optimum design of the container was very important to control the container pressure and temperature [102]. Another disadvantage of the LNG is the need of highly trained personnel for refuelling because of the potential severe human tissue damage [3]. In terms of the engine operation, an LNG engine is generally the same as the CNG one because it is the fully vaporised liquid that is fuelled into the engine intake system.

Recently a new method to store the gas on board by using solid adsorbent materials such as the activated carbon has been put into test [103]~[105]. The carbon could be produced from coal derived materials, cellulosic materials or polymer based materials. There are different methods to increase the carbon surface area or micropore volume per unit volume of carbon. Conventional activation process such as the treatment with steam, carbon dioxide or air at elevated temperature over 600 °C for the removal of

carbon could increase the surface area to over 1500 m^2/g [103]. Lin, Y. C. and Huff, G. A. [105] developed a new activation method which could obtain a surface area of 3000 m^2/g. A number of non-friable smaller shaped pieces could be packed into the vessel at ambient temperature and high pressure. Due to the physical characteristics of the adsorbents, the natural gas could be adsorbed into the micropore at high pressure and could be desorbed or delivered out of the adsorbents at low pressure with a delivery efficiency over 80% for the pressure controlled storage. For temperature controlled storage, the pressure was relatively low (1~20 bar) and the storage capacity could be larger than the pressure controlled storage [104].

The adsorbed natural gas (ANG) technology has great potential to increase the fuel storage capacity per unit storage volume while decreasing the compressor output pressure, which will greatly reduce the safety and the refuelling infrastructure cost. At 25 °C and 500 psig (3.5 MPa), which is near the gas saturation pressure, the maximum methane density in the micropore was about 230~270 g/*l*. When the pressure reached a certain value, the amount of gas storage per unit volume become equal between the ANG and CNG because of the saturation and the volume of the adsorbent itself [105].

To sum up the review carried out above, the following theme can be drawn on current natural gas engine technologies. To further reduce the main regulated emissions from natural gas engines, two main strategies can be applied. One is the engines equipped with three-way catalyst converter and a closed loop mixture air fuel ratio control unit operating at stoichiometric mixture. The other one is the engine equipped with closed loop mixture air fuel ratio control system operating at a lean mixture. Compared to the stoichiometric mixture operation, a higher thermal efficiency, a lower thermal loading and lower cost can be achieved by applying the lean burn operating scheme. The stoichiometric operation equipped with the 3-way catalyst converter can offer more stability and lower emissions. Both strategies demand a well designed combustion system and a high quality mixture preparation system. To overcome the low energy density drawback of the engines fuelled with natural gas, either turbocharging or high compression ratio techniques can be used benefiting from the fuel high knock resistant ability. The high boost pressure or the high compression ratio will result in a high engine thermal efficiency as well. When natural gas engines are applied for automobile applications, any of the three gas storage methods can be used to cover a reasonable operating range.

In order to further reduce natural gas engine emissions and retain their power output and efficiency, the mixture prepared for the engine plays a very important role. In the engines with lean burn system, the mixture prepared governs the engine's torque

fluctuation and lean burn limit. In the engines equipped with three-way catalytic converter and operating at stoichiometric mixture, it is critical for the mixture to be within the λ window to keep the emissions at low level. For the EGR system, the recirculated hot exhaust gas must be well mixed with fresh air and gas. Otherwise the engines performance and emissions will be poor. Research work carried out in the mixture air fuel ratio control system has been very encouraging. However, further knowledge on the mixing part of the mixture preparation system is still demanded. For either the stationary or the automobile applications, the existing mixture preparation systems can not provide a satisfactory mixture quality required by the engines under different operating conditions. A better understanding on the mixing behaviour is required and a better mixing device is desired.

For the immature natural gas engines, there are also some other areas which are worthy of being studied. For example, the three existing methods of gas on-board storage are not very satisfactory and there is still much work which needs to be done. In order to better understand the performance and emissions formation in natural gas engines, numerical prediction techniques will be very helpful. Effort in this area is yet to be made. To do this, some fundamental research into the combustion mechanism and the emissions formation mechanism associated with natural gas should be carried out.

1.2.2 CFD and its applications to engines

In support of the advanced experimental methods, many engine numerical analysis codes with various sophisticated models have been developed and some of them have already been tried in industry [106]~[108]. The on-coming low cost, powerful workstations and personal computers further encouraged these computational activities. Among the numerical analysis tools, the CFD technique, which is trying to cover the majority of the existing engine performance and emissions simulation models, is becoming popular in engine research activities. The CFD analysis is to exert the same influence on engine research and development as have the other CAE methods.

1.2.2.1 Computational fluid dynamics

Generally, CFD is a technique which concerns the mathematical representation of fluid transportation processes and the numerical solution of the governing equations for different categories of fluid dynamics. For Newtonian fluid, the widely used fluid dynamics description at present is the unsteady Navier-Stokes (the N-S) equations, which have been known for more than a century. They are given in Appendix II together with those equations involved in the case of thermally driven flows and/or the flows driven by species concentration differences. The N-S equations are generally considered

to govern both laminar flow and turbulent flow. However these partial differential equations are so complicated that an exact analytical solution is unavailable. With the development of numerical methods and the improvement of computer technology, the differential equations can be replaced with systems of algebraic equations which can be numerically solved by using computers. The obtaining and solving of the algebraic equations is one of the main interests for the CFD developers. For Non-Newtonian fluid, the mathematical description of the flow behaviour is at a less advanced stage and is still an active research area in the CFD community as is the turbulence representation and the description of chemically reacting flows and two-phase flows for either kind of fluids.

The CFD technique has spanned a wide spectrum of engineering applications including aerodynamic and aeronautical, automotive, mechanical, civil, nuclear, chemical, medical, meteorological, biological engineering [109]~[112]. It emerges as a new tool with which to enhance and partially offset the need for experiments in many fundamental and practical flow behaviour investigations, especially in the case where the experimental methods are restricted or prohibited by financial, technological or environmental difficulties. For example, during aircraft design full scale measurement of the fluid dynamics characteristics using a wind tunnel is economically unavailable. In this case the CFD analysis supported by some model experimental work will be very effective in the early elimination of competing design configurations and will therefore significantly reduce the cost and lead time in design and development while giving detailed information throughout the region which would be prohibitively expensive if only experimental methods were used. There are many other cases such as the heat and coolant flow studies in nuclear stations, geophysical fluid dynamic studies for oil exploration and astrophysical fluid dynamic studies for weather pattern prediction where it is too dangerous for the intrusive experimental work to be conducted or too remote in time and space for the problems to be simulated experimentally. Thus it is necessary to resort to the CFD technique to make realistic studies on the flow behaviours of interest.

1.2.2.2 Applications of the CFD technique to engines

With the rapid development of powerful computers, numerical simulations of complex flow problems like the flow in internal combustion engines have become feasible and affordable. The research work carried out both experimentally and theoretically on transport phenomena studies including unsteady turbulent flow, fuel air mixing, combustion, emissions formation and heat transfer in engines and in the related thermofluid sector had laid down a sound foundation for the fluid dynamic computation. Therefore several attempts have been made to apply the CFD analysis to engines. The requirement of better understanding of the complex engine processes, driven by the

more and more stringent emissions standards, will speed up this trend because the processes such as the induction, mixture preparation, ignition, combustion, emissions formation and after treatment, cooling and heat transfer are all linked to the 3-dimensional flow behaviour which is the original concern of the CFD technique.

Presently there are a few sophisticated CFD codes such as the KIVA, PHOENICS, STAR, SPPED and FIRE specifically developed or tailored for engine applications. They have been tested by engine researchers and manufacturers for various purposes. The application cases of these general purpose CFD codes to engines will be examined below in order to assess the capability of the technique and its current use in the engine community.

1.2.2.2.1 CFD applications to natural gas engines

In order to assess the capability of the CFD analysis in assisting engine development, Johns, R. J. R. and Jones, P. M. [113] initiated an investigation into the application of CFD to the flow and mixing in the pre-chamber of a lean burn natural gas engine. The geometric model created in the calculations is given in Figure 1.7. The model included the spark plug central electrode and the gap between the electrode and the main body. The turbulence effect was incorporated via the k-ε model. The friction and heat transfer were allowed for at the surface through the boundary setting. Initial conditions of pressure, temperature and composition in both the pre-chamber and main chamber were determined from a filling-emptying cycle simulation and were imposed at BDC because only the compression stroke was considered in the study. Spatial uniformity was assumed within each chamber at the beginning. The velocity field and air fuel ratio distributions within the pre-chamber at different crank angle from BDC to TDC were obtained for different initial main chamber air fuel ratios. The calculations helped to clarify a number of phenomena observed during the experiments previously carried out and gave a better understanding of the fluid dynamics and associated mixing in this type of engine. A comparison with the measured ignition limits was made and the result was encouraging. It was concluded through the study that CFD can provide valuable guidance to designers and developers.

To design the combustion system of a single cylinder lean burn natural gas engine, Moore, D. S. carried out an investigation into the parameters which affect the mixture formation and distribution in the pre-chamber of the engine [34]. In parallel with the experimental study, CFD modelling was applied for the simulation of mixture formation in the pre-chamber. The effects of pre-chamber volume, pilot mixture ratio, pilot gas supply pressure and inlet manifold pressure on the mixture formation were studied by using the early version of the PHOENICS package. Although there was no relevant

experimental data to validate the computational results, the prediction attempt provided a valuable insight into the mixing process and guided the combustion system design. Based on this preliminary computation, Jager, D. J. and Charlton, S. J. [32] [33] conducted a further investigation into the mixture preparation in the pre-chamber of a natural gas engine using both experimental and computational approaches. The STAR-CD code was used in their computational study. The pre-chamber of the engine was modelled by using a 10 degree single layer axisymmetric model having 400 cells. The mixture distributions during the compression stroke at positions around the pre-chamber perimeter, which was vitally important to the success of this type of lean burn combustion system particularly in the region of the spark plug, was simulated, see Figure 1.8. The effects of changing the concentration of the mixture supplied to the chamber and increased nozzle size were also investigated. Comparisons between the CFD modelling and experimental results of the mixture concentration distributions were also made. The study showed that a reasonable agreement had been obtained. It was demonstrated through the comparative study that much detailed information could be gained from the CFD results in addition to the cost benefit.

A similar kind of CFD simulation work was also conducted by Chmela, F. G. and Kapus, P. [29] [44] using the FIRE code developed at AVL LIST GmbH Graz, Austria. Instead of the pre-chamber, it was an open combustion chamber for which the simulation was performed. With the aid of the CFD work, the flow patterns and turbulence distributions within the combustion chamber of a lean burn natural gas engine were better understood, which was extremely helpful in due course for the combustion chamber configuration development. The comparison of flow patterns and turbulence distributions between the conventional chamber and the CFD optimised symmetric one showed that high turbulence was generated around the initial flame kernel, unlike the eccentric hemisphere conventional chamber, without having excessive flow velocities at the spark location, see Figure 1.9. These features were essential for low ignition energy, short and safe ignition, fast and stable flame propagation. The results were verified on a test engine in terms of engine heat release rate with different combustion chambers, which showed that the CFD optimised chamber displayed a very stable and short ignition delay in combination with the shortest duration of combustion.

Another application attempt was made by Mendonca, F. G. and Bretton, A. S. [114] using the PHOENICS code to simulate the fuel mixing process in a Ruston RK 270 natural gas engine during the non-combustion part of the four stroke cycle commencing as the inlet valves open and ending at compression TDC, advancing with 5 degree crank angle equivalent time steps. A three dimensional curvilinear mesh was used which comprised 52×32×19 cells in the circumferential, axial and radial directions, respectively. The grid refinement studies were performed to ensure that the mesh

created was suitable enough to represent the geometry of the pre-chamber, piston and valves, and to capture the main flow features. The slided mesh with regeneration and removement was used to model the transient motion of the piston and inlet valves. Initial conditions were derived from a set of separate quasi-steady state calculations based on the measured steady state inlet mass flow data and modelled direct pre-chamber fuel injection. Comparison of the CFD predictions with the measured hydrocarbon concentration at two measurement points using a sampling probe [48] was made and a qualitative agreement was achieved. The discrepancy meant that a more accurate inlet boundary conditions was needed. The comparison of the predicted and the measured average cylinder pressure changes with crank angles was very encouraging.

To assist natural gas direct injection development, Zhang, J., et al. [86], Jennings, M. J. and Jeske, F. R., [84] [85] applied CFD analysis to the modelling of the turbulent fluid flow within gas injectors under different operating conditions. Zhang, J. and his colleagues examined the impact of the injector exit boundary conditions such as the velocity and temperature profiles on the modelling of direct injected natural gas engines based on their 2-D finite volume CFD code. Jennings, M. J. and Jeske, F. R. [84] [85] investigated the dynamics of the natural gas plume and its interaction with the combustion chamber surface. The effect of key engine design parameters such as the injector configurations on the dynamics and the resulting fuel air mixing were studied. Their computation model comprised of 80 cells in the axial direction and 50 cells in the radial direction. Stretching of the grid was applied in the computation. The natural gas fuel was treated as pure methane. The pressure ratio across the injector was assumed to be the critical ratio. The temperature of the natural gas in the injector was assumed as 350 K and the temperature at the nozzle exit was computed by assuming an isentropic expansion of the gas to the critical pressure. Because the grid resolution across the nozzle was not high enough to capture secondary effects of non-uniform velocity profile, the jet velocity profile at the nozzle exit was assumed to be uniform, which was strongly disputed by Zhang, J., et al. [86]. At the first stage, a single hole nozzle was studied and the injection characteristics were investigated. Then a parametric study was made on the number of holes, the size of the holes, the angle of the nozzle and the height of the nozzle tip. Finally an optimised combustion chamber geometry was designed by fitting the geometry to the computed plume shape.

1.2.2.2.2 CFD applications to diesel engines

In diesel engines, the combustion chamber design is a fundamental factor for the engine performance and emissions. Due to more and more stringent emissions standards, there is an increasing requirement for a better understanding of the processes within the combustion chamber and cylinder. This encouraged a number of CFD applications

concerning flow behaviour and chemical reactions in diesel engines. In support of the experimental investigations, researchers at Ricardo [115] applied the CFD analysis to model in-cylinder events of air motion and fuel spray in a Ricardo 4-valve high speed direct injection diesel engine at engine peak torque and rated power operating conditions. The interactions of air motion and fuel spray/vapour was better understood, which appeared to be very important to the development of future ultra low emissions and high performance diesel engines. The successful simulation encouraged them to examine the effect of the combustion chamber geometry on the interactions by using CFD in their on-going research project.

Somerville, B. J., et al. [116] [117] applied the STAR-CD code to examine the effect of the engine speed and the effect of the engine glow-plug locations on swirl and turbulence in the combustion chamber of a small passenger car IDI diesel engine during the engine compression and part of the expansion stroke. Three models of identical geometry with different numbers of mesh were generated using PATRAN in order to test the sensitivity of the mesh density to the computation results. Two differencing schemes were also tested to examine their effect on the predicted velocity and turbulence. The test results showed that the solution was mesh dependent for the variables of interest. The finer meshes better resolved the flow. For a given mesh, the Filtered Central Differencing Scheme predicted significantly higher velocity, swirl and turbulence levels than that of the standard Upwind Scheme. The underpredicted variables of interest were attributed to inexact representation of the turbulence model. After the validating tests, the effect of design changes on the engine performance was investigated and the results from the numerical model were compared with data taken from engine performance testing.

A similar CFD study was also conducted by other researchers [107] [108] on flow behaviours in IDI diesel engine combustion chambers but with the addition of the combustion process simulations by using the SPEED code. The results indicated that the influence of the geometry of the piston recess, the connecting passage between the two chambers, the positions and dimensions of the glow-plug on the flow field in the pre-chamber could be characterised during the compression process, but the simulation of the injection and combustion processes needed to be further exploited through modelling improvement.

To improve the combustion process in diesel engines, people have tried a number of means to generate swirl by using specifically designed intake ports or valves. A correctly directed air motion can enhance pre-ignition turbulence and increase the flame propagation speed. To match the swirl level to its combustion chamber, Seeley, W. A. and his co-workers in Coventry University [118] applied the CFD analysis in parallel to

a steady state flow rig test using both Laser Doppler Anemometry (LDA) and hot wire anemometry (HWA). Meshes consisted of 70,000 and 200,000 cells were used in order to obtain a mesh independent solution. Inlet and outlet boundary specifications were used with the three inlet velocity components specified based on HWA measurement. Combinations of different differencing schemes and turbulence models were tested. The results were compared with the experimental data obtained from LDA measurement. Of the combinations tested, the Self Filtered Central Differencing Scheme with the RNG k-ε model produced the best agreement for the axial velocity profile but none of the combinations could give an acceptable swirl velocity correlation between the experimental data and the CFD predicted values. Nevertheless, the general form of the flow was characterised by the detailed prediction results.

In order to reduce the engine inlet ports design and development time, Jaguar launched an investigation on the integration of CFD into their engine design process [119] [120]. Due to the length of time needed to build the complex model of flow domain, it became critical to reduce the model building time drastically in order that the CFD technique was able to be incorporated into engine process. To reduce the elapsed time on modelling, a CAD modellar was used to create geometrical data. The CAD data were then transferred into an International Graphics Exchange Standard (IGES) file via the I-DEAS (Integrated Design and Analysis System) modelling system. Because the CAD model had problems of mesh surface overlap, discontinuity and convention mismatch, the IGES file had to be modified and a basic solid description of the geometry of the flow domain was then read by the CFD package used. During the converting process, not only the geometry of the flow domain, but also the mesh and its shapes had been converted. With the model created, calculations were made with the standard two-equation turbulence model for an inlet flow speed of 19.7 m/s. To enable the calculation to proceed smoothly only the velocity and pressure were calculated initially, then the turbulence quantities were calculated and finally the density solver was activated. The simulation results were compared to data obtained from a parallel project conducted in Imperial College by using Laser Doppler Velocimetry. The comparison showed various degrees of agreement from place to place of the flow domain. In the middle of the cylinder, both means sensored the existence of the double vortex structure. Despite the errors from the mesh quality, geometric resolution and turbulence modelling, the research work exhibited the potential for using the CFD technique in the design process of the engine inlet port as part of CAE environment.

Based on intensive experimental and theoretical research, mathematical models describing the injection, mixing between fuel spray and air, ignition, combustion and emissions formation processes of diesel engines have been implemented into some of the CFD packages. To model the diesel engine combustion and emissions formation

processes, researchers [121] used the KIVA-II code, developed by Amsden, et al. at Los Alamos National Laboratory for 2-D or 3-D unsteady flow with or without chemical reactions of ideal gas mixtures, to study the combustion and NO emission in a Ricardo Hydra direct injection diesel engine. Two combustion models were used and compared. One was the standard chemical kinetics based on the single reaction Arrhenius model (SR model) without considering the effect of turbulence on combustion, which was suitable for premixed combustion systems such as spark ignition engines. The other was the eddy break up model (EBU model) of Magnussen accounting the effect of turbulence on the mean chemical reaction rates through the presentation of the diffusion combustion process. The values of the Arrhenius coefficient and the activation temperature were adjusted in the SR model to achieve a good agreement between the computational and experimental results. Both models resulted in a reasonable agreement with the engine experimental data using hexadecane and dodecane as fuels under varying engine operating conditions. The EBU model produced a slower combustion rate than the SR model, resulting in a lower gas temperature and NO emission. The emission result from the SR model showed a better agreement with the test data when the Arrhenius coefficient, A_f=9.0×E+10 and the activation temperature, E_f=1.5×E+4 K were selected.

The KIVA-II code was also used by Dillies, B. and his co-workers for diesel engine combustion modelling [122]. Unlike in pre-mixed spark ignition engines, the formation and evolution of spray droplets, the mixing of fuel and air, the auto-ignition of the mixture, and the propagation of the flame have all to be modelled in order to simulate the combustion process properly in diesel engines. The mixture formation process was modelled by the Taylor analogy break-up (TAB) model, and the ignition process by a four-step reaction Arrhenius ignition model which was constructed by applying Arrhenius law exponents to fit the experiment data obtained. After the ignition, a turbulent combustion flamelet model which not only considered the mixing and diffusion controlled turbulent combustion, as the Magnussen model does, but also accounted for the partially premixed combustion in the early stages of turbulent combustion. This approach was based on the hypothesis that the chemical reaction times were much shorter than the characteristic time scale of the turbulence. The coherent flame model replaced the original Arrhenius combustion model in the KIVA-II, and the simulation results were compared to experimental data available from a Cummins optically accessible DI diesel engine. In terms of the cylinder pressure and heat release rate, the comparison showed a good agreement between the experimental and computational results provided that adequate information about the injection conditions was specified to the spray models.

In order to obtain a better spray simulation, Liu, A. B. and his colleagues proposed a new fuel drop drag and break-up submodel for the KIVA-II code based on experimentally measured trajectories and sizes of single drops injected into a high relative velocity gas flow [123]. Computation results on using the new submodel and those on using two other popular models were all compared to the measured data. With respect to the drop trajectories prediction, all models gave a good agreement with the measurements but not to the break-up process. Robinson, et al. [124] modified the initialisation routines and combustion sub-model of the KIVA-II code to enable the code to be capable of modelling the asymmetric, fully three-dimensional pentroof chamber geometry and taking account of turbulent mixing. Ignition was simulated by increasing the internal energy of the cells corresponding to the spark plug electrode. The Arrhenius coefficient, A_f and the activation temperature, E_f in the rate of fuel consumption model were obtained empirically. The computation results were validated against data obtained from a parallel experimental study using through piston double exposure photography and an acceptable agreement was achieved. As encountered by other users [125], the quantitative improvement of the turbulence treatment which linked to several transport phenomena was needed in order to obtain more accurate simulation results. An attempt on the model modifications had been made by Amato, U., et al. [126] on the turbulence and spray submodels backed by experimental studies. But the comparison showed that the models still could not give satisfactory results.

1.2.2.2.3 CFD applications to two stroke engines

In two stroke cylinder port type engines, fresh charge loss during scavenging will reduce charging efficiency for direct in-cylinder fuel injection, and increase fuel consumption and HC emission for engines with a premixed fuel supply system. It is very important for the two stroke cycle engines to have well designed scavenging and exhaust systems which lead to minimum fresh charge loss during the gas exchanging process. Due to the complexity of the exchanging process, the CFD simulation was resorted to by many researchers in addition to experimental studies [127] [128]. Their experience showed that CFD analysis could correctly identify the main features of the gas exchanging process and guide the related systems design irrespective of the fuel used and the scavenging format. However it was found to be difficult to predict the absolute level of such parameters as the scavenging efficiency and turbulence. Advanced models representing the inter-linked unsteady gas exchanging process are still required.

There is another type of two stroke engine in which the gas exchange system uses a valve mechanism. Due to its lower specific weight and volume, better fuel economy, smoother operation and better commonalty to existing four stroke engines, this type of

direct injection overhead valve two stroke engine has recently received a renewed interest in the automotive industry. To simulate the flow field within the cylinder with varying intake valve orientations, a modified version of the KIVA-II code was applied to simulate the scavenging flow in a four-poppet-valve type engine intake system [129]. Compared to the experimental data, the simulation produced qualitatively correct results for the velocity field, turbulence kinetic energy and fresh air mass fraction distribution in the cylinder. Parametric studies showed that the intake port orientation did not have much effect on the scavenging efficiency due to the strong flow diversion caused by the valves.

1.2.2.2.4 CFD applications to catalyst converters and blow-by flows

With the advent of increased exhaust emissions controls, catalyst converters have become widely used in engines fuelled with both conventional fuels and natural gas. The flow field within the converter monolith effects the temperature distribution and consequently the chemical kinetic reaction and the thermal stress distribution. An uneven temperature distribution can result in the monolith cracking and the catalyst ageing. It is generally accepted that a uniform mass flow (or velocity) distribution of the exhaust gas over the catalyst is necessary to obtain a satisfactory emissions conversion efficiency and catalyst life time. For a certain conversion efficiency required, a shorter catalyst length can be used if the exhaust gas is uniformly spread over the converter, which will result in lower cost and lower back pressures. In order to achieve uniform velocity distributions without using long narrow angled diffusers, the CFD technique was resorted to by several companies and institutions involved with catalyst design.

Baxendale, A. J. [130] applied the CFD technique to the calculation of the distribution of exhaust gas within the monolith of two different designs of catalytic converters, see Figure 1.10. The mesh was generated by using I-DEAS^{TM} and PATRAN^{TM}. The standard k-ε turbulence model was used and steady state incompressible calculations were performed by using the STAR-CD code. Calculations were performed for each port open in turn at an inlet condition corresponding to a 1.4 litre engine at the peak exhaust mass flow rate of 0.09 kg/s with a temperature of 850 °C and density of 0.4453 kg/m^3. To represent the catalyst monolith approximately the porous media facility embedded in the code was evoked. The experimentally correlated velocity-pressure drop through the monolith was used to define the resistance field in the flow direction and a very large value was assumed in the cross stream direction to represent the physical constraint to the flow. Based on the calculated velocity distributions within the monoliths and pressure drops across the systems, the two alternative designs were

assessed. Clarkson, R. J. and his co-workers [131] also applied the STAR-CD code to investigate the detailed steady flow fields in a catalytic converter assembly. Four turbulence models and two differencing schemes were tested to test the sensitivity of the predictions to the changes. A known uniform inlet flow field was specified for the boundary condition setting. The predicted velocity profiles and pressure drops across the assembly were compared to the experimental results. Though the RNG two-layer turbulence model and the hybrid differencing scheme could give an improved prediction, there was still considerable difference between the predicted results and the experimental data. It was identified that the weakness in the existing turbulence models and in the catalyst pressure drop representation were the likely causes for the discrepancies. Although transient calculations involving flow and chemical kinetics at an exact converter monolith geometrical representation (about a order of 10^7 cells) were not realistic, Baxendale, A. J. claimed that useful design data for different designs and design changes could be obtained at the present time without waiting for the models to be numerically perfect [130].

Apart from the CFD simulations of the flow behaviour in the engine intake manifold, inlet port, combustion chamber, cylinder, exhaust port and the catalytic converter, the technique was also applied to some of the other engine flow processes. Due to the fact that a portion of the engine HC emissions originates from the mixture entering piston-cylinder-ring crevices during the compression stroke, an investigation into the amount of the mass flow and its contribution to the HC emissions was conducted by Shih, L. K. and Assanis, D. N. [132]. A ring motion model which described the piston ring dynamics was created and implemented into KIVA-II for the prediction of trapped cylinder mass and pressure (the closed part of the cycle) together with the crevice flow model which described the flow motions through the ring-side clearances and through the ring gaps developed by Namazian and Heywood. They applied this modified KIVA-II and baseline code to a 2.5 litre petrol engine to investigate the effects of the engine speed and selected piston-cylinder-ring design parameters on the crevice flows and their contribution to HC emissions. The prediction was verified with the tested results. The study revealed that the peak cylinder pressure predicted with and without activation of the sub-models was 5% different, because the amount of the fresh charge blowby (about 0.58% of the cylinder charge) was not counted in the baseline code. The contribution of crevice flows on unburned HC emissions was reduced at higher speeds because there was a larger fraction of the HC vapour returned from the crevice during the expansion stroke which was oxidised. The increase of piston-cylinder side clearance would increase the blowby and dramatically reduce the cylinder peak pressure.

To sum up the applications of the CFD technique in engines research activities, the following framework can be constructed. With the evolution of computers and numerical methods, the CFD technique has become more and more acceptable to engineers for flow behaviour examination. The intensive experimental and theoretical research on thermofluid behaviour are producing more sophisticated but realistic models to describe the physical phenomena encountered in engineering. There have been some applications of the CFD analysis to engines fuelled with natural gas and conventional fuels. For the natural gas engines, the CFD simulations were focused on the flow behaviour and the mixture formation within the pre-chamber or the open chamber irrespective of the types of mixture preparation systems used. For diesel and petrol engines, applications were mainly centred at the swirl and turbulence arrangement in IDI or DI four stroke cycle diesel engines and at the scavenging system arrangement in two stroke engines. The simulation of the intake process, fuel spray process, combustion process and the emissions formation process were also attempted by a number of CFD developers and package users. Some of the simulations were compared with relevant experimental data and the agreements were reasonably acceptable with respect to some of the variables. All of these CFD applications showed that the CFD technique was capable of being used as an analysis tool in current mixture preparation studies. Due to the complexity of the mixing problems of concern, however, it is very difficult for any of the existing CFD codes to simulate quantitatively the process with a high accuracy. At the present time, an effective remedial method is to validate the computational results by using relevant experimental data. Such validation will give users more confidence in the appropriate applications of the packages in matters such as boundary conditions specification and models selection.

The CFD technique has been developed to such a stage that the relative evaluation of the superiority or inferiority of the flow behaviour related engine component design proposals can be reliably made by experienced users who understand both the technique and the physical phenomena investigated. It can be used as a complementary tool to costly and time consuming experimental testing in some of the engine component design and research activities. It is only through consideration of individual applications where the CFD model is compared with experimental results, that the weakness of the numerical solutions embedded in existing CFD packages can be exposed and the solutions improved. The more accurate simulations will inevitably lead to a better understanding on the complex engine processes and ultimately give more confidence in the design procedure compared to empirical approach alone. It can be foreseen that the joint effort made by the CFD developers and engine practitioners will promote more user friendly and CAE applicable CFD packages to a level where the CFD analysis is one of the main tools to the engineers engaged in engine design and development.

1.3 The scope and contents of this thesis

The first step of the study was focused on the examination of the mixing mechanism in a venturi type mixer. The CFD technique was used as one of the main tools after being validated through various means. The CFD package used and its validations will be discussed in the second chapter of the thesis.

The simulations of the flow behaviour and the mixture formation in the novel venturi mixer will be reported in the third chapter. The simulation results visualised the flow pattern and the mixture distribution within the entire gas-air mixer flow domain, which revealed the relationship between the flow pattern and the mixture strength distribution in the mixing unit of interest and pinpointed the factors that govern the mixture preparation quality. With the better understanding of the flow phenomena occurring inside the mixer, the effects of design parameters on mixture formation were computationally examined. Sensitivity tests on some of the computation boundary specifications were also conducted.

Aware of the fact that the CFD technique was a relatively young discipline. Many aspects such as the turbulence models and the methodology of decoupling the pressure term from the continuity equations were still in the development stage. Reasonable cautions were exercised on the CFD results in the variables which had not been validated. To prove the computational results and to compare the mixer performance between the newly design venturi mixer and the three proprietary mixers, experimental studies were carried out. These will be described in chapter four. To measure the mixture concentration distribution out of each of the mixers tested, a novel flame ionisation detector technique was used. The technique and its applications to engines will also be described in the chapter. Further validations on the predictive results and the findings and the comparisons of different mixers will then be presented.

After the mixers performance comparison, attention was then moved to the effects of the mixture prepared on engine performance and emissions. Chapter five will report the engine performance and emissions results with each of the mixers installed on a natural gas engine test rig in turn. The mixture formation within the whole intake system will then be discussed in chapter six. Finally, more design concepts evaluation work and CFD aided mixer scaling-up design for engines with different engine power outputs will be presented in chapter seven together with more findings about the venturi type mixers. At the end of the thesis, conclusions drawn from the study will be given and recommendations for future work will be suggested.

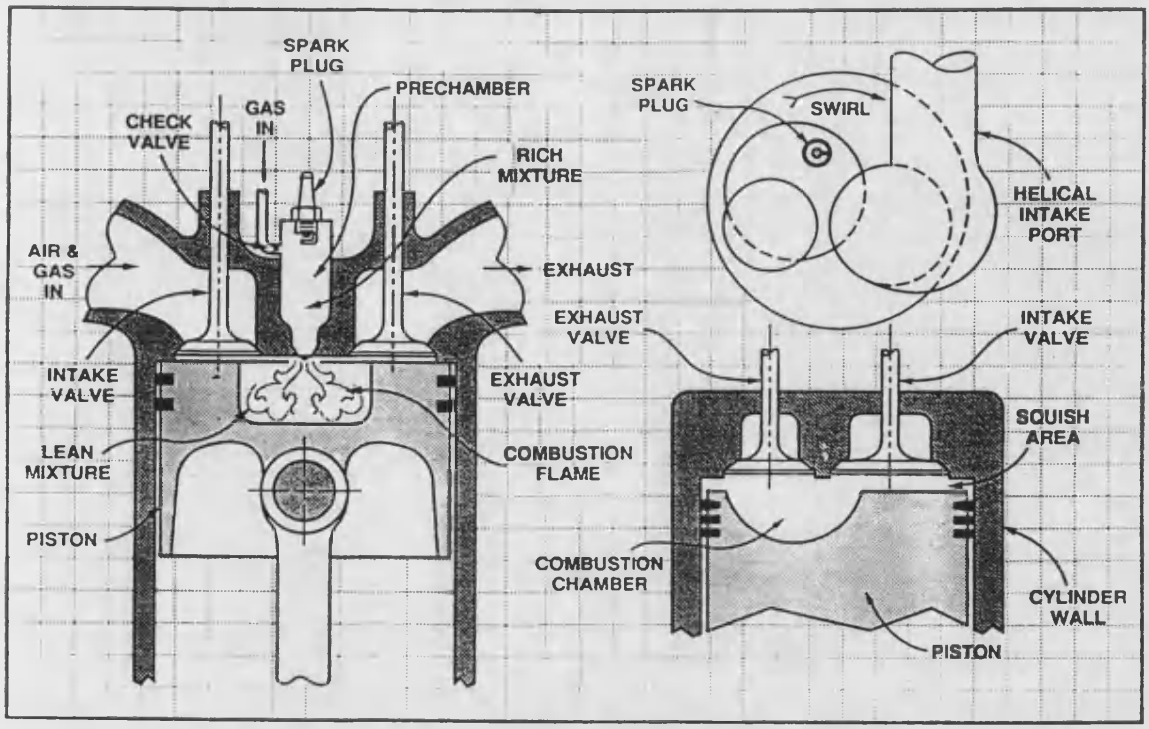

a) Pre-combustion chamber b) Open chamber

Figure 1.1 Typical lean burn combustion systems [28]

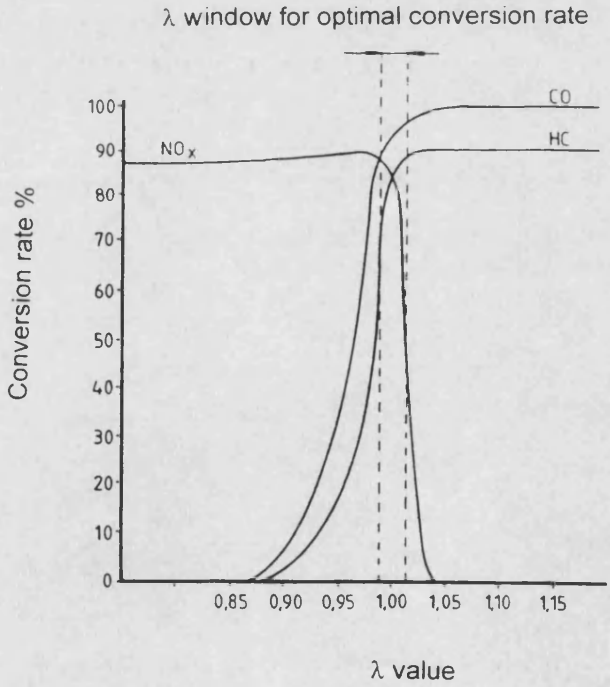

Figure 1.2 λ window for optimal catalyst conversion rate [53]

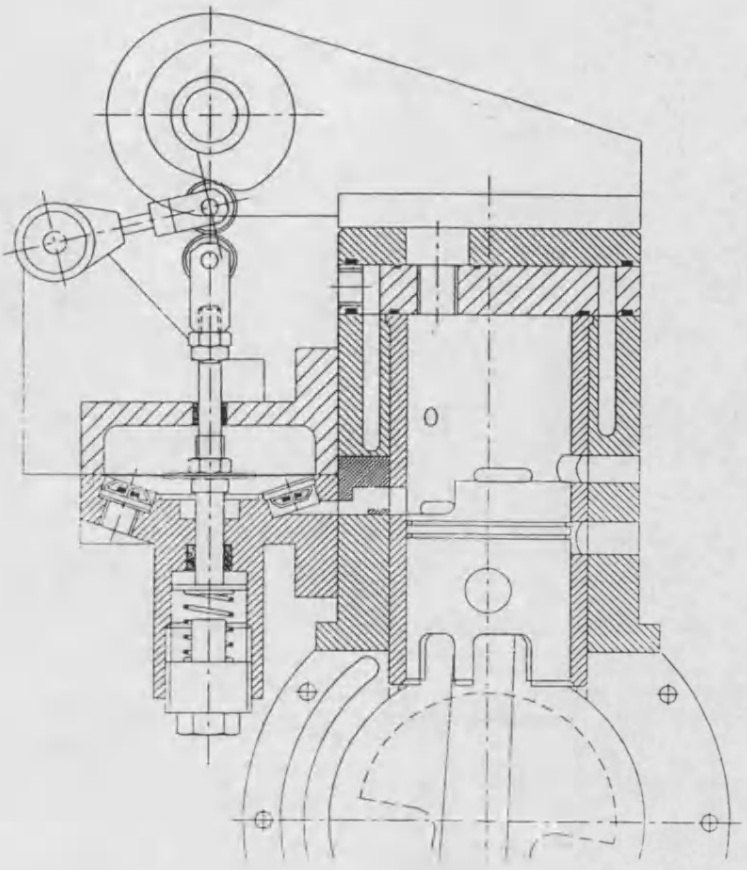

Figure 1.3 Diaphragm type natural gas injector schematic [21]

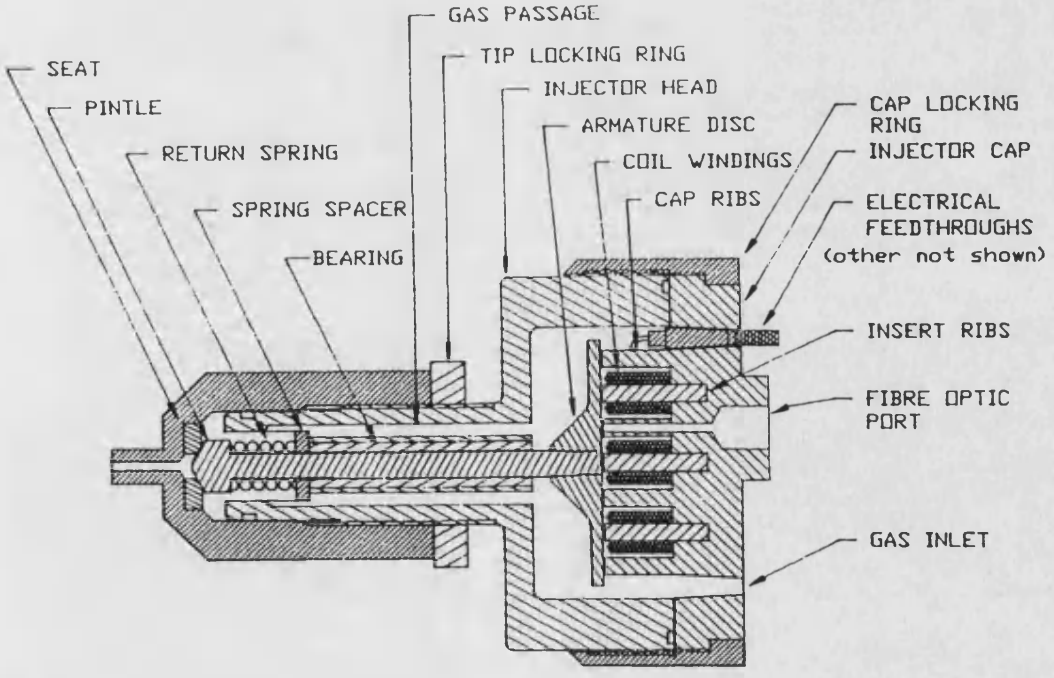

Figure 1.4 Solenoid type natural gas injector schematic [68]

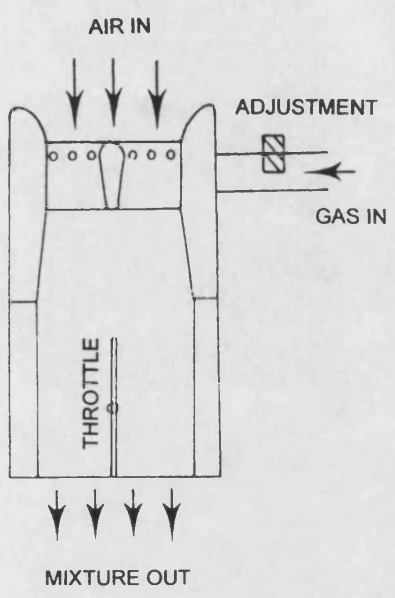

a) The venturi carburettor

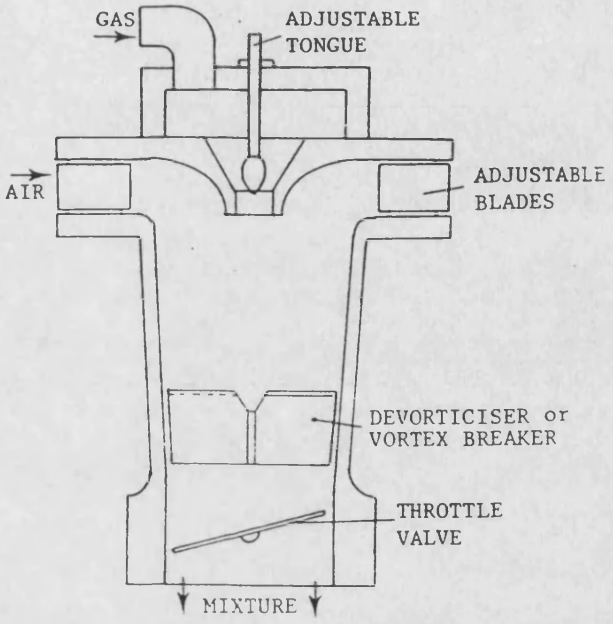

b) The vortex carburettor

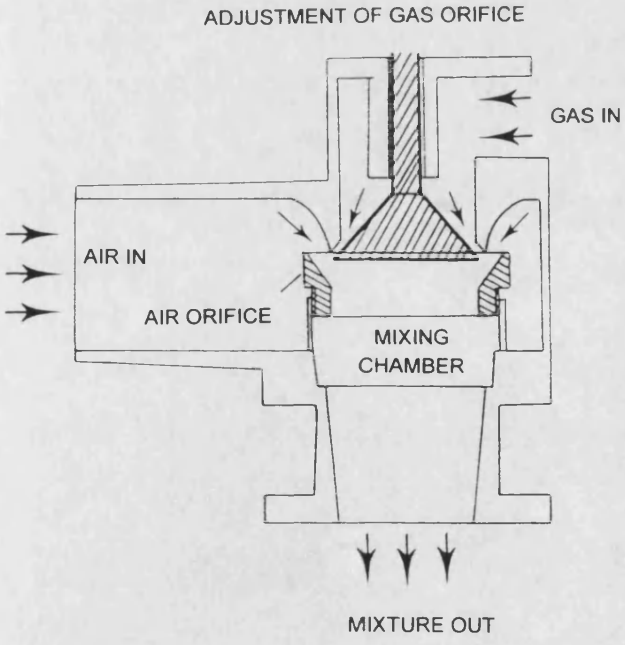

c) The orifice carburettor

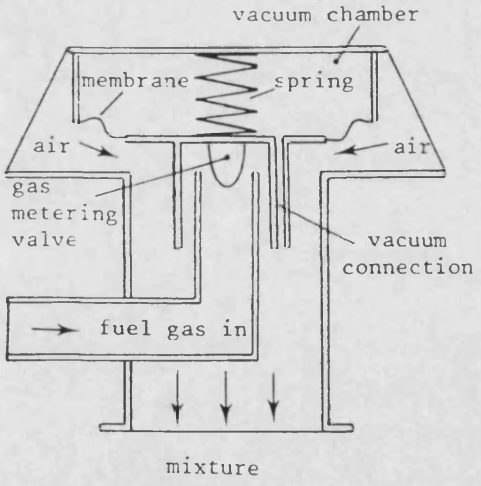

d) The variable restriction carburettor

Figure 1.5 Typical natural gas carburettors schematic [87]

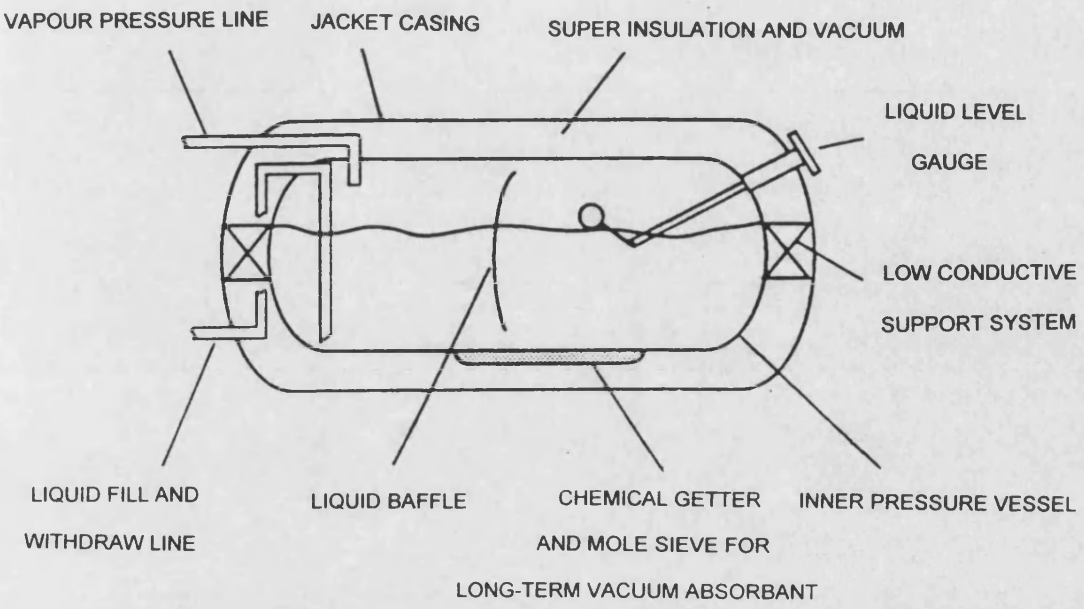

Figure 1.6 Liquefied natural gas storage container schematic [101]

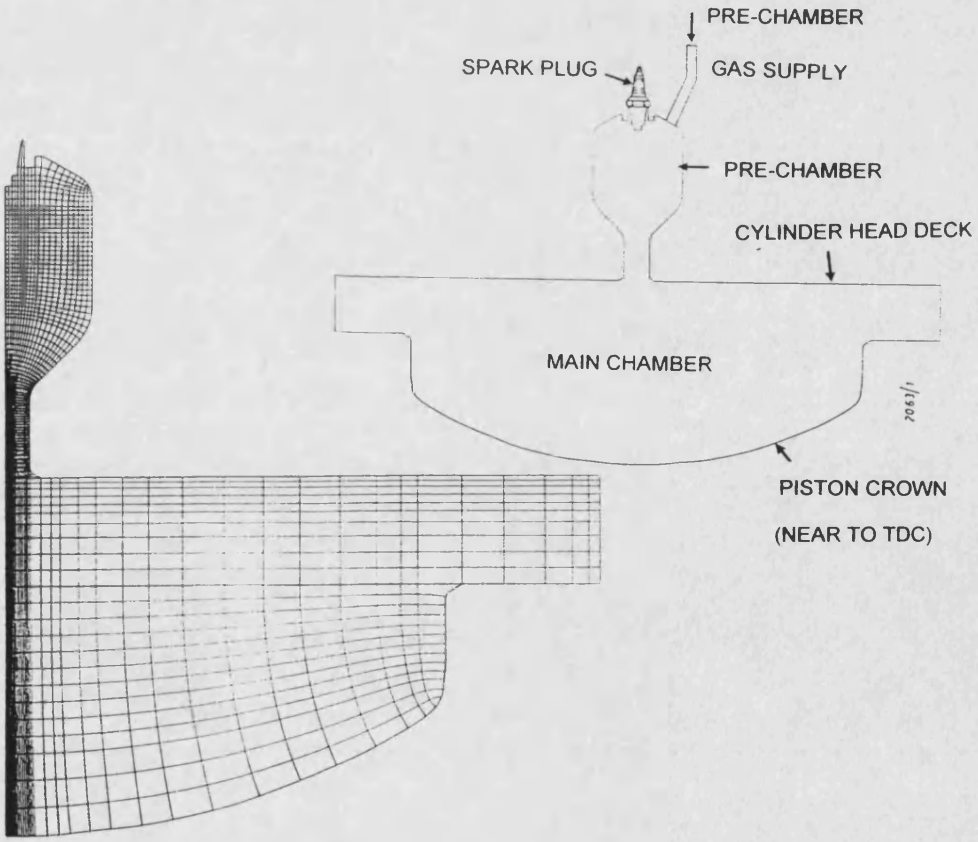

Figure 1.7 Pre-chamber configuration and its CFD mesh [113]

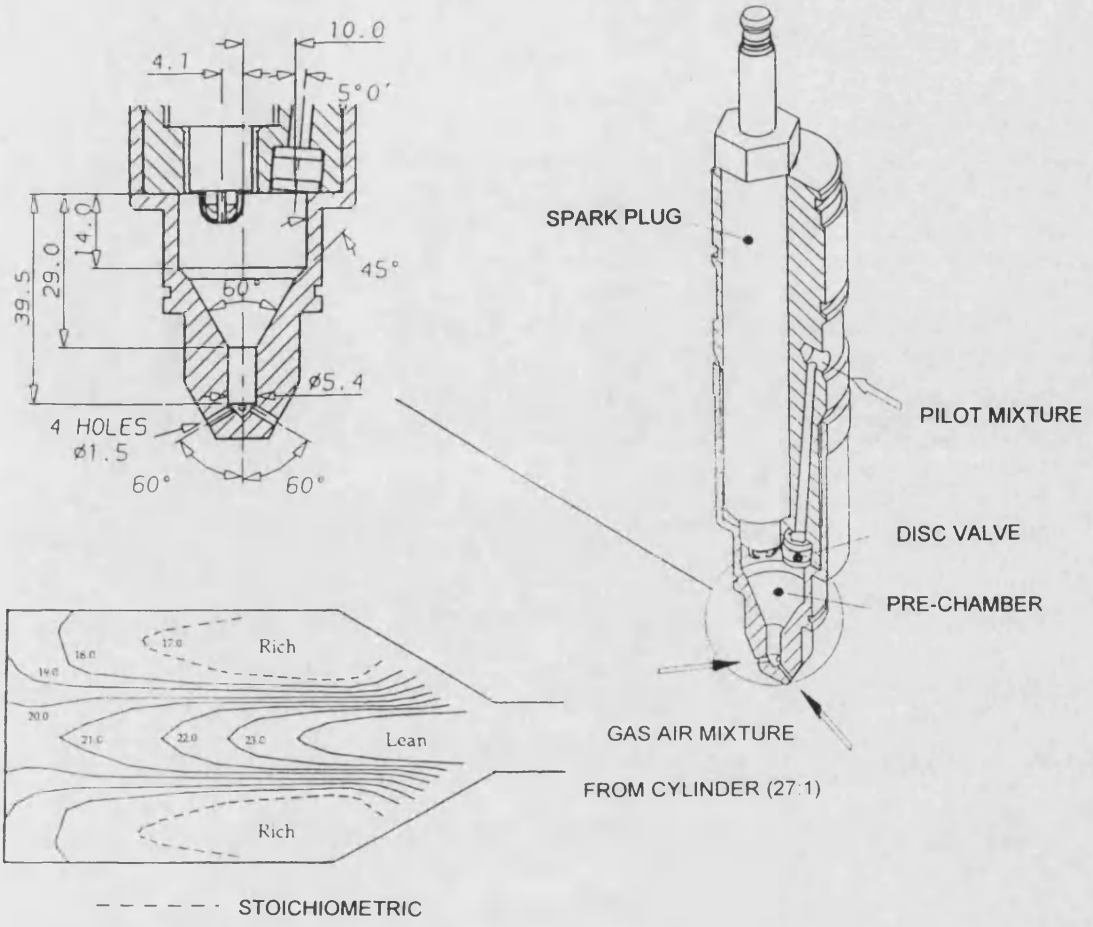

Figure 1.8 Pre-chamber detail and CFD predicted mixture distributions [32]

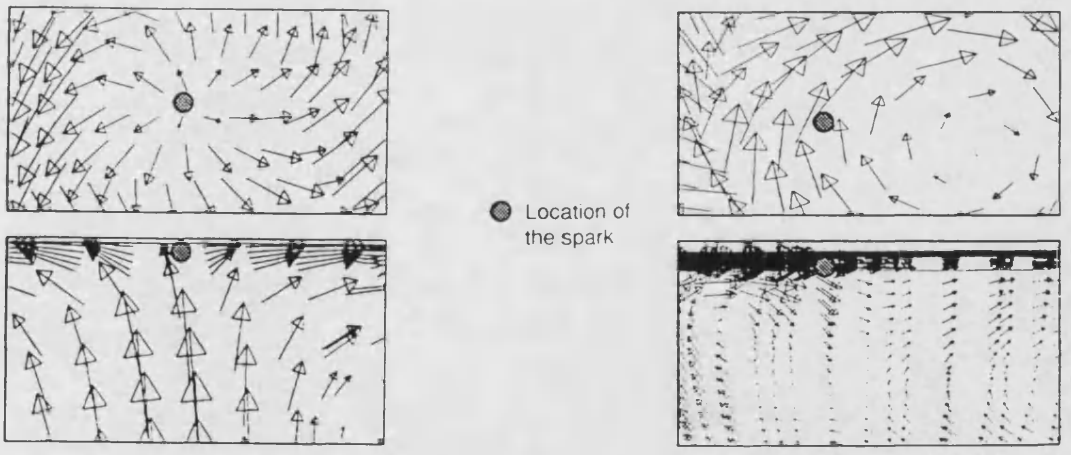

a) CFD optimised chamber b) Conventional chamber

Figure 1.9 Predicted in-cylinder gas flow with different combustion chambers [44]

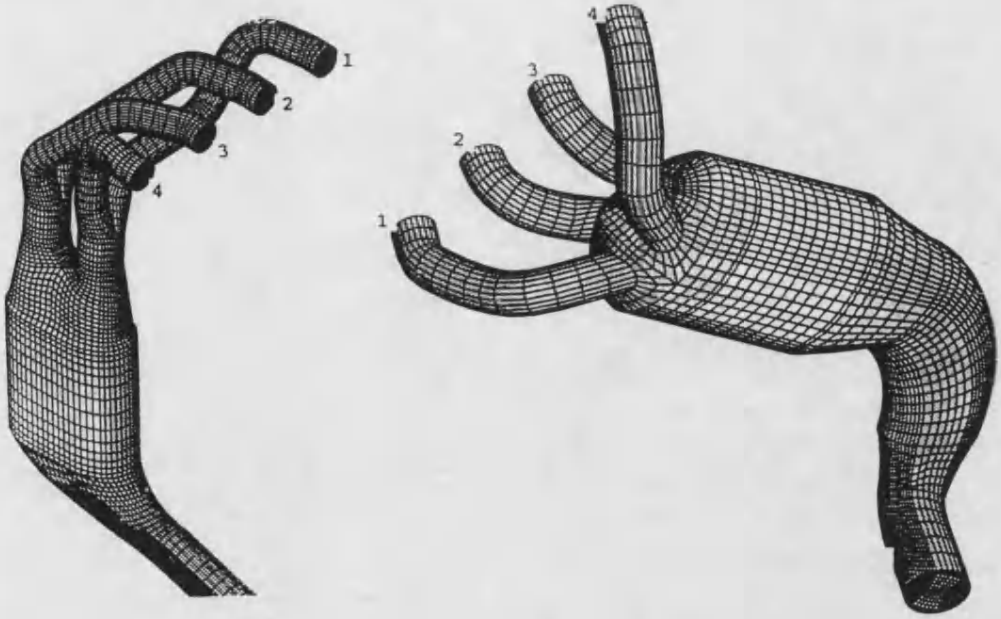

Figure 1.10 CFD models of different catalyst converter designs [130]

2 Description of STAR-CD code and its validations

2.1 Introduction

As has been discussed in the previous chapter, the CFD technique is becoming more and more acceptable in the prediction of flow behaviour in engineering systems. The mixture preparation system in natural gas engines operates on the principles of fluid dynamics and turbulent mass transportation between two species. This feature makes it possible for investigations into the mixture preparation in a natural gas engine to be conducted through either an experimental or a computational approach. The latter one often provides valuable insight into the flow phenomena without distorting the flow field and gives better understanding of the effects of design parameters on the mixture formation with low cost in terms of time, money and human resources. A computational approach at the initial stage of a novel design is a very effective way to proceed if no experimental data are available.

Presently, whether a CFD analysis result can be achieved for a specific problem and what kind of result it will be if it has been obtained all depends on the user. It is still a subjective aspect of the CFD technique and is independent of the package used. For the same problem and using the same package, it is quite possible that different users may obtain different answers [133]. Actually with the same nominal flow conditions, there may be several different steady state flow patterns. Due to the complexity of the fluid dynamics itself and the immaturity of CFD modelling, validation of the CFD package for a particular application is very important if the computational results are to be used with confidence [133] [134]. Models developed by researchers may have been validated on certain problems within their parameter ranges. CFD developers often verify their software to demonstrate that their codes correctly represent the mathematical models used and are bug-free and reliable for the problems within the capability of the codes. The majority of CFD programmes in existence have evolved from different origins each being designed to solve a particular physical phenomena. It is not realistic for the model researchers and CFD developers to validate the package on every physical problem encountered in engineering. Thus it is up to each of the individual users to acquire the necessary experience from applications of the package to certain experimentally resolved problems which are similar to the particular problem to be resolved.

This chapter is concerned with the computational tool to be used in the investigation. The general purpose commercial CFD code, STAR-CD, was used as the major computational means in the prediction of the mixture preparation. A brief description of the package is firstly presented. To prove the feasibility of the technique on the problem in question, validation tests on the package carried out by modelling a well documented

fluid flow problem and a duct flow with which experiments were performed will then be reported.

2.2 The STAR-CD CFD code

The STAR-CD thermofluid analysis system was developed by Computational Dynamics Limited for the calculation of fluid flow, heat and mass transfer and chemical reaction in industrial and environmental circumstances. The package comprises the main analysis code, STAR (stands for Simulation of Turbulent flow in Arbitrary Regions) which numerically solves the flow physics governing equations on a computational mesh, and the pre-processing and post-processing code, PROSTAR which is an interactive command-driven processor functioning to model geometry, to define the problem, to manipulate and display the mesh generated and results calculated, and to manage files of its own and link them to external CAD/CAE systems if necessary [112]. The code system is a self-contained, fully integrated and user friendly CFD tool with built-in models representing an extensive range of flow phenomena encountered in various kinds of complex configurations.

2.2.1 Basic equations and the numerical solution techniques

The basic differential conservation equations solved in STAR are listed in Appendix II. There are five user selectable state equations. Facilities are also available for user specified property functions to be inserted in STAR-CD. There are several turbulence models employed in STAR-CD to determine the Reynolds stresses and turbulent scalar fluxes based on an ensemble averaging approach. The main options available in the latest version are variants of the well known k-ε model including the standard one, the Renormalisation Group (RNG) theory version for high Reynolds number and the Two-layer model in which the near wall flow is simulated via one equation low Reynolds number model and the rest of the flow region is simulated using the standard k-ε model. In addition to the above, there are another two alternative turbulence representations. They are the 'k-*l*' model, where *l* is a user specified spatial distribution of the turbulence length scale used to dispense with the differential ε equation over the entire flow, and the directly prescribed turbulent viscosity model where there are no differential turbulence equations involved. Details of these models are given in Appendix II. The choice of these models are primarily based on the user's experience. The generality, cost effectiveness and availability of performance data favour the three k-ε model variants. Usually the standard and RNG models are the most economical and require minimal numerical resolution. In the case where the assumptions of flow in the near wall layer are not valid, the two layer models may perform better with the penalty of high numerical resolution and low cost effectiveness. However, it is a generally recognised

fact that none of the existing models can accurately represent the physical behaviour and the degree of inexactness of a given model depends on the nature of the flow.

In addition to the basic equations listed in Appendix II, there are many extra equations for the distributed resistance, such as the flow through a region containing fine scale geometrical structures and the flow through a thin porous baffle; for chemical reaction and combustion, such as the flow behaviour in the internal combustion engines where the chemical species and energy are linked with the flow field via density changes brought about by temperature and concentration variations; and for dispersed multiphase flow where the flow consists of a continuous phase, gaseous or liquid, and one or more dispersed phases in the form of solid particles or liquid droplets or gas bubbles. Because these models were not encountered in the study, they are not given here in the thesis. Details of these equations can be obtained from the package manual [112].

2.2.1.1 Mesh generation

In order to solve the differential conservation equations, the flow domain or solution domain needs to be subdivided into a number of small cells, or control volumes in the case of the finite volume approach. The STAR employs a highly flexible computational mesh system. This facilitates its application to the complex geometry which is often encountered in actual CFD problems. The mesh flexibility can also be exploited to selectively refine those meshes in regions of steep flow gradients and to cater for moving boundaries with the capability of cells addition and removal, as in the situations of sliding walls, rotation and distortion. For example, the mesh generated for the prediction of flow in reciprocating engine combustion chambers features enormous distortion due to moving piston and valves. The facility of mesh dynamic movement with cells addition and removal becomes very useful to cope with this kind of application. Of course, the mesh motion is not entirely arbitrary, because there are limits on the degree of distortion which can be tolerated, imposed by accuracy and stability considerations.

Cells or sub domains used in STAR are straight edged cells which may be shaped and jointed face-to-face in an arbitrary manner. The cells can have any of the following alternative shapes: haxahedra, tetrahedra, triangular prisms and pyramids, as illustrated in Figure 2.1. In order to provide continuous meshes, faces and vertices on the joint edge of different cell forms must be coincident. In principle, a mesh may be constructed from any of the shapes mentioned above. In terms of efficiency of computer coding and suitability for flow calculation which often requires long thin cells in boundary layers, the hexahedra structure should be predominantly used with other options used locally for reasons of convenience or necessity. Vertices and faces which define a cell should be

assigned in a sequence which follows the right hand rule in a global Cartesian co-ordinate system or in a locally selected alternative system (e.g. cylindrical, spherical, toroidal). For cells indexed with shapes other than hexahedra, attention should be paid to the coincident vertices formed by collapsing cell faces to lines and/or points. When meshing for the simultaneous calculation of heat transfer in a fluid and an adjacent solid (i.e. conjugate heat transfer) or for multiple stream applications, the continuity of mesh at the solid/fluid interfaces should be carefully treated.

A mesh for the STAR-CD simulation can be produced either directly by using PROSTAR commands or by using an external wire frame type surface modular and then importing the data into the CFD code through the built-in interfaces with the following well known CAE packages:

ANSYS™	IDEAS™	CAEDS™
NASTRAN™	PLOT3D™	PATRAN™

The linkage with some popular proprietary CAD/CAE system is a unique feature of the STAR-CD package and it inevitably makes the package a part of the CAE repertoire, which enable the CFD code particularly suitable for applications in a CAE environment. The STAR-CD package also accepts data from surface modular which provide data in either the widely used standard IGES or VDA formats.

2.2.1.2 Discretisation of conservation equations

The discretisation of the differential equations is conducted in STAR by the finite volume method in which the physical quantities are integrated over the individual computational control volume and/or time increment. The physical variables are located at the centre of the control volume and the integrated fluxes are approximated at the faces in terms of the neighbouring nodal values of the dependent variables. The conservation equations in general vector form are composed of three terms as follows:

$$\frac{d}{dt}\int_{v_p}\rho\Phi dV+\sum_j\int_{s_j}(\rho\vec{u}_r\Phi-\Gamma_\Phi grad\Phi)\bullet d\vec{S}=\int_V s_\Phi dV \qquad (2.1)$$

$$T_1 \qquad T_2 \qquad T_3$$

where $\vec{S}$ is the surface vector , $\vec{u}_r$ is the surface velocity, Vp is the volume of the computational cells and Sj (j=1, total number) the discrete faces which close the cell, Φ stands for any of the dependent variables, Γ_Φ and s_Φ are diffusion and source coefficients which associate with those variables, and ρ is density.

Thus the first term T_1 can be discretised by an interval δt between old ('o') and new ('n') time levels over the volume as

$$T_1 \approx \frac{(\rho\Phi V)_P^n - (\rho\Phi V)_P^o}{\delta t} \tag{2.2}$$

The second term T_2 can be split into the separate contributions due to convection and diffusion respectively. Each one is expressed in average values over cell faces, denoted by $(\,)_j$, thus:

$$T_2 \approx \sum_j (\rho\vec{u}_r\Phi \bullet \vec{S})_j - \sum_j (\Gamma_\Phi grad\Phi \bullet \vec{S})_j \equiv \sum_j C_j - \sum_j D_j \tag{2.3}$$

The diffusion terms D_j are assumed to depend on a linear variation of the nodal variable across the interfaces of the control volume and are approximated directly by face-centred linear expressions under the consideration of its neighbouring cells, i.e.

$$D_j \approx \Gamma_{\Phi,j}\left[f_j^l\left(\Phi_n - \Phi_p\right) + \sum_k f_j^k \delta\Phi_j^k \right] \tag{2.4}$$

where the first term in the brackets represents the gradient between the point considered and the neighbouring cell-centred node n and the second term is the summation over all vertex pairs on face j with the interpolated Φ values from surrounding nodal values. The f_j are geometrical factors and $\Gamma_{\Phi,j}$ is the interpolated face diffusivity.

The convection terms C_j rely on the values of certain nodal variables upstream and downstream of the control volume. As mentioned before, the increase of spatial discretisation can reduce the deviation between the differential and approximated algebraic equations. But the refinement of control volumes are constrained by computer storage limitations, machine precision and calculation speed. Accuracy of the solution therefore depends, to a large extent, on the approximation methods of the variables at the faces of the control volume. The approximation is sometimes crucial to obtain a stable and accurate discretisation scheme. Basically there are three widely used schemes, that is the low-order, the high-order and the filtered or blended schemes. The first one often suffers from inaccuracy due to its low order of approximation and the second from instability such as non-physical spatial oscillations. Thus many variants and alternatives have been put forward attempting to get a scheme which is numerically stable and computationally accurate as well.

There are five options available in STAR to discretise the convective terms. They are:

(a) Upwind Differencing (UD)--first order;

(b) Linear Upwind Differencing (LUD)--second order;

(c) Central Differencing (CD)--second order;

(d) Self -Filtered Central Differencing (SFCD2);
(e) Blended Differencing (BD).

STAR allows the user to individually select from the above options for each of the transport equations solved. Thus it becomes possible to specify the SFCD scheme for the momentum equations and the UD scheme for the 'k-ε' turbulence model equations. It is even possible for some schemes that different factors can be specified for each equation. This flexibility makes the STAR very suitable for some flow phenomena where instability may be involved. However, none of these can be universally suitable for all the flow behaviour encountered in engineering. Compromise has sometimes been made between the accuracy and cost under condition of obtaining a stable result.

The third term, source term (or sink) is averaged over the whole control volume in a general linear form:

$$T_3 \approx s_1 - s_2 \Phi_p \tag{2.5}$$

After some mathematical manipulations, the final form of the discrete finite volume equations 3.1 are converted as the following algebraic equations:

$$\left(\sum_m A_m + s_2 + \frac{(\rho V)^o}{\delta t}\right)\Phi_p^n = \sum_m A_m \Phi_m^n + s_1 + \left(\frac{(\rho V)^o}{\delta t}\right)\Phi_p^o \tag{2.6}$$

where A_m represents the effects of convection and/or diffusion; the summation is over all neighbour nodes used in the flux discretisation.

2.2.1.3 Solution algorithm and boundary conditions

After the finite volume discretisation process, a variable coupling method has to be devised in order to treat the velocity components and the pressure terms. STAR currently incorporates three different implicit algorithms to temporarily de-couple the flow equations from each other so that they can be sequentially solved using the so called prediction-correction strategy while enforcing the continuity features of the mass and momentum. They are the well known SIMPLE method (semi-implicit pressure linked equation), the more recent and efficient PISO method (pressure-implicit with splitting of operators) and their combination variant SIMPISO. The SIMPLE and SIMPISO are used solely for steady state flow problem calculations where the time derivative terms are deleted from the FV equations. The PISO is applicable to both transient and steady state flow calculations.

To find a numerical solution for the equations obtained, imposition of the appropriate boundary conditions is required. Boundary condition definition is performed by

PROSTAR, which allows the conditions to be imposed directly on each of the relevant cell faces or on the entire boundary surfaces. The available boundary condition options built-in are as follows:

1) Prescribed flow;
2) Outlet ;
3) Prescribed pressure;
4) Impermeable wall;
5) Cyclic boundaries;
6) Symmetry plane or axes;
7) Prescribed stagnation conditions;
8) Free-stream transmissive;
9) Transient transmissive;
10) Slip surface;
11) Prescribed wall temperature or concentration;
12) Prescribed wall heat or mass flux;
13) Prescribed surface reaction.

Generally these options can be specified in conjunction with each other depending on the physical problem. But cautionary treatment given in the manual should be carefully consulted when the boundary specification is to be embarked on.

2.2.2 The capabilities of STAR-CD version 2.21

Due to the rapid development of the technique and fierce market competition, the package developer has been updating the code to a new version in almost every half year. The author of this thesis has experienced six versions since the start of this investigation. The modelling capability of the package is advancing with each new version, which is accompanied by improved pre/post-processing facilities such as the mesh generation and the results processing. But it should be aware of that some of the commands in newly released versions are not compatible to the previous release. The latest version used in this study was the version 2.21.

1) The types of flow phenomena capable of consideration in the version are:

- Steady and transient;
- Laminar and turbulent;
- Newtonian and non-Newtonian;
- Incompressible and compressible;
- Heat transfer (convection, conduction and radiation);
- Mass transfer;
- Chemical reaction and combustion;
- Distributed resistance (porous media);

- Buoyancy and rotation;
- Dispersed multi-phase flows;
- Multiple streams.

2) The type of geometry capable in the version are:

- Unstructured meshes;
- Mesh movement;
- Embedded refinement;
- Sliding interface;
- Multiple rotation zones;
- Dynamic cell addition and deletion.

In addition to the above capabilities, the user can further extend them by the user programmability feature via FORTRAN coding.

2.2.3 Application procedure

The application of STAR, as for any other CFD packages, requires sound knowledge of fluid mechanics and dynamics. The more a user knows about the package and the problem which is going to be solved, the more likely it will be for the user to get an answer with the appropriate accuracy. Some essential operations which are commonly encountered when the package is used for prediction of thermofluid dynamics problems are discussed here.

Firstly, the physical problem to be solved must be correctly defined. The nature of flow should be well understood and the question of whether the flow problem falls within the capability of STAR-CD should be answered before any further implementation is taken. To answer this, many aspects of the problem need to be examined. For example, if the flow is a multi-phase fluid problem, it is out of range of any version previous to STAR-CD Version 2.2. In this case other packages or a new version of STAR have to be considered.

Secondly, the creation of a geometrical model which represents the flow domain is the next step to be carried out. It is the most time consuming stage of setting up a CFD simulation, which takes about 80% of the total effort of the users. The mesh generated can effect whether a solution is obtainable, the speed to obtain the solution and the accuracy of the simulation. The main considerations in this step are accuracy and cost. The structure of mesh and mesh density arrangement will govern this consideration. A compromise between accuracy and cost has sometimes to be made. A high mesh density will produce less mesh distortion for a certain mesh structure and give a better

representation of the flow domain. But the fine meshes need much time for a user to create and more space for the computer to store the necessary information. Needless to say the CPU time required for each iteration or time step will be greater. A commonly used method to deal with this is local refinement of the mesh, especially for a flow with sharp variable gradient changes. STAR-CD facilitates such selective local refinement. No matter what kind of mesh is used and what density it is, the degree of mesh distortion must be checked using the three factors defined in the manual.

Thirdly, the initial conditions and boundary conditions should be specified. The initial condition refers to the values assigned to the dependent variables at all mesh points prior to the start of calculation. In transient calculation the initial conditions not only affect the course of the solution, as in the calculation of steady flows by iterative means, but also affect the result of the solution. Boundary conditions specification is perhaps the most difficult stage in CFD application. Decisions on where to place the boundaries, what type of boundaries to be defined and what boundary values to be ascribed are very important to achieve a successful solution. Correct and consistent specifications depend mainly on the user's understanding of the problem and of the package. Sometimes different options embodied in the package have to be tried with careful analysis of the results. It will be better and helpful to the user if relevant experimental data or the data from well documented literature are available.

Next, thermophysical properties of the fluid and control parameters need to be set. Clearly properties like density depend on the nature of the flow and the circumstances prevailing such as ambient conditions and species. These related conditions or variables should be taken into account during the definition. Setting the control parameters is one of the key steps for achieving a successful solution, because these parameters control all aspects of the operation, such as data processing and solution procedure. The solution procedure is the first thing to be selected at this stage between the alternatives, SIMPLE, PISO, and SIMPISO, depending on whether the flow is unsteady or not. Once the algorithm is selected, the control parameters such as residual convergence tolerances, sweep limits and relaxation factors are the next to be prescribed. Normally, the default values can be used for these factors. Only when it is difficult to get a satisfactory solution, will these settings require adjustment under guidance of the manual. For simulations of mixing problems, chemical reactions and other fluid behaviours in the versions later than version 2.1, the related solvers should be turned on at this stage and specifications of the variables of concern posed.

Finally, the calculation under consideration can be pursued and the assessment of results can be made. The results may be presented in ways such as x-y graphs, flow animation, neutral files and the data or files acceptable by other CAE packages.

For each step, attention must be paid to the specification of the built-in options. Experience from other users are sometimes helpful for achieving a reasonable solution. One of the best ways to evaluate the outcome of a CFD prediction with each set of options specified is by validating the results either indirectly or directly with experimental data.

2.3 Validation of the code though BS 1042

The validation, here, is defined as a process in which the CFD computed results are independently compared against the well documented data or experimental data that represent or are related to flows of real engineering interest. There have been some specifically conducted experimental data available for CFD code validation [135]~[137]. The data are presented in such a detail and format that they can be used to test or validate CFD codes and mathematical models without difficulties on defining necessary boundary, inlet and/or initial conditions. However, these data only highlight some particular fluid flow phenomenon or influence. There is no universally accepted data for all sort of CFD codes validation. Therefore it is up to each user to select the data or obtain data by conducting experiments which are most relevant to the flow phenomena that are to be simulated.

The objective of this validation work and the one followed was to accumulate knowledge on using the STAR-CD package by modelling a well documented fluid flow problem and a conventional pressure driven internal flow system in which some of the flow parameters can be experimentally measured. The two problems simulated were similar to the potential mixture formation system. The study also included the effect of the mesh selections and the boundary options on computation performance for the problems simulated. The experience and understanding acquired on using the tool to predict those basic fluid dynamics parameters in the actual flow domain were then transferred confidently to the research work on mixture preparation in collaboration with experimental facilities.

2.3.1 Introduction to British Standard 1042

British Standard 1042 is a standard for measurement of fluid flow in closed conduits. The device inserted in circular cross section conduits can be one of the three pressure differential units: square edged orifice plates, nozzles and venturi tubes. The Standard specifies the geometry of these devices and their installation, operating conditions and necessary information for calculating the flow rate when each of these devices is used under the conditions specified. The device used in this study was a classical venturi tube

because the majority of existing carburettors were based on this principle. The definition of the sections which make up a classical venturi tube is stated by the standard. When the device is used for the measurement of flow with a known flow rate, the pressure difference between the two pressure tappings whose positions are specified by the standard should follow the relationship given below with the appropriate flow coefficient or discharge coefficient.

The mass flow rate can be derived from the following formula when the pressure difference is measured:

$$q_m = CE\eta\frac{\pi}{4}d^2\sqrt{2\Delta p \times \rho_1} \qquad (2.7)$$

where E is called the velocity of approach factor and can be derived from the following equation:

$$E = \frac{D^2}{\sqrt{D^4 - d^4}} \qquad (2.8)$$

here D is upstream diameter of the classical venturi tube. Thus the discharge coefficient C will be:

$$C = \frac{q_m}{E\eta\frac{\pi}{4}d^2\sqrt{2\Delta p \times \rho}} \qquad (2.9)$$

The numerical values of the coefficient given in the standard are based on data determined experimentally. Therefore with a known input value of the flow rate, a CFD computational value of Δp and hence a computational discharge coefficient will be obtained. The computational discharge coefficient was expected to be within the range given in the standard if the CFD predicted pressure distribution coupled with other variables such as the velocity was accurate enough.

2.3.2 Geometry model creation for a classical venturi tube

A geometrical model of a classical venturi tube was created with a straight cylindrical pipe line of constant cross sectional area installed in the system. The model and its original geometry which follows the specification given in the standard are shown in Figure 2.2. To reduce computation cost, only a slice of the tube was considered in the model, which is reasonable for this kind of symmetrical flow. According to the flow phenomena through a venturi tube, the mesh refinement was used in order to save the computer storage space. Fine meshes were defined in the conical convergent section, the divergent section and the cylindrical throat section where the flow variables change with

a steep gradient. Coarse meshes were used in the other part of the flow system. The regular hexahedral cells were mainly used with some regular prism cells adjacent to the symmetrical axis. Taking the mesh distortion, the flow domain geometry representation and computation cost into account, ten layers of mesh in the radial direction and ten degrees of angle in the circumferential direction were chosen. The surfaces of each cell were defined, as far as possible, either parallel to or perpendicular to the anticipated streamlines. The geometric model was composed of 800 cells.

2.3.3 Boundary condition settings

The upstream boundary was specified as the prescribed inlet boundary with constant flow velocity along the axis and with constant fluid temperature. The prescribed pressure boundary was also tested for the upstream boundary specification. For incompressible flow problems, the fluid density was set to be constant. Thus the flow rate through the system was specified. In the case of high velocity gas flows, the fluid density was assumed to hold to the ideal gas law in order to minimise the compressibility effect on the computation results. In this situation the mass flow rate can be derived from the calculated density and velocity on the upstream boundary. The downstream boundary was specified as the outlet boundary, whilst the upstream boundary was defined as the inlet, with zero gradients of all variables normal to the outflow surface. To see the difference between the two options embodied within the STAR-CD, prescribed pressure for the downstream boundary was also defined.

The outer surface which is the interface between the flow domain and the pipe wall was defined as an impermeable wall boundary with a known roughness number. The characteristics at the wall, the velocity, the heat flux across the wall and the distribution of chemical species flux through the wall were prescribed as zero. The two splitting surfaces were defined as symmetry planes because the assumption of no circumferential flow in the flow domain was made. The centre axis was defined as the symmetry axis which can be inferred from the grid structure and other already specified boundary conditions.

2.3.4 Other settings

For the fluid property setting, gas was used rather than liquid in the study because the future work would be mainly on gaseous flow phenomena. Specifically, air was assumed to be the fluid used for the convenience of getting those necessary fluid properties. In all the cases, the pressure datum was set to be the standard atmospheric pressure for the air.

For the inlet velocity specified, the Reynolds number was calculated in order to decide whether the turbulence switch embodied in the code should be switched on or not. With the velocity of 20 m/s specified at inlet boundary, the Reynolds number exceeded the critical value with an air kinematic viscosity of 1.568×10^{-5} m^2/s at temperature of 300 K. The turbulence switch was in the ON position. The wall roughness number will affect the results of the computation. For a given flow velocity, three different roughness numbers were specified. The small number 1.2 represents a rough wall. The big number 20 represents a smooth wall. The default number 9 covers most of the commonly used wall roughness features. When the critical value of the Reynolds number was exceeded, the 'k-*l*' turbulence model was used based on the well documented relationship between the turbulence kinetic energy and the inlet velocity with an assumed turbulence intensity. The turbulence length scale l was assumed to be one tenth of the characteristic dimension of the flow cross section. For comparison, the 'k-ε' model was used in one of the calculations and the switch was even set in the OFF position for the turbulent flow.

In solution parameters setting, the SIMPLE solution algorithm was chosen appropriate to the steady nature of the flow. The default relaxation factors and tolerances were used during the solution. Two hundred iterations were allowed for the computation before it was forced to stop. In order to check the solution progress, the solution was monitored through variables at a cell in the throat section.

2.3.5 Validation tests

Based on aforementioned model and specifications, a series of computations were carried out by running STAR-CD with specifications listed in Table 2.1. With the computed pressure difference under the specified velocity and density, the derived discharged coefficient C should be about the same as that has been given in the Standard if the computational results are within a certain accuracy. To validate these results, firstly, the mass flow rate at the inlet boundary was calculated using the averaged velocity and density at the boundary. Secondly, the upstream pressure at a position where the tapping is defined in the Standard was read off. It was the average value of cells at the cross section (cell 81 to 90 for this study) used to simulate the pressure tappings in the actual measurement. Thirdly, the pressure tapping values at the throat cross section were averaged. Finally, the discharge coefficient for each computation was calculated using equation 2.9. The computational values of the discharge coefficient are given in Table 2.1. The distributions of the pressure and velocity along the axis with different boundary definitions and mesh densities are given in Figure 2.3 and Figure 2.4.

Table 2.1 Variable specifications and computation results

Case No.1	Upstream boundary Inlet, u=20 m/s	Fluid density 1.17 kg/m^3	Fluid viscosity/Temp. 1.568 E-5 m^2/s /300 K
	Roughness Number 9	Downstream boundary Pressure, 0 N/m^2	Turbulence model OFF
	Cell number 800	Discharge coeff. 0.933	Iteration steps/CPU time 62/260
Case No.2	Upstream boundary Inlet, u=20 m/s	Fluid density Ideal gas	Fluid viscosity/Temp. 1.568 E-5 m^2/s /300 K
	Roughness Number 9	Downstream boundary Outlet, split=1	Turbulence model 'k-ε'
	Cell number 800	Discharge coeff. 0.975	Iteration steps/CPU time 73/300
Case No.3	Upstream boundary Inlet, u=20 m/s	Fluid density Ideal gas	Fluid viscosity/Temp. 1.568 E-5 m^2/s /300 K
	Roughness Number 1.2	Downstream boundary Outlet, split=1	Turbulence model 'k-ε'
	Cell number 800	Discharge coeff. 0.969	Iteration steps/CPU time 73/300
Case No.4	Upstream boundary Inlet, u=20 m/s	Fluid density Ideal gas	Fluid viscosity/Temp. 1.568 E-5 m^2/s /300 K
	Roughness Number 20	Downstream boundary Outlet, split=1	Turbulence model 'k-ε'
	Cell number 800	Discharge coeff. 0.977	Iteration steps/CPU time 73/300
Case No.5	Upstream boundary Pressure, 0 N/m^2	Fluid density Ideal gas	Fluid viscosity/Temp. 1.568 E-5 m^2/s /300 K
	Roughness Number 9	Downstream boundary Pressure,-5000~-800N/m^2	Turbulence model 'k-ε'
	Cell number 800	Discharge coeff. /	Iteration steps/CPU time (Divergent)
Case No.6	Upstream boundary Pressure, 0 N/m^2	Fluid density Ideal gas	Fluid viscosity/Temp. 1.568 E-5 m^2/s /300 K
	Roughness Number 9	Downstream boundary Pressure,-656 N/m^2	Turbulence model 'k-ε'
	Cell number 800	Discharge coeff. 0.975	Iteration steps/CPU time 341/1420
Case No.7	Upstream boundary Inlet, u=20 m/s	Fluid density Ideal gas	Fluid viscosity/Temp. 1.568 E-5 m^2/s /300 K
	Roughness Number 9	Downstream boundary Outlet, split=1	Turbulence model 'k-*l*'
	Cell number 800	Discharge coeff. 0.930	Iteration steps/CPU time 63/260
Case No.8	Upstream boundary Inlet, u=20 m/s	Fluid density Ideal gas	Fluid viscosity/Temp. 1.568 E-5 m^2/s /300 K
	Roughness Number 9	Downstream boundary Outlet, split=1	Turbulence model 'k-ε'
	Cell number 3200	Discharge coeff. 0.97	Iteration steps/CPU time 113/3212

The results showed that the discharge coefficient C increased with the increased wall roughness number. It was 0.969, 0.9756 and 0.977 for the roughness number 1.2, 9 and 20, respectively. This agreed with that the smoother the wall, the larger its discharge coefficient would be. When the turbulence model was switched off, the wall roughness number had no effect on the result at all. It only affected the computation result for the

turbulent flow. For all of the results, however, the computed discharged coefficient C was slightly smaller than those given in the Standard (0.984~ 0.995). This meant that the pressure differences were over estimated by STAR. As shown in Figures 2.3 and 2.4, the turbulent wall roughness number also influenced the pressure distribution and the velocity distribution along the venturi tube, especially in the divergent section. The pressure recovery in the section was smaller for a rough wall than that for a smooth wall.

When both upstream and downstream boundaries were defined as prescribed pressure boundaries, as in computation No. 5, it was likely that a divergent solution would be obtained if the pressure gradients between the two boundaries were large. Since the gradient was excessively large in the throat section of the venturi tube, this sometimes caused numerical instability and led to a failed solution. In computation No. 6, the two pressure values were those resulting from the previous computation No. 2 with specified inlet and outlet boundaries. Not only the discharge coefficients but also all of the other parameters and their distributions were identical to each other. This is to say that the two kinds of definitions did not give any deviation of the result. However the time cost to complete the computation was very different. The pressure-pressure definition used threefold of the time taken for the inlet-outlet definition. Therefore the pressure-pressure boundary definition should be avoided whenever possible.

To see the effect of mesh density on the computation results, a much more refined mesh with 3200 cells was created, see Figure 2.5. A brief comparison between the two models with different mesh densities was made. With respect to velocity magnitude distribution, the effect of mesh density was relatively small, as shown in Figure 2.4. The discharge coefficients computed using the two models with different mesh densities were nearly the same. With respect to the pressure distribution, there were differences between the two models having different mesh densities. A fine mesh revealed a more detailed information about the pressure changes particularly in areas such as the transition between the convergent and throat sections.

2.4 Validation of STAR-CD through duct flow experiments

In the aforementioned validation, the code was validated through the British Standard 1042 with respect to two parameters which are derivatives of the fluid dynamics variables. The objective of this test was to validate the code further on some of the directly computed variables by comparing them with experimental results. Among those parameters directly computed by STAR, it is pressures and velocities that can be measured using conventional instruments such as pitot tubes and manometers. Therefore this further validation was carried out by measuring the pressure distribution

along a duct with different diffusers installed in turn. The reason for using diffusers was because of their similarity to the venturi type carburettors.

2.4.1 The duct flow tests with different diffusers

The test rig is shown schematically in Figure 2.6. The source of flow came from a motor driven centrifugal fan which was run with a constant speed of 2870 rpm. The duct was made of a rough welded sheet iron. A pitot tube was inserted in the upstream flow in order to measure the total pressure of the flow at the cross section where a static pressure tapping was positioned. Downstream of the flow, two different diffusers were set up using flange clamps. For the conical diffuser configuration A and B, the convergent and the throat sections were identical. Diffuser A, however, was arranged to have a narrow divergent angle which was only 13 degrees. Diffuser B had a very wide divergent angle which was 32.8 degrees and was of short length. The configurations of the two diffusers are given in Figure 2.7. Another pitot tube was positioned in the throat section where the flow velocity was expected to be very high. The total pressure tube was set to point into the air upstream and was traversed across the duct accurately using a displacement mechanism. Thus the velocity profile and the mass flow rate at each section could be determined.

All the pressure tappings were connected to a multi-tube manometer. The relative density of the manometer fluid was carefully calibrated using a hydrometer in case of evaporation which could change the marked value. After post processing the experimental data for each diffuser, the pressure distribution along the duct and the velocity distribution across the flow at the throat section were achieved. The results are given in Table 2.2. The average axial velocities at the upstream section where the axial distance is zero were also measured for both diffusers and they were 7.53 m/s for diffuser A and 6.52 m/s for diffuser B.

2.4.2 Duct flow simulation using the STAR-CD code

It was very difficult and unnecessary to simulate the flow within the fan used in the experiment. The flow of interest was at the downstream sections with the diffuser installed. The flow variables like static pressure at the section where the upstream pitot tube was positioned were known. Therefore the flow domain which was to be studied was chosen from this section downwards. The measured profiles of mean flow and estimated turbulence at the section were taken as the duct inlet conditions. According to the configurations used in the test, a geometrical model was created for each of the duct flow domains, which are shown in Figures 2.8 and 2.9. To reduce the cost of computation, only a slice of cells was created to represent the axisymmetrical flow. As

before ten layers in the radial direction of the duct were used and mesh densities were locally refined at the section where large gradients of variables existed. Because the pressure distribution in other parts of the flow domain was also important for the validation, the mesh density used was quite high in these parts as well. The mesh distortion factors were checked during the mesh creation. A total number of 1740 cells was used for configuration A and 1410 cells for configuration B.

Table 2.2 Experimental results of a duct flow

(a) Pressure distribution along the diffuser A

Axial distance (mm)	0	154	381	609	756	796	832
Static pressure (N/mm^2)	415	415	405	390	376	326	191
Axial distance (mm)	972	1020	1123	1265	1316	1367	1418
Static pressure (N/mm^2)	-614	-631	-738	-450	-290	-224	-158
Axial distance (mm)	1469	1520	1571	1622	1673		
Static pressure (N/mm^2)	-116	-74.6	-58	-33	-1.36		

(b) Velocity distribution at a throat section of diffuser A

Radial distance (mm)	0	3	5	8	10	13	14
Axial velocity (m/s)	42.6	42.6	42.6	42.6	42.6	42.6	42.6
Radial distance (mm)	16	18	19	20	21	22	
Axial velocity (m/s)	42.4	42.3	41.4	39.8	37.8	32.6	

(c) Pressure distribution along the diffuser B

Axial distance (mm)	0	154	381	609	756	796	832
Static pressure (N/mm^2)	679	679	677	675	663	630	514
Axial distance (mm)	972	1020	1123	1270	1310	1346	
Static pressure (N/mm^2)	-149	-160	-207	-41	-33	-24	

(d) Velocity distribution at a throat section of diffuser B

Radial distance (mm)	0	3	5	8	10	13	14
Axial velocity (m/s)	38	38	38	38	38	38	38
Radial distance (mm)	16	18	19	20	21	22	
Axial velocity (m/s)	37.8	37.7	37.1	35.7	33.3	29.4	

The upstream boundary conditions were defined as to be the same as those measured in the experiment. Therefore both the inlet velocity and the prescribed static pressure could be specified by using the value derived from the test. To enable the inlet boundary conditions to be defined separately, five regions were set with each of two cells forming an inlet region. This setting made it possible to define a fully developed velocity profile

on the boundary. Both single stream outlet and prescribed pressure boundary conditions were tried for the downstream boundary condition. When the upstream boundary condition was a known velocity, the downstream one could be the outlet or prescribed pressure. When the upstream one was a pressure boundary condition, the downstream one could only be defined as pressure boundary condition. Otherwise the computation would be likely to fail. The boundary settings for the two configurations are listed in Table 2.3 and 2.4.

The ambient pressure and temperature were specified as for those measured in the test. The density of air was defined as using the ideal gas law with a molecular mass of 28.96 kg/kmol for air. Thus the density of the fluid was automatically determined by the equation of state. The viscosity was defined as constant with a value of 1.51×10^{-5} m^2/s at the temperature of 20 °C. The outer circumferential surface was specified as an impermeable wall with different roughness numbers tried in the computations. The two symmetry planes and the symmetric axis were set to be the same as in the previous validation.

The Reynolds number of the flow was larger than the critical value. Therefore the 'k-*l*' turbulence model was used in the calculations with a turbulence length scale of one tenth of the duct characteristic dimension. The turbulence intensity was specified using different values from 0.05 to 0.4. The number of iterations to be performed was set to 500 steps and the overall residual tolerance value was set to 0.005 in order to save the computer time with reasonable accuracy of the results. Because the flow was steady, the SIMPLE solution algorithm was chosen. The pressure datum was set to be the same as the measured ambient pressure. Those settings not mentioned here were specified as their default ones.

Computed pressure and velocity distributions along the diffuser for different boundary settings are given in Figures 2.10 and 2.11 together with the tested pressure data. Comparisons of the pressure distributions showed that agreement between the computed and experimental results was very good no matter which kind of boundary setting was used. The velocity traverse comparison given in Figure 2.12 gave the same conclusion. With prescribed pressure upstream boundary definition the agreement was better than with the prescribed inlet velocity definition. When the turbulent roughness number used was small, the resulting difference between the calculated pressure and the measured pressure was very small. It was that only when a higher roughness number was used, the difference between the computed pressure in the upstream part of the flow and the tested results were slightly greater, and similarly for the velocity traverse comparison.

Table 2.3 Variable settings for each computation of diffuser A

Case No.1	Upstream boundary Inlet, u=5.3 m/s	Fluid density Ideal gas	Fluid viscosity/Temp. 1.51E-5 m^2/s /293 K
	Roughness Number 9	Downstream boundary Pressure, 0 N/m^2	Turbulence model 'k-*l*', I=0.1, *l*=0.0123
	Cell number 1740	Air molecular mass 28.96 kg/kmol	Iteration steps 99
Case No.2	Upstream boundary Inlet, u=5.3m/s	Fluid density Ideal gas	Fluid viscosity/Temp. 1.51E-5 m^2/s /297 K
	Roughness Number 9	Downstream boundary Outlet, split=1	Turbulence model 'k-*l*', I=0.1, *l*=0.0123
	Cell number 1740	Air molecular mass 28.96 kg/kmol	Iteration steps 99
Case No.3	Upstream boundary Inlet, u=5.3 m/s	Fluid density Ideal gas	Fluid viscosity/Temp. 1.51E-5 m^2/s /293 K
	Roughness Number 1.2	Downstream boundary Pressure, 0 N/m^2	Turbulence model 'k-*l*', I=0.1, *l*=0.0123
	Cell number 1740	Air molecular mass 28.96 kg/kmol	Iteration steps 102
Case No.4	Upstream boundary Pressure, 415.2N/m^2	Fluid density Ideal gas	Fluid viscosity/Temp. 1.51E-5 m^2/s /293 K
	Roughness Number 1.2	Downstream boundary Pressure, 0 N/m^2	Turbulence model 'k-*l*', I=0.1, *l*=0.0123
	Cell number 1740	Air molecular mass 28.96 kg/kmol	Iteration steps 337
Case No.5	Upstream boundary Inlet, u=5.3 m/s	Fluid density Ideal gas	Fluid viscosity/Temp. 1.51E-5 m^2/s /293 K
	Roughness Number 9	Downstream boundary Pressure, 0 N/m^2	Turbulence model 'k-*l*', I=0.4, *l*=0.0123
	Cell number 1740	Air molecular mass 28.96 kg/kmol	Iteration steps 112
Case No.6	Upstream boundary Inlet, u=5.3 m/s	Fluid density Ideal gas	Fluid viscosity/Temp. 1.51E-5 m^2/s /293 K
	Roughness Number 100	Downstream boundary Pressure, 0 N/m^2	Turbulence model 'k-*l*', I=0.4, *l*=0.0123
	Cell number 1740	Air molecular mass 28.96 kg/kmol	Iteration steps 123
Case No.7	Upstream boundary Inlet, u=5.3 m/s	Fluid density Ideal gas	Fluid viscosity/Temp. 1.51E-5 m^2/s /293 K
	Roughness Number 1.2	Downstream boundary Pressure, 0 N/m^2	Turbulence model 'k-*l*', I=0.4, *l*=0.0123
	Cell number 1740	Air molecular mass 28.96 kg/kmol	Iteration steps 110
Case No.8	Upstream boundary Inlet, u=5.3 m/s	Fluid density Ideal gas	Fluid viscosity/Temp. 1.51E-5 m^2/s /293 K
	Roughness Number 9	Downstream boundary Pressure, 0 N/m^2	Turbulence model 'k-*l*', I=0.05, *l*=0.0123
	Cell number 1740	Air molecular mass 28.96 kg/kmol	Iteration steps 92

Table 2.4 Variable settings for each computation of diffuser B

Case No.1	Upstream boundary Inlet, u=6.52 m/s	Fluid density Ideal gas	Fluid viscosity/Temp. 1.51E-5 m^2/s /293 K
	Roughness Number 1.2	Downstream boundary Pressure, 0 N/m^2	Turbulence model 'k-*l*', I=0.1, *l*=0.0123
	Cell number 1410	Air molecular mass 28.96 kg/kmol	Iteration steps 77
Case No.2	Upstream boundary Pressure, 696.9 N/m^2	Fluid density Ideal gas	Fluid viscosity/Temp. 1.51E-5 m^2/s /293 K
	Roughness Number 1.2	Downstream boundary Pressure, 0 N/m^2	Turbulence model 'k-*l*', I=0.1, *l*=0.0123
	Cell number 1410	Air molecular mass 28.96 kg/kmol	Iteration steps 184
Case No.3	Upstream boundary Inlet, u=6.52 m/s	Fluid density Ideal gas	Fluid viscosity/Temp. 1.51E-5 m^2/s /293 K
	Roughness Number 1.2	Downstream boundary Outlet split=1	Turbulence model 'k-*l*', I=0.1, *l*=0.0123
	Cell number 1410	Air molecular mass 28.96 kg/kmol	Iteration steps 80
Case No.4	Upstream boundary Inlet, u=6.52 m/s	Fluid density Ideal gas	Fluid viscosity/Temp. 1.51E-5 m^2/s /293 K
	Roughness Number 1.2	Downstream boundary Pressure, -24 N/m^2	Turbulence model 'k-*l*', I=0.5, *l*=0.0123
	Cell number 1410	Air molecular mass 28.96 kg/kmol	Iteration steps 85

The computed velocity distribution for diffuser B in the flow domain showed that flow recirculation appeared in this diffuser because of the large divergent angle. This was shown experimentally by positioning a thread at the downstream boundary. Because of the short length of the diffuser, the pressure distribution showed the flow did not fully recover at the end of the diffuser. The pressure here was still much lower than the ambient pressure and the variable gradient normal to the section was not zero. Therefore the downstream boundary set as outlet would definitely lead to a failed simulation of the flow. This is shown by the comparison made between the computed results and the experimental results, see Figures 2.13 and 2.14. The agreement for both the pressure distribution and the velocity traverse was not good whether it was the outlet boundary or the prescribed pressure boundary. When it was the prescribed pressure boundary posed for the downstream boundary, a single pressure was used rather than a series of pressures. Clearly the pressures across this surface changed quite a lot from computation cell to cell. To get a good agreement between the computed result and the tested one, the information on pressure distribution across the section is necessary. Otherwise it is difficult to achieve a successful simulation. The velocity distribution along the central line of the diffuser is given in Figure 2.15. The velocity at central area of the downstream section was very high and even higher than the velocity at the upstream surface. That was because the flow in outer area of the surface had recirculated.

2.5 Summary

As a powerful computation and simulation tool, the CFD package STAR-CD was introduced. To gain confidence in its application, the code was validated by two different ways. The validations were carried out mainly on conventional dynamics parameters such as pressure and velocity.

The different boundary condition definition studies showed that these options had a great effect on the solutions and their results. The boundary positions of the flow domain chosen were also very important to flow problems as that in duct flow configuration B. If possible, the upstream boundary of the flow domain should be chosen at a section where either the velocity or the pressure distribution is known. The downstream one should be at a section where either the pressure distribution is known or all the gradients of variables normal to the surface are zero.

To obtain a good agreement between the experimental and computational results with respect to pressure distribution, a small roughness number was preferred. The relationship between the actual mechanical roughness number and the computational roughness number was needed in order that the correct number was chosen for the computation. With the venturi type configuration variables such as pressure and velocity were not sensitive to turbulence intensity. The effects of turbulence conditions on the computation results of variables like mixture concentration remain to be found. The mesh density test carried out showed that the mesh density did not cause any serious problems for the configuration simulated. Otherwise several refined mesh densities had to be tried until they no longer affected the variables concerned. Another way to obtain an accurate solution is to use a different discretising scheme in order to minimise the computer time consumed but preserve the accuracy required.

After a series of computations and the subsequent experimental validation it can be concluded that the STAR-CD package can reliably predict fluid behaviours quickly and at low cost compared with experimental methods. With the experience gained, the STAR-CD can be used confidently to predict the outcome of mixture formation and to aid novel mixers development.

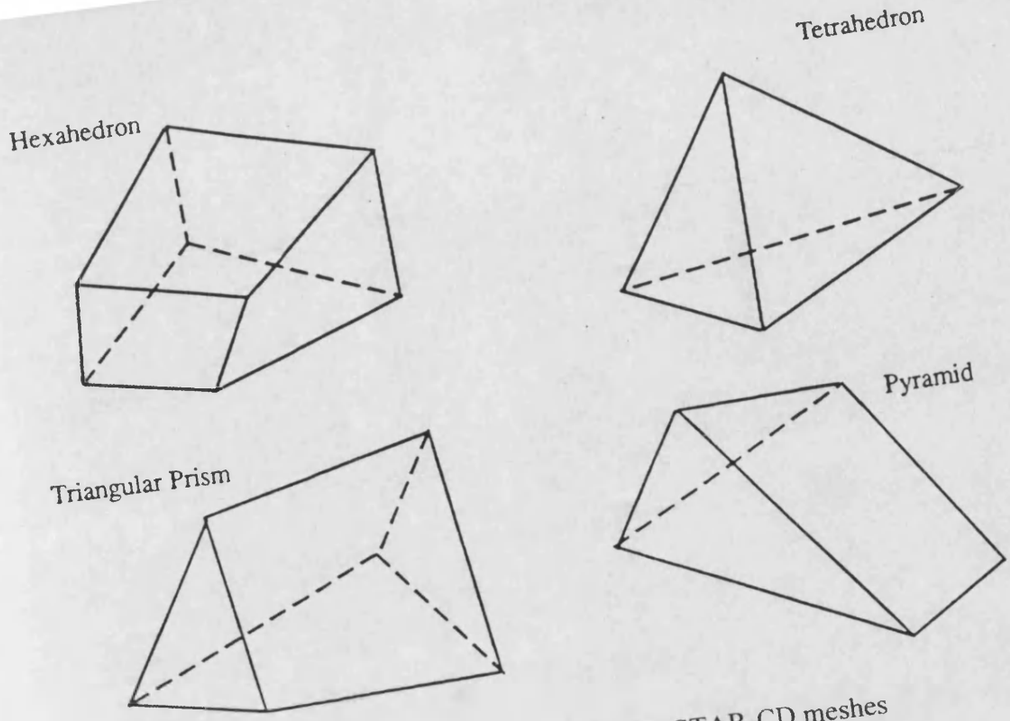

Figure 2.1 Cell structures admissible in STAR-CD meshes

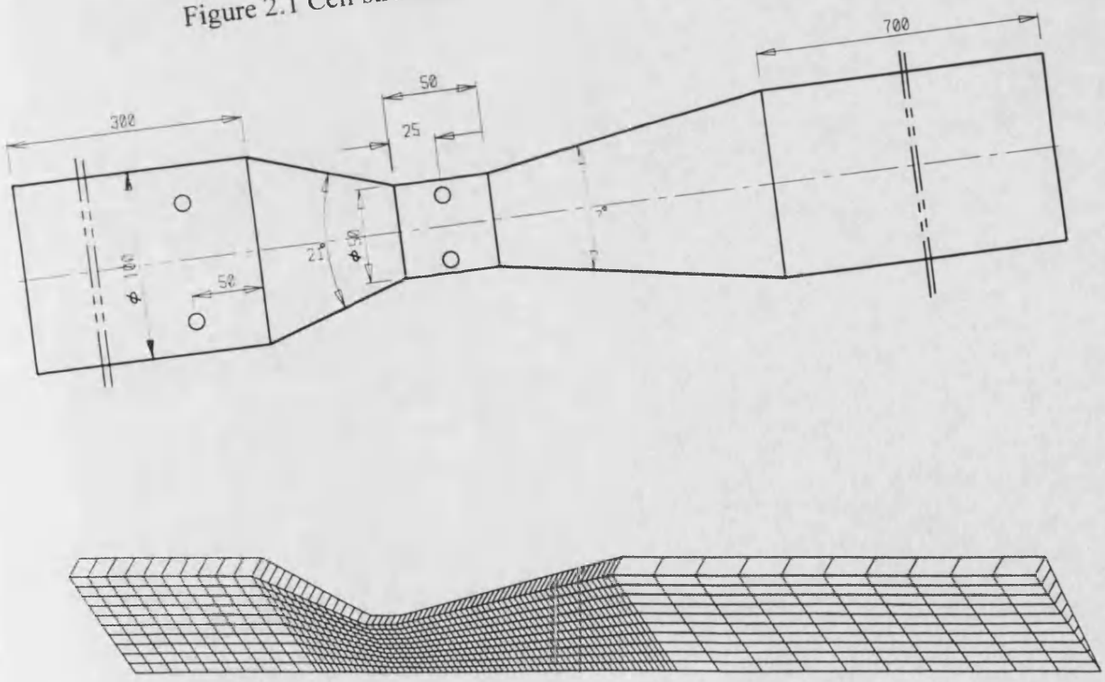

Figure 2.2 Geometry and computational model of the classical venturi tube

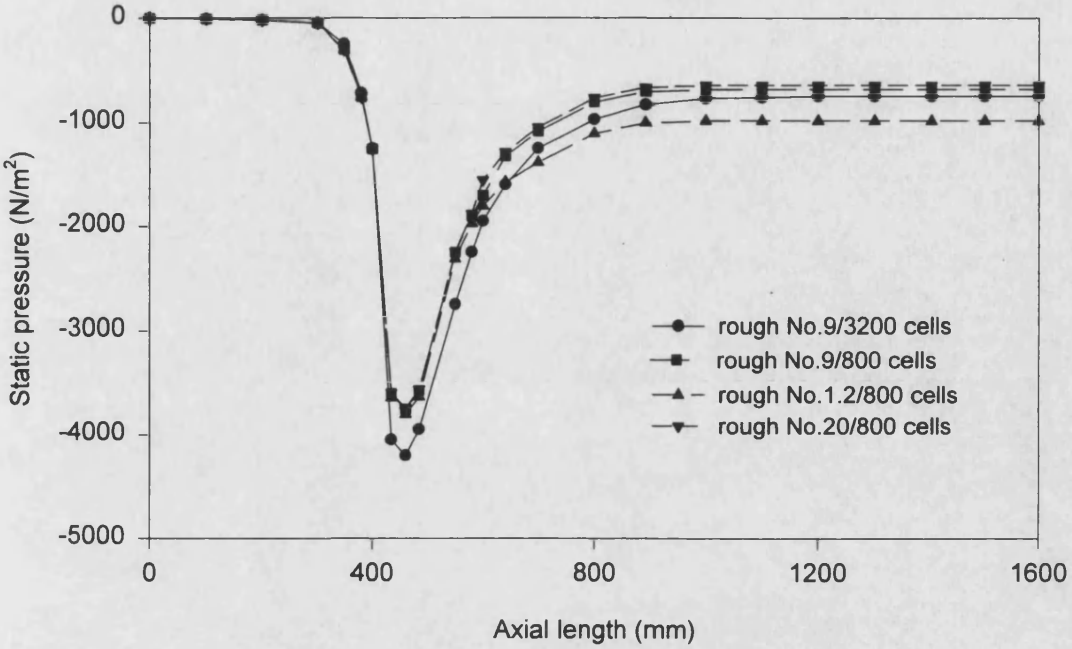

Figure 2.3 Pressure distributions along the venturi tube with different boundary condition settings and mesh densities

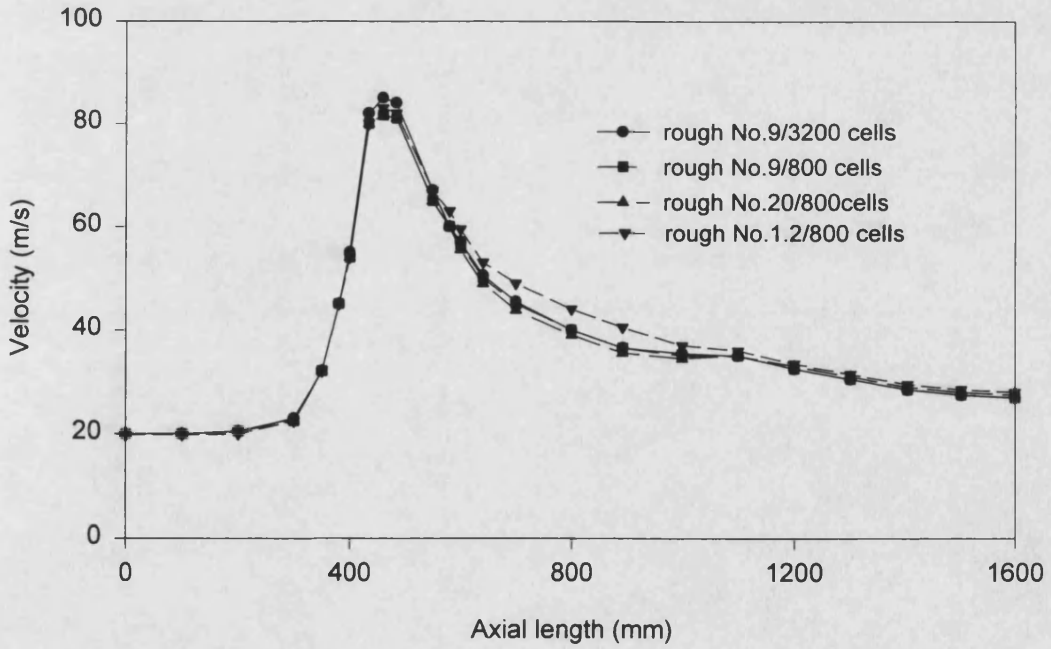

Figure 2.4 Velocity distributions along the venturi tube with different boundary condition settings and mesh densities

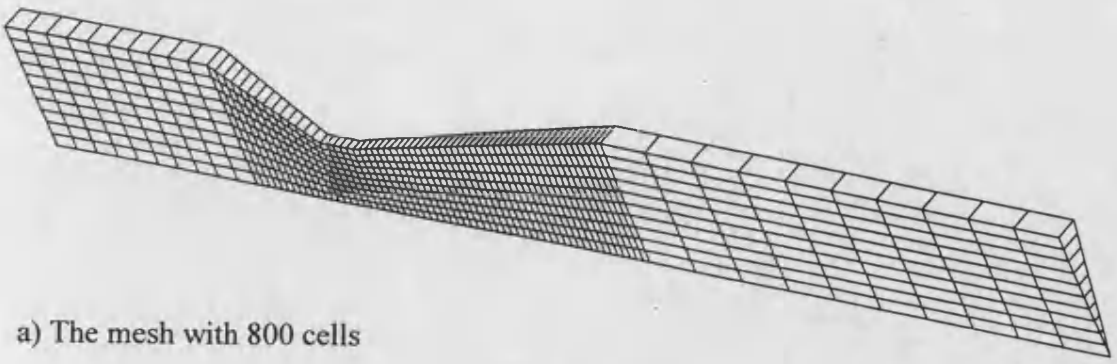

a) The mesh with 800 cells

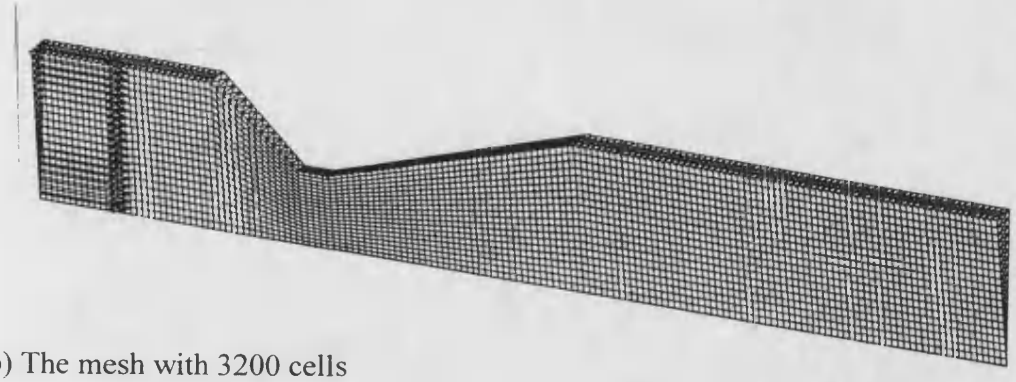

b) The mesh with 3200 cells

Figure 2.5 Computational models of the venturi tube with different cells numbers

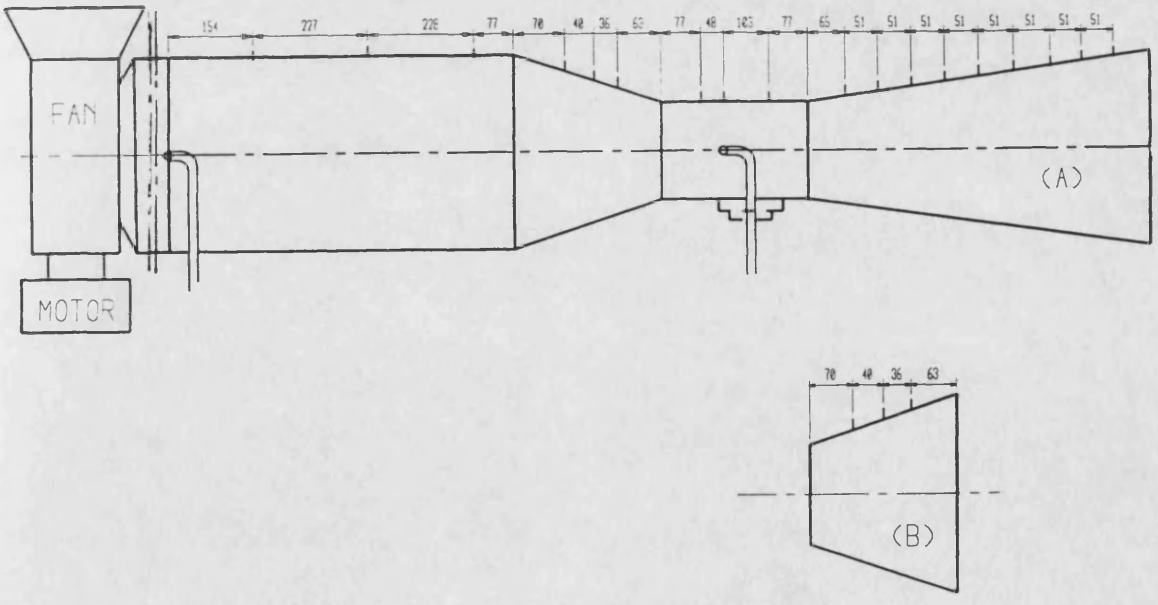

Figure 2.6 Duct flow test rig with different diffusers

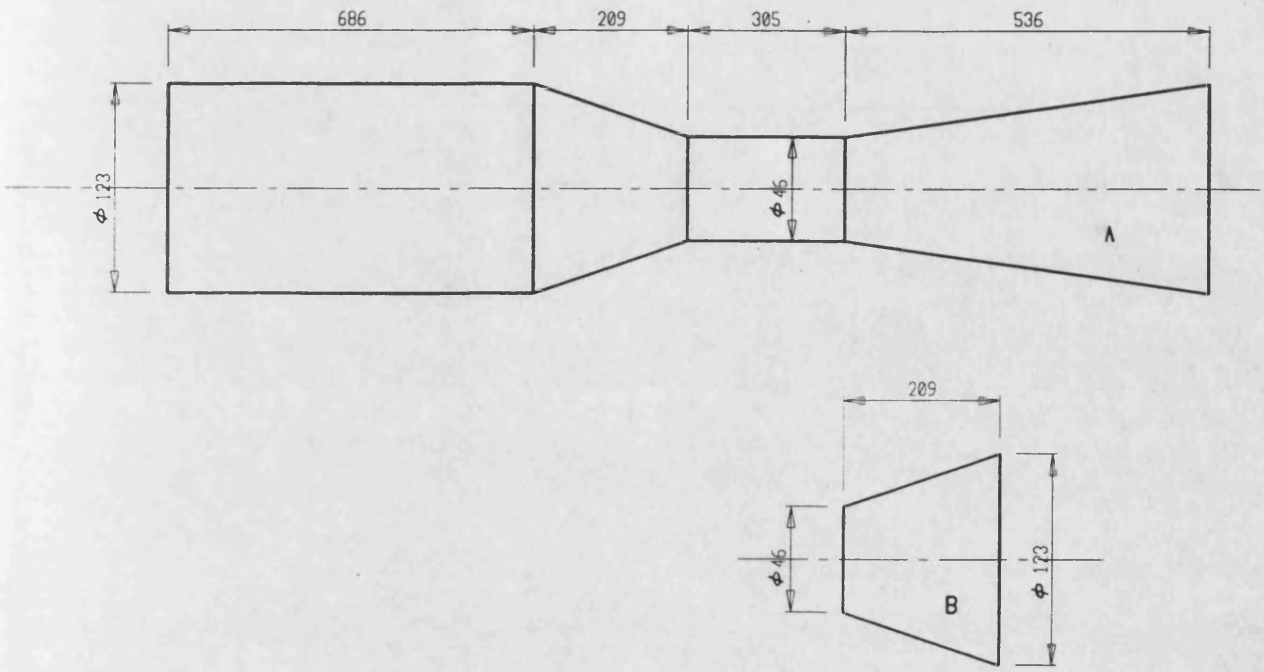

Figure 2.7 Configurations of the diffusers

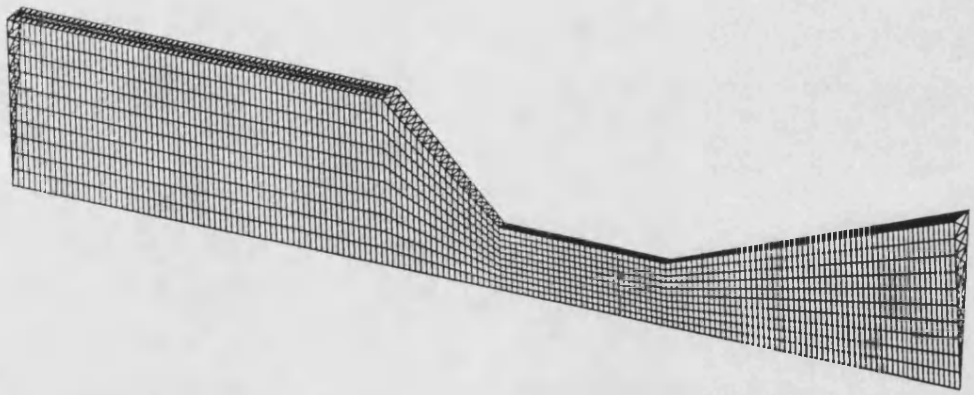

Figure 2.8 Computational model of the diffuser A

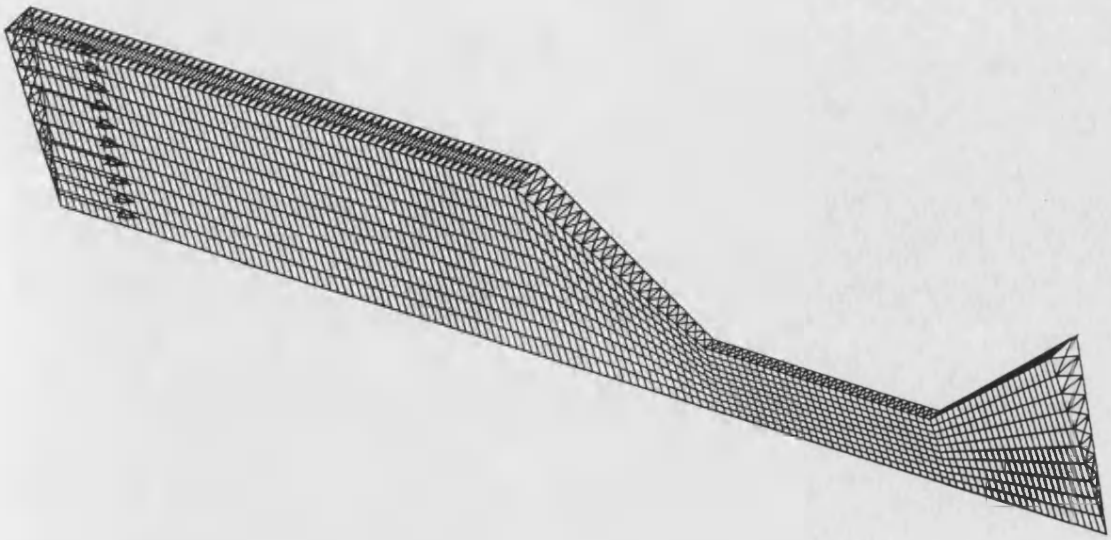

Figure 2.9 Computational model of the diffuser B

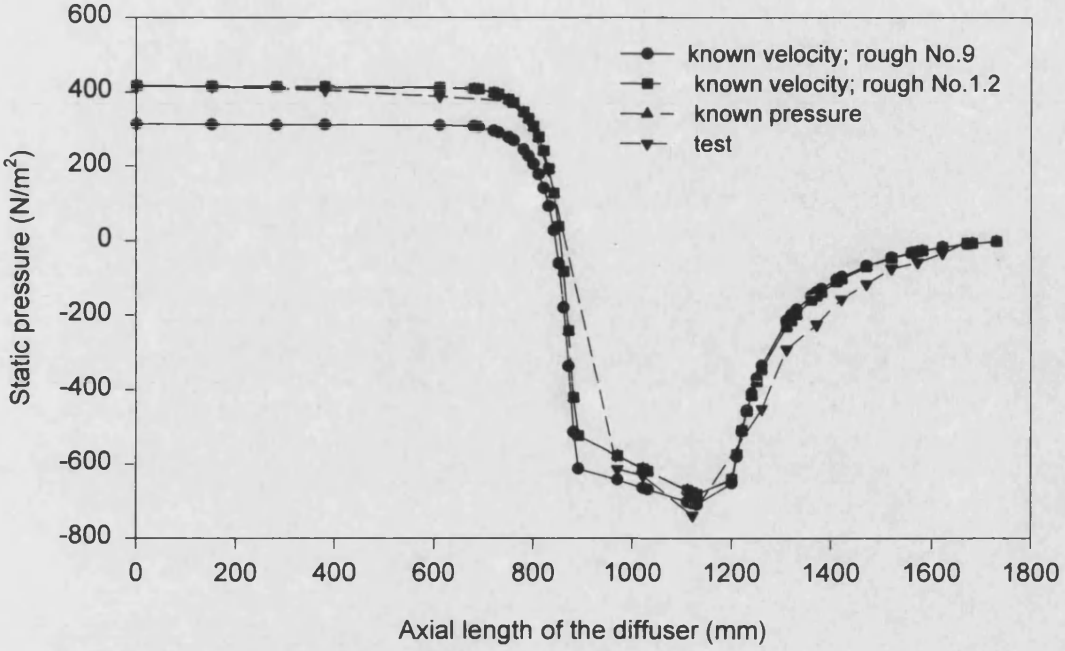

Figure 2.10 Comparison of pressure distributions along the diffuser A

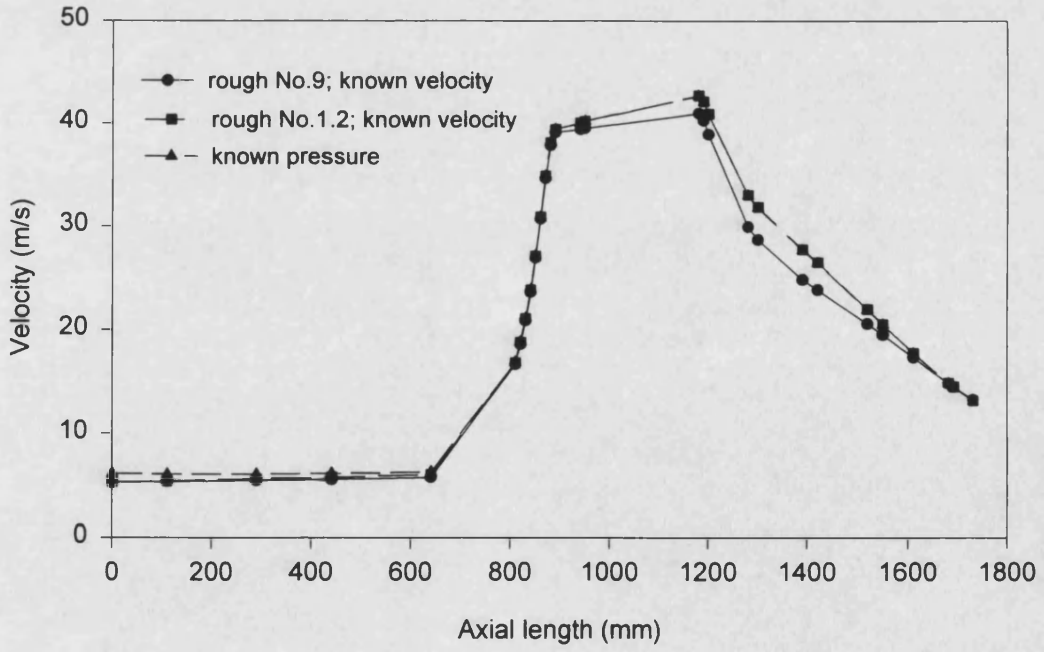

Figure 2.11 Velocity distributions along the diffuser A with different upstream boundary settings and wall roughness numbers

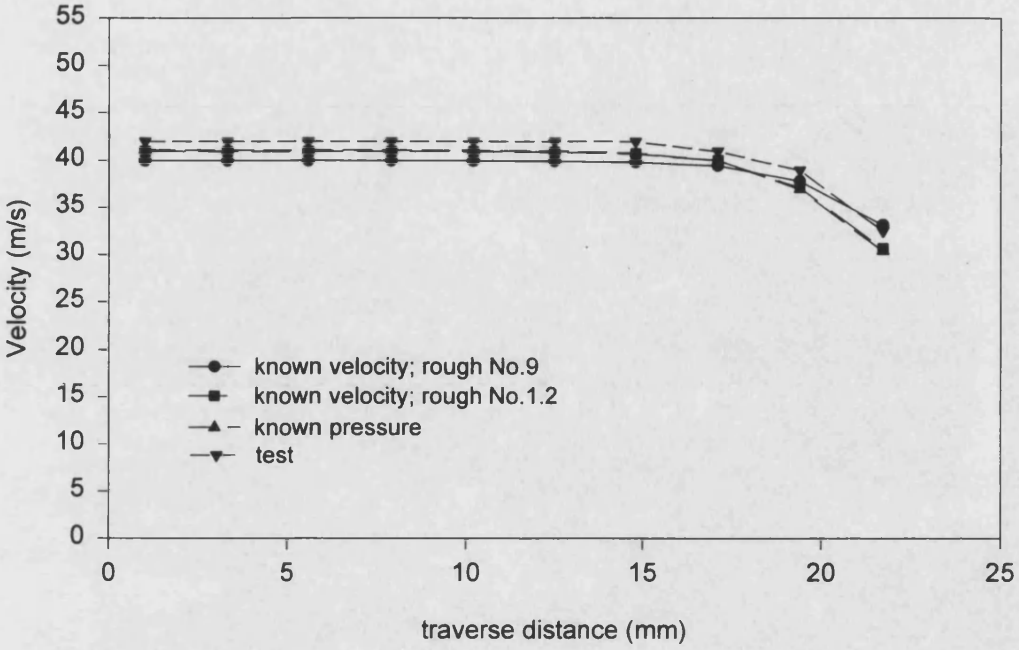

Figure 2.12 Comparison of traverse velocity distributions across the throat section of the diffuser A

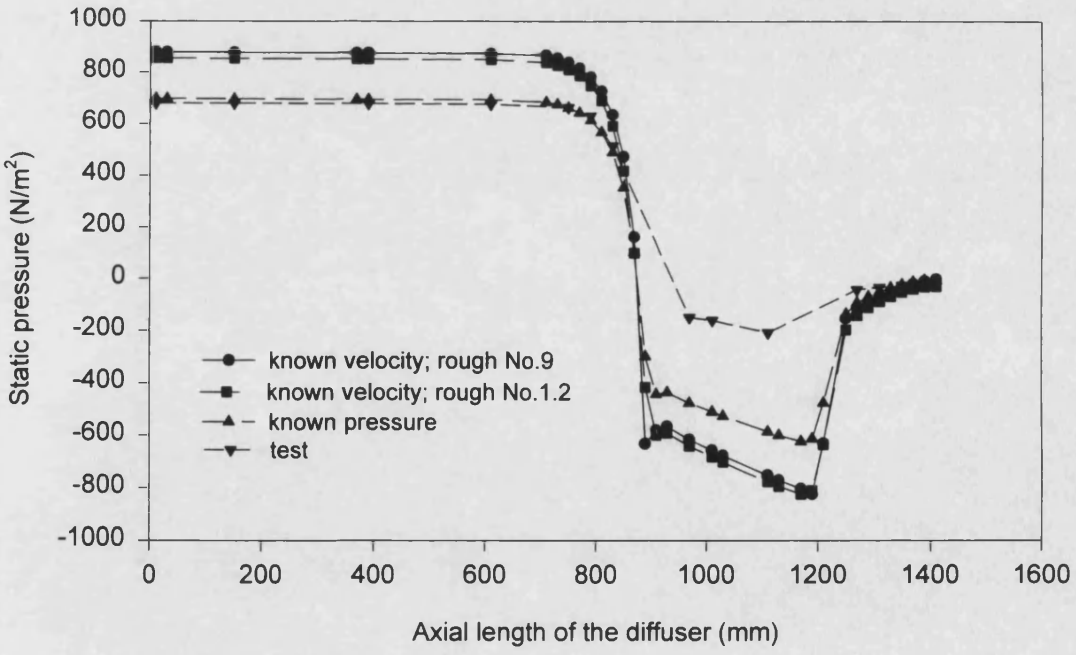

Figure 2.13 Comparison of pressure distributions along the diffuser B

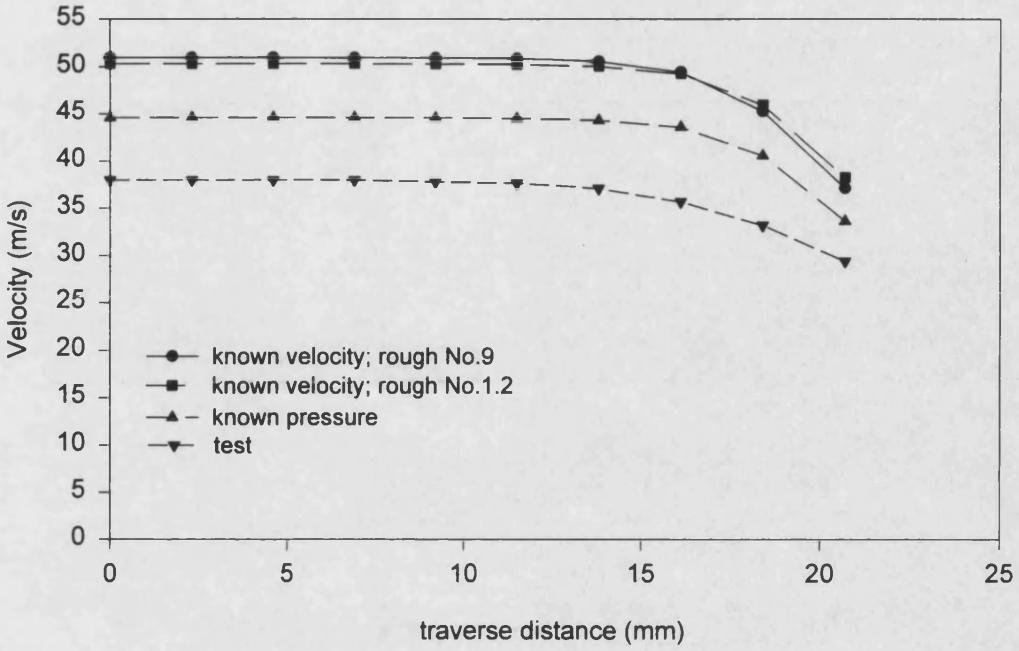

Figure 2.14 Comparison of traverse velocity distributions across the throat section of the diffuser B

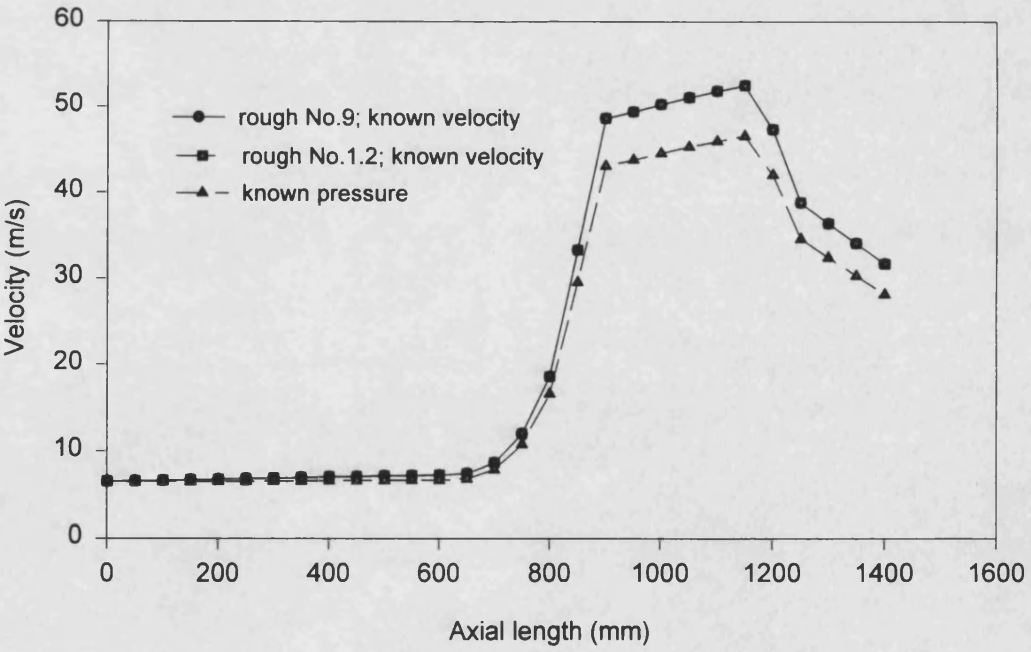

Figure 2.15 Velocity distributions along the diffuser B with different upstream boundary settings and wall roughness numbers

3 Prediction of mixture formation in venturi type gas-air mixers

3.1 Introduction

As in engines fuelled with conventional fuels, the carburettor of a natural gas engine has a duty of supplying the engine with a metered amount of fuel and air. Not only the overall mixture air fuel ratio, but also the mixture concentration distributions have a profound effect on ignition of the mixture and propagation of the flame in the engine combustion chamber and hence on the engine performance and emissions. The quantity and quality of the fuel air mixture must be appropriate to different engine operating conditions. Relatively small deviation from the demanded characteristics of the carburettor may depreciate the engine power and economy noticeably and increase exhaust emissions substantially. It is a widely accepted fact that throttle controlled SI engines fuelled with gaseous fuels like natural gas have the disadvantage of lower volumetric efficiency, which reduces the engines specific power output or power capacity. To offset this disadvantage, a reduction of flow restriction throughout the intake system is very important. Thus a homogeneous mixture prepared with a low flow restriction at the correct air fuel ratio over the engine operating range is essential to minimise emissions from natural gas engines while maintaining good engine performance and fuel economy. However, to meet all of these requirements in one mixer is very difficult because of their inherent contradiction. For example, high turbulence intensity which aids the mixing of air and fuel will increase flow resistance and hence the pressure loss. Therefore optimisation of design parameters such as dimensions of a mixer becomes very important throughout the design process in order to achieve a successful development of the gas-air mixer. Traditionally, the design parameter optimisation is based on component prototype testing and modification. Today the testing method is still an invaluable tool of the component development, but it is time consuming and expensive and often can not give a clear explanation of the observed phenomena. Apparently, the mixing behaviour between the two species in all of the existing gas-air mixers is governed by the fluid dynamics, not by mechanical impellers, as often used in chemical mixers. Therefore the newly emerged CFD technique offers another possible approach for the study of the flow behaviour under different configurations of the flow domain.

The objective of this study was to use the validated STAR-CD CFD code to simulate the mixture development process within a conceptually designed mixer under normal engine operating conditions. With the computer visualised flow dynamics and mixture concentration distributions, the mechanism governing the performance of venturi type gas-air mixers was better understood. A computational investigation into the effect of design parameter changes on mixture formation was conducted for this type of mixer.

The findings were very helpful in the novel mixer design and development process. Details of the study and its findings will be reported in the following sections of the chapter.

3.2 Preliminary design of the mixer

To aid the novel mixer design for a stationary natural gas engine, a study of the existing mixers in various kinds of natural gas engine carburettors was conducted. To do this, three proprietary mixers were purchased and each of them represented one of the commonly used mixers. They are the variable restriction type, the fixed orifice type and the venturi type. Their basic configurations have been schematically shown in Figure 1.5. These proprietary mixers were firstly analysed and then experimentally evaluated [138].

The variable restriction type mixer, or the I-mixer, is a non-symmetrical design, as the inlet and outlet are at 90 degrees to each other. It has flow dependent restrictions in both the air and gas streams. A valve plate restricts the air flow, and supports a gas metering valve in the gas stream. As the air flow increases, the low pressure in the restriction is used to produce a pressure drop across the diaphragm and valve plate and lift it upwards against an opposing spring. This produces increased flow areas for both the air and gas flows. The high flow restriction at low flow rates is unimportant since otherwise the flow would need to be further throttled by the throttle valve instead. Control of air fuel ratio supplied to the mixer with increasing flow is mainly controlled by the ratio of flow areas for the air and gas flows. By changing the shape of the gas metering valve it is possible to alter the air fuel ratio schedule that occurs with flow rate variations. Due to the pressure changes in the gas main, especially when containers are used, a pressure regulator is inserted to regulate the gas supply pressure. The regulator has the same effect as the float chamber valve in a petrol engine carburettor. To cope with different throttle opening positions, an impact tube is connected between the inlet of the mixer and the regulator. This keeps the regulated gas pressures consistent with the air inlet pressures under all engine operating conditions.

The fixed orifice type mixer, or the H-mixer, is also a non-symmetrical design. The gas signal, which is the pressure difference between the air at the orifice and the gas in the supply passage, is produced by accelerating the flow through a restriction. Gas is admitted by a narrow slot around the inner edge of the orifice. This slot width can be adjusted by a stepper motor to provide external control of the air fuel ratio supplied to the mixer. In this design, some of the flow energy is converted into turbulence as the air passes through the restriction, which is to aid mixing of the gas and air, but as a result,

pressure loss is increased. Flow through this mixer is not symmetrical as the inlet and outlet are at 90 degrees to each other, as with the I-mixer. Provision is made for adjustment of the restriction width to accommodate different engine flow requirements.

The fixed venturi type mixer, or the D-mixer, is a symmetrical design. A difference between the gas pressure and the static pressure at the venturi throat is produced as the flow is accelerated through the throat of the venturi. The difference, i.e. the gas signal, sustains and regulates the flow of fuel. The gas signal is a function of the air velocity and the gas pressure. Because the air velocity is determined by the geometry of the venturi and throttle opening positions, an aerofoil shaped cross is placed in the throat of the venturi to further reduce the flow area. This cross divides the air flow into four quadrants and gas is admitted into the air streams in each quadrant by six 1.5 mm holes placed along the surfaces of the winged cross which is connected to the gas supply. This is to distribute the gas more evenly over the air flow. Additional fuel is supplied into the air stream through another three 1.5 mm holes in each quadrant around the circumference of the throat at a upstream section of 6 mm from the throat. This brings the number of gas admission holes up to 36 in total and gives a total gas admission area of 63.585×10^{-6} m^2, which is only 3.24% of the air inlet area and 12.96% of the throat area. Flow through this mixer is symmetrical about its axis. The expansion section beyond the throat maintains an approximately constant expansion rate, which is expected to exhibit good pressure recovery, although the trailing edge of the aerofoil profile is blunt and may incur a wake at higher flow rates. The gas pressure supplied to the mixer is determined by the positions of the control valve and the gas supply pressure from either the gas main or gas container. Thus adjustment of the air fuel ratio can be achieved by using a variable restriction valve fitted in the fuel supply system.

The experience gained in the analysis of proprietary mixers [138] played an important role in designing a novel mixer. The analytical results indicated apparently that the novel mixer should be designed to operate on the venturi principle. To reduce the cost of the development and to prevent non-symmetrical flow patterns in the unit, a symmetrically fixed straight venturi outer body was selected as a gas admission signal producing unit. Gas was admitted into the main air stream at the throat section of the venturi. In order to sustain an adequate amount of gas under the limited gas supply pressure, the pressure depression at the throat section had to be great enough. However, a higher gas signal might lead to a higher pressure loss due to the difficulty in recovering the pressure depression. Thus the factors associated with the gas signal and capability of pressure recovery should be well balanced. A higher gas supply pressure can effect a high enough gas signal without higher pressure depression at the throat section. But for mains gas, the pressure is often fixed and difficult to raise. Thus the pressure depression and the gas discharge area have to be carefully examined in addition

to factors that affect gas discharge coefficient and air pressure recovery. To avoid high pressure loss caused by sharp geometry changes while maintaining a high enough gas signal level, not only the outer body was designed to form a mild venturi but also an inner bulbous obstruction, or "bullet", was placed into the main air stream. The inner bullet was coaxial to the outer body and a symmetrical annular venturi was formed smoothly by the outer body and the inner bullet together in order to increase the pressure depression gradually ahead of the throat and to recover the pressure after the gas was drawn in.

There were several ways to introduce the gaseous fuel into the main air stream. To ease the machining process of the prototype mixer, a single circumferential annular slit on the inner bullet was initially considered. The slit was connected through six holes to a hollow conduit in the bullet. The end of the bullet was threaded onto an elbow pipe through which the fuel was supplied. The slit width was designed to be adjustable by using a threaded stud at the bullet head. The entire bullet assembly could be changed should it be necessary to test a different bullet size. This flexible design would avoid the need to manufacture completely new units during prototype development and enable testing to progress more efficiently.

The principal dimensions of the mixer were decided initially using the knowledge gained from the analysis of the proprietary mixers. The inlet diameter was 50 mm and the diameter at the throat section was 40 mm. The convergent angle was 29° which was the same as the divergent angle of the outer body. The total axial length for the convergent part and the divergent part was 40 mm. The length of the throat part was 50 mm, which gave a long length for mixing. The diameter of the central bullet was 30 mm and its head was a hemisphere with a radius of 15 mm. The cylindrical length of the bullet was 5 mm. The angle of the bullet tail was 21 degrees which was designed to produce an early pressure recovery. A schematic drawing of the initial design is given in Figure 3.1.

3.3 Simulation of mixture formation in the mixer

As with any other computing code, the STAR-CD is a tool which can assist the engineer in gaining a better understanding of physical phenomena. Success or failure of a simulation depends to a very large extent upon the input information such as the geometry of the flow domain, nature of the flow, boundary conditions, etc., provided by the user. Correct definition of the physical problem to be solved is a prerequisite to obtaining the right solution or any prediction at all. The first step should be posed on physical rather than numerical terms.

3.3.1 Problem definition

The nature of the flow in a venturi type gas-air mixer depends largely on both the geometry of the mixer and the engine operating conditions. The characteristic of the flow within a four cylinder engine intake manifold is unsteady. Because each of the four cylinders takes more than 180 degrees in its suction process, the unsteady flow is greatly damped and tends to be steady with slight fluctuations during an entire operating cycle. For the sake of computation cost, the flow was treated as steady flow. The steady flow rates of air and gas under certain engine operating conditions were derived from the engine power outputs. For a 5~50 kW power output engine, the inlet air flow rate was about 0.0145~0.048 kg/s and hence the average steady flow velocities at the inlet surface of the mixer with the dimensions designed were about 6~20 m/s when the air density was assumed to be 1.22 kg/m^3. At any other sections of the mixer, flow velocities were higher than that at the inlet surface because of the reduced flow areas. If the kinematic viscosity of the fluid was 1.51×10^{-5} m^2/s, the Reynolds number of the flow at the inlet surface within the engine operating range would be 1.98×10^4~7.28×10^4, which was far greater than the critical Reynolds number. At the throat section the Reynolds number was also far above the critical one because of the great contribution from the high flow velocity even though the flow characteristic dimension was small. Clearly the flow was turbulent throughout the flow domain.

At low engine output operating conditions, the Mach number of the flow was quite low. However for high output running, the compressibility of both air and gas had to be taken into account in order to increase the computation accuracy. The densities of air and gas were determined using the ideal gas law. So the nature of the flow was steady, turbulent, compressible and the flow was accompanied by a mixing process of two species. The appropriate algorithm and mathematical models related to the nature embodied in STAR-CD were invoked during the simulation.

3.3.2 Geometry modelling

The flow domain of the mixer was apparently a three dimensional axisymmetrical flow except at the area of the elbow gas supply pipe. The elbow pipe was treated as a bullet with a radius equal to the bending radius of the pipe, which was supposed not to affect the flow characteristics in the main part of the flow domain. Thus the flow and the geometry of the flow domain were reasonably simplified and the computation cost significantly reduced. For the axisymmetrical flow only a slice of the domain was considered which can represent the whole flow domain.

To create a set of computation meshes which best described the flow domain, much attention had to be paid to the surface mesh definition to make sure that the boundary topography was adequately characterised. For a cylindrical geometry, the circle was represented by a polygon. In order to minimise the difference between the area of the circle and the area of the polygon, two approaches could be used. One was to cut a thin slice of the domain, for example 10 degrees or smaller. The other was to cut a thicker slice but generating several layers of meshes.

With respect to the mesh density, there were no rigid constraints. To compromise between the cost and the numerical discretisation errors, local refinement was used in the regions of convergence, throat and divergence by defining the same number of cells in the radial direction as that in the inlet and outlet regions. Thus the highest mesh density was at the area where flow dynamics parameters including concentration distribution had steep gradients along and across the flow streamlines. As shown in Figure 3.2, there were 10 cells in the radial direction and 132 cells in the axial direction which were formed by 5133 vertices. The gas admission slit position and its width were accurately defined by its co-ordinates of four vertices which consisted of the inlet boundary for gaseous fuel. A hexahedra shape was chosen to be the predominant cell structure with triangular prisms used in the vicinity of the symmetrical axis.

To ensure that the mesh distortion was within the limit when both the accuracy of the solution and the cost were considered, three factors which measured the mesh deformation, see Figure 3.3, were checked. Aspect ratios of length/height, length/width and width/height for all cells defined were much less than the limit given. Non-orthogonality of those cells, which refers to the degree of departure from 90° internal angle of cell edges, were 90°±5°. They were quite near 90° and much larger than 45° which was the limit of non orthogonality which could be used. Face warp angle of all cells were also within their given constraints.

3.3.3 Boundary conditions definition and turbulence model setting

Boundary conditions definition are probably the main area of difficulty in a CFD application. Problems often come from identifying the correct type of condition; from posing an acceptable mix of boundary types; and from defining appropriate values of boundary variables. These often indicate where to place these boundaries.

3.3.3.1 Boundary regions definition

There were two essential steps to specify the boundary conditions. The first step was to identify each individual boundary with a regional group and a given region ID number.

The region referred to a series of external surfaces of the calculation mesh which had the same flow dynamics features. An individual boundary was defined by indicating a region number and the vertices which made up the cell face. In the flow problem in question, there were eight external surfaces which enveloped the geometric model, see Figure 3.4. They were the upstream air surface, the upstream gas surface, the downstream mixture surface, two split surfaces, inner and outer wall surfaces and the symmetrical axis. It was apparently not necessary to further identify the upstream gas admission boundary which consisted of only one cell in the geometrical model created. And neither was it necessary for the wall boundaries, the two symmetrical boundaries and the symmetrical axis, because those boundaries on the same surface had the same features. Due to the fact that the upstream air surface was directly open to the atmosphere rather than any upstream pipe line, the velocity on the surface was assumed to be uniform. The downstream mixture surface was well behind the recovery part and the cylindrical section of the mixer. Boundaries on this surface were supposed to have the same features. Therefore they did not need to be further divided into different regions. Thus eight boundary regions were defined for the model created.

3.3.3.2 Boundary types definition and conditions specification

The second essential step was to define the type of the boundary conditions for each specified boundary region and pose a value to each variable related. Region one was the boundary region through which air was admitted into the mixer and region two was the region for gas to be admitted. The average velocities of air and gas through their boundary regions were derived from the engine power output. The pressure distribution on the boundary was supposed to be the atmospheric pressure for region one and the fuel supply pressure for region two if the prescribed pressure boundary option was chosen. It was the prescribed inlet velocity rather than the prescribed pressure distribution which was specified for these two regions for the sake of computing time and solution stability. For the engine operating condition simulated (1500 rpm and 100 Nm), the engine power output was about 15 kW with a thermal efficiency of 22%. The gas flow rate was about 0.00118 kg/s and the air flow rate 0.0196 kg/s when a stoichiometric mixture was expected. In the normal atmospheric state the air density was assumed as 1.22 kg/m^3. With the supplied gas pressure and room temperature, gas density was assumed to be 0.68 kg/m^3. Thus the average velocity of air in region one and the average gas velocity in region two which depended on the slit width used could then be specified.

Region three was the downstream mixture boundary region which was connected directly with the intake manifold in the actual applications. The pressure on this boundary region depended on the engine operating condition. It could be calculated

using some especially developed engine performance simulation package such as SPICE. To get the precise value was another area of the simulation work. Because the upstream boundaries had been defined as the prescribed inlet boundaries, this boundary region was simply defined as the outlet with the flow everywhere on the plane outward directed. This was another reason why the upstream boundary regions were specified as prescribed inlet velocity boundaries. The flow features on this plane and cell layers designated adjacent to the plane made it possible for the boundary region to be defined as the outlet. No flow parameters were needed for an outlet boundary specification.

Region four and five were the two interfaces where the calculated flow domains were cut off from the rest of the mixer flow. These two regions were specified as symmetrical planes because of the axisymmetrical flow nature through the mixer assumed above. The components of the air velocity and gas velocity normal to these planes were set to be zero during the inlet boundary definitions. There was no user input required for these symmetry planes.

Region six was the interface between the inner bullet and the flow domain. Region seven was the interface between the mixer outer body and the flow domain. Both of them were defined as non-slip impermeable walls with zero wall velocity and zero chemical species flux. The heat flux across the wall was neglected. Thus the temperature distribution on both sides of the wall did not need to be specified. Wall roughness number which was discussed before was defined as 9.0 for each wall because of the finely machined wall surfaces.

The last region, number eight, was a special region--the symmetrical axis, so only a wedge of cylindrical mesh was modelled. If a full flow domain was created, this region would have automatically vanished. For an axisymmetrical region, there was no user input required. Region specifications posed are listed in Table 3.1. Any external cell face which was not included in a user defined region was, by default, assumed to be a wall with region number zero.

3.3.3.3 Turbulence model setting

No matter which kind of boundary conditions were posed on boundary region one to three, the turbulence key embodied in STAR-CD had to be switched on because of the turbulent nature of the flow. Once the turbulence key was set on, the optional models and their parameters had to be chosen. As described in the previous chapter, there were options available in STAR-CD. Each of the models had its own way to treat the near wall region to deal with the difference of viscous effects and turbulence scales in the neighbourhood of the non-slip wall, the region where the mixing between the gas and

Table 3.1 Boundary region specifications for single inner slit

Region No.	Region Type	Variable Specification
1	prescribed inlet	u=8.2; v=0; w=0; ω=0; I=0.2; *l*= 0.005; T=293; ρ=1.22; scalar 1=0;*
2	prescribed inlet	u=0; v=44.7; w=0; ω=0; I=0.2; *l*= 0.0005; T=293; ρ=0.68; scalar 1=0;
3	prescribed outlet	stream split=1;
4	symmetry plane	/
5	symmetry plane	/
6	impermeable wall	adiabatic; adiabatic;
7	impermeable wall	adiabatic; adiabatic;
8	symmetry axis	/

* where scalar 1 is the concentration of the mixture on the inlet boundary in kg/kg.

air mainly happens. Due to the popularity of the models and the ease of mesh creation, the standard 'k-*l*' model was selected in which the law of the wall was used within the single layer of the mesh. The values of the empirical constants appearing in the model (Eqs. A-II. 21 and A-II. 22), were taken as those recommended in reference [112] and are listed in Table 3.2. There were only two parameters needed for the model. The value of the local relative turbulence intensity which was usually much less than unity. It is a well accepted fact that the turbulence is asymptomatic in pipe flows and each of the turbulence intensity components varies with the radial distance [136]. The experimental flow conditions and pipe radial dimension used in [136] are similar to the upstream section of the mixer. Thus their measured turbulence intensity results were referenced in the turbulence boundary specification. For the mean velocity considered, a mean axial intensity value of 0.2 was specified, which was nearly the average of the measured intensity components (0.1~0.4). The other key parameter needed in the turbulence 'k-*l*' model was the mixing length scale which is usually an order of magnitude smaller than the characteristic dimension of the cross section bounding the duct flow.

Table 3.2 Values of the empirical constants in the k-ε model

C_μ	$C_{\varepsilon 1}$	$C_{\varepsilon 2}$	$C_{\varepsilon 3}$	$C_{\varepsilon 4}$	σ_κ	σ_ε	κ	E
0.09	1.44	1.92	1.44	-0.33	1.0	1.20	0.419	9.0

3.3.3.4 Other boundary conditions description

Apart from the velocities and turbulence parameters defined above, the temperature of the air and the temperature of gas were also posed on the two inlet regions. Both of them were specified as room temperature 20 °C. The density of air and the density of gas on inlet boundary regions at the initial state were posed as being the same as those used during their velocities derivation. Mixture concentration on region one was specified as zero, which meant that no gas existed in this region. The concentration in region two was posed as 1, which implied that there was no air in the gaseous fuel supply system in STAR-CD version 2.1 (in later versions Scalar models were implanted separately).

3.3.4 Fluid properties and control parameters setting

3.3.4.1 Fluid properties setting

After mesh generation and boundary definition, the next step was to specify fluid properties such as viscosity, specific heat, Prandtl and Schmidt numbers. As discussed before, the compressibility factor should be taken into account when considering the high velocity of the flow in the throat area. Both air and gas were treated as perfect gases with the density being a function of both pressure and temperature. The value of laminar kinematic viscosity was set as 1.51×10^{-5} m^2/s, which was the value of air at the ambient condition with 1 atm and 293~300 K. Specific heat at constant volume was set as the default value of 0.719 kJ/kg K. The turbulent Prandtl number was set as 0.9, its default value. The species equation was turned on for the mixing problem and the values of laminar Schmidt number and turbulent Schmidt number were set as 0.5 and 0.9 respectively. The value of the source terms for momentum, turbulence, temperature and reaction equations were ignored in this simulation because they were not relevant to this problem, as also were the values of body forces.

3.3.4.2 Control parameters setting

There are two separate tasks in the setting of the parameters which control the progress of a STAR run. The first is to set the solution parameters, such as the type of solution, the nature of run, the number of iterations, relaxation factors and tolerances used during

the solution. The other is to set the parameters which control the printing of run time output and storage of post-processing data.

When getting into the control module, those default settings were firstly checked. Additional solvers for the temperature and concentration were turned on. The SIMPLE solution algorithm was chosen because of the steady nature of the flow. The second-order central differencing scheme (CD) with a linear factor of 1.0 was used for the density and the first-order upwind scheme (UD) for the rest due to the consideration of both accuracy and stability of the solutions. The number of iterations was allocated as 1000 conservatively. The overall residual tolerance, the value of the relaxation factor and the number of sweep limit used in the solution for each of the variables were set at their recommended values in [112]. The solver tolerance for each of the respective variables was also set at the suggested value. There was no problem of stability encountered during the simulation with these settings. Cell 305 was chosen as the calculation monitoring cell where the flow was very sensitive.

3.3.4.3 Initial conditions setting and data files writing

The initial values of the dependent variables at all mesh points prior to the start of the calculation were set as standard initial conditions because it was the prescribed inlet velocity rather than the prescribed pressure that was assigned for the upstream boundary condition. If the upstream boundary region was defined as the prescribed pressure or if the problem was a transient one, the setting of the initial conditions should be carefully provided, because that would affect not only the speed of the solution but also the course of the solution. In some extreme cases, special techniques had to be employed in order to obtain a reasonable result.

By this stage the pre-processing was completed and the geometric details about the model created were written on file No.08. The problem data like fluid properties and control data were written on file No.10. Before writing file No.08, the SI unit for each of the three dimensions was checked again to decide if unit changes were needed while writing the file. When leaving PROSTAR, all the pre-processing data were saved on file No.16 for later use. After linking the related files, an executable file having a user imposed file name was created with a double precision option selected in order to reduce the round-off errors of the solution.

3.4 Computational results and analysis

After successful running of STAR, PROSTAR which was used for pre-processing needed to be run again for data post-processing and analysis of the results. With the data

file resumed and the result file loaded, both scalar data and vector data were stored in the memory for printing, plotting and manipulating. There were several variable distributions which could be post-processed by the CFD package. When the vector data were requested, the data of the cells should be stored. When the scalar data were needed, it was the data of vertices rather than the cells that should be invoked. To make the computational results directly comparable to those of the experimental results, the concentration distribution of the gas-air mixture across the outlet boundary was converted into air fuel ratio (AFR), the term commonly used in internal combustion engine performance. At the same outlet plane, the velocity distribution was also printed during the post-processing. In order to assess the mixer performance another important performance criterion, the pressure loss across the mixer, was calculated as well.

The vector velocity distribution given in Figure 3.5 showed that the maximum velocity was 35.5 m/s in the throat area of the mixer. In the vicinity of the central bullet after the gas was admitted, the velocity was lower than that of the area adjacent to the outer body. The magnitude of velocity distribution given in Figure 3.6 showed the same pattern. The pressure distribution, see Figure 3.7, stated that stagnation appeared on the front area of the bullet, which gave a positive pressure. The depression in the throat area was about 1100 N/m^2 and the lowest pressure was at the place just after the gas admission slit. The pressure depression recovered greatly after the divergent section of the mixer. The static pressure loss across the mixer was about 348.5 N/m^2 for the operating condition simulated.

The converted concentration distribution, mixture air fuel ratio, given in Figure 3.8 showed that the mixture was very rich in the neighbourhood of the slit area and thereafter. Most of the gas admitted was gathered around the central bullet. On the outlet plane of the mixer, the mixture was still very rich in the central area and very lean in the area near the outer body. It was believed that the ejected gas had a small momentum flux which made it difficult for the gas stream to penetrate into the main air flow which had a large momentum flux. Even when the slit width was designed as 0.41 mm and the gas inlet velocity reached a value of 44.7 m/s, the momentum flux of the gas flow was still about ten times smaller than that of the air flow. The main part of the gas flow was squeezed to the flow between the main air flow stream and the bullet with a portion of the gas mixed by diffusion into the air on the interface between the two species.

The perpendicular gas flow had an effect on the air flow as well. The air stream in front of the slit was pushed outwards by the gas flow. This was the reason why the lowest pressure within the throat area appeared just downstream of the slit. The gas flow direction was bent by the air flow stream, which greatly changed the gas flow

momentum flux in the axial direction. This was the reason for the non-uniform velocity distribution across the mixer downstream, as shown in Figure 3.9.

To verify the analysis above, another simulation was carried out with the same geometric model and the same boundary conditions except that the gas admission slit was closed by defining the cell face as part of the inner bullet wall. The result showed that the velocity distribution in the throat area and downstream was much more uniform than that with the gas induced through the slit. The maximum velocity of the main flow was reduced. The pressure depression in the throat area was reduced to about 568 N/m^2 and the place where the lowest pressure appeared was also moved to the transitional area between the convergent and the throat sections. This meant that the assumed gas blocking effect did exist. The gas flow stream influenced not only the pressure depression, but also the pressure loss across the mixer.

3.4.1 Effect of gas slit positions on mixture formation

According to the analysis conducted, it was predicted that if the gas admission slit was placed in the outer body instead of the inner bullet, the pressure loss across the mixer would be the same. The velocity distribution downstream would be higher in the central area and lower in the outer annular area where gas accounted for the majority of the mixture. A lean mixture was expected in the central area and a rich mixture in the area near the outer body.

To confirm this prediction, a new geometric model was created with the gas slit placed in the outer annular body, see Figure 3.10. The boundary regions definition and the boundary conditions specification were identical to the previous one, except that the gas admission velocity was reduced because the slit diameter was increased from 30 mm to 40 mm. The gas inlet velocity was 33.5 m/s for the gas flow rate simulated. All other settings and definitions were identical to that of the inner slit calculation. The computational results given in Figures 3.11 to 3.13 indeed verified the analysis above. The maximum velocity was 38.01 m/s which was slightly higher than that at the inner slit, because the slit was located at the transition between the convergent and the throat sections. The lowest pressure was -1165 N/m^2, which was at the location just downstream of the slit. This further demonstrated the existence of the gas blocking effect. The pressure loss across the mixer was 345.2 N/m^2, which was nearly the same as that of the previous inner slit. The mixture homogeneity was slightly worse than that of the inner gas slit placement because of the rear configuration of the central bullet and the divergent dimension of the venturi tube type outer body. The concentration distribution for the outer gas slit design, shown in Figure 3.14, was exactly the reverse of that for the inner gas slit design.

3.4.2 Effect of gas slit widths on mixture formation

Further simulations were conducted by using the geometric models similar to those used above but with wider gas inlet slit width. Instead of 0.41 mm, the slit width was increased to 1.25 mm for these further computations. For the same mixture strength and the same slits diameters, a wider slit reduced the gas inlet velocities for both the inner and outer slits if the mixture air fuel ratio was kept constant. Apart from this, there was no other difference in the simulations with a wider slit. The computational result showed that the pressure loss across the mixer was 293.6 N/m^2 for the inner one and 291.6 N/m^2 for the outer. These were slightly reduced because of the lower gas inlet velocities and hence the weaker blocking effect. All other parameters of interest and their distributions showed tiny differences from those with a narrower slit width. The mixture air fuel ratio distribution and the velocity distribution in the mixture outlet plane are given in Figures 3.15 and 3.16 together with the results of the mixer having a narrower slit width.

These graphs clearly showed that the gas admission slit width did not affect the mixture formation. The reason was believed to be the momentum flux ratio between the main air stream and the gas flow drawn into the air flow. When the slit was enlarged from 0.41 mm to 1.25 mm, the gas flow velocity was reduced from 44.7 m/s to 14.66 m/s for the inner one and from 33.5 m/s to 10.98 m/s for the outer one. With such a great gas admission velocity difference, however, the ratio of air flow momentum flux over the gas flow momentum flux was still of the same order, which is one order of magnitude larger than unity. As long as the mixture air fuel ratio and the gas density remain of the same order of values, the momentum flux ratio which dominates the mixture formation of venturi type mixer will be in the same order.

3.4.3 Effect of gas slit numbers on mixture formation

To improve the mixture quality, two other approaches were tried. One of them was to increase the contact interface area between the two species. The other was to enhance the mass transfer coefficient. With regard to the increase of the interface area in the prototype mixer, an effective way was to place two gas admission slits on both the inner bullet and the outer body. Simulation was conducted for this design concept. The implemented configuration of the concept and its CFD computational model created are given in Figures 3.17 and 3.18. Both slits were of the width of 0.41 mm at first. Then the width was widened to 1 mm and 1.25 mm for the two slits. To avoid the effect exerted on the pressure distribution by the convergent section of the venturi body, the outer slit was moved downward to the position where the pressure depression was at the same level as that at the inner gas slit. In addition to the eight boundary regions used for

the single slit geometrical model, one further region was added for gas inlet flows. The gas inlet velocities through the two slits were treated as equal, assuming that the gas supply pressure drops across the two slits were identical. With the gas flow rate simulated, the gas admission velocities were 19.16 m/s, 7.8 m/s and 6.28 m/s respectively for slits width of 0.41 mm, 1 mm and 1.25 mm. All other boundaries and parameters specifications were set to be the same as those used in the previous single slit simulations, see Table 3.3 for the slit width of 0.41 mm. When the gas slit widths were widened to 1 mm and 1.25 mm, the region definition differences were in the region of 2 and 3. The gas admission velocities through the two slits changed to 7.8 m/s and 6.28 m/s.

Table 3.3 Boundary region specifications for double slits (0.41 mm)

Region No.	Region Type	Variable Specification
1	prescribed inlet	u=8.2; v=0; w=0; ω=0; I=0.2; * *l*= 0.005; T=293; ρ=1.22; scalar 1=0;
2	prescribed inlet	u=0; v=19.16; w=0; ω=0; I=0.2; *l*= 0.0005; T=293; ρ=0.68; scalar 1=0;
3	prescribed inlet	u=0; v=-19.16; w=0; ω=0; I=0.2; *l*= 0.0005; T=293; ρ=0.68; scalar 1=0;
4	prescribed outlet	stream split=1;
5	symmetry plane	/
6	symmetry plane	/
7	impermeable wall	adiabatic; adiabatic;
8	impermeable wall	adiabatic; adiabatic;
9	symmetry axis	/

The velocity distributions on the mixture outlet plane are given in Figure 3.19. The results showed that the velocity distribution was much more uniform than that of the single gas slit. However because of the gas blocking effect, the near wall friction effect and the mixture concentration difference, the velocities in the vicinity of inner bullet and outer body were lower than that in the middle annular area between the two walls. This can also be clearly seen from the velocity magnitude distributions given in Figure 3.20 for the mixer with different gas slit widths.

When two gas slits were used, pressure distributions did not change very much, no matter which slit width was used, see Figure 3.21. The pressure depressions were slightly reduced. The computed static pressure loss across the mixer was 284.23 N/m^2 for the slit width of 0.41 mm, 266 N/m^2 for 1 mm and 251.33 N/m^2 for 1.25 mm. The wider the gas slit, the lower the gas admission velocity, and the lower the static pressure loss across the mixer. Compared to the pressure losses in the single gas slit design, the two gas slits reduced the loss by 15%, which is a very favourable aspect of the two slits design.

The mixture concentration distributions with different gas slit widths within the flow domain are given in Figure 3.22 and the mixture air fuel ratio distributions on the outlet plane are given in Figure 3.23. The mixture was rich in the central area of the mixer and also in the area near the outer body of the mixer, because the two slits drew the gas into the mixer from both sides. In the annular area from radius of 7.5 mm to 18 mm the mixture was on its lean side. The leanest mixture appeared at the area where the radius was about 15 mm because it was difficult for the gas from both slits to be transferred into this part. Even though the mixture strength distributions were not perfect with the two gas slits design, the mixture homogeneity had been greatly improved compared to the single gas slit design no matter what slit width was used. This means that the increase of interface area between the two species is a very effective way to improve the mixture formation in venturi type gas-air mixers.

3.4.4 Effect of inner bullet dimensions on mixture formation

The mixture formation was shown to be very sensitive to the interface area between the two species. The two gas slits design gave an acceptable mixture homogeneity with a bullet diameter of 30 mm. But with a single venturi type mixer, it was very difficult to increase the area further just by increasing the number of gas slits. One possible way to further increase this area was to use the double venturi principle which is often used in high performance petrol engine carburettors. Another approach as mentioned above was to increase the turbulence intensity by enlarging the inner bullet diameter. High turbulence gives high mass diffusion transfer rate, which would result in a more homogeneous mixture. The enlarged bullet diameter would increase the inner gas flow area as well. The shortened distance between the two slits would make it easier for the gas flows to penetrate into the far area of the main air stream. Of course the pressure loss across the mixer would be increased. The idea was implemented by using an inner bullet with 33 mm in diameter.

A computational model was created for this new version of the design. The model was quite similar to the previous one which had two gas slits with a width of 1 mm on both

sides. Boundary regions were defined in the same way as before. The only difference in the region specifications was the gas admission velocity because of the change of the inner slit area. The simulation result showed that the maximum velocity in the throat area of the mixer was 49.19 m/s, a very big increase compared to that of the 30 mm one which was 35.45 m/s. The pressure depression in the throat was increased too, from 892 N/m^2 to 1730 N/m^2, and so was the static pressure loss across the mixer, which was from 248.9 N/m^2 for the 30 mm one to 522.6 N/m^2 for the 33 mm. The pressure loss was nearly doubled. Because of the enhanced turbulence, the mixture homogeneity was improved. This can be clearly seen from its air fuel ratio distribution on the mixture outlet plane given in Figure 3.24. The pattern of these distributions were the same as those with the 30 mm inner bullet.

From Figure 3.24 it can be seen that the mixture strength distribution was still uneven at the outlet plane of the mixer. The reason was in the different circumferential areas between the two gas slits. The outer slit had a larger diameter than the inner one. To adjust this, a small width was used for the outer gas slit, which changed the mixture strength distribution. To show this, the geometrical model created for the 33 mm bullet was modified and the boundary region definitions were re-specified. The outer slit width used in the new simulation was 0.5 mm. The inner gas slit was kept unchanged. The results showed that the static pressure losses across the mixer were slightly changed after the outer gas slit width was narrowed. The maximum velocity, the turbulence kinetic energy and its dissipation rate did not change with the different gas slit widths. The mixture air fuel ratio distributions on the outlet plane were affected. When 0.5 mm was used for the outer slit width and 1 mm was used for the inner slit, a rich mixture gathered in the central area and a lean mixture in the area of the outer body.

The increased bullet diameter improved the mixture homogeneity but with an increased pressure loss. A trade-off between the pressure loss and the mixture homogeneity had to be made. Thus a bullet diameter of 32 mm, rather than 33 mm, was tested. A new computational model was created in which the inner bullet diameter was 32 mm and the gas slits width was 1 mm. The computed result showed that the static pressure loss was 458.7 N/m^2, which was better than that for 33 mm bullet. The mixture strength distribution was nearly the same as that for the 33 mm bullet design, see Figure 3.24. Other values of interest were at the same level as those for the 33 mm inner bullet.

3.4.5 Effect of engine operating conditions on mixture formation

All those simulations above were carried out for the air flow rate of 0.0196 kg/s which corresponds to the engine operating condition of 1500 rpm and 100 Nm. For a higher operating speed or load, the air flow rate and the gas flow rate will increase. To see the

effect of the air flow rate on the mixture formation, two other simulations with higher air flow rates which relate to higher engine output were conducted. One of them was for the 33 mm bullet diameter design and the other was for the 30 mm. The air flow rate of 0.0508 kg/s, which was for the engine to run at about 2000 rpm and 200 Nm, was used for the former one and 0.0677 kg/s was used for the latter when over load was expected for the engine. For the 33 mm diameter bullet, the two gas slits widths were 1 mm and for the 30 mm the two widths were 1.25 mm. After modification of the geometrical model, the boundary region specifications were re-posed and the computer was run again. The results of both calculations showed that the mixture strength distributions on the outlet plane of the mixer changed little with different air flow rates simulated. This can be seen from Figure 3.25. The explanation for this is the same as that given for the different gas slit widths. Within the engine operating range the momentum flux ratio of the air and gas flows, which governed the mixing feature, was of the same order. The difference resulted from the high turbulence generated. Thus the mixture homogeneity stayed unchanged within the engine operating range. The velocity distributions given in Figure 3.26 showed that the high mixture mass flow rates resulted in high velocities on the plane. Its maximum velocity in the throat area was very high too. The static pressure loss across the mixer was significantly increased for the high flow rates. The loss was 251.3 N/m^2 for air flow rate of 0.0196 kg/s and was 3163.9 N/m^2 for 0.0677 kg/s when the bullet diameter was 30 mm and the two gas slits widths were 1.25 mm. With the one whose bullet diameter was 33 mm and gas slits width was 1 mm, the pressure loss was 522.6 N/m^2 for the flow rate of 0.0196 kg/s and 3831 N/m^2 for 0.0508 kg/s. This was because of the high friction between the mixture and the mixer body.

3.4.6 Effect of inner bullet nose on mixer flow restriction

In all of the simulations discussed above, the inner bullet nose was of a hemispherical bulbous shape around which the flow obstruction was suspected to exist from the pressure distribution results. If the bulbous nose had been replaced by a pointed one, the flow restriction through the nose and the entire mixer would have been less than that had been obtained. To prove this, three pointed inner bullet noses were designed and simulations were performed for each of them. Their CFD geometrical models are given in Figure 3.27. Instead of improvement of the flow restriction from the nose configuration A, the restriction deteriorated from the pressure loss of 378.68 N/m^2 for the bulbous one to 396.6 N/m^2. The reason for this was that the flow at the transient section between the convergent part and the throat part was directed towards outer area of the circumference by the nose. The flow direction change in this area caused an increase of turbulence, which tended to increase the friction and the pressure losses across the mixer. Though with the subtle pressure penalty, the mixture concentration

distribution did show a little improvement. When the length of the nose was shortened with the same end diameter, as the configuration B, the further increased nose convergent angle dramatically changed the flow stream lines. Consequently, the pressure loss increased further from 396.6 N/m^2 to 456.2 N/m^2 with more mixture homogeneity gain.

In order to eliminate the drawbacks caused by the flow stream line changes, a third nose configuration was designed, as illustrated in model C, which gave a smoothly changing section area that the flow stream line was expected to follow tangentially to the downstream section. The mixture formation within the mixer with this bullet was simulated and results showed that pressure loss was reduced to 386 N/m^2 which was still a little higher than the hemisphere bullet nose. This meant that the flow restriction or the pressure losses across the mixer were not as sensitive to the inner bullet nose shape as was expected.

3.4.7 Effect of venturi outer body on mixture formation

The simulations conducted above were all based on the same annular venturi configuration which was produced by an outer venturi body and an inner bulbous bullet. There was another design option which could also produce an annular venturi just by using one single inner bullet. This design concept was aiming at reducing the manufacturing complexity while seeking for the same mixture quality and flow restriction. One of the easy ways to implement this was to use a straight outer body without any curvature, see Figure 3.28b. The original venturi outer body was replaced by a straight pipe-like body with a diameter of 40 mm which was the dimension at the throat section of the original venturi outer body. All other configurations and dimensions were unchanged. After the geometry modelling, a simulation was performed for the design under the same air flow rate and gas flow rate conditions. Due to the reduced air inlet area, the prescribed air inlet velocity was increased compared to its parent venturi outer body configuration. The results showed that the maximum flow velocity and the turbulence level in the throat area were similar to each other; and so were the pressure losses across the mixers. The mixture concentration distributions on the outlet plane of the mixer is given in Figure 3.29 together with the results obtained from the mixer with the original venturi outer body configuration. It is apparent that the mixture homogeneity was not as good as that from the original venturi outer body configuration. Another simulation was performed with this new design concept but with a pointed inner bullet nose instead of the hemispherical one. There was not much difference between the two different nose shapes for this design either. It can be concluded that straight line venturi outer body design is not a better alternative to the

already quite simple venturi shaped outer body configuration in terms of mixture homogeneity.

3.5 Sensitivity test on boundary conditions settings

Throughout the calculations given so far, two parameters have been kept unchanged and their specifications were based on the estimations. In order to see their effect, a series of values of these two parameters were defined in turn while keeping all others unchanged. Ten turbulence intensity values from 0.01 to 0.6 were tested in turn for the air inlet boundary, gas inlet boundaries and mixture outlet boundary specifications. Five different wall roughness numbers were posed in turn for the wall of the inner bullet and of the outer body. The variables of interest were processed for these tests.

The mixture concentration distributions on the outlet plane of the mixer with different turbulence intensities are shown in Figure 3.30. The mixture air fuel ratio was affected by the turbulence intensity. The higher the intensity, the more homogeneous the mixture tends to be. But when the value was changed from 0.01 to 0.6, that was a sixty times increase, the mixture homogeneity was not improved significantly. The mixture velocity distributions on the same plane for different intensities are given in Figure 3.31, which showed the velocity on this plane was sensitive to the turbulence intensity specified. A higher intensity gave a more uniform velocity distribution on the outlet plane of the mixer. The pressure loss across the mixer was sensitive to the turbulence intensity too, as shown in Figure 3.32. When the intensity posed was lower than 0.1, the pressure loss increased with the decrease of the intensity value. For the value of 0.1 to 0.2 specified, the pressure loss reached its minimum value which was about 510 N/m^2. Once the intensity exceeded the value of 0.2, the pressure loss increased with the intensity again. The reason for this was believed to be the combination of two effects. One was that the high turbulence intensity tended to cause high friction and hence high pressure loss. The other was that the high intensity value gave a more uniform velocity traverse of the mixture, which reduced the friction between the fluid layers and hence reduced the pressure loss. Therefore there was a minimum pressure loss at a certain turbulence intensity value for this kind of mixing problem. The maximum velocity in the throat area of the mixer was unchanged with these different turbulence intensities, see Figure 3.33, because it was mainly governed by the venturi dimensions. The turbulence kinetic energy and its dissipation rate increased with the turbulence intensity because of their inherent relationship.

The results of sensitivity test of the wall roughness numbers are given in Figures 3.34 to 3.38. The air fuel ratio of the mixture on the outlet plane of the mixer was not sensitive to the wall roughness number defined and neither were the velocity distributions on the

plane. The pressure loss across the mixer increased with the increase of the numbers. The maximum velocity in the throat area of the mixer did not change with the wall roughness numbers defined. The maximum turbulence kinetic energy in the mixer changed a little when different numbers were defined. Apparently the smoother the wall surface, the lower the pressure restriction and the lower the turbulence.

3.6 Summary

The fluid dynamics and mixture formation simulations for a prototype mixer were conducted by using the validated CFD package. The geometrical models created, the boundary regions defined, the fluid properties specified, and the control parameters posed had been shown to be very successful by the satisfactory results obtained. With the aid of the computer simulation, flow distributions were visualised within the mixer and the mechanisms governing the performance of venturi type gas-air mixers were better understood. With a fixed order of flow momentum flux ratio between the air stream and the gas stream, it is very difficult for the gas stream to penetrate into the air stream which has a higher momentum flux. Increase of the interface area, the contact time and the turbulence between the two flow streams are essential to achieve a homogeneous mixture. The mixer slit dimensions, positions and numbers all affect the mixture formation. With respect to the mixture homogeneity, the single gas slit concept was unacceptable and the two gas admission slits design gave favourable results no matter what width of gas slit was used.

A parametric study showed that the inner bullet diameter affects both the mixture homogeneity and the pressure loss across the mixer. A compromise has to be made between the good mixture quality and the low pressure loss. The relationship between the flow pattern and the mixture distribution was revealed by the simulation. An asymmetrical air flow pattern will cause a non-homogeneous mixture distribution and the non-homogeneous concentration distribution impairs the flow symmetry downstream of the mixer. Different inner bullet nose and venturi outer body configurations can effect various flow restrictions and mixture homogeneities. But too simple a configuration will give rise to disadvantages on some aspects of the fluid dynamics variables of concern.

Guided by the proprietary mixers study and the CFD simulations, the initial design of the prototype gas-air mixer was finished at this stage with several configuration modifications in mind. Due to the awareness of the drawbacks that the current CFD techniques have, however, the final design decisions can only be made after the CFD analysis has been validated by the pertinent experimental data.

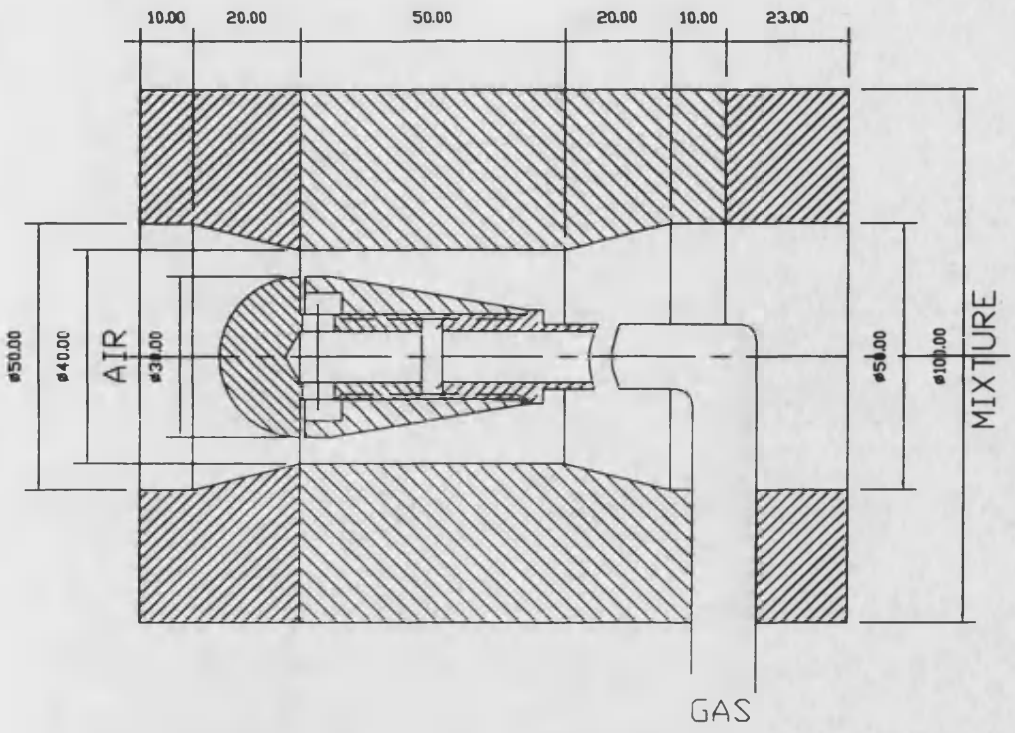

Figure 3.1 Initial design of the gas-air mixer

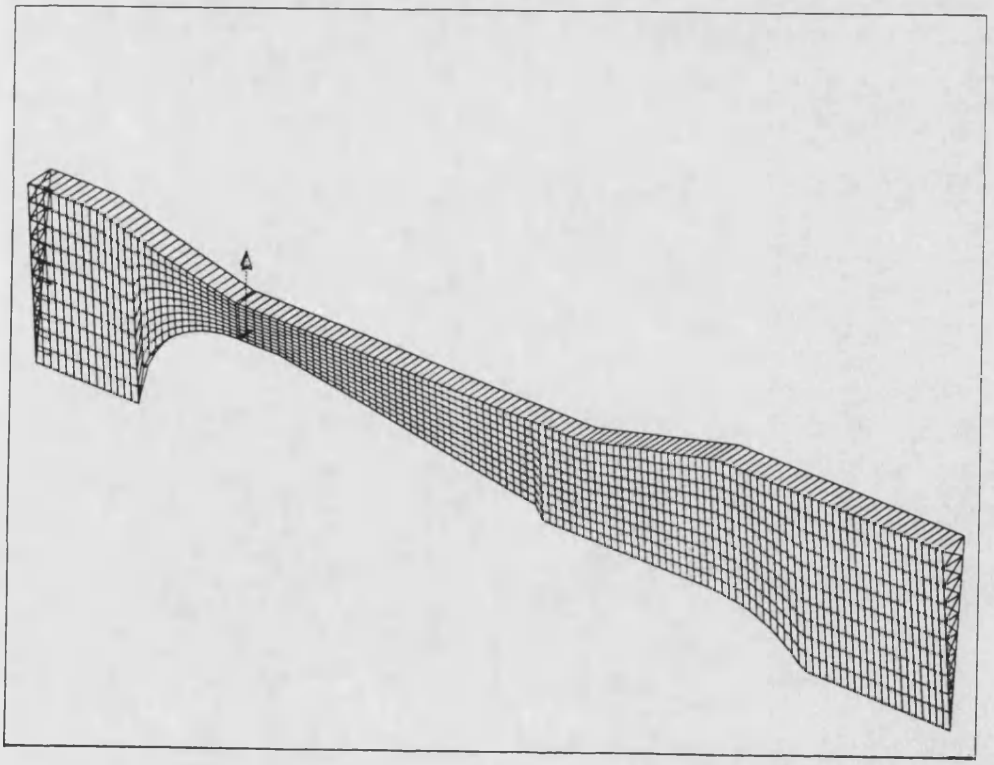

Figure 3.2 Computational model of the mixer with single inner gas slit

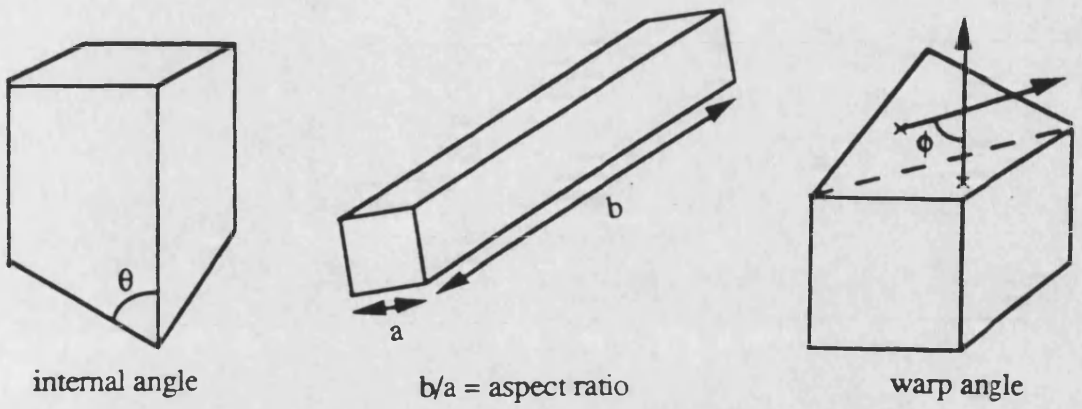

Figure 3.3 Measures of cell deformation

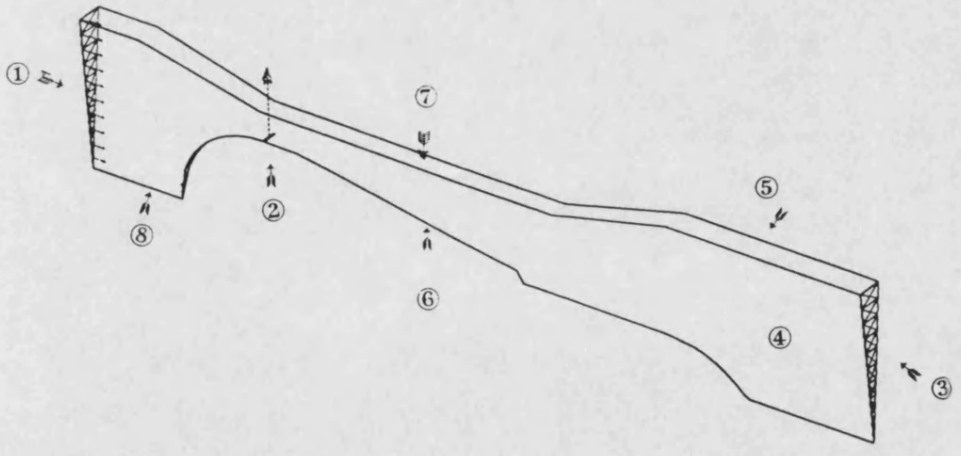

Figure 3.4 Boundary regions definition

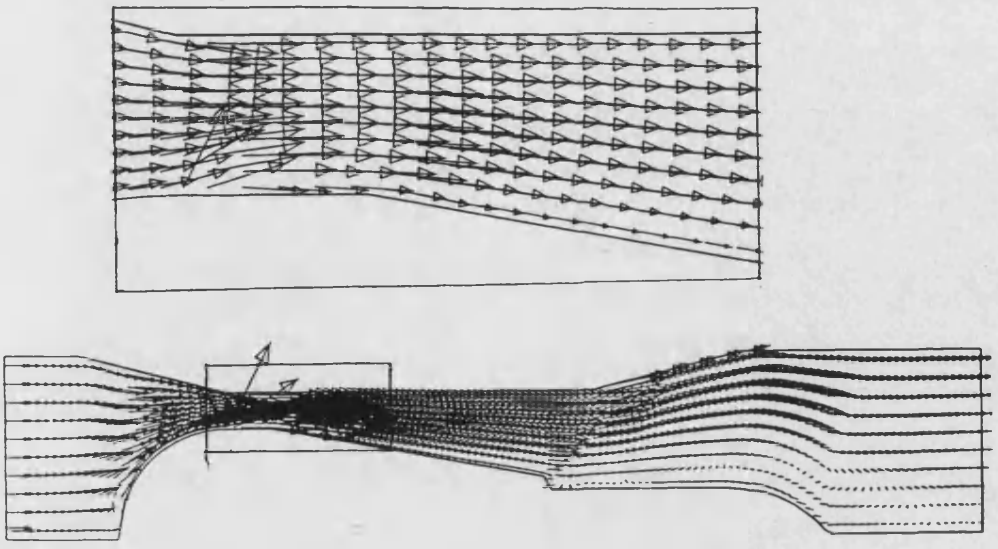

Figure 3.5 Vector velocity distribution of the mixer with single inner gas slit

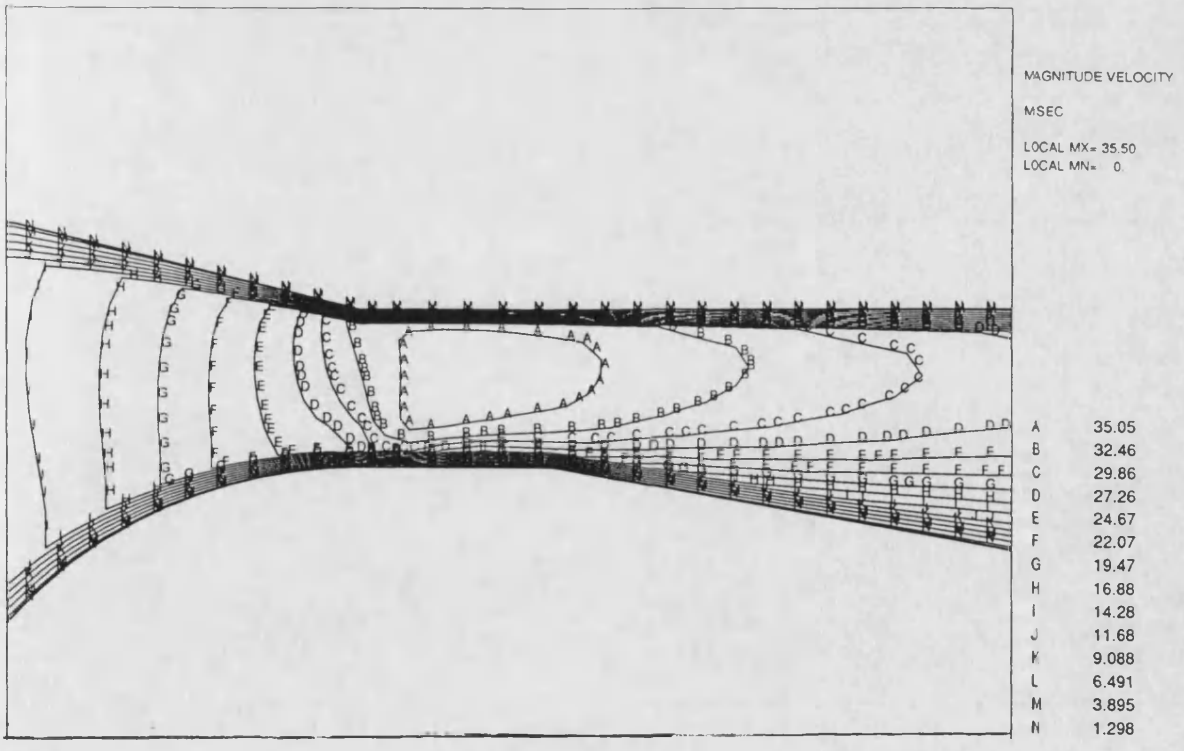

Figure 3.6 Velocity magnitude distribution of the mixer with single inner gas slit

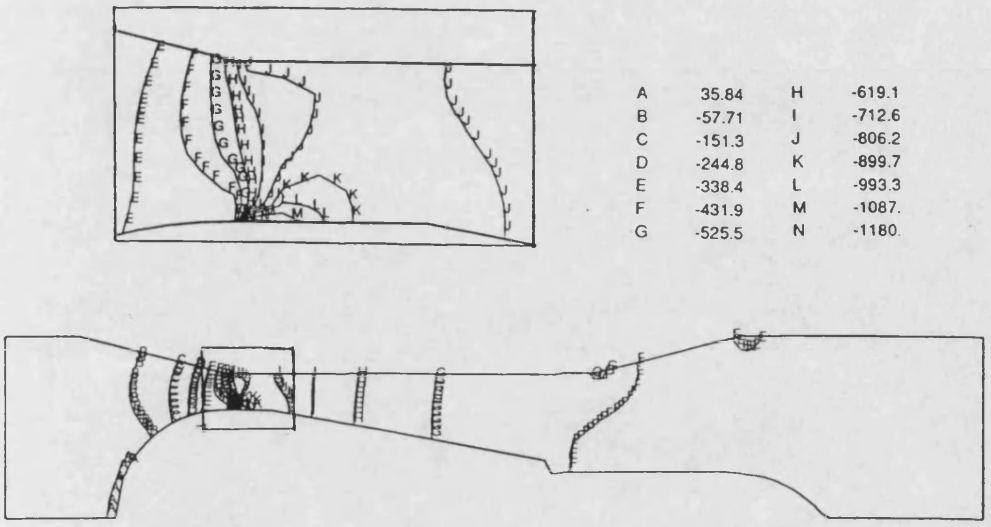

Figure 3.7 Pressure distribution of the mixer with single inner gas slit

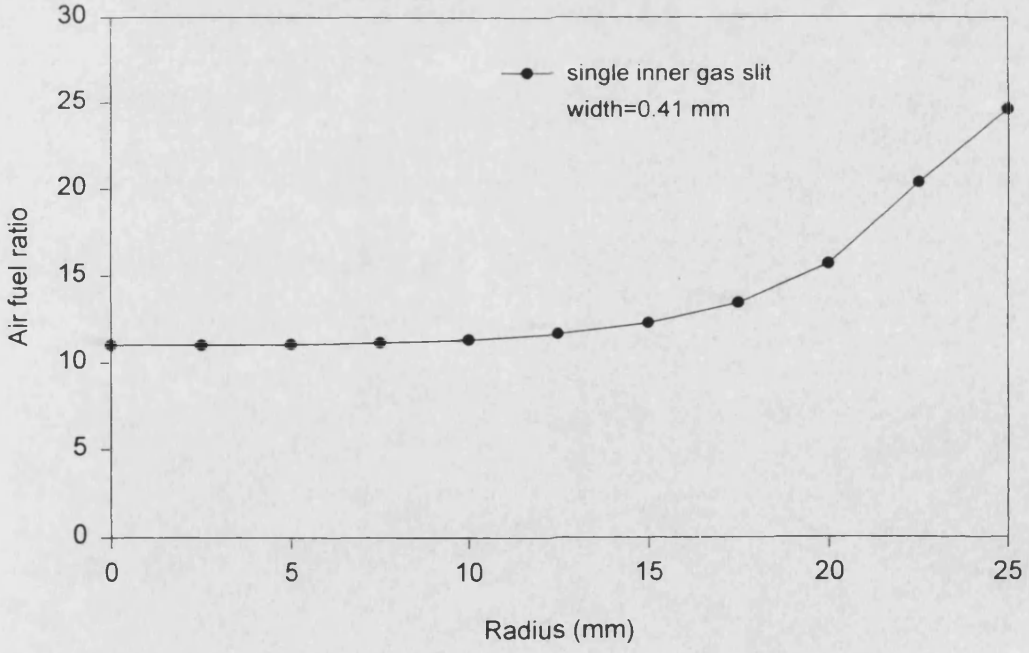

Figure 3.8 Mixture AFR distribution on the outlet plane of the mixer

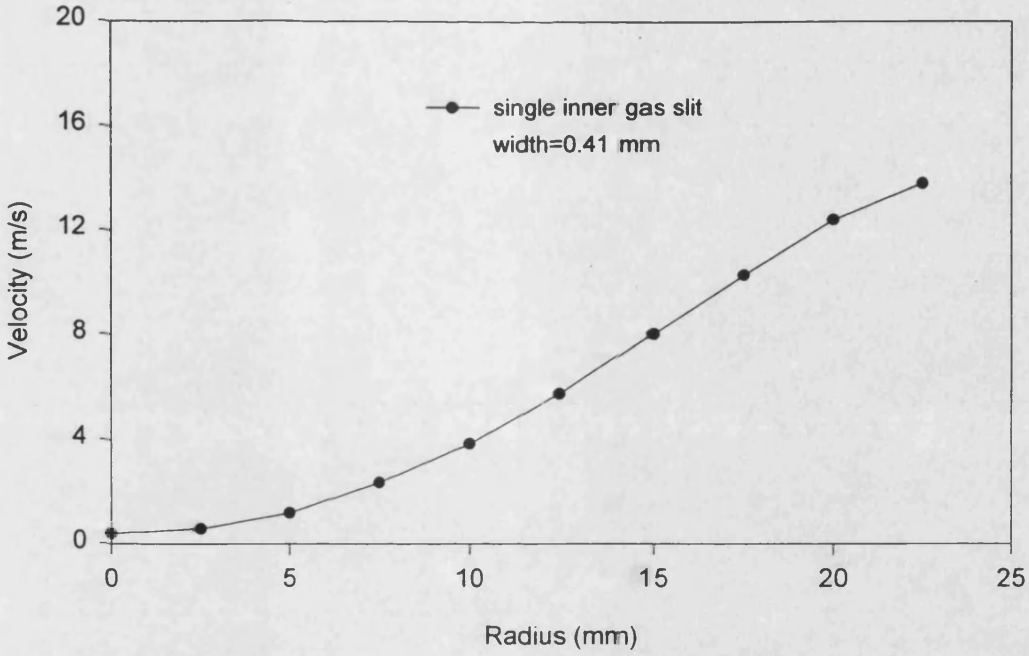

Figure 3.9 Velocity distribution on the outlet plane of the mixer

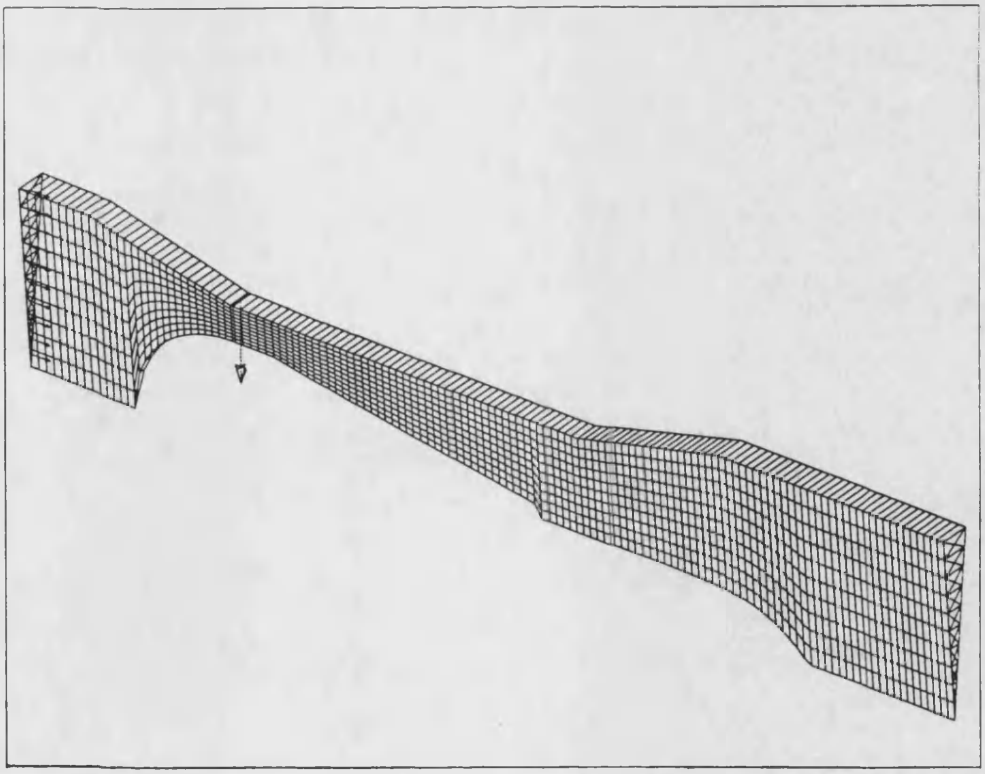

Figure 3.10 Computational model of the mixer with single outer gas slit

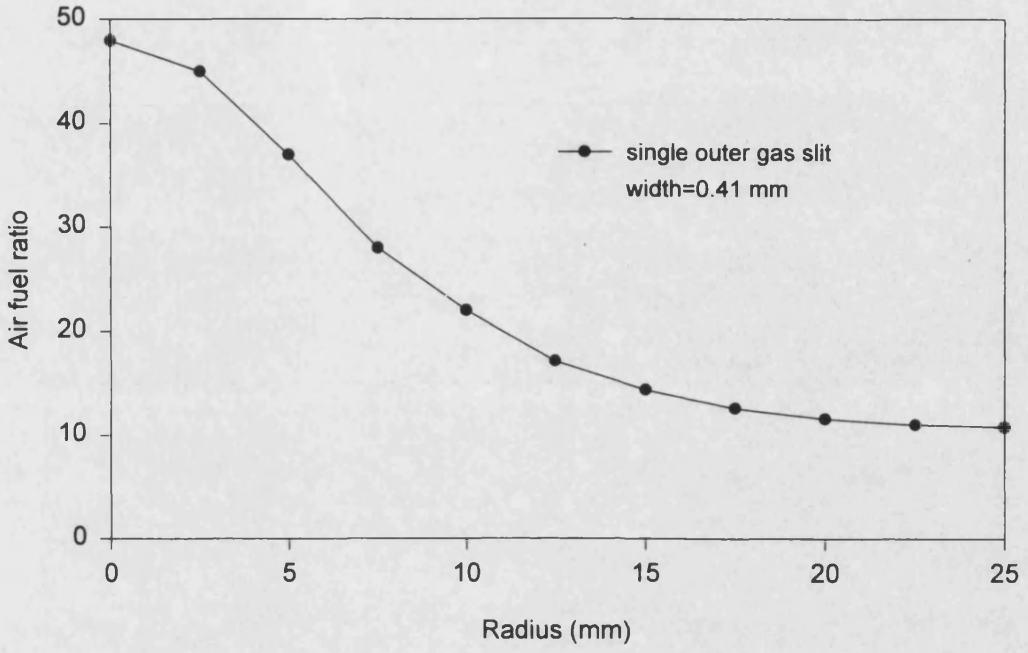

Figure 3.11 Mixture AFR distribution on the outlet plane of the mixer

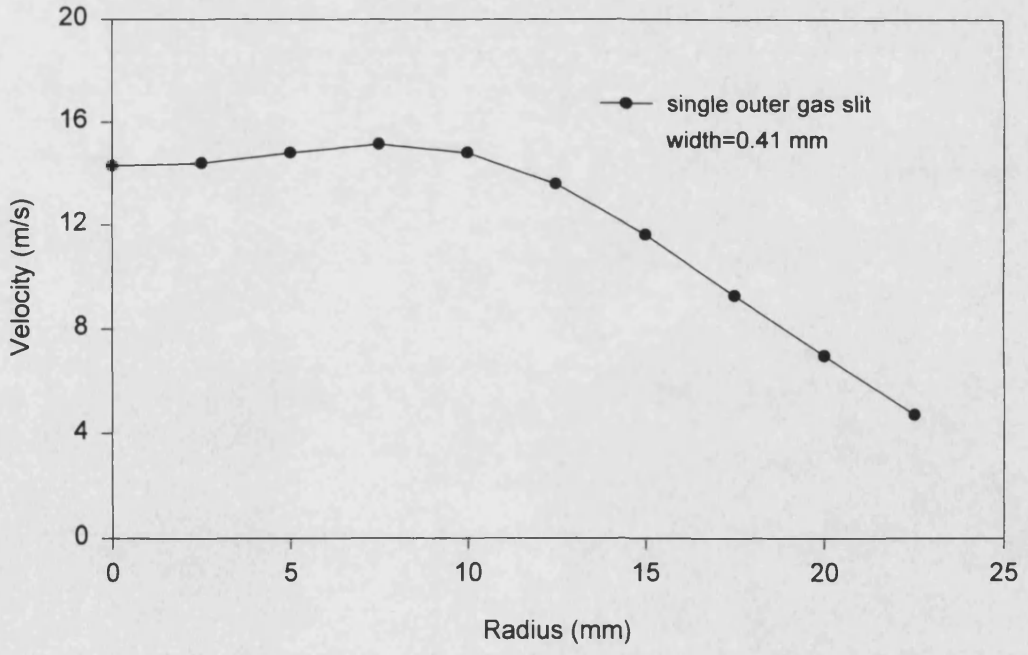

Figure 3.12 Velocity distribution on the outlet plane of the mixer

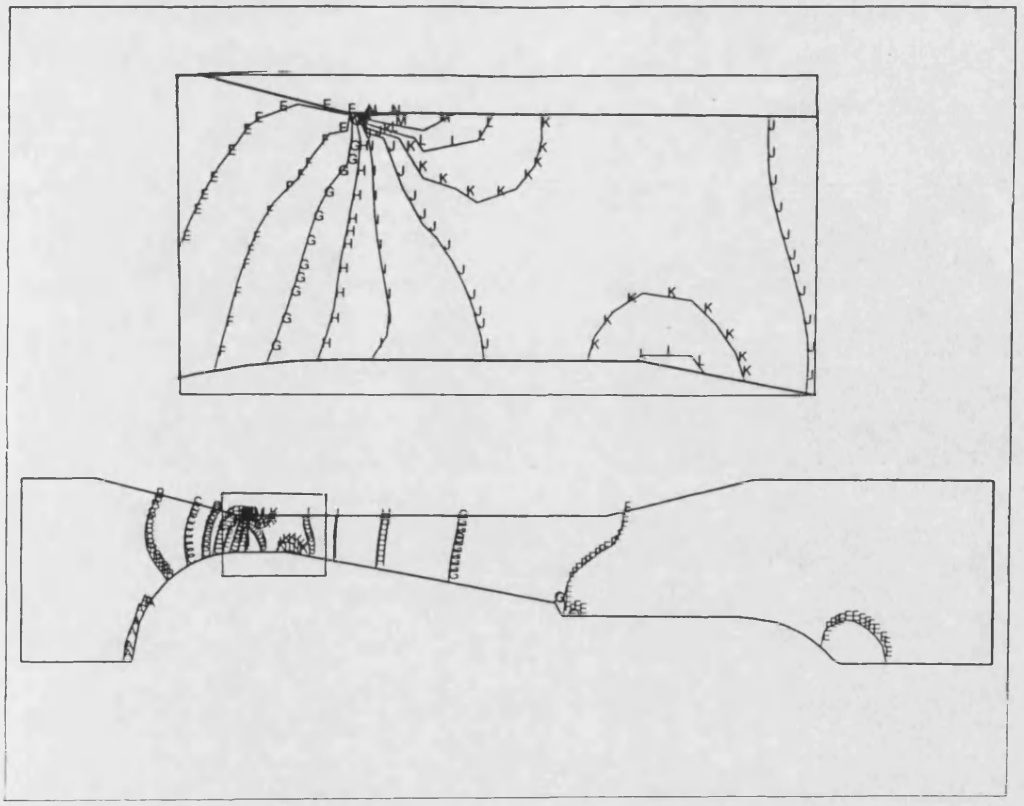

Figure 3.13 Pressure distribution of the mixer with single outer gas slit

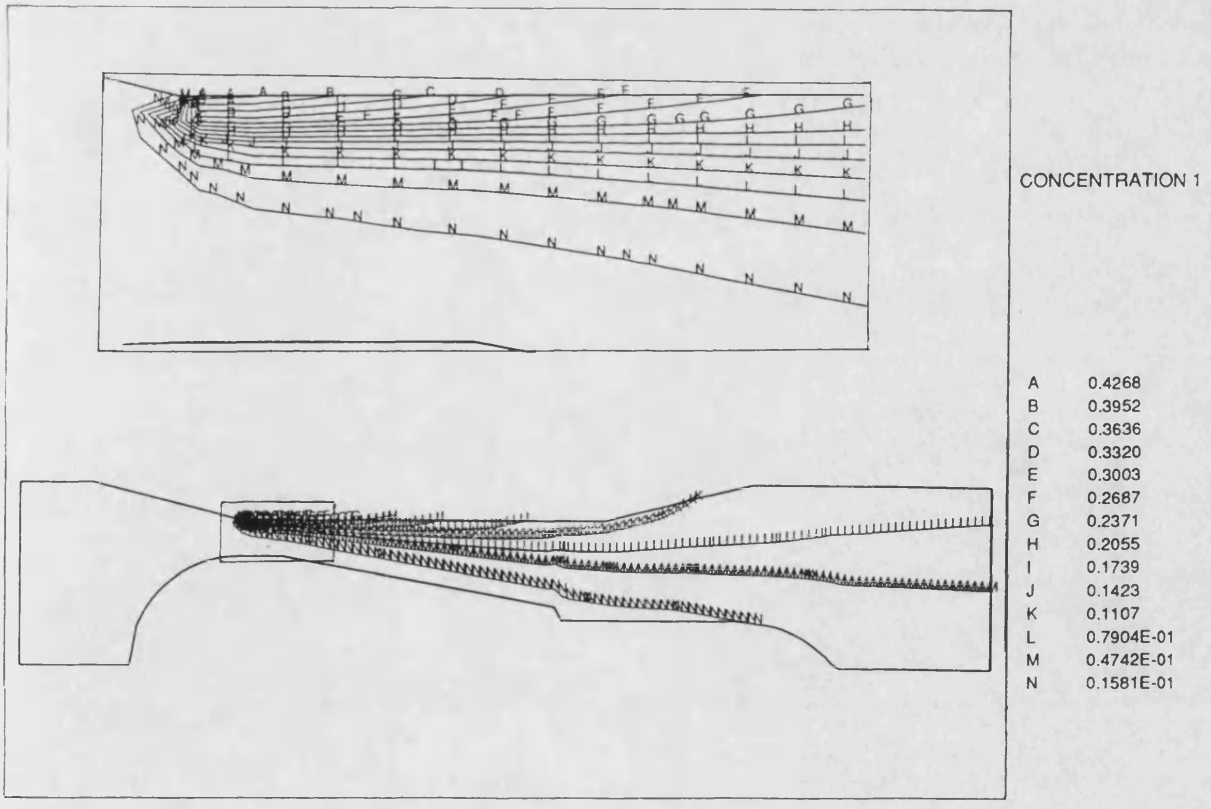

Figure 3.14 Concentration distribution of the mixer with single outer gas slit

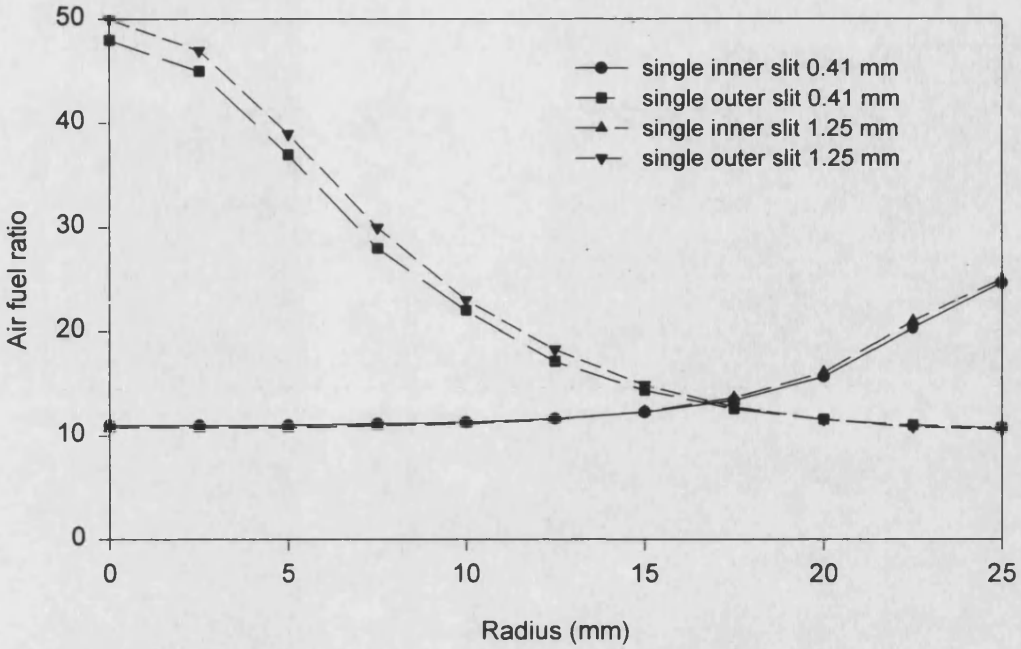

Figure 3.15 Mixture AFR distributions for different gas slit positions

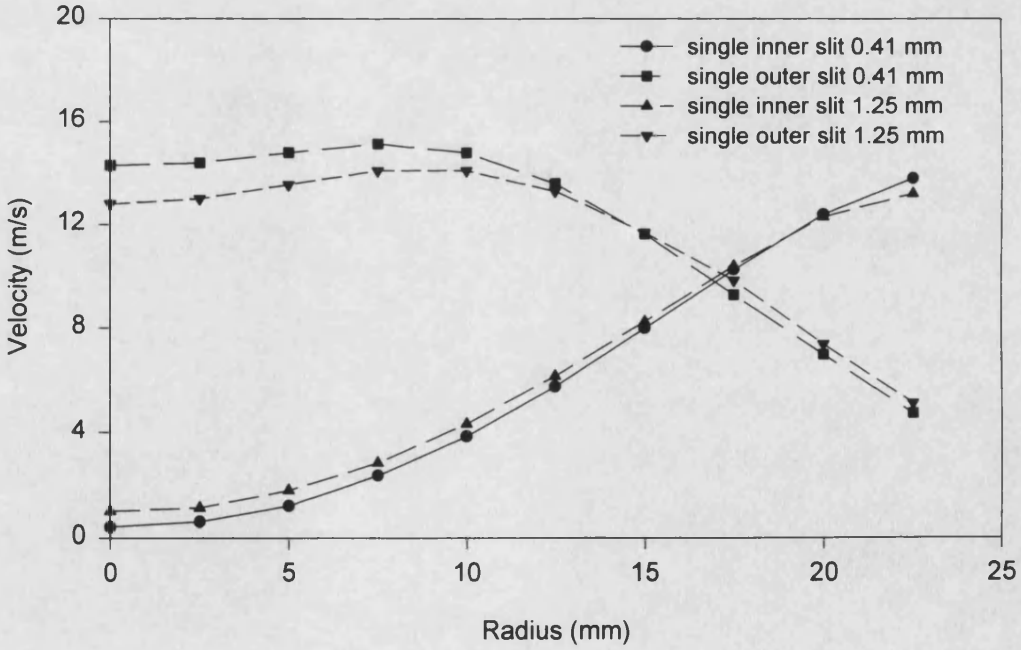

Figure 3.16 Velocity distributions for different gas slit positions

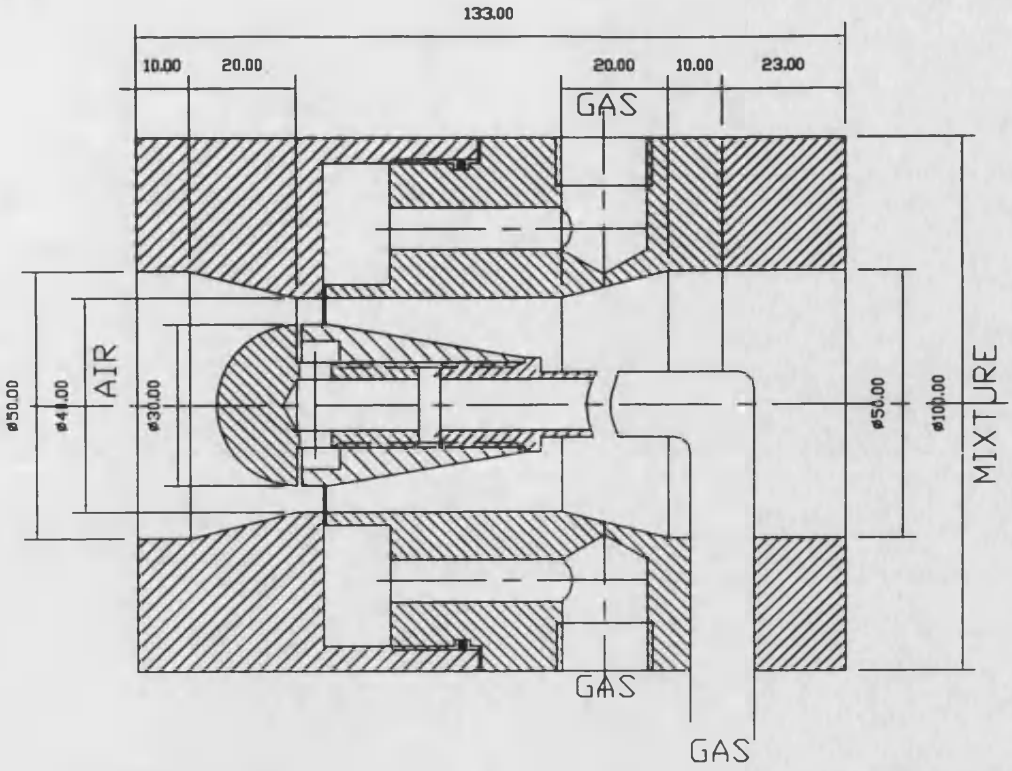

Figure 3.17 Configuration of the mixer with two gas slits

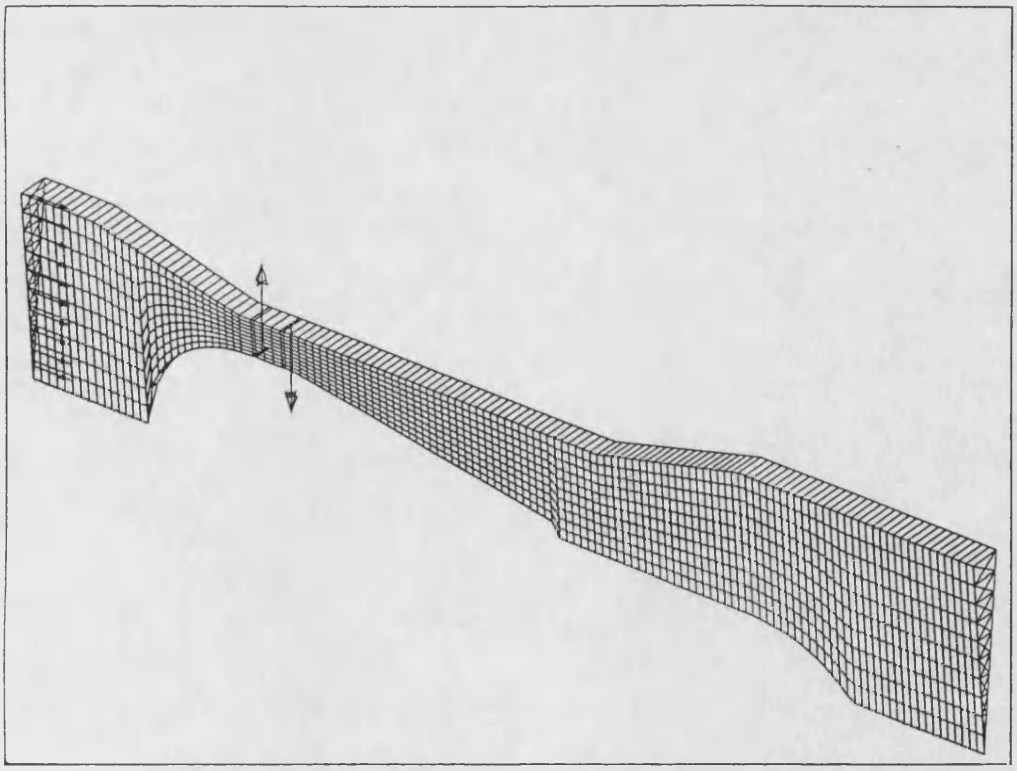

Figure 3.18 Computational model of the mixer with two gas slits

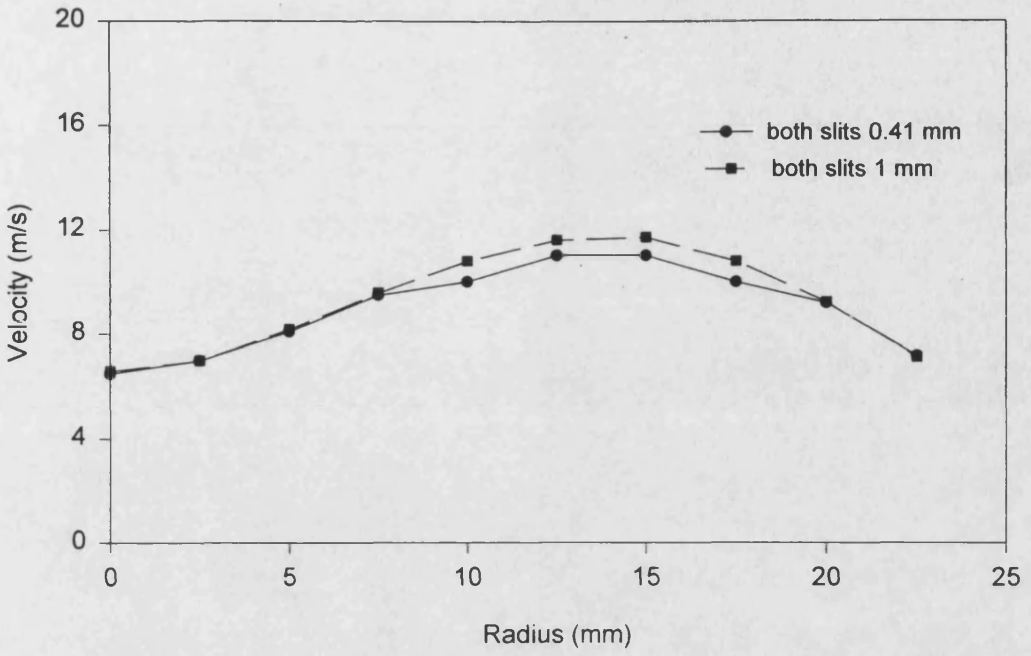

Figure 3.19 Velocity distributions of the mixer with two slits

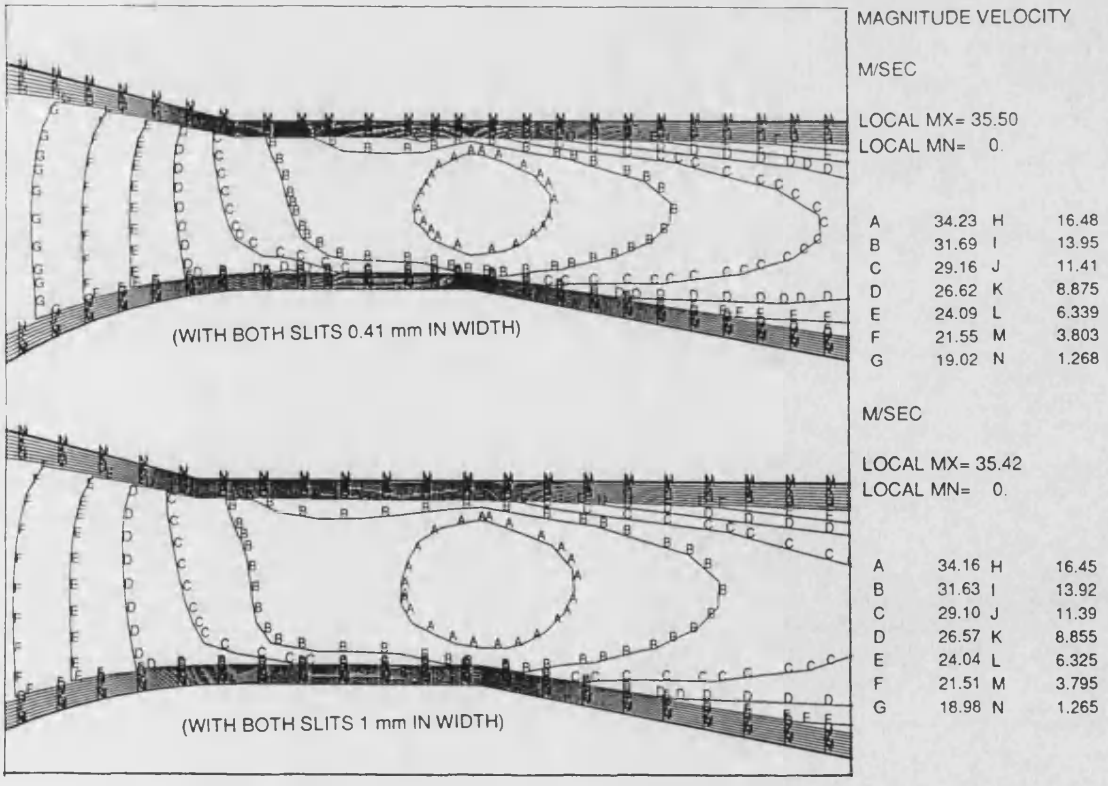

Figure 3.20 Velocity distributions of the mixer with different gas slit widths

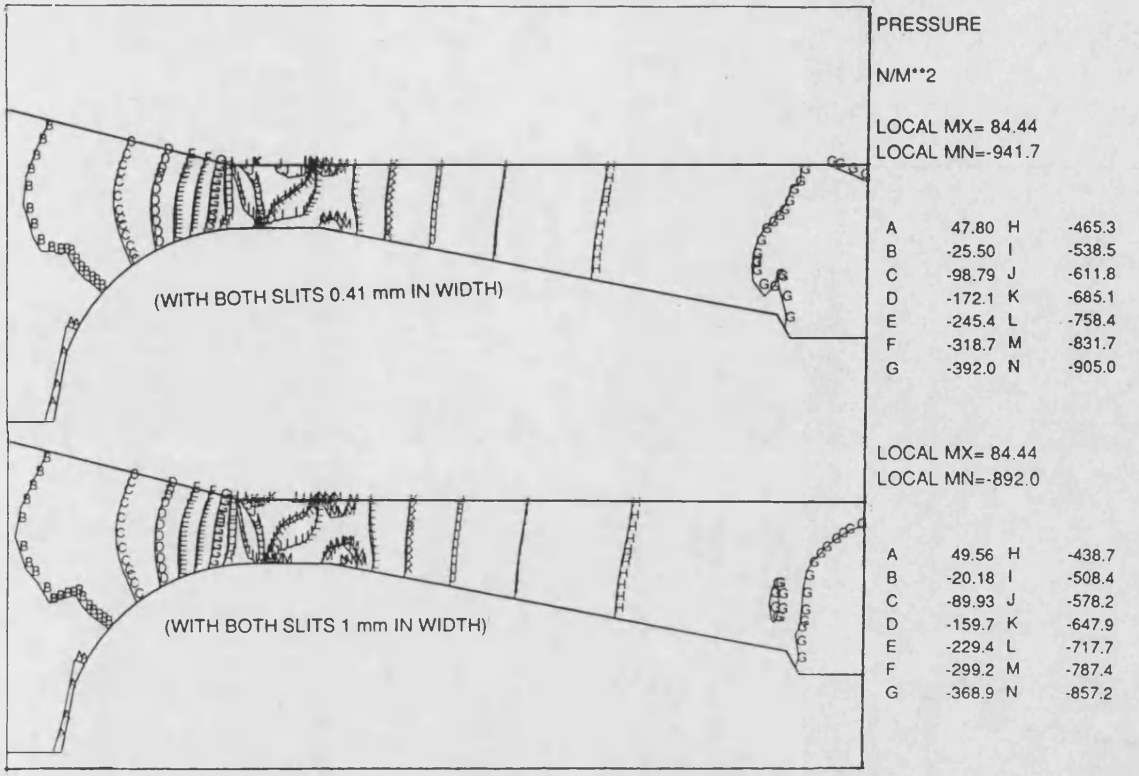

Figure 3.21 Pressure distribution of the mixer with different gas slit widths

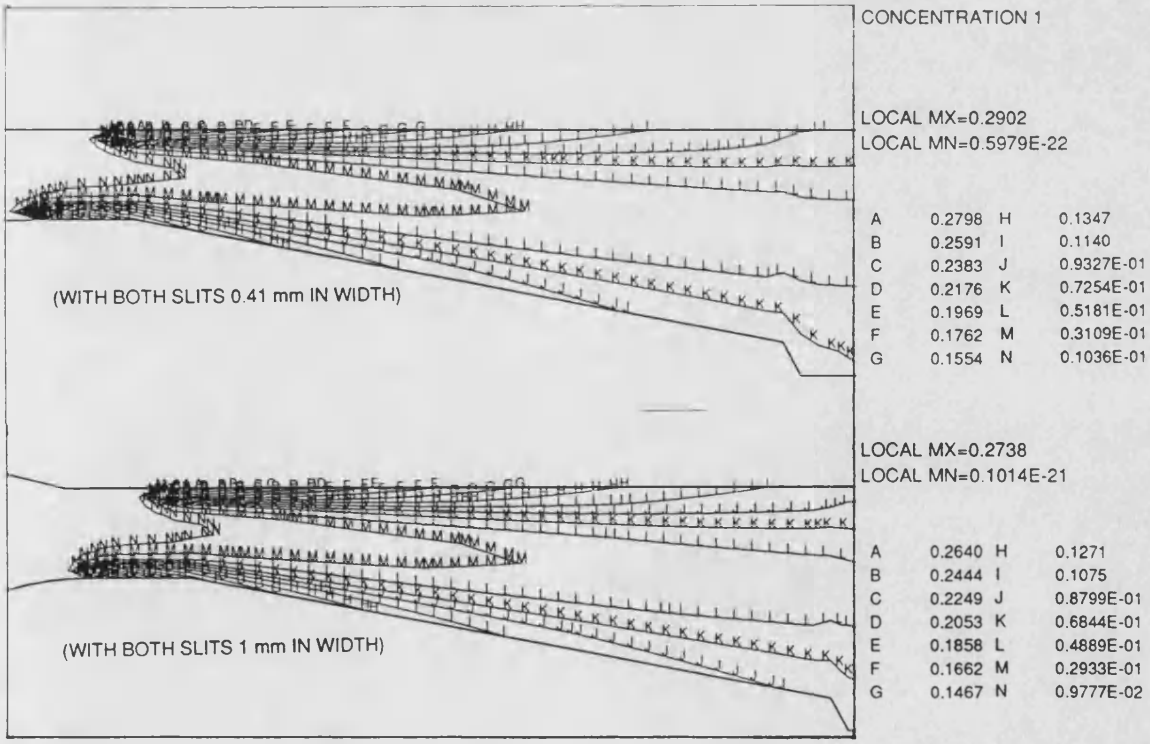

Figure 3.22 Concentration distribution of the mixer with different gas slit widths

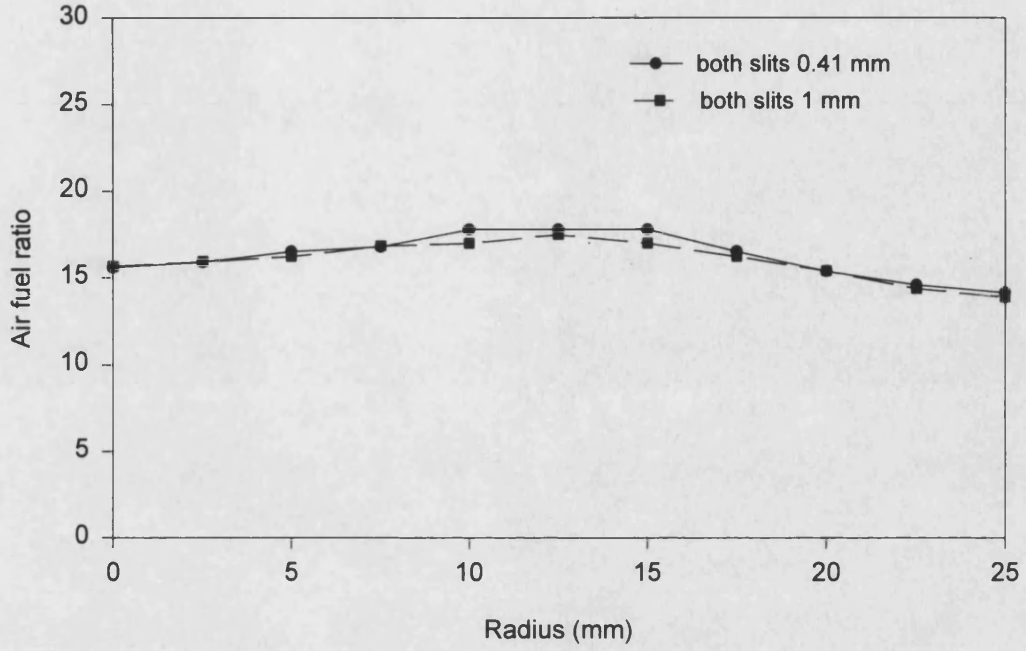

Figure 3.23 Mixture AFR distributions of the mixer with two gas slits

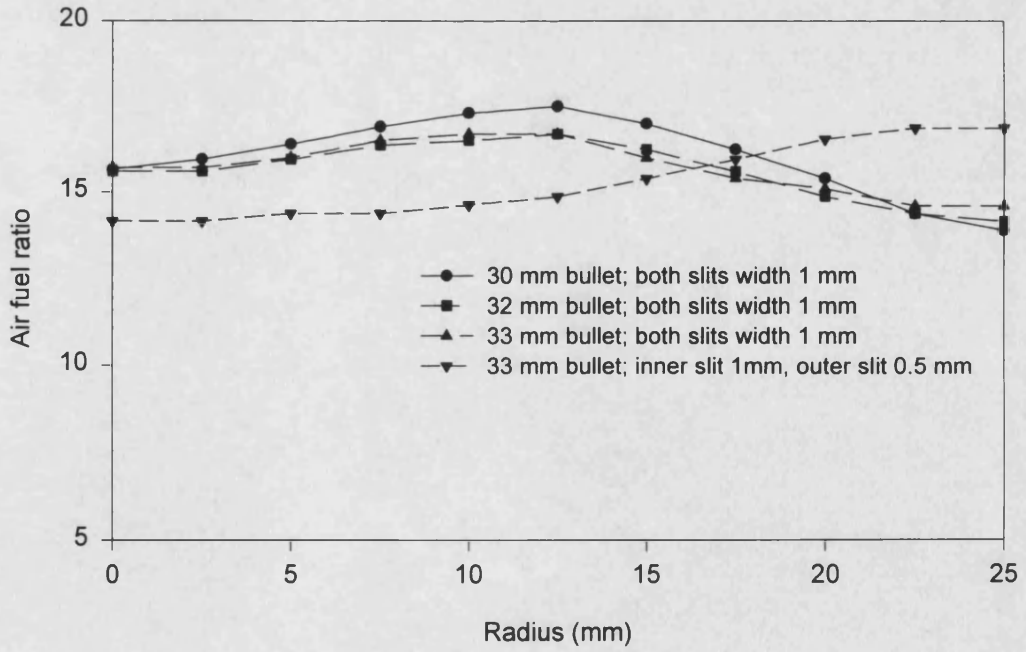

Figure 3.24 Mixture AFR distributions for different inner bullet diameters

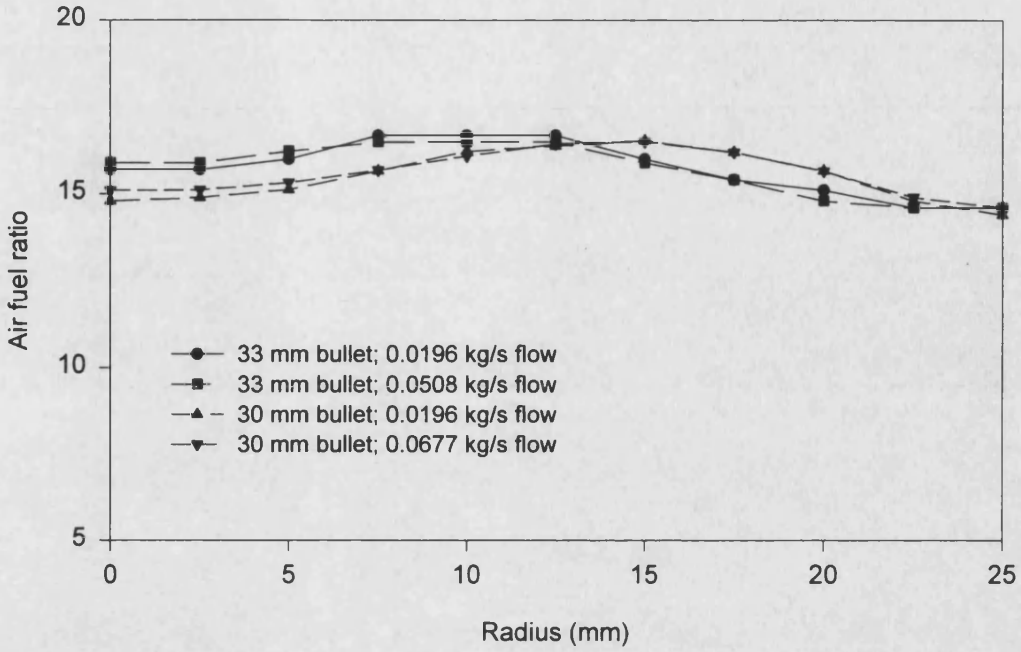

Figure 3.25 Mixture distributions for different flow rates and bullet diameters

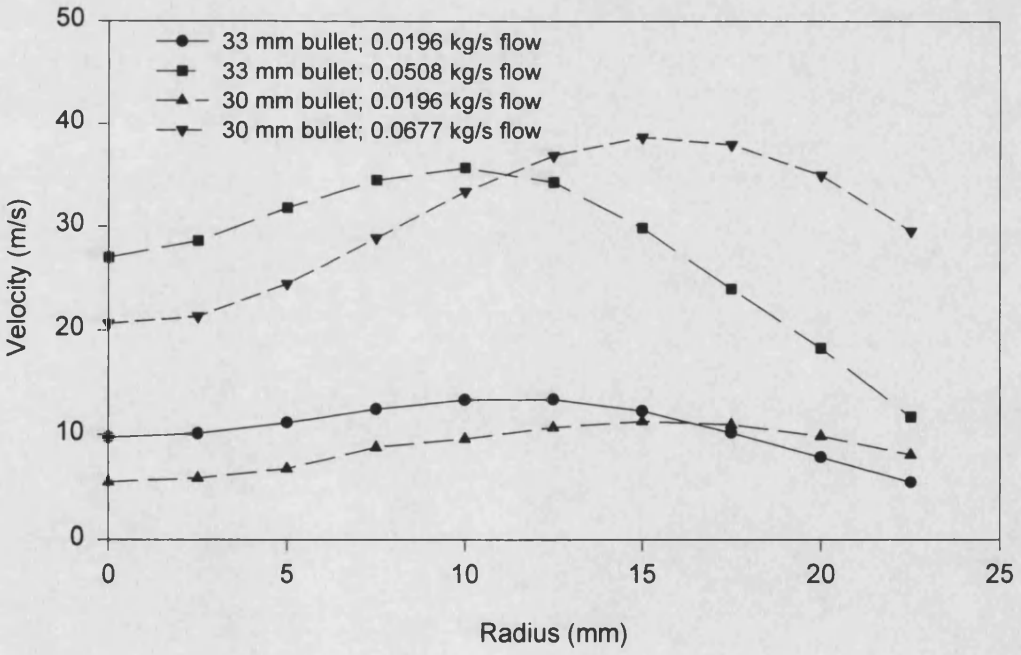

Figure 3.26 Velocity distributions for different flow rates and bullet diameters

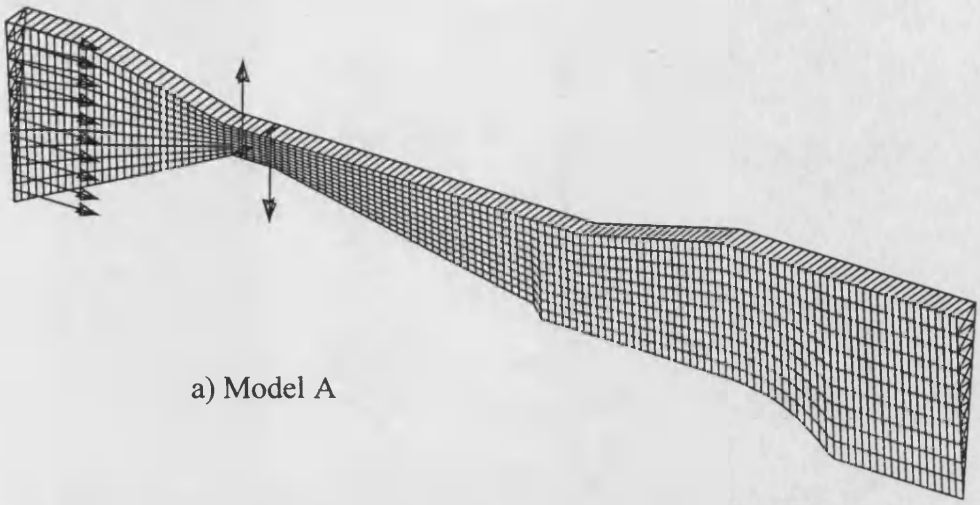

a) Model A

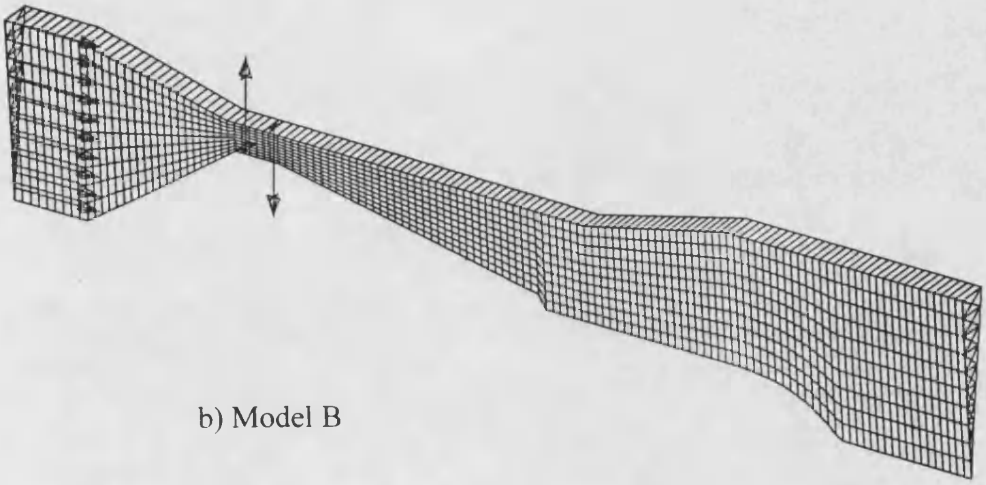

b) Model B

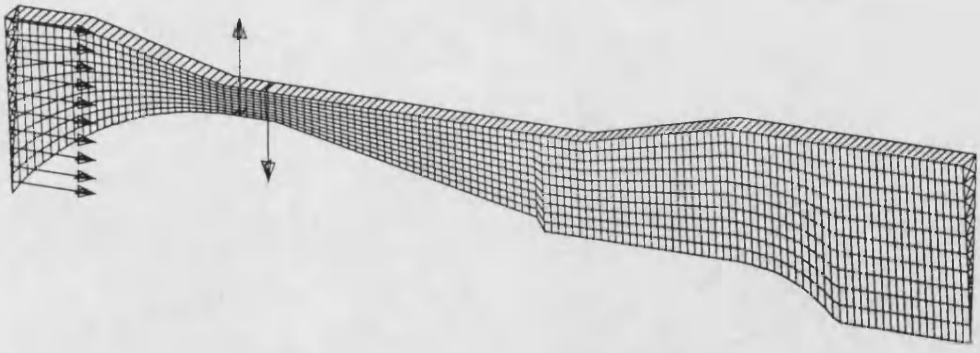

c) Model C

Figure 3.27 CFD models of the mixer with different inner bullet nose configurations

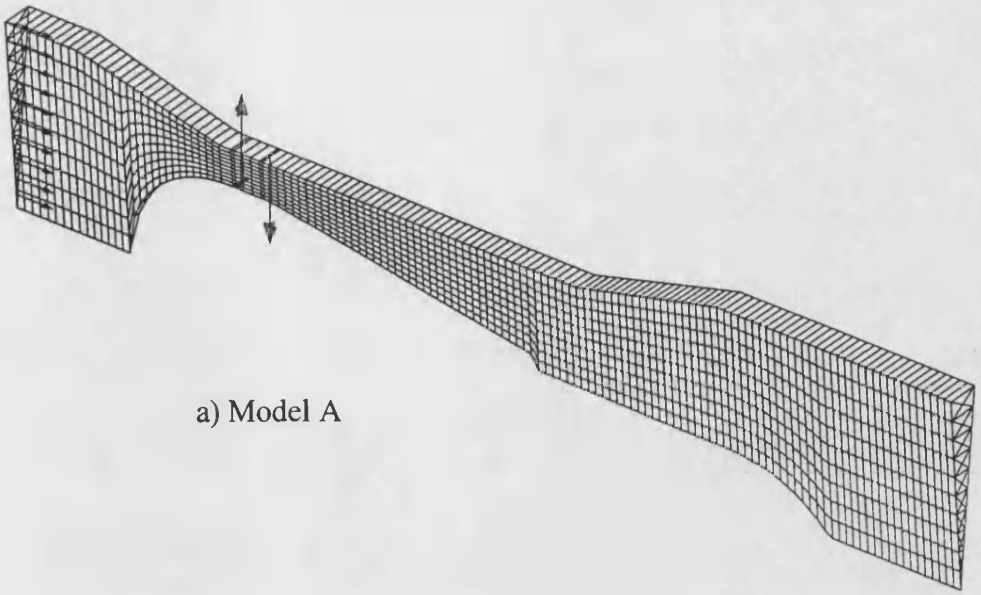

a) Model A

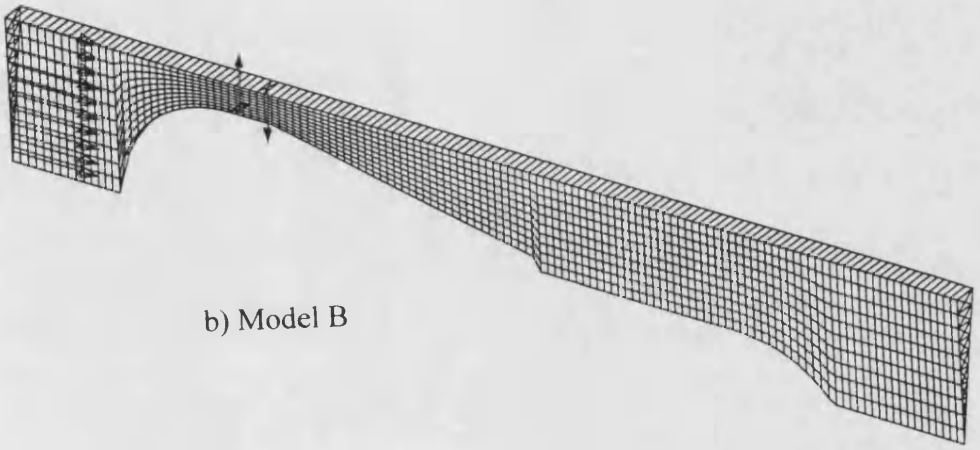

b) Model B

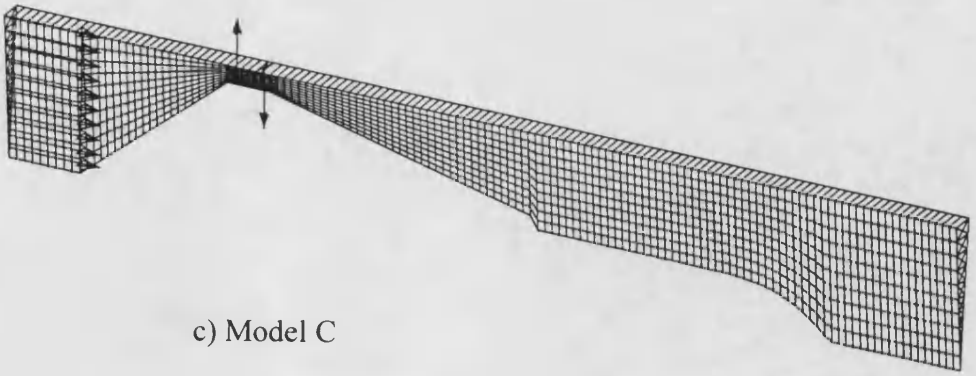

c) Model C

Figure 3.28 CFD models of the mixer with different outer body configurations

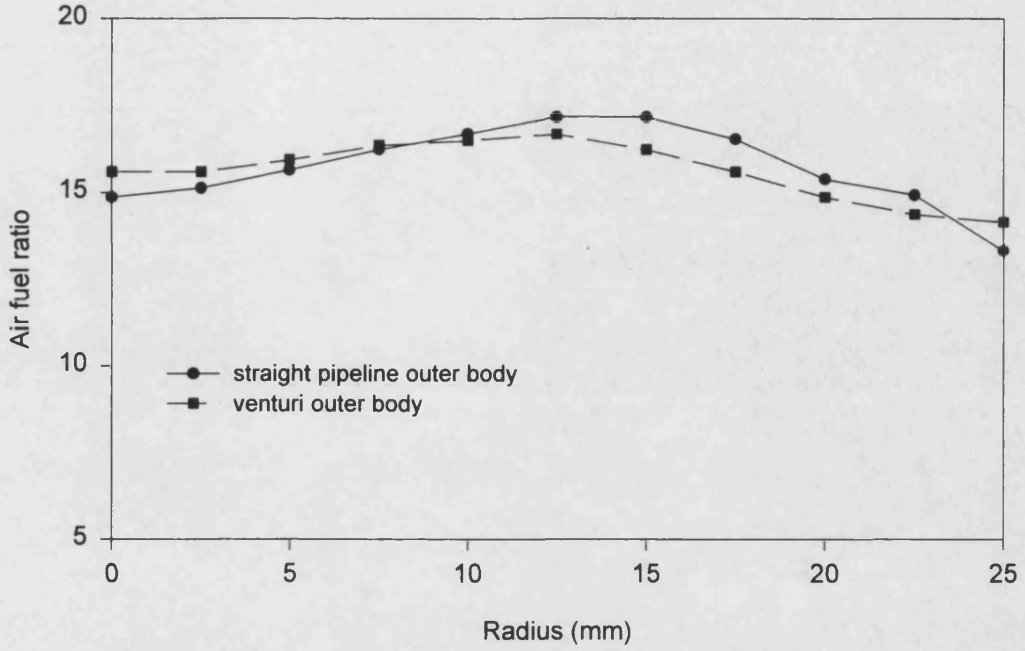

Figure 3.29 Mixture distributions for different mixer outer body configurations

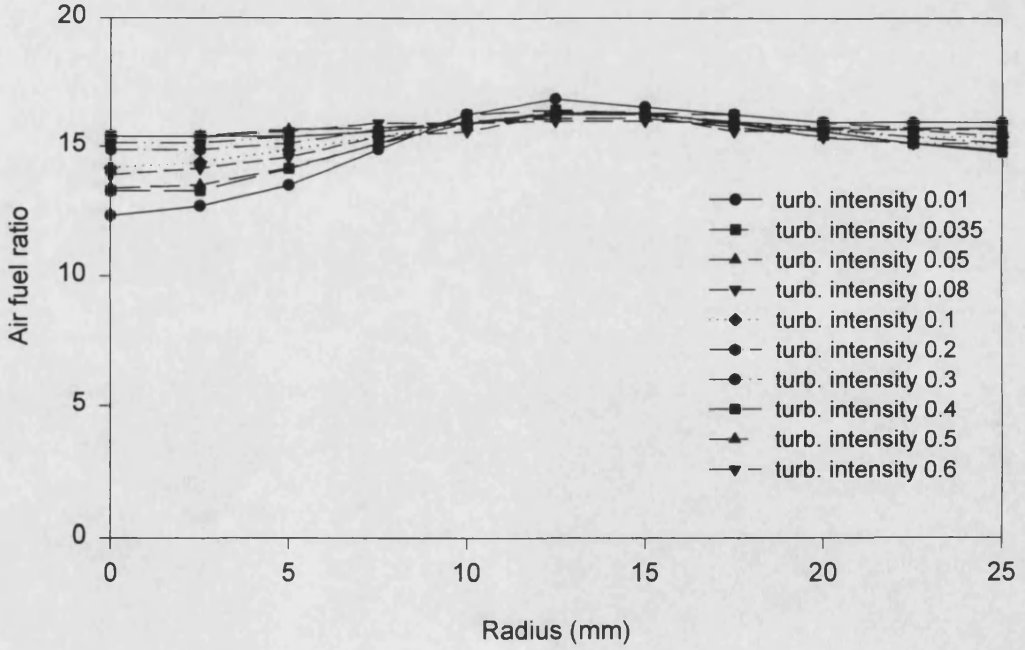

Figure 3.30 Mixture distributions for different turbulence intensities specified

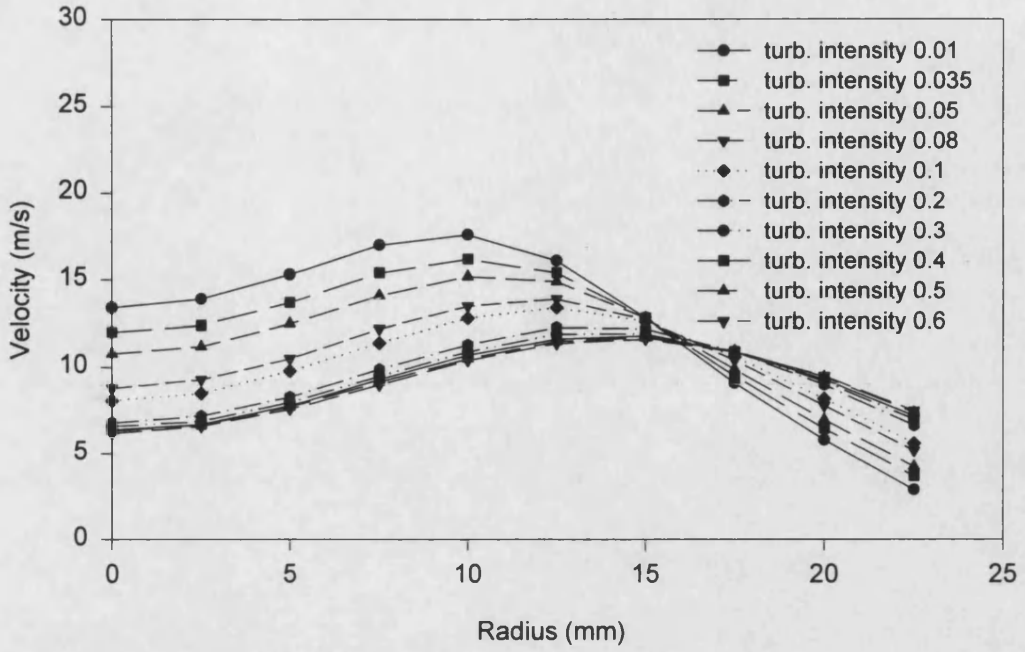

Figure 3.31 Velocity distributions for different turbulence intensities specified

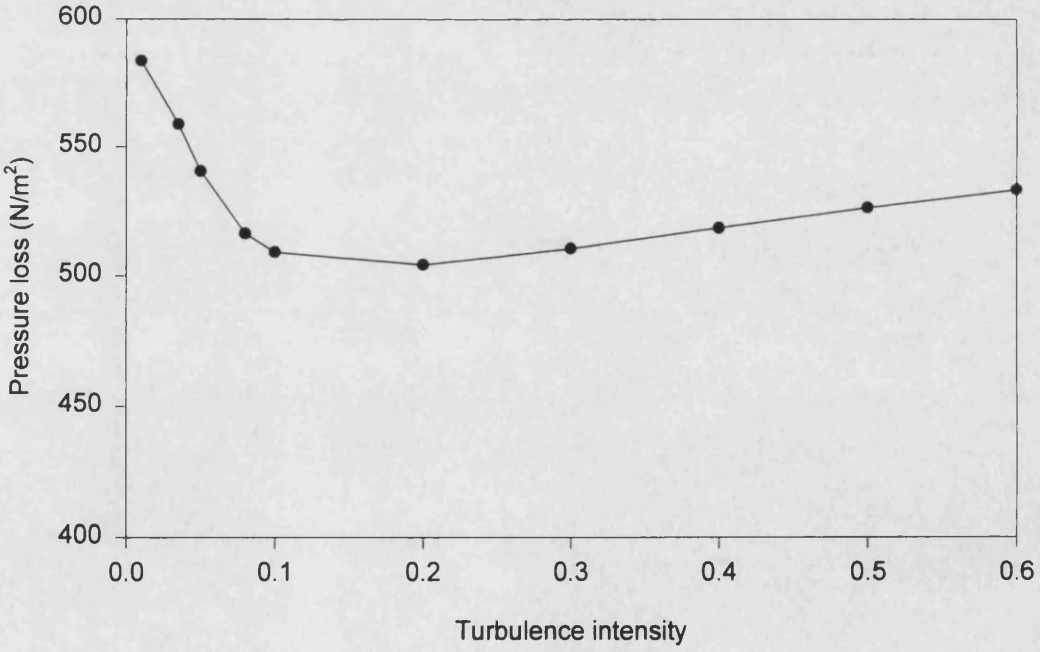

Figure 3.32 Pressure losses for different turbulence intensities specified

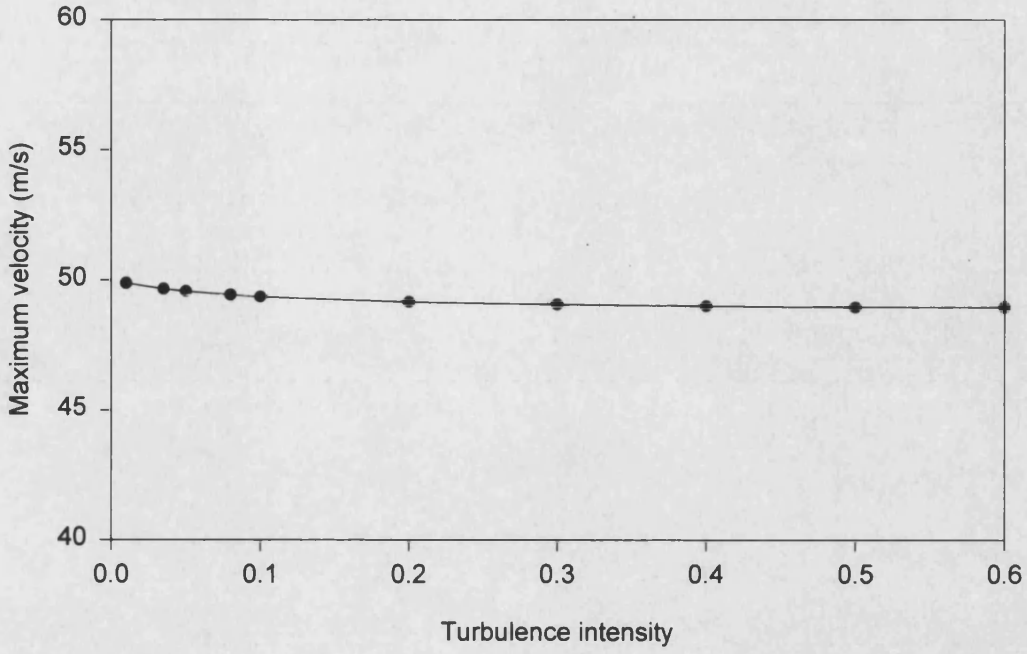

Figure 3.33 Maximum velocity in the throat area of the mixer

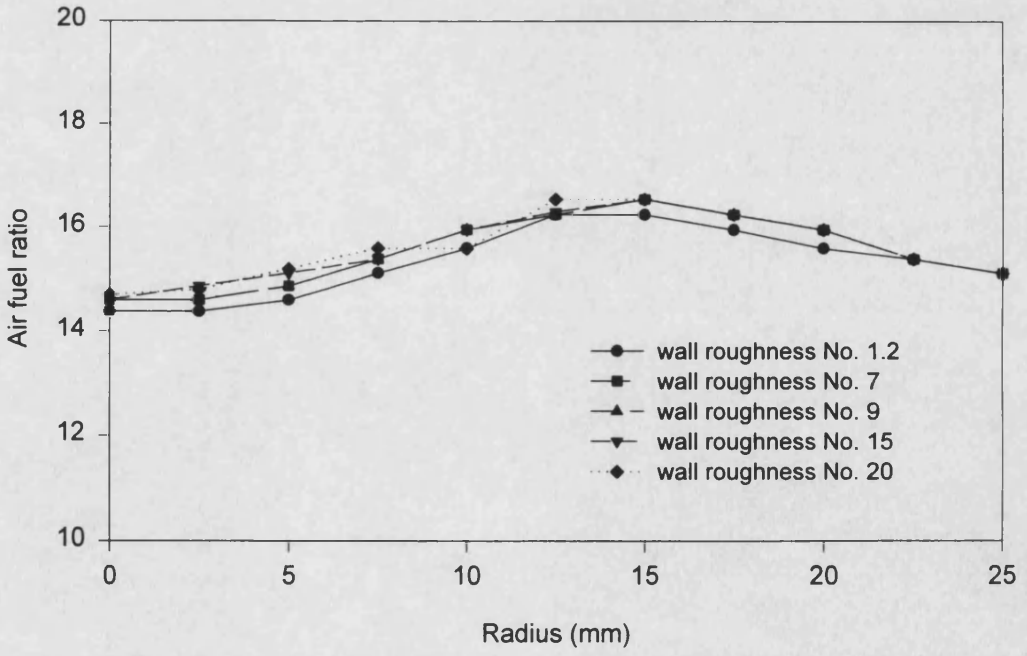

Figure 3.34 Mixture AFR distributions for different wall roughness numbers

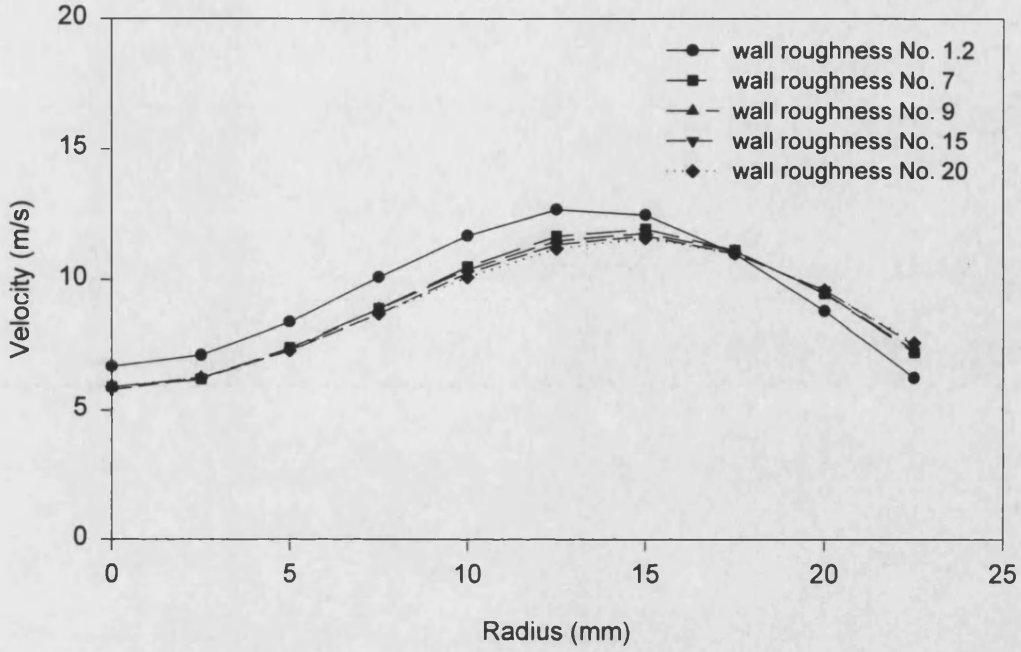

Figure 3.35 Velocity distributions for different wall roughness numbers

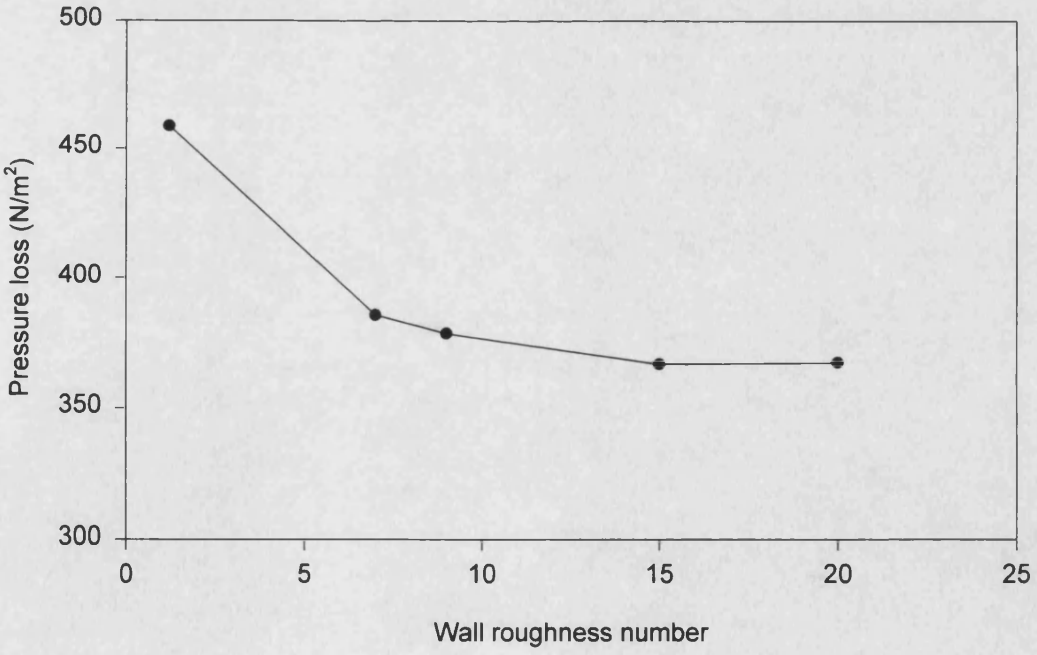

Figure 3.36 Pressure losses across the mixer for different wall roughness numbers

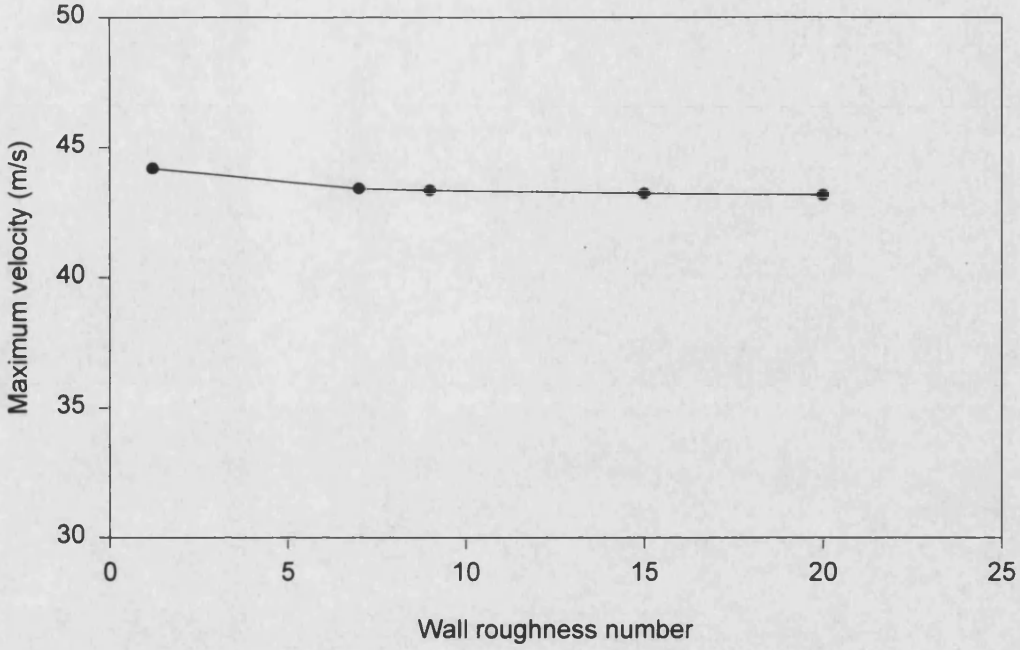

Figure 3.37 Maximum velocity variations in the throat area of the mixer for different wall roughness numbers

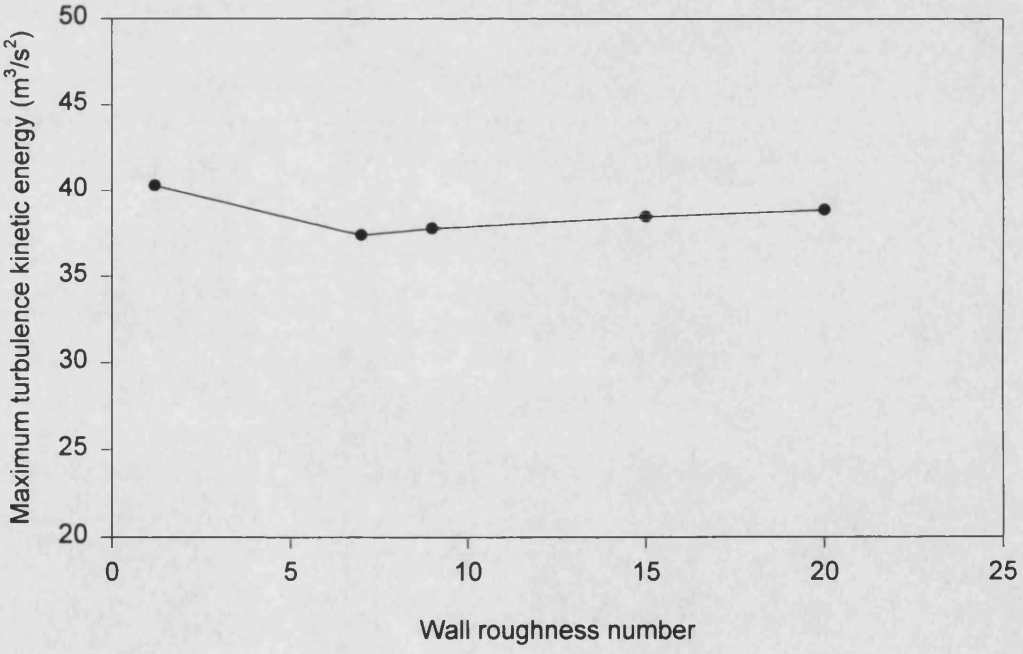

Figure 3.38 Maximum turbulence kinetic energies for different wall roughness numbers

4 Experimental study of mixture formation in the gas-air mixer

4.1 Introduction

The CFD simulations reported in the previous chapter showed that the computationally optimised novel venturi type gas-air mixer could produce a satisfactory mixture for stationary natural gas engines. For the annular venturi type mixer, the single gas slit design was eliminated because of its unacceptable computational mixture concentration distributions. Due to the shortcomings mentioned in chapter one about the turbulence models, it was borne in mind that the CFD findings on the predicted turbulence behaviour and its related variables like the scalar species composition can be fully accepted only when some of the predictions have been validated by experimental results. The validation work reported in chapter two was the validations made on some of the simulated parameters such as the pressure and the velocity. These validated parameters did not ensure the simulated results of the mass transportation or turbulent mixing between different species. Therefore, an experimental study of mixture formation in the mixer was carried out and experimental comparisons of the performance between the novel mixer and three different proprietary mixers were made.

The objectives of this study were to examine experimentally the mixture formation characteristics of the novel annular venturi mixer, to confirm the simulation results and the analysis made in the previous chapter, and to compare the mixer performance with that of proprietary mixers. The comparison between the computed and the tested data not only validate the simulation results, but also test the CFD package on different applications. The evaluation of the mixture prepared by mixers based on different operating principles will provide valuable information for both natural gas engine mixture preparation unit developers and natural gas engine users.

After the prototype mixer was machined according to the initial design, it was installed on the natural gas engine for which the mixer was designed. A series of experiments were then carried out on an engine test rig with both the novel mixer and three proprietary mixers installed in turn. The engine was operated under a wide range of speeds and loads which covered those used during the CFD computations. Therefore the simulation results such as the mixture concentration distributions and pressure losses across the mixer could be compared directly with the results obtained from the experiments.

4.2 Test facilities

The mixer performance test rig consisted of a naturally aspirated 4 cylinder Power Torque natural gas engine, coupled to a Heenan MK1 eddy current dynamometer. The gas engine was converted from a Ford Dover diesel engine for combined heat and power plant application. An engine was used here rather than any other flow generator, which would create a more representative operating condition for the measurement and would be safer in that it consumed the flammable gas air mixture. The engine speed was controlled by a Heinzmann electronic governor operating a throttle valve placed on the engine intake manifold. The dynamometer load exerted on the engine could be controlled independently of engine speed. The prototype mixer was mounted remotely from the engine, separated from the intake manifold by a length of 1.4 m straight pipe aiming at easing the assessment. The arrangement of the test rig used is shown schematically in Figure 4.1. Natural gas is spontaneously flammable in the air for a certain range of concentrations and temperatures. To ensure the safety of the experiment surroundings, a gas alarm was installed inside the test cell and two Maxson shut-down valves were inserted into the gas supply system. In case of an emergency stop of the engine or any type of failure, the main gas supply would be automatically shut off.

There were several boundary conditions specified during the CFD simulations. The prescribed air and gas velocities derived from the related flow rates for the engine operating conditions simulated were two of them. To measure the air flow rate flowing through the mixer, an orifice plate to BS 1042 specification was firstly used in the engine intake supply system. The gas flow rate supplied to the mixer was measured by a positive displacement roots flow meter, a very accurate unit for gas flow rate measurement. As an assistant instrument, a natural gas float meter was inserted into the gas supply system, which made the engine operation adjustment easier because of its direct reading. To measure the density of the gas and air supplied to the mixer, their temperatures were measured using K-type (nickel-chromium alloy / nickel-aluminium alloy) thermocouples, pressures were measured by water manometers.

Overall mixture air fuel ratio from the mixer was measured by the excessive amount of oxygen contained in the engine exhaust, which was detected by a heated oxygen sensor placed in the exhaust. Signals from the oxygen sensor were input to a Horiba Mexa-110 air fuel ratio analyser which could display digital readings of the mixture air fuel ratio supplied to the engine intake system or volumetric percentages of the oxygen in the exhaust or λ values of the mixture. The analyser settings such as the sensor constants, the recorder constants, the fuel constants were specified according to the application conditions and the fuel used. The air flow rate flowing through the mixer could also be

deduced from the accurately measured gas flow rate and the overall air fuel ratio, which was more accurate than that given by the orifice plate measurement.

The velocity traverse measurements on the mixer outlet plane were achieved jointly by a pitot tube which gave the total pressure distribution and a static pressure tapping on the same plane. Both pressure tappings were connected to a water multi-manometer. By positioning another pressure tapping at the air inlet boundary, the average static pressure losses across the mixer were then measured. Ambient conditions of pressure, temperature and relative humidity were measured using the barometer, thermometer and whirling sling hygrometer respectively. Mixture concentrations in the intake system out of the mixer were measured using a Cambustion HFR 200 high speed FID. For CHP applications, the engines are mainly run under steady operation condition at constant speed and load. It was therefore reasonable to assume that the flow behaviour including the mixture concentration distributions within the mixer flow domain were in steady state, as were assumed during the CFD simulations. The mixture concentration distributions were obtained by traversing the sampling probe of the FID at points across the diameter of the mixer outlet plane using a displacement mechanism. Instead of the entire flow domain, only the mixture concentration distributions across the outlet plane of the mixer were measured at discrete positions. The validation of the predicted mixture formation on this single plane can be regarded as the validation of the simulation within the entire flow domain without much flow behaviour distortion, especially when the axial distribution of certain variable such as the static pressure amongst the mixer was measured. Details of the FID technique and its calibrations will be discussed in the following section.

4.3 The flame ionisation detector and its calibration

4.3.1 Operating principle

The flame ionisation detector is an instrument to measure the number of carbon atoms burnt in hydrocarbon form. The principle is based on the phenomenon that pure hydrogen-air flames produce very little ionisation, but when a few hydrocarbon molecules are introduced, a quantity of ions are formed and the number of ions produced is nearly proportional to the number of the carbon atoms present in the hydrocarbon molecules, which applies to all classes of hydrocarbons such as paraffin, olefin and aromatics, but not to hydrocarbon molecules containing oxygen or nitrogen atoms [139]. For a hydrocarbon C_mH_n, experimental results show that the maximum FID ion current i is correlated to the sample flow in the following way:

$$i = \frac{Q \times [HC] \times N_a \times c \times e}{60 \times 10^9} \times \frac{p}{R_0 T} (\mu A) \qquad (4.1)$$

where Q is the sample flow (cc/min) at pressure p (N/m^2) and temperature T (K); [HC] is the concentration of hydrocarbons (ppm); N_a is Avagadro's number which is 6.023×10^{23} molecules/mole; c is the number of carbon atoms in HC molecule; e is the electronic charge which is 1.6×10^{-19} Coulombs; and R_0 is the universal gas constant which is 8.3144 J/mole K.

The correlation given above shows that the ion current generated is proportional to both the hydrocarbon concentration and the sample flow. The sample flow rate has to be either measured or kept unchanged at a certain known value in order to measure the hydrocarbon concentration. In the conventional FID, the flows of fuel gas, air and sample are controlled via capillary tubes and pressure regulators, which works very well except for its poor frequency response. The FID used in this study was arranged in such a way that the sample gas was introduced directly to the exit tip of the burner nozzle through a small connecting tube, as illustrated in Figure 4.2. This significantly improved the response of the instrument because of the elimination of its long and narrow sample capillary and pumps in some of the conventional FID. However, the new arrangement of the novel FID, which was developed in Cambridge University and called Cambustion FID, gives rise to problems of the sample flow control and its signature interpretation. The interpretation depends on the setting and calibration of the instrument carried out by each of its individual users. Another disadvantage of the Cambustion FID is the difficulty of the flame chamber pressure maintenance. To ensure an adequate amount of sample, the pressure in the FID flame chamber must be below that of the sample source. Thus a partial vacuum is often required when the instrument is applied to the mixture measurement in the engine intake system where a relatively high level of vacuum is present.

4.3.2 Construction of the FID

The Cambustion FID has been developed into a series of models since its first release. The one used in this study was the HFR 200 model which consisted of a sampling head, a gas handling sub-system and an electronics sub-system. The sampling head, as shown in Figure 4.2, was a small unit and could be installed close to the sampling position in order to obtain a fast response. The diffusion flame of the combustible hydrogen-air mixture in the burner was initiated by a glow plug and the temperature of the burner was measured by a thermocouple. Negative ions (mostly electrons) generated in the flame were collected on to an electrode where a positive electrostatic field was applied by exerting a +180 voltage. The signal produced in the collector depended on the number

of ions formed, which was proportional to the number of carbon atoms in the flame. The signal generated was put into the electronic sub-system for signal conditioning. The output signal was displayed by a digital meter in this study. The electronic sub-system also functioned to monitor the temperatures and pressures in the FID, which would automatically shut-off the fuel and air system in case of instrumentation failure. The gas handling sub-system controlled actual flow rate of the fuel (hydrogen in this case) and air supplied to the flame chamber by adjusting two needle valves installed and the flow rates were obtained directly from the built-in rotameters. The sub-system also controlled the sampling flow rate. In order to reduce the effect of pressure fluctuations at the sampling source on the FID sample flow, a constant pressure (CP) chamber was installed at the bottom of the sampling head. With this CP chamber, the pressure difference between the CP chamber and the FID flame chamber was easily adjusted and a constant sampling flow rate ensued.

4.3.3 Applications of the FID

Since the Cambustion FID increased the response dramatically, its inventors have made a significant effort to apply the instrument to a variety of engine research activities associated with hydrocarbon compositions. So far the FID has been accepted and increasingly used by engine researchers in many countries. The reported applications of the FID have been focused on two kinds of hydrocarbon measurements. One was the in-cylinder local gas compositions measurement and the other was the measurement of the engine exhaust HC emissions.

Collings, N., one of the Cambustion FID developers in the University of Cambridge, monitored hydrocarbon levels in real time during the compression and firing stage in a firing petrol engine. The sample system was made using a modified sparking plug in which a small hole through the centre electrode was drilled and a 0.12 mm stainless steel capillary tube was welded in it [140]. The reason for using the very small sample tube was not to disturb the ignition process or the hydrocarbon source by the sample flow. A small tube could also minimise the turbulent diffusion controlled mixing of the sampled gases in the sampling tube, which ensured a better time resolvement. The assessed hydrocarbon level or the mixture strength was correlated to the measured cylinder pressure developed and a good agreement was achieved.

After the first attempt, an unsteady flow simulation was carried out jointly between Massachusetts Institute of Technology and Cambridge University for the sampling unit which consisted of a transfer tube, an expansion tube, a connecting tube and a constant pressure chamber [141]. The time delay of the sampling system was obtained for selected engine loads and speeds. The time delay referred to the finite transit time

through the sampling unit to the measuring device, which was a function of the engine cylinder pressure history. The analysis result showed that the sample mass flow rate to the FID could be constant if the pressures within both the FID flame chamber and the CP chamber were kept constant and the exit to the expansion tube was not choked, a condition which ensured the pressures on the expansion side of the connecting tube equalled to the pressure of the CP chamber. With a constant sample mass flow rate, the FID signal output was uniquely related to the hydrocarbon concentrations when the sample pressure and temperature were able to be kept constant. Based on the technique mentioned, the FID was then used to examine the in-cylinder charge inhomogeneity and residual gas concentration in spark ignition engines by different users [142] [143].

The Cambustion FID was also used to monitor the mixture strength within the engine cylinders, on a cycle by cycle basis after sudden throttle opening during the transient operations of a gasoline port-injected engine [144] [145]. In order to obtain a sufficient time for the FID signal to reach its peak value, i.e. the plateau, and to stay at its peak value until the flame arrives, two methods were tested for the already very low-capacity sample tube. One of them was to locate the sample point far away from the spark plug so as to delay the flame arrival. The other method was to disable the cylinder spark for the cylinder examined. Both methods worked satisfactorily with the carefully selected tube diameters and the FID flame chamber pressure. To further reduce the FID signal sensitivity to cylinder pressure even during the engine transient operation period, a sample tube T-piece was incorporated in addition to the original FID T-piece, i.e. the piece composed of the expansion tube and the connecting tube. As a result of the modification, the sensitivity of the FID signal to the sample pressure change was virtually eliminated. The engine monitored in the study showed a transient mixture excursion to its lean side of stoichiometric mixture existed only for the first cycle after the rapid throttle opening. The excursion was believed to be caused by a brief imbalance in the air and fuel flow rates into the engine cylinder due to their inertia difference. This mixture excursion had demonstrated a very good correlation with the cylinder pressure record and its associated heat release analysis result.

The use of the FID to measure the exhaust HC emissions was tried first by Collings, N. and Willey, J. and then the technique was improved and extended to the study of the exhaust catalysts response [146]~[149]. With the modified FID sample system, the HC emissions signature from individual cycles was simply monitored, which gave an insight into the cyclic HC concentration structure at different periods of the exhaust process. By using two sample heads located at each side of the catalyst converter, the HC concentrations difference was cyclically monitored. As a result of the studies, the transient behaviour of the catalysts at different mixture strengths was examined in real time.

To look at the influence of sampling location on exhaust HC concentration versus crank angle signatures of the FID, a simple one dimensional plug-flow model was used to analyse the exhaust flow [150]. The model analysis showed that the variation with sampling location was due to a combination of a variation of concentration and the intermittent flow in the exhaust pipe. This sampling location influence on the measured HC values was also experienced by Rouveirolles, P. and Roy, J. P. in their cyclically resolved HC emissions study in the exhaust port of a firing SI engine [151]. A similar kind of exhaust HC emissions measurement was conducted for monitoring the HC emissions during the blow-down period when the engine load was changed suddenly [152]. All of these studies demonstrated that the Cambustion FID could trace the sequential process of the HC pollutant formation and gave a good understanding of the phenomena.

4.3.4 Calibration of the FID

Since the FID signal output is proportional to both the sample flow rate and the concentration of hydrocarbons, a direct interpretation of the signal output into an HC concentration value becomes difficult. The sample flow can be measured by using a rotameter provided on the gas handling sub-system or any other mini-flow rate measurement unit. This method is not accurate because of the difficulties of measuring small flow rates. Instead of the direct sample flow rate measurement, there is another way to separate the sample flow rate effect from the hydrocarbon concentration measurement. If the sample inlet can be supplied with a source of hydrocarbon gas having a known concentration at the same pressure as that at the sampling point, the actual sample flow rate can be deduced from the known concentration and the FID signal output. The purpose of the identical pressure control was to maintain the sample flow rate to the same value as the sampled span gas. The key issue here was how to control and measure the pressure accurately. To achieve this identical flow rate, the pressure difference between the flame chamber and the CP chamber was accurately controlled, and the pressure of the sampled span gas was adjusted to be identical to the pressure at the measuring mixture source point. To control these pressures and pressure differences, the pressure of the burner flame chamber and the pressure difference between the chamber and the constant pressure chamber were monitored by a built-in unit. The pressure at the sampling point was measured by using a special pitot tube. A three-way valve switch was inserted in the sampling and calibration system, which switched the sample gas flow between the measured point and the span gas source, see Figure 4.3. The pressure of the span gas was adjusted by using a pressure regulator and an orifice restriction valve to the same value as that of the sampling source point. In this way the FID system was calibrated and the signal was interpreted into mixture concentration without measuring the sample flow rate directly.

The span gas had a known concentration value which was 6% of methane by mass in a balance of nitrogen. The FID was also calibrated against zero gas. The zero gas used was dry air. Calibrations were carried out during the entire measurement process in order to monitor the sample flow rate and to avoid the influence of the FID time drift which was experienced at the very beginning of the calibration test. It was the nitrogen used as the balance in the span gas rather than the air because of the safety regulations. As an calibration gas, the 6% of methane in air would be more appropriate if it could be legally purchased. It is a widely accepted fact that the oxygen presents an interference with the FID signal output [154]. Fortunately, the interference can be reduced to a minimum by careful operating point setting [139].

Due to the pressure fluctuation inside the natural gas engine intake manifold, however, it was very difficult to keep the pressure difference constant. Thus a plenum was inserted between the FID sampling head and the sampling probe for steady measurement purposes, which isolated the FID sample flow from the source pressure fluctuations. Therefore the sampling flow rate was strictly controlled via the accurate control of the pressure difference between the flame chamber and the constant pressure chamber of the sample head, and also between the constant pressure system and the measuring points.

In an aspirated throttle controlling natural gas engine, the pressure after the gas air mixer is always in vacuum state. In order to sample the mixture into the FID sampling head, a vacuum pump was installed into the gas handling system through which the vacuum inside the CP chamber was ensured. The vacuum pump was also connected to the FID flame chamber in order to obtain a higher vacuum than that in the CP chamber and to draw off burned substances from the chamber. The vacuum level within the CP chamber and the flame chamber were adjusted separately by using two built-in regulators. Because there was no liquid fuel condensation problem or high temperature exhaust gas condensations in this study, the sample line heater provided was not used. To avoid the vacuum line water vapour disturbance to the FID output, the condensation collection bowl was periodically purged.

The pressure within the flame chamber of the FID varies with the flow rates of the air and the hydrogen fuel. Because the pressure decides whether adequate amount of low pressure mixture can be sampled into the FID for the vacuum pump used, a series of parametric tests were carried out in order to find out the relationship between the

thermodynamic status and the flow rates of the air and hydrogen fuel supplied to the flame chamber. The result would help to enlarge the FID operating range under the required engine operating conditions. There is another factor which also affects the selection of the FID setting point with respect to the H_2 and air flow rates. Because the characteristics of the FID are affected by the flow rates of the sample, the concentration of the sampled mixture hydrocarbons and the air to hydrogen ratio which is defined as the air flow rate divided by the hydrogen flow rate; the setting point of the H_2 and air flow rate should be of such values that they are offering a high sensitivity, a good linearity and present a low oxygen interference. Because the single carbon atom CH_4 accounts for about 90 percent in mass in natural gas, the FID output signal is extremely weak. Thus the maximum sensitivity setting is desired. Of course it is very difficult to satisfy all these requirements at the same time. For example, a high vacuum in the flame chamber will cover a wide range of low pressure sampling sources, but produce a low signal output for a fixed sample flow rate. In order to find out the best compromise of all the possible settings, a sensitivity test was also carried out on a range of air flow rates and hydrogen flow rates by sampling the span gas with a known mixture concentration and sampling pressure.

For a fixed span gas pressure and a fixed pressure difference between the CP chamber and the flame chamber, the flow rate of hydrogen was firstly fixed at 70 cc/min. The air flow rate was then adjusted from 250 cc/min to 1400 cc/min. The results of the flame chamber pressure and the FID signal output with different air flow rates are given in Figures 4.4 and 4.5. The vacuum pressure in the flame chamber decreased with the increase of the air flow rate. The higher the air flow rate, the more the excessive air supplied to the FID chamber, the lower the vacuum in the flame chamber. For a fixed pressure difference between the CP chamber and the flame chamber, the lower the vacuum pressure in the flame chamber, the lower the vacuum pressure in the CP chamber. The sensitivity of the FID signal output to the air flow rate increased with the increase of the air flow rate. In order to draw the sample into the CP chamber and the flame chamber, the pressure difference between the sampling source and the CP chamber and the pressure difference between the CP chamber and the flame chamber should be great enough. This demanded a lower pressure or higher vacuum in the flame chamber. Thus a low air flow rate was required. But to obtain a high signal sensitivity, a high air flow rate was required. For the engine used, the intake pressure or the sampling vacuum pressure was in the range of 430 mmHg to 20 mmHg for the engine operating range encountered. Thus the air flow rate should be lower than 1100 cc/min in order to be able to sample the mixture from the mixer with a pressure margin of 100 mmHg. The sensitivity result showed that the signal output was too weak if the air flow rate was lower than 800 cc/min. Therefore for the hydrogen flow rate tested, the air flow rate

should be in the range of 800 cc/min to 1100 cc/min. To examine the effect of the hydrogen flow rate on the flame chamber pressure and signal output sensitivity, the hydrogen flow rate was changed from 50 cc/min to 250 cc/min at a fixed air flow rate of 900 cc/min. The results given in Figures 4.6 and 4.7 showed that the vacuum in the flame chamber changed from 530 mmHg to 543 mmHg, which did not vary significantly. The signal sensitivity result showed that at the hydrogen flow rate of about 70 cc/min, the maximum value was obtained. At this flow rate the temperature in the chamber was not too high, which was about 580 °C. When the hydrogen flow rate exceeded the flow rate of 120 cc/min, the temperature in the flame chamber was over 700 °C and even reached above 800 °C when the hydrogen flow rate was 200 cc/min, which was not safe for the sampling system. Therefore an air flow rate of 900 cc/min and a hydrogen flow rate of 70 cc/min was set for the flame chamber air-fuel supply, which gave a reasonable compromise between the flame chamber vacuum and the FID signal output. At this setting the sampling mixture vacuum could be as low as 430 mmHg, which was the operating condition of the engine at just above its idling operation. As has been reported by other researchers [139], this setting was also in the range of good linearity and low oxygen interference. A linearity test was conducted at this setting with the engine running at steady state, that is, with a fixed engine speed, throttle position and cooling status. With the engine overall mixture air fuel ratio changed from 14 to 24 by changing the fuel supply system, FID signal outputs at the same sampling point were measured and the result showed that its linearity was quite good, see Figure 4.8. To keep the pressure and temperature at the sampling point constant under all of the mixture air fuel ratios, the load exerted by the dynamometer was adjusted to obtain a constant engine speed and throttle opening position. The linearity result was similar to those obtained by some other researchers in their Cambustion FID calibration tests [142] [145].

The setting of the pressure difference between the CP chamber and the flame chamber depended on the signal sensitivity and the engine operating condition. When the engine was run at higher loads and speeds, the pressure difference was kept constant at 100 mmHg and it was 50 mmHg when the engine was run at lower loads and speeds in order to sample adequate amount of mixture from the sampling source points. If the sample flow rate had been too low, the insufficient signal would have required a higher amplification gain, which would have resulted in a relatively low signal/noise ratio. If the sample flow rate had been too large, the measuring flow field would have been distorted and the FID burner flame would have been disturbed, which would have reduced the degree of accuracy.

4.4 Test procedure and results

4.4.1 Test procedure

To make the experimental results directly comparable to the results from the CFD simulations conducted, the engine was initially run under a steady operating condition with a brake power output of 15 kW, which was at about 1500 rpm in speed and 100 Nm in torque. After the engine and all the instruments were warmed up, the engine was adjusted to give the output wanted. The outlet of the mixer was probed at discrete positions by a pitot tube which was oriented into the mixture flow. The probe was traversed along the full diameter of the pipe. The probe also measured the total pressure, which allowed discrete values of velocity to be calculated at each location of the probe when a static pressure at the same plane was also detected. The analysis of samples was undertaken continuously by the FID and a map of mixture concentration variation across the mixer outlet was obtained at the engine operating condition. A single gas admission slit placed either in the inner bullet or in the outer body was firstly investigated which was a similar arrangement to that considered in one of the CFD simulations. Then the effect of gas admission slit dimensions and numbers on mixture formation were studied. This included changes of the single inner slit width over a range of 0.41 to 2.2 mm and gas slits placed both in the inner bullet and the outer body. The effect of changing the throat area by varying the bullet size on the mixture formation was next examined. With the optimised dimension of the slit width and inner bullet or throat area, the engine was operated under different operating conditions, which revealed the effect of air flow rate on the mixture formation. After this, the measurements were conducted when the mixer was installed in the engine intake system with and without the matched throttle valve aiming at examining the effect of the throttle plate on the mixture concentration distributions and the pressure losses across the mixer. Finally the axial pressure distributions along the mixer were measured in order to obtain another direct parameter for the validation of the CFD simulation results. In addition, the pressure axial distributions and the pressure loss across the mixer with different inner bullet nose shapes were compared in order to verify the effect of the nose configurations on the mixer flow restriction.

4.4.2 Experimental results and analysis

The results for operating the novel mixer with inner and outer slits independently and simultaneously are shown in Figure 4.9 at the engine operating speed of 1500 rpm and load of 100 Nm, which was correlated to the air flow rate of about 60 m^3/h. For the single inner slit, mixing was found to be extremely poor. The core of the outlet of the mixer was rich in fuel, but the mixture was extremely lean in the periphery. With an

additional slit incorporated around the outer diameter of the throat, mixing result was greatly improved. Single outer slit gave a similar mixing result to the inner one, but in an inverse manner. The reason for this was believed to be the same as what had been found from the CFD simulations. Due to the penetration ability and turbulence intensity, the low momentum gas stream could not easily penetrate into the far side of the air stream. When a single slit was used, the momentum of the gas jet was forcing the air flow to the other side of the mixer and the momentum of the air was forcing the gas jet to change its direction and to flow downward in the near region. When the gas was admitted from both sides, the effect of air flow diversion was expected to be countered. This not only increased the intersurface area significantly, but also shortened the distance needed for penetration dramatically. At the same time the turbulence of the air stream was increased owing to the gas blocking effect from both sides of the air stream rather than from one side. The actual effective flow area for the air stream was smaller than that for a single gas admission slit. The entrainment of the gas into the air from two sides of the annular air stream significantly increased the mixture homogeneity at the outlet plane of the mixer. Clearly the mixture distribution variations when operating with either the outer or inner slit independently were unacceptable, but favourable results were obtained when operating with both slits simultaneously. In terms of the pressure loss across the mixer, it was about 300 N/m^2 for the single inner slit, 294 N/m^2 for the single outer one and 255 N/m^2 for the double slits. The mixer exhibited an extremely good pressure recovery irrespective of which kind of gas admission was used, primarily due to the low gas signal and the mild geometry changes. It was interesting to notice that the mixer operating with both slits simultaneously not only produced a better mixing, but also produced a lower pressure loss, which had also been predicted by the CFD simulations.

Even with the two gas admission slits, the mixture concentration was still having a large variation. The lean mixture existed in the middle area between the centre and outer edge of the mixer, the rich mixture in the central and outer part. Thus following the similar steps as in the CFD simulations, three different slit widths were tested for the initial design with the inner bullet diameter of 30 mm. The effect of changing slit width when operating with the inner slit only is shown in Figure 4.10. Changing the slit width, and therefore the gas velocity entering the air stream had little effect on mixing performance. This had also been predicted using CFD modelling, and it was believed that the momentum of the gas, which determines how far the gas can penetrate into the air stream, had not been changed much as the velocities were varied. With the velocity changes, the gas momentum flux was still of the same order because of the lower gas mass flow rate. With respect to the pressure losses across the mixer, there was not much difference between the three widths tested. The values were about 300 N/m^2 for the 0.41 mm one and a little smaller with the increased widths. Changing slit width tests were

also made when operating with the outer slit only and with both slits together. The same results were reached, but with the adjustment of the gas flow area on each slit separately, the amount of gas through each slit could be balanced according to their annular diameters, which did affect the mixture distributions. When the same slit width was used for both gas admission slits, the gas flow rate drawn into the mixer from the outer slit was higher than that from the inner one because of the larger outer slit circumferential diameter. In this case the rich mixture occurred in the outer annular area of the mixer outlet plane. For this reason the humps appeared in the mixture concentration distributions curve of the double slits were shifted by adjusting the slit width on each side separately.

Another experiment was made on the effect of the throat area by changing the diameter of the inner bullet. Figure 4.11 shows the mixing performance for different sizes of bullet from 30 mm diameter to 33 mm diameter, tested without a throttle valve and with the slit width fixed at 1 mm for the inner and 0.5 mm for the outer. The larger diameter bullet produced better mixing as the turbulence in the throat and the mixing intersurface area was increased, and the distance between the inner and outer slits was reduced. However the larger diameter bullet produced a higher pressure loss, which was about 255 N/m^2 for the 30 mm inner bullet, 536 N/m^2 for the 32 mm and 646 N/m^2 for the 33 mm. Thus compromise had to be made between the mixing and the pressure loss. Comparing the three sizes the 32 mm bullet produced good mixing and reasonable pressure loss. Because the tests were carried out without the throttle valve attached, the mixture homogeneity was expected to be improved for each of the three sizes if a throttle valve was added. This was verified in a later study.

The experimental mixture concentration distributions results given above, however, showed that the distributions were not symmetrical. This should not be a feature of the symmetrical geometry design. This was believed to be caused by the fact that it was difficult to locate the bullet coaxially. The bullet radial position was carefully checked after the experimental work. It was found that the gas supply pipe elbow was loose causing the decentralisation of the bullet during the test. It was this malfunction of location that caused the non-symmetrical mixture concentration distributions. The inner bullet location method needed to be modified in a future design.

All of the results given above were achieved under the engine operating condition of 1500 rpm in speed and 100 Nm in load. To see the effect of the engine operating conditions and hence the air flow rate on mixture formation, some of the measurements were also carried out at an engine operating speed of 1500 rpm and load of 200 Nm, which was correlated to the air flow rate of about 100 m^3/h. Figure 4.12 gives the mixture concentration distribution results under the two engine operating conditions

with identical mixer dimensions. As had been predicted by CFD simulations, the mixture concentration distributions were not sensitive to the engine operating conditions, but the pressure loss across the mixer was. The higher the engine load or the greater the air flow rate, the higher the flow velocities within the mixer and the higher the flow restriction. The pressure losses were increased from 646 N/m^2 at 60 m^3/h to 1846 N/m^2 at 100 m^3/h for the 33 mm bullet diameter. The mixture velocity at the outlet plane of the mixer was increased as well, which corresponded to the flow rate increase.

The presence of throttle plate was tested for this prototype novel mixer, and results given in Figure 4.13 show that the throttle plate did play a part in mixture preparation. The presence of throttle plate improved the mixing, but increased the flow restriction, see Figure 4.14, which was also corroborated in reference [22].

In order to obtain some fluid dynamics variable distributions within the flow domain for further CFD validations, the static pressure distributions in the mixer axial direction were measured. Of the variables of interest, the static pressure was the one which could be easily obtained without much interference to the flow behaviour. Six small pressure tappings were made along the mixer at different characterised positions. Two other tappings were also placed inside the gas supply plenums which were just ahead of the inner gas admission slit and the outer slit, in order to measure the gas pressure losses on passing through each of the passages. The results of the axial pressure distributions along the mixer under different engine operating conditions are shown in Figure 4.15 for the 32 mm inner bullet diameter with a 1 mm inner and 0.5 mm outer slit width. For all the flow rates tested, the lowest pressure or in other words the highest pressure depression appeared in the throat area, which resulted from the venturi effect. The pressure started to recover gradually after the cylindrical section of the inner bullet. The divergent part of the venturi outer body further recovered the pressure. At the end of the mixer divergent part, the pressure was still recovering but with a very small gradient. On the outlet plane of the mixer, the pressure could not be recovered to the same level as when the air was drawn into the mixer due to the turbulence and friction. Some of the energy had to be used to help the mixing.

The gas pressure drop across the passages against the air flow rate are given in Figure 4.16. The gas pressure loss from the gas inlet to the inner gas admission slit was different from that to the outer one. The pressure loss to the outer one was a little less than that to the inner one because of the small connection holes used in the inner bullet.

To see the effect of the inner bullet nose configuration on the pressure distributions or the pressure losses across the mixer, a pointed nose was machined which was identical

to one of the configurations simulated by CFD modelling. Results are given in Figure 4.17 together with the pressure distributions obtained from the hemispherical nose or round nose under the same engine operating condition. Comparison of the pressure distributions from the different bullet nose configurations showed that the pointed bullet nose could not reduce the pressure loss across the mixer. It was the throat dimension and the dimensions of the annular venturi bodies in the mixing part, the area immediately after the throat, and the divergent part of the mixer that played a very important role in pressure recovery. Comparisons of the two nose configurations under different engine operation conditions gave the same conclusion as above.

4.5 Comparison of the computational and experimental results

The mixture concentration distribution comparisons are shown in Figure 4.18. It can be seen that the computational results and the experimental results have a good agreement with each other no matter what width of gas slit was used, in what position the gas slit was located or how many slits the mixer had. However, the velocity distributions, see Figure 4.19 failed to give such close agreement, at least not as good as that of the concentration distributions because of the non-symmetrical test results. However, the agreement is still within a reasonable range.

The good agreement obtained on the mixture distributions at the mixer outlet plane showed that the findings from the CFD simulations with regard to the mixing mechanism, the gas blocking effect and the entire mixing processes of the mixture formation within the venturi type mixers were truly described. The findings were very helpful not only for the understanding of the physical process taking place within the mixer, but also for further gas air mixer design and development programmes.

Comparing the effect of the inner bullet diameters on the mixture formation, it can be seen from Figures 4.20 that the measured results gave exactly the same conclusions as that obtained from the computed results. The 33 mm bullet diameter gave the best mixture homogeneity and the 30 mm one produced the worst of the three diameters tested. The diameter of 32 mm gave both a reasonable mixture homogeneity and an acceptable pressure loss across the mixer. The measured results given in Figure 4.12 showed that different air flow rates under different engine operating conditions had little influence on the mixture concentration distributions at the outlet plane of the mixer, which had been predicted by the CFD simulations.

The measured pressure losses across the mixer were 255 N/m^2 and 646 N/m^2 for the bullet diameter 30 mm and 33 mm respectively with the double gas admission slits arrangement. They agreed very well with the predicted results which were 248.9 N/m^2

and 507.5 N/m^2. The measured pressure axial distributions along the mixer for the 32 mm inner bullet diameter with double slits and the CFD predicted results are given in Figure 4.21. They showed a very good agreement with each other. The predicted axial pressure distributions along the mixer gave much more detailed information than did the measurement at a number of limited discrete points, especially at the transient sections region. The difference in the convergent part was because of the difficulties of wall roughness number specification. Comparison of the predicted and measured pressure losses across the mixer with the pointed nose gave a very good concordance too. All other pressure losses predicted under different conditions were in good agreement with the measured ones.

However some subtle differences existed between the measured and the predicted mixture concentration distributions. From the predicted results the mixture was often far richer in the outer annular and the central area of the mixer than the measured mixture distributions. There were two possible reasons for this. One was the turbulence intensity value specified during the computation which should have been larger than 0.2. The lower value was also the possible reason for the underestimated pressure loss across the mixer. The other was the default values used for those parameters like the Prandtl number and Schmidt number which affected the mixing problems. For the flow domain considered and the physical problem simulated, coefficients in the turbulence model and species mixing model needed to be examined in order to achieve better agreement between the predicted and measured results should it be the absolute value of the fluid dynamics variables rather than the comparative study that had been of interest. By carefully adjusting these parameters, better agreements could be expected.

Another disagreement between the tested and predicted results was when a narrower outer slit width of 0.5 mm was used, the predicted mixture distribution showed that the outer area had a leaner mixture, which was different from the tested result. This was because the gas pressure drop across the two gas slits and their passages were not identical. As the gas pressure measurement showed in Figure 4.16, the gas pressure drop to the outer gas admission slit was less than that to the inner one. The gas pressures behind each of the slits were not equal, nor was the pressure in front of the slits because the local pressure varied in a radial direction. Thus the equal gas inlet velocity assumption made during the CFD prediction was believed to be the main reason for the disagreement. The underestimated species transportation was another contribution to the discrepancy.

At this stage it is necessary to point out that all experimental work is subject to errors in accuracy despite all precautions. It is not possible to completely eliminate the errors. Similarly computational work involves errors which are either incurred by

approximations of the models themselves at the conceptual stage or produced by the geometrical and numerical assumption during the computation process. Thus when differences occur between experimental and computational results, it is very difficult to pinpoint which of them is more plausible, especially in the case where both techniques are newly emerged ones.

4.6 Comparison between the Gem and proprietary mixers

For the purpose of comparison and performance evaluation, the mixture concentration distribution, pressure loss and mixture regulation for the three proprietary mixers described in chapter three were measured by the same methods as used for the prototype novel gas engine mixer, hereafter named as Gem.

The mixture concentration distributions for the three proprietary mixers and the Gem are shown in Figures 4.22 to 4.25 for two flow rates, 60 & 100 m^3/h, and two perpendicular diametric traverses across the outlet plane of each mixer. As had been tested with the Gem that the throttle plate had an effect on the mixture relative air fuel ratio and the pressure loss across the mixer. The measurement for the Gem was made with a throttle valve which was the one used for the similar type D-mixer due to the fact that each of the proprietary mixers were supplied together with their own matched throttle valves. Thus the results for the mixers were directly comparable. In each case the throttle plate was set to the wide open position and the engine operating condition was controlled through another throttle valve installed directly on the engine intake manifold. To represent the distributions of mixture concentration, the mixture λ value is used. A schematic diagram in each figure shows the orientation of the mixer and throttle plate with respect to each traverse.

The I-mixer showed variation in λ value of between 30 to 40 % from minimum to maximum values in both traverse directions for both the lower and higher air flows (60 & 100 m^3/h). This inhomogeneity was attributed to the gas and air inlet arrangement because the mixture was rich on the gas inlet side and lean on the air inlet side. These results were also achieved by Klimstra, J. [87]. To increase the mixture homogeneity, the means of gas admission needs to be rearranged and the configuration of the gas/air mixing chamber needs to be modified. The mixture homogeneity from the H-mixer showed that the variation in λ value for the same flow rates was between 8 & 11 %, again with little difference between the higher and lower flow rates. The larger gas distribution orifice and the existence of a mixing chamber made the mixture a little

more homogeneous than from the I-mixer, but it was still unsatisfactory. By comparison the D-mixer showed variations in λ value of between 3 to 4 % for the same flow rates. This was believed to be due to the relatively symmetric gas air inlet arrangements which resulted in a more homogeneous mixture than that from the previous mixers. Aside from the presence of one rich core in the centre of the carburettor, as being assumed by Klimstra, J. [87], there was another rich core which was located in the circumferential area of the carburettor, see the two humps in Figure 4.24. These two humps revealed that the gas entered into the main air stream from holes placed in the aerofoil shaped cross mainly gathered in the central area and the gas from holes around the circumference of the throat in the outer area. It was the air and gas entrainment and the turbulent mass transportation which partly mix the gas and air together at their interface. The bigger the interface area or the higher the turbulence intensity, the more homogeneous the mixture would be, but which would result in a higher flow restriction.

Figure 4.26 shows results of mixture distributions for all the mixers. The D-mixer clearly produces a near homogeneous mixture, superior to either the I-mixer or H-mixer. Results for the D-mixer showed little variation in either traverse direction as a result of the geometric symmetry of this design. The mixture homogeneity for the Gem mixer appeared as good or better than the D-mixer tested at the same conditions. Figure 4.27 shows comparative pressure loss for each of these mixers against air flow shown as percentage of the maximum flow rating stated by the manufacturer for each mixer. Clearly the Gem mixer showed the lowest pressure loss of the mixers tested. But it should be noticed that the lower flow rate range tested for the I-mixer which was a variable restriction type and the pressure loss at high flow rates would be different. Even so the Gem was still a low flow restriction type mixer, which was the inherent feature of the venturi configuration.

Mixture regulation with increasing flow is another parameter often used for evaluation of mixers. Measurement was made on this characteristic for the Gem and the three proprietary mixers. In this test the gas pressure entering the mixers was maintained equal to the air pressure at inlet to the mixers aiming at eliminating the effect of the gas pressure fluctuations. As shown in Figure 4.28, both the Gem mixer and the H-mixer maintained relatively constant air fuel ratio over most of the flow range, however the D-mixer mixture became leaner at high flow rates. This resulted from the increasing loss in gas pressure across the complex internal passageways and the control valve used in the design. The I-mixer showed the phenomenon of mixture enrichment with increasing flow. This was to allow lean mixture at part load for economy and stoichiometric mixture at high load for power output. The variable geometry design also allowed slight losses in pressure in the gas supply system as flow rate increased.

4.7 Summary

By using a carefully calibrated novel instrument Cambustion FID, mixture concentration distributions and pressure loss across the Gem mixer were measured together with some other mixer performance evaluating parameters. Because of the inherent properties of natural gas, the gas flow stream does not easily penetrate the high momentum air flow stream. In order to obtain a homogeneous mixture, a large mixing interface area and a reasonable turbulence intensity are essential. An even inlet gas distribution over the air stream will aid the mixing under the arranged mixing intersurface. The throttle valve effects both the mixing and the flow restriction. But the inner bullet nose configurations have little effect on the mixer performance.

By comparing the CFD computational and experimental results, the package was further validated with respect to the concentration distribution which was one of the key parameters to evaluate the performance of mixers. Of the three variables measured, all of them gave excellent agreement between the predicted results and the measured results. The predictions not only gave information about the variables of interest on the outlet plane of the mixer, as the experiments did, but also gave more detailed fluid dynamics information within the whole mixer on every variable involved. This was one of the advantages for CFD work compared to the high cost experimental approach. Having the experience and the confidence obtained so far, further development work can then be carried out with the aid of the CFD simulation in collaboration with the necessary experimental work.

By evaluating three proprietary mixers in the same way as that used during the performance measurement for Gem, the Gem mixer was experimentally compared with the other mixers. The Gem mixer exhibited similar or superior performance to the three proprietary mixers tested. Pressure loss was some 20 % lower than that for the D-mixer, which was the lowest of the three proprietary mixers, when tested with the same throttle plate. The variation in λ value across the outlet plane was about 3% for the Gem, compared to approximately 4% for the D-mixer, also the best of the three. The simplicity of the Gem design can result in potentially lower manufacturing costs. The use of slits which can be simply altered in size means that the mixer can be readily adjusted for different engine configurations or operating regimes such as stoichiometric or lean burn applications, which will widen the application range of the mixer.

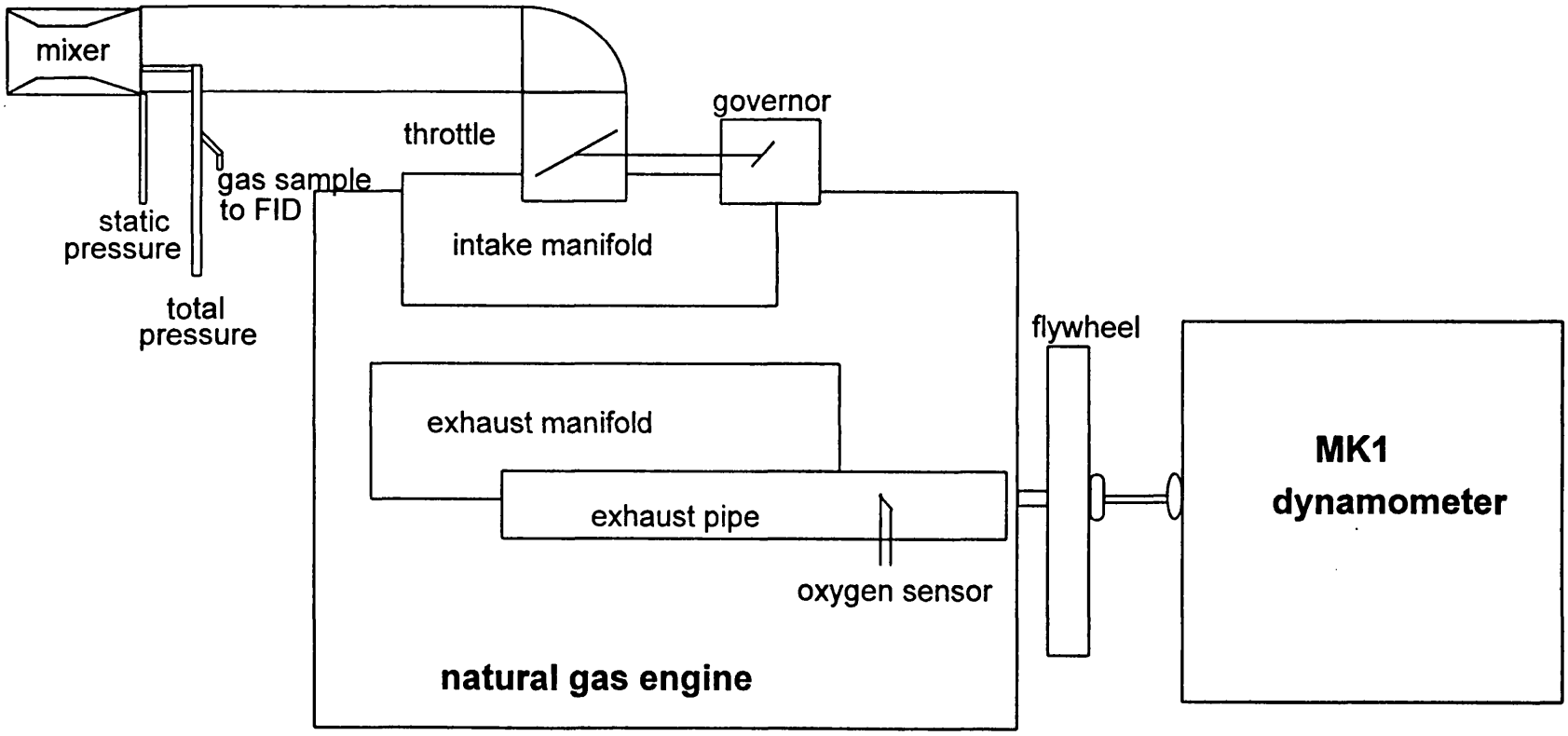

Figure 4.1 Arrangement of the mixer performance test rig

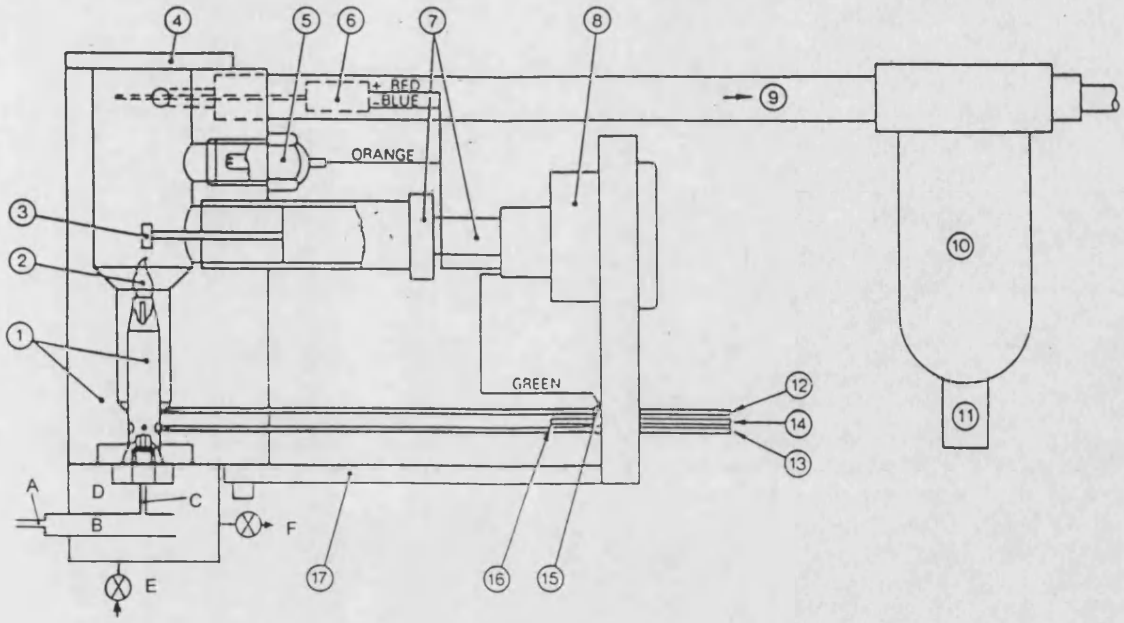

1 burner/flame chamber
2 flame
3 collector electrode
4 lid
5 glow plug igniter
6 thermocouple
7 collector insulator assembly
8 electrical connector
9 vacuum supply
10 condensate collection bowl
11 non-return valve
12 air supply
13 fuel supply
14 sample connection
15 earth tag
16 sample connection
17 base plate
A. transfer tube
B. expansion tube
C. connecting tube
D. CP chamber
E. bleed valve
F. vacuum valve

Figure 4.2 The Cambustion FID sampling head and CP chamber

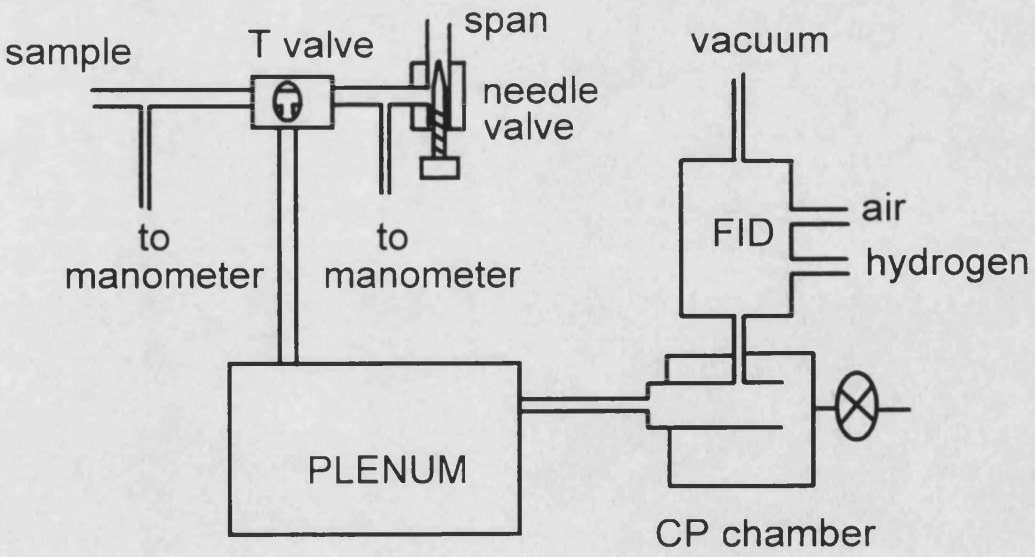

Figure 4.3 Sample and calibration switch system schematic

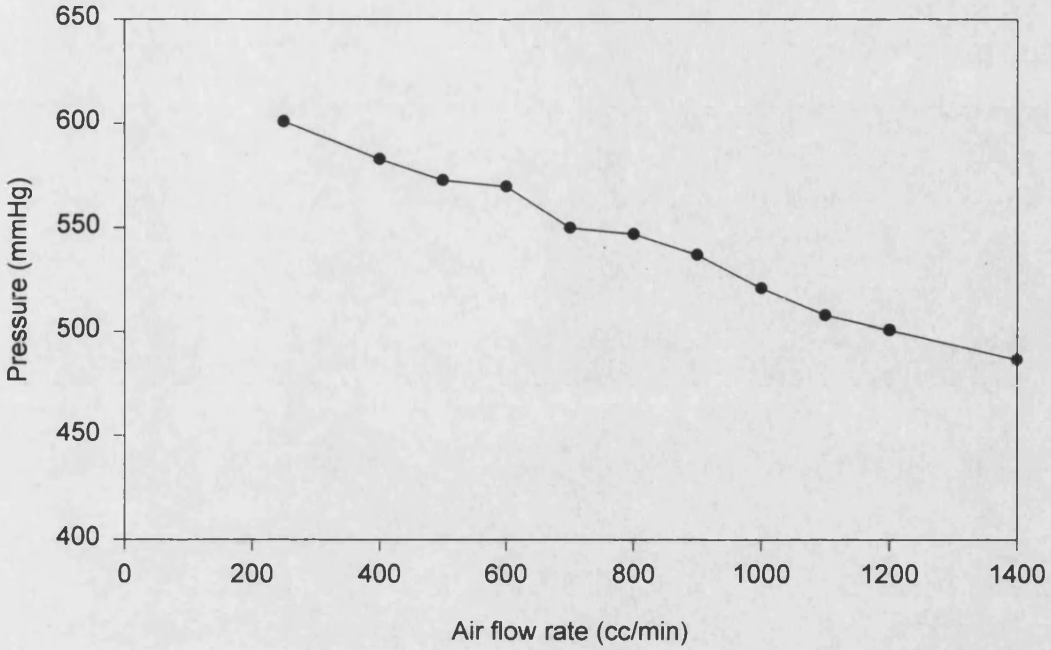

Figure 4.4 Pressures for different air flow rates in the FID chamber

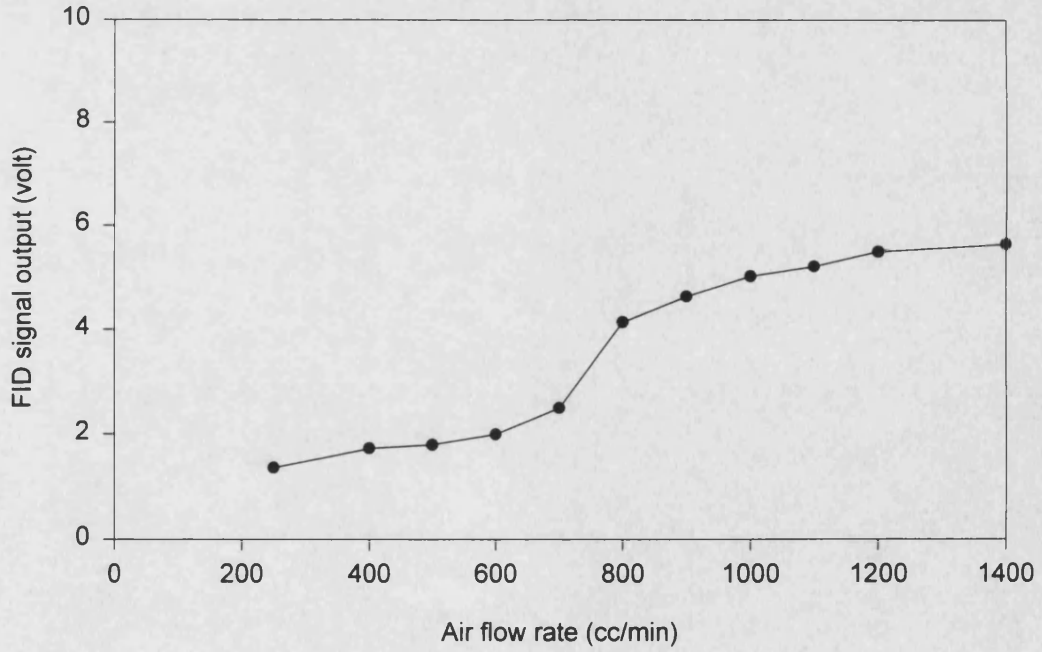

Figure 4.5 Signal outputs for different air flow rates in the FID chamber

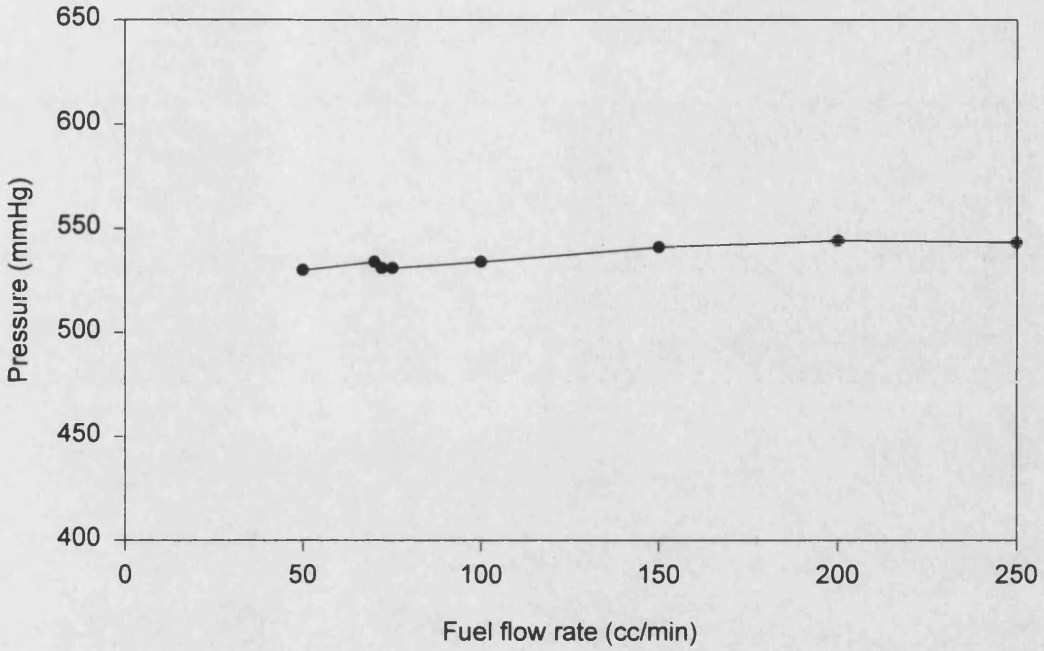

Figure 4.6 Pressures for different H_2 flow rates in the FID chamber

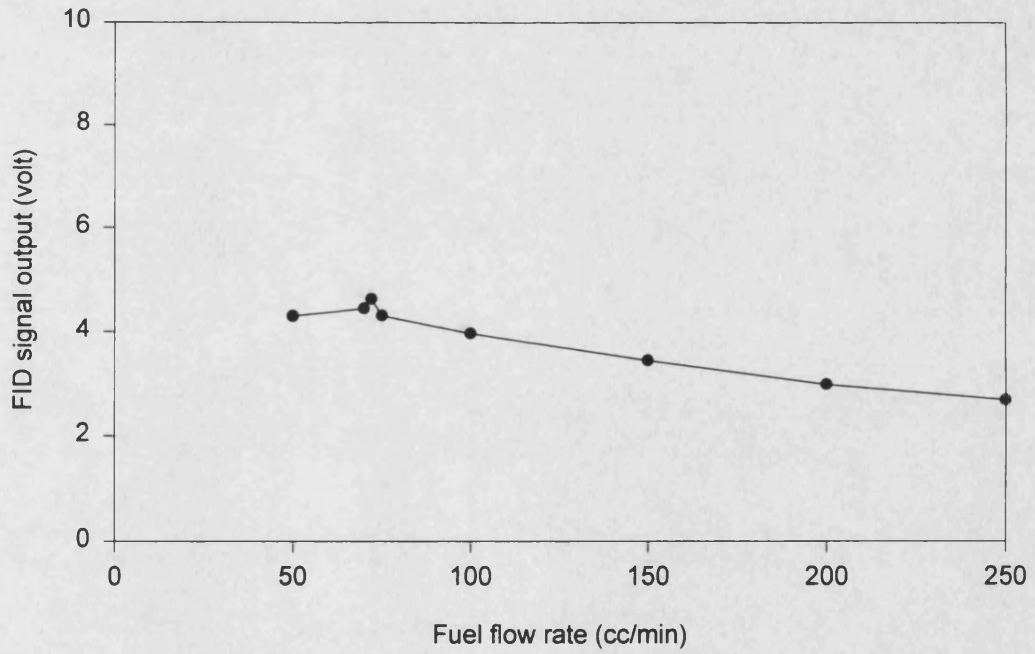

Figure 4.7 Signal outputs for different H_2 flow rates in the FID chamber

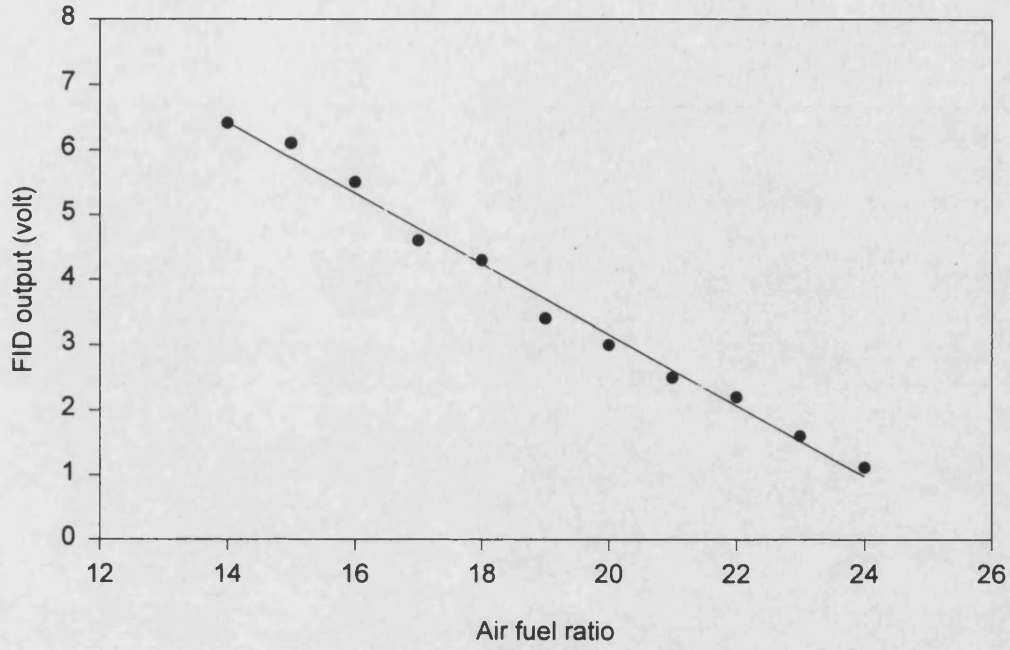

Figure 4.8 FID signal outputs with different mixture strengths

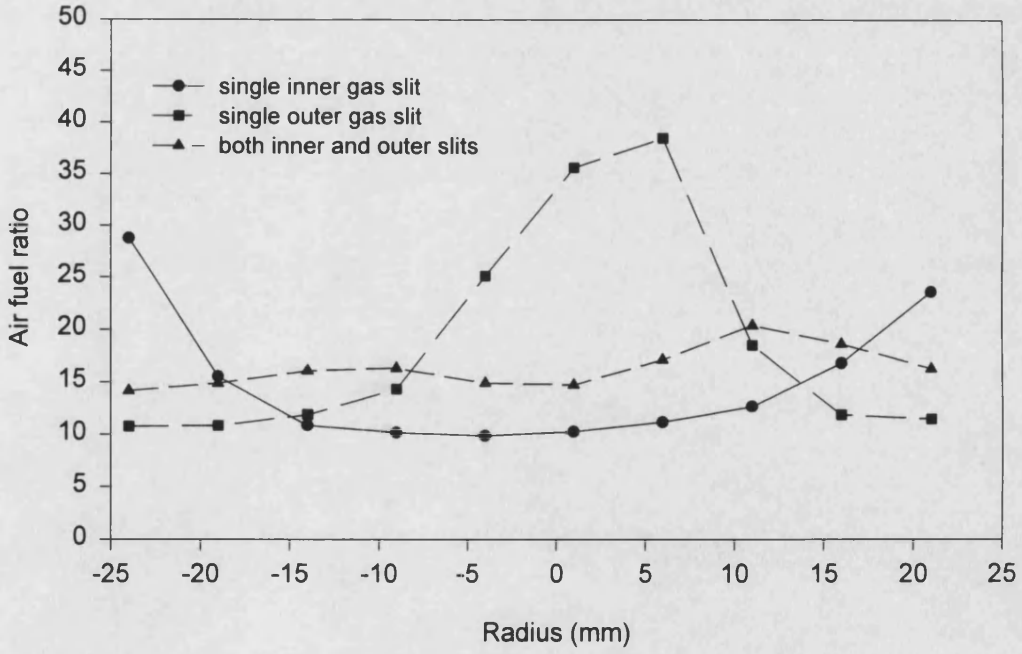

Figure 4.9 Air fuel ratio distributions on the outlet plane of the mixer

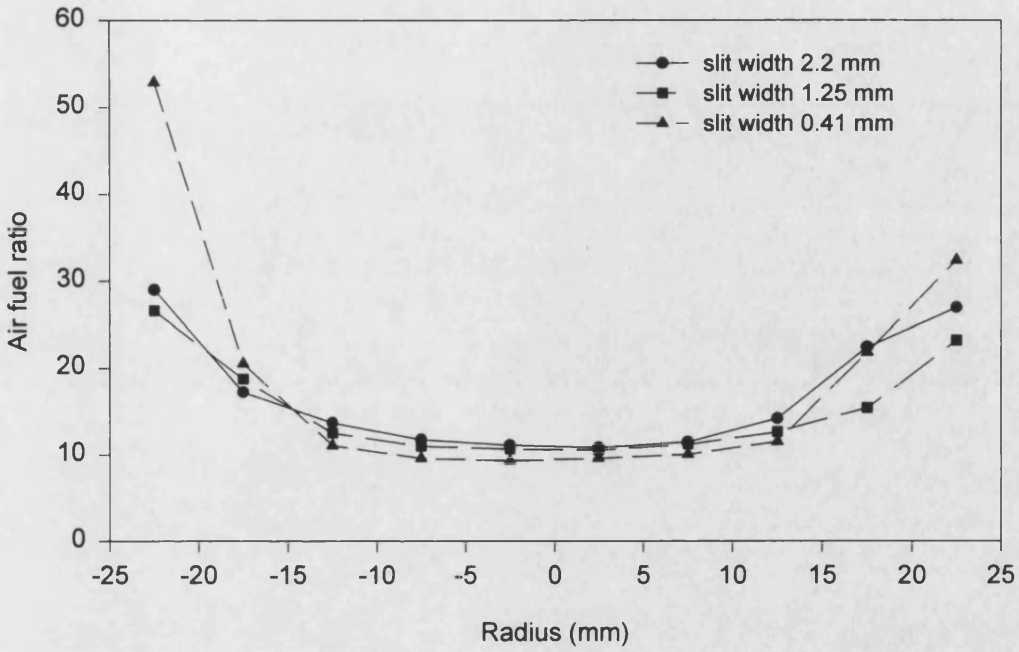

Figure 4.10 Effect of slit widths on mixture formation of the mixer

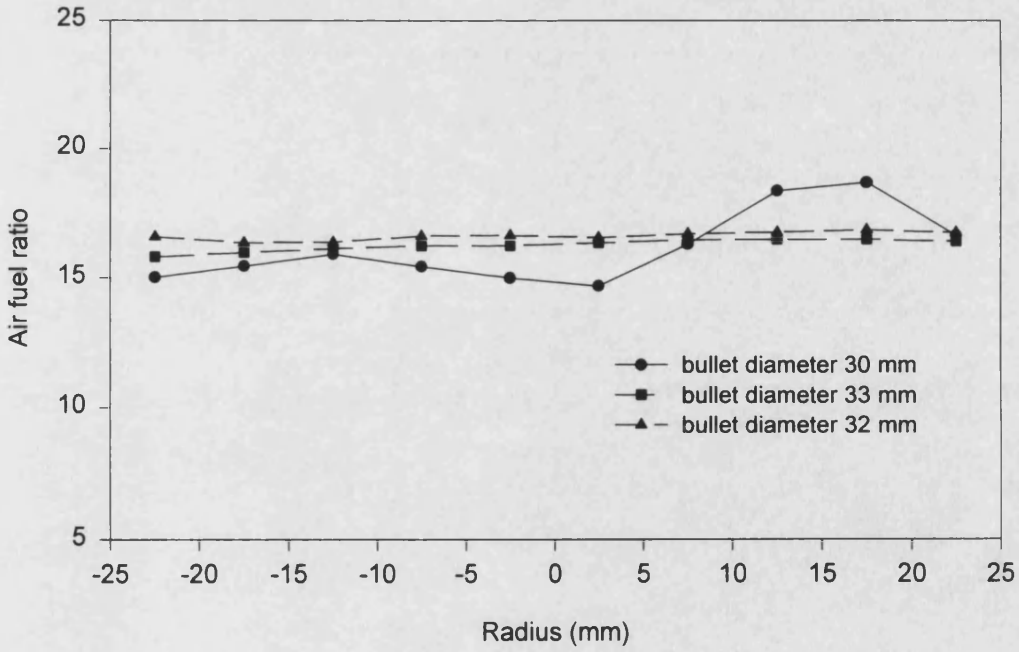

Figure 4.11 Effect of the inner bullet diameters on mixture formation

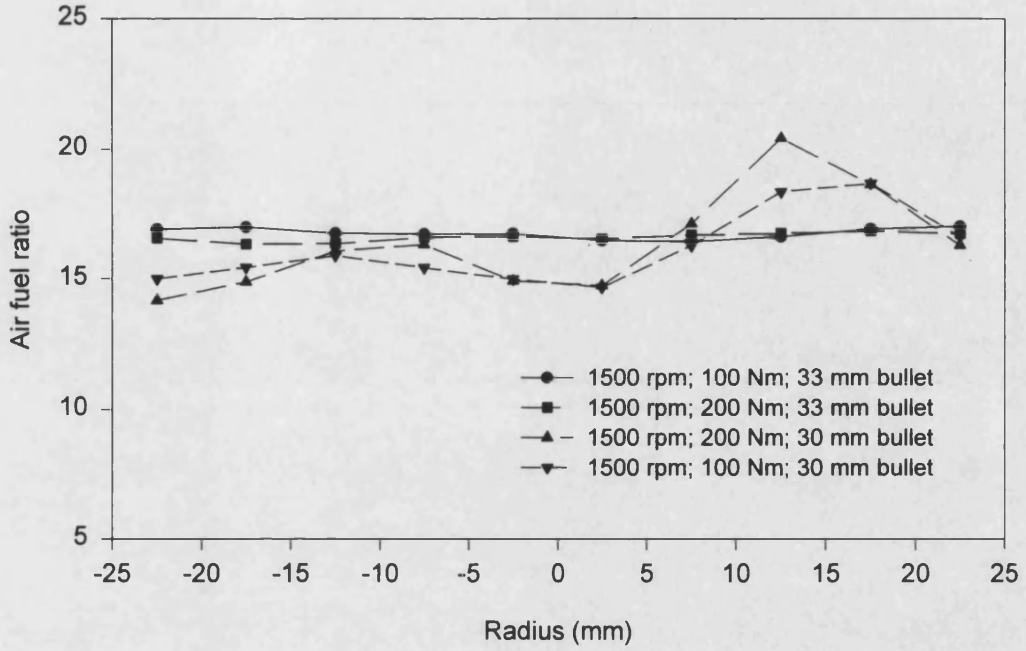

Figure 4.12 Effect of the engine operating conditions on the mixture formation

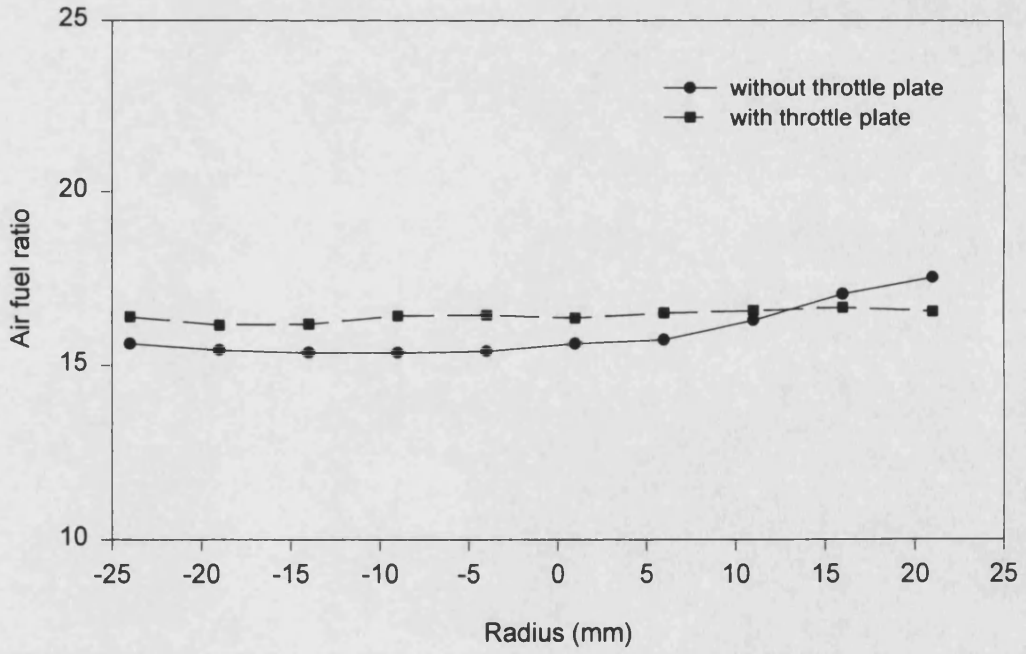

Figure 4.13 Effect of throttle plate on the mixture formation

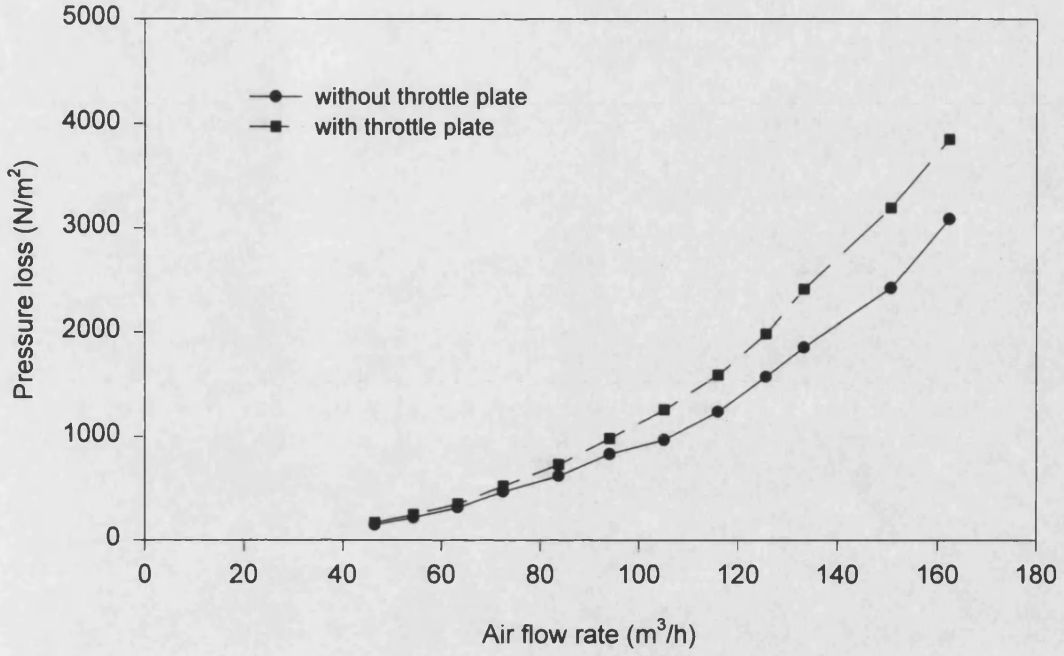

Figure 4.14 Effect of throttle plate on the pressure loss across the mixer

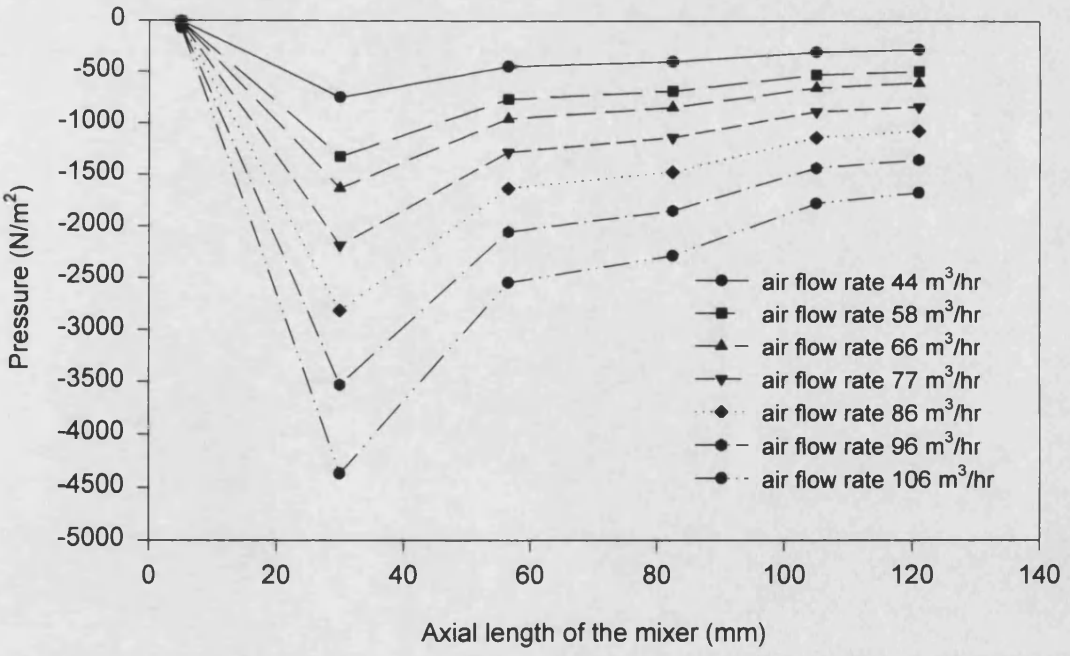

Figure 4.15 Pressure axial distributions along the mixer for different air flow rates

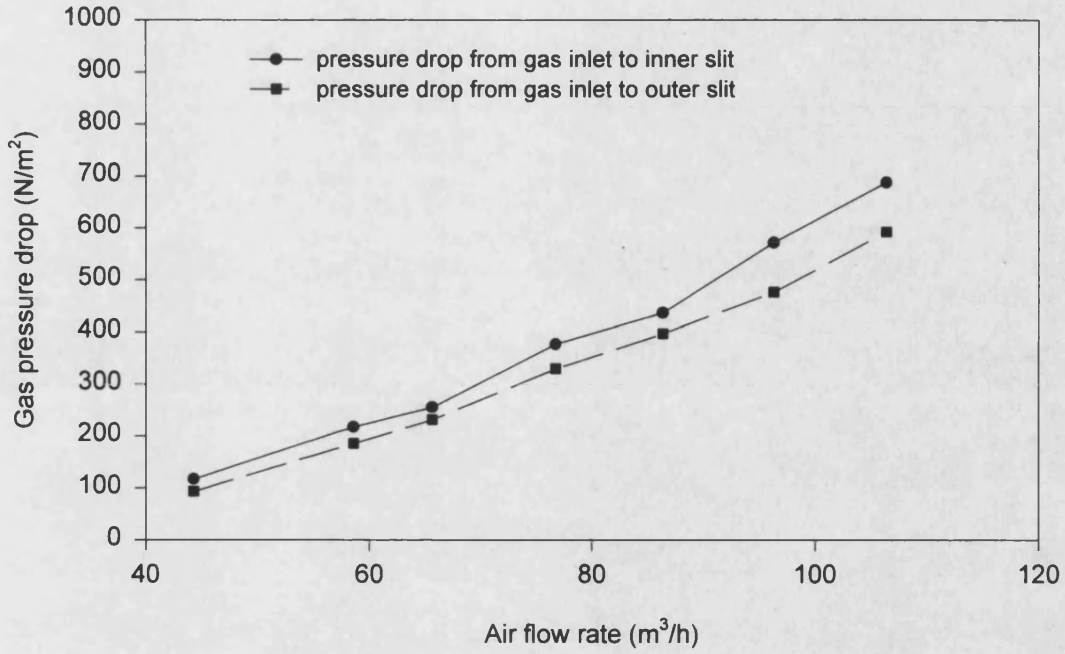

Figure 4.16 Gas pressure loss through the passages within the mixer

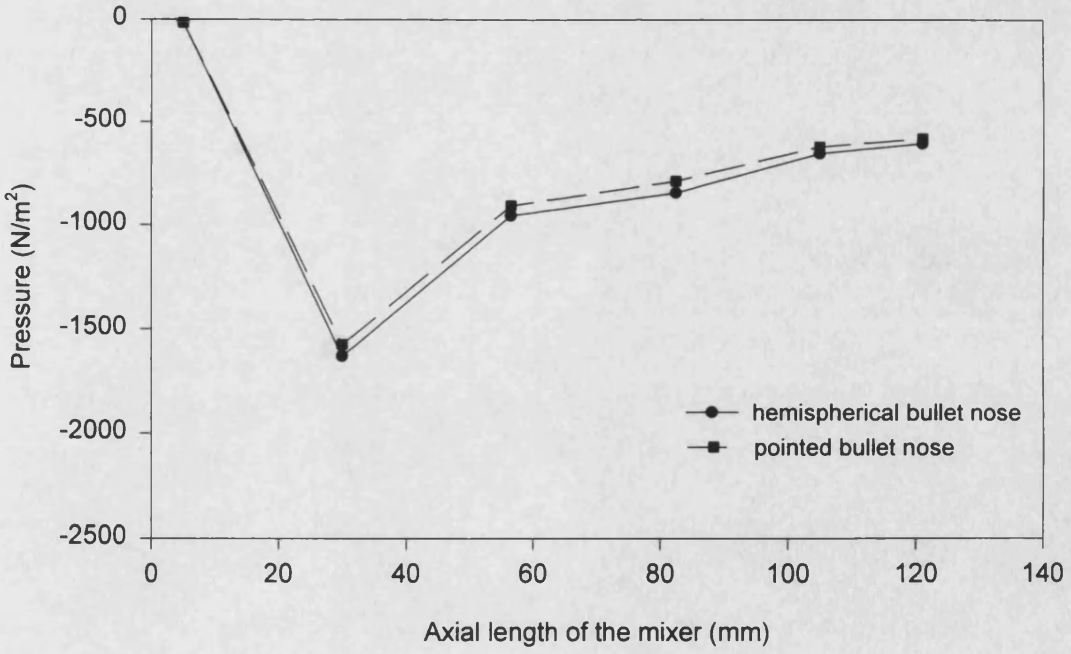

Figure 4.17 Pressure axial distributions along the mixer for different bullet noses

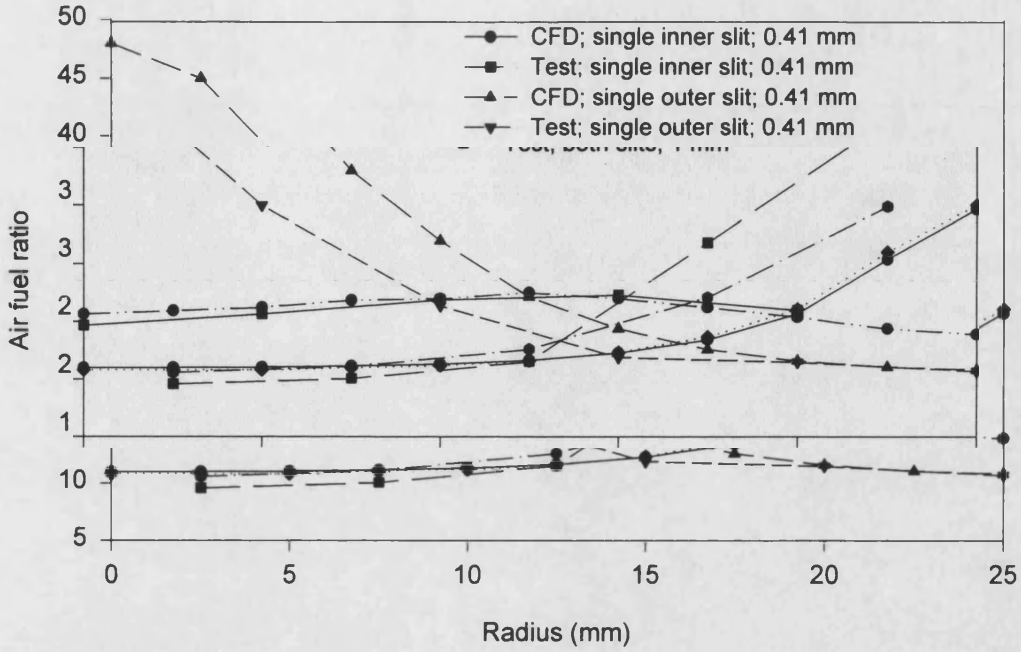

Figure 4.18 Comparison of AFR distributions between the CFD and tested results

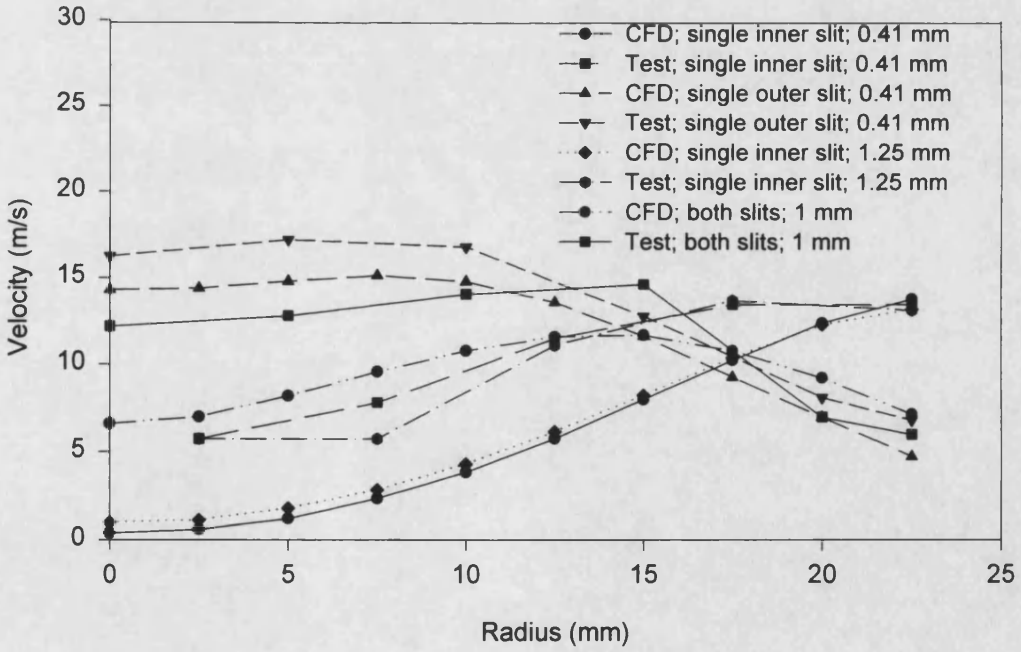

Figure 4.19 Comparison of velocity distributions between the CFD and tested results

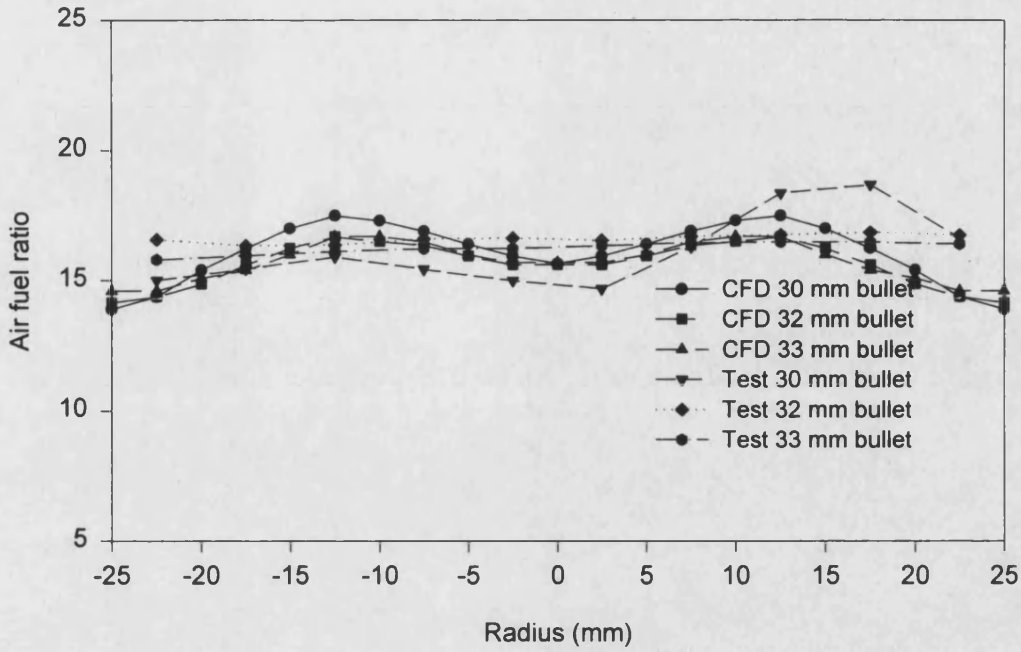

Figure 4.20 Comparison of the predicted and tested results for different bullet sizes

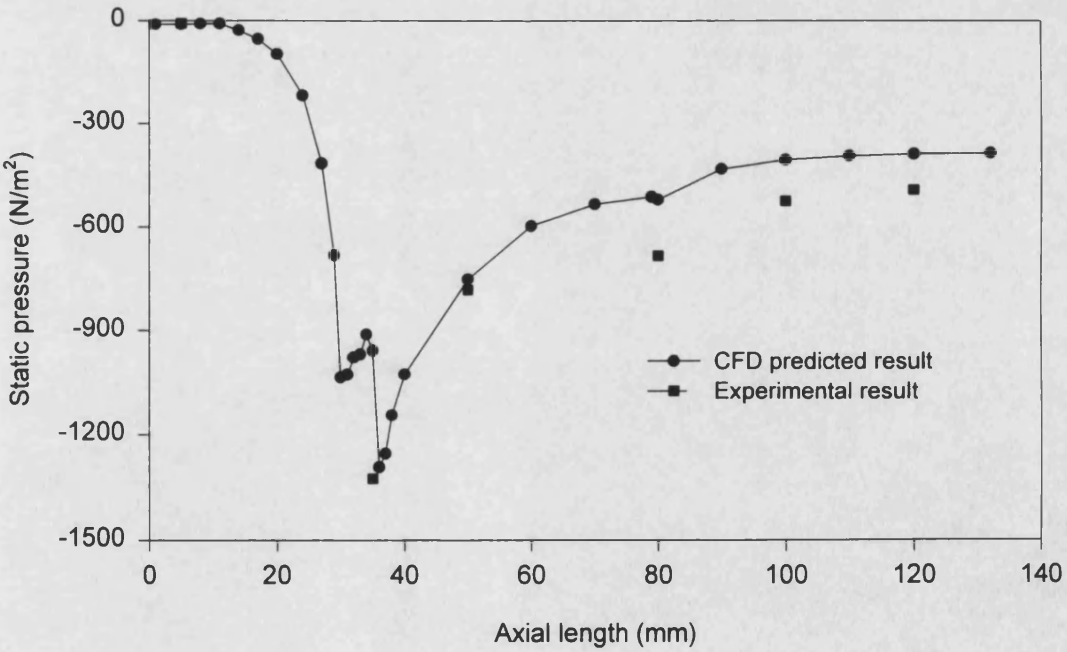

Figure 4.21 Comparison of the predicted and tested axial pressure distributions

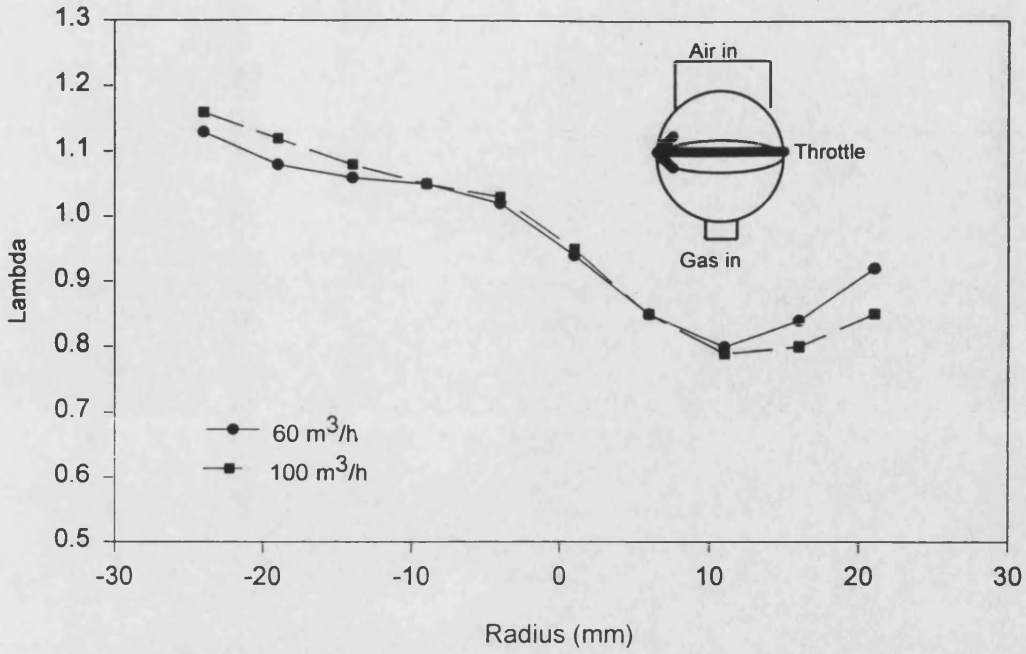

(A) Horizontal traverse

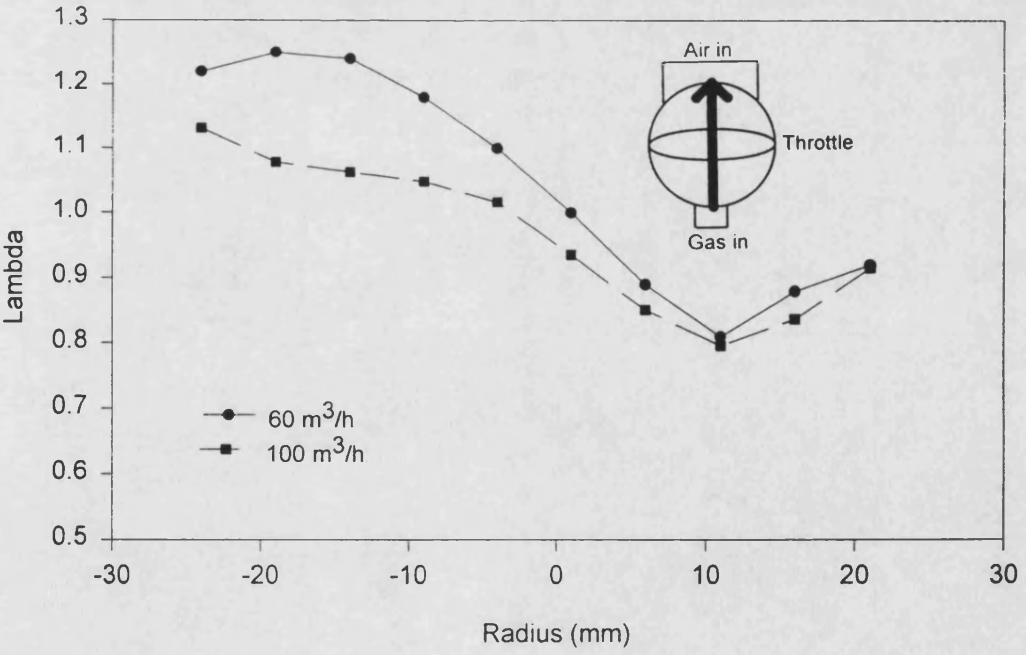

(B) Vertical traverse

Figure 4.22 Mixture distributions for the I-mixer

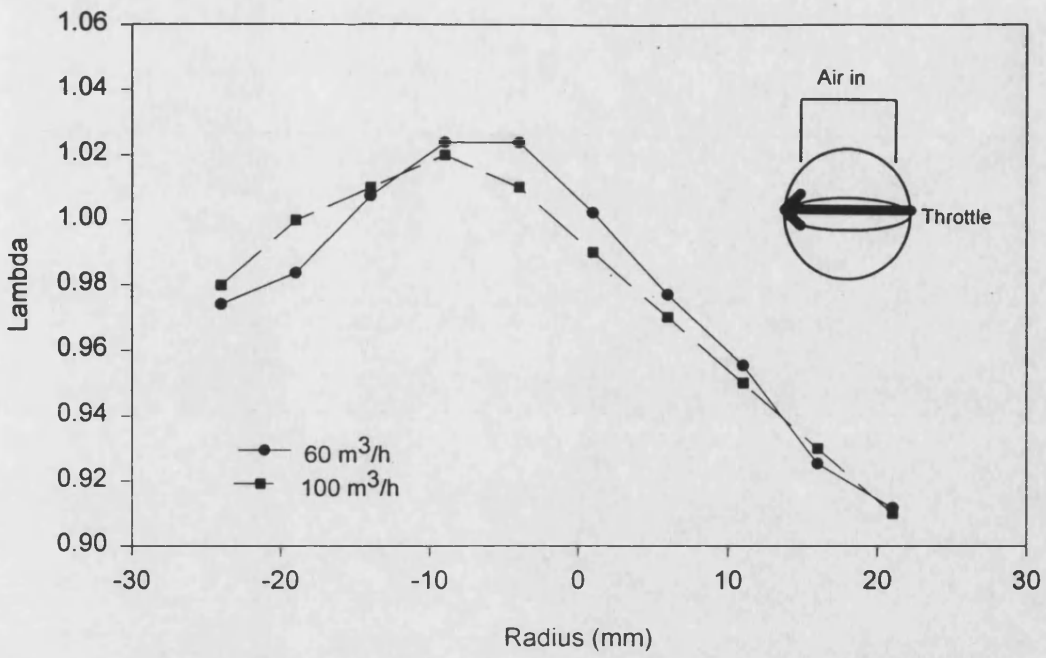

(A) Horizontal traverse

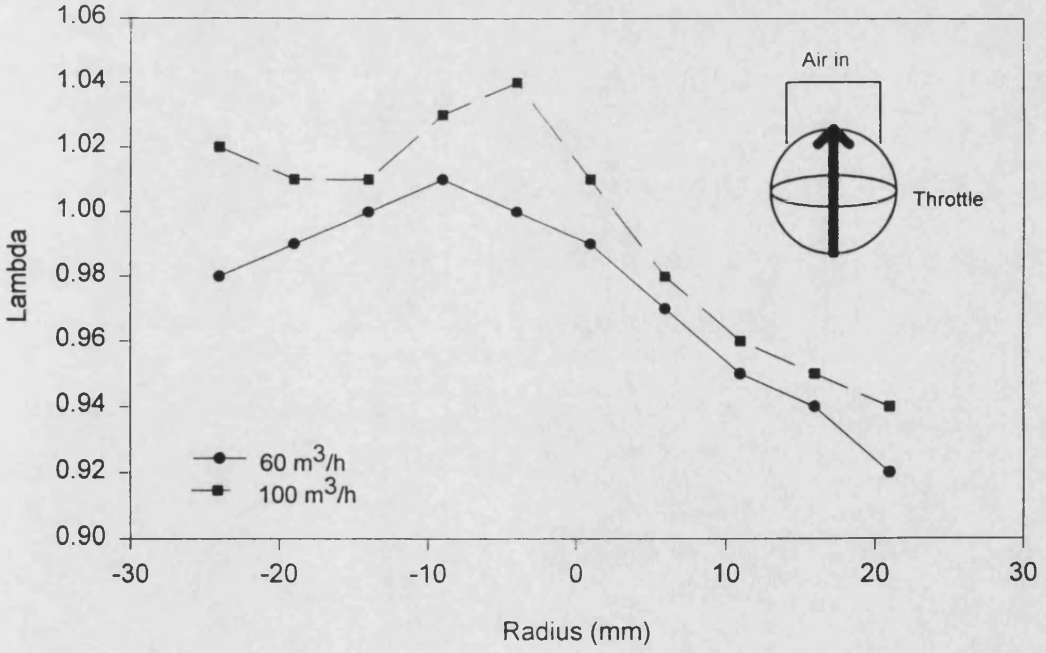

(B) Vertical traverse

Figure 4.23 Mixture distributions for the H-mixer

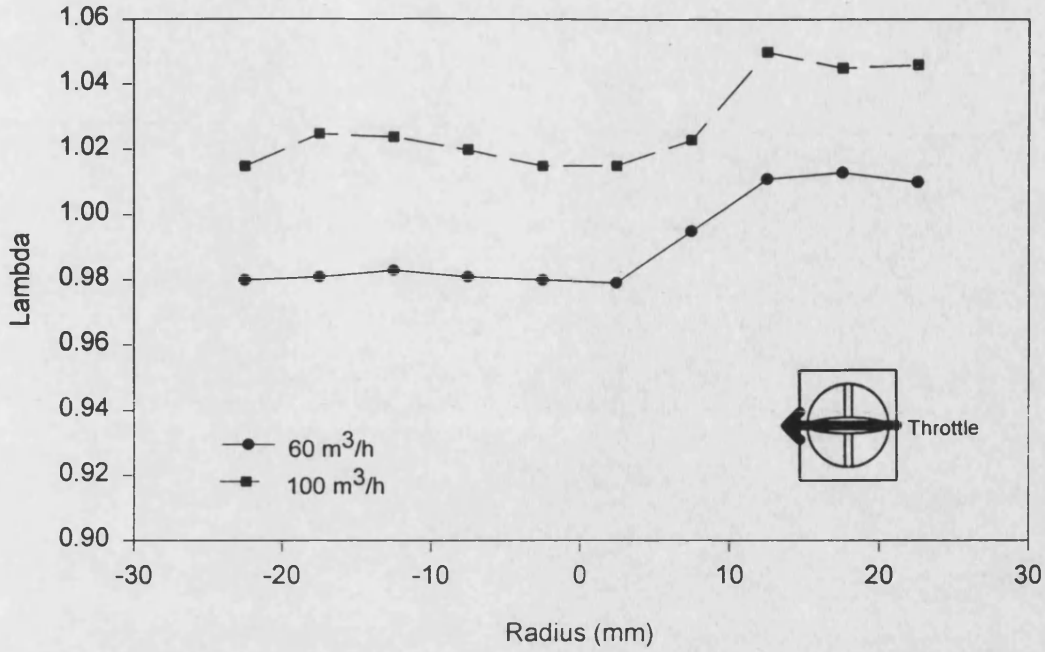

(A) Horizontal traverse

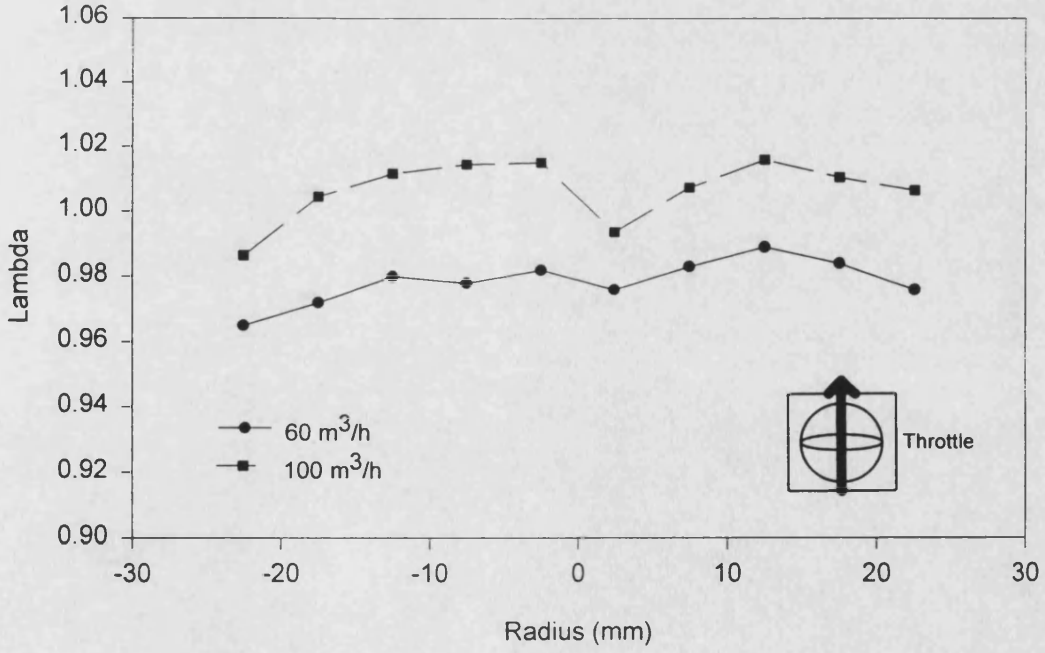

(B) Vertical traverse

Figure 4.24 Mixture distributions for the D-mixer

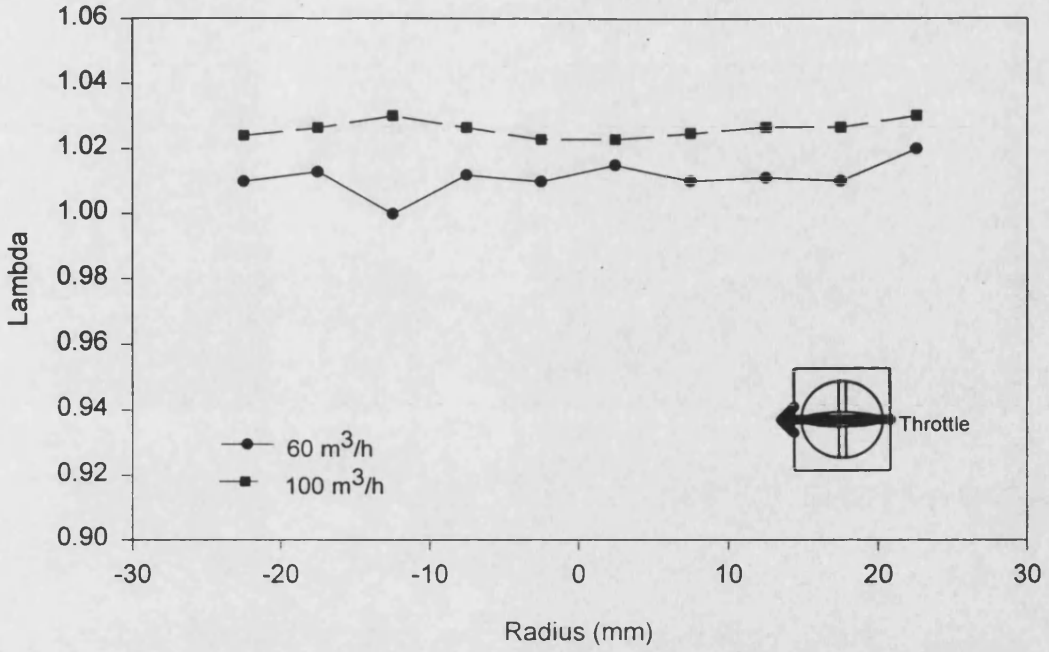

(A) Horizontal traverse

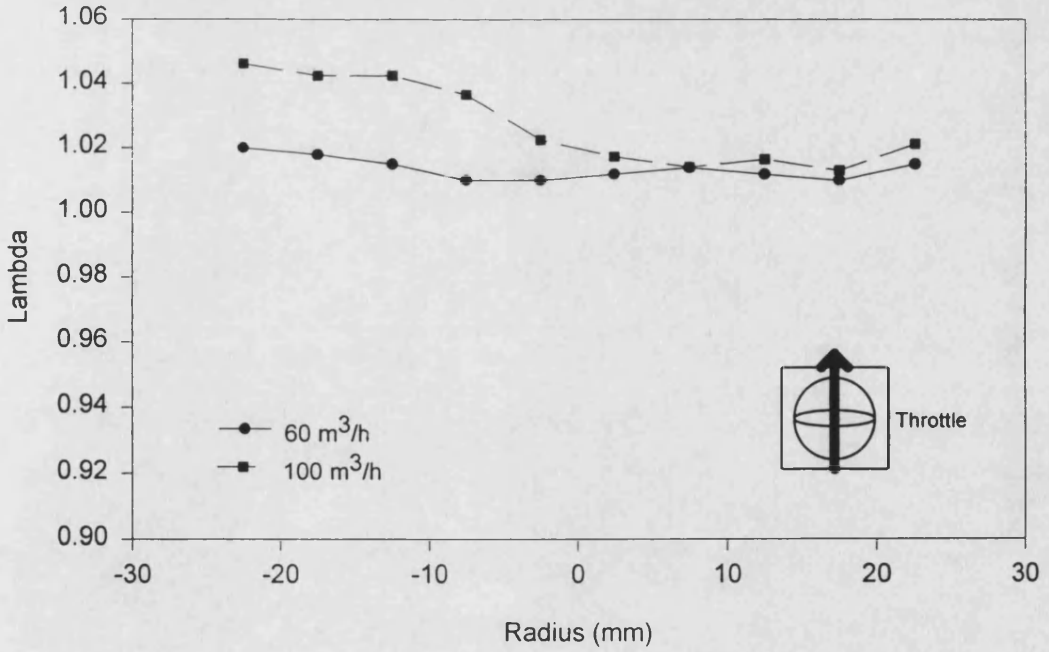

(B) Vertical traverse

Figure 4.25 Mixture distributions for the Gem

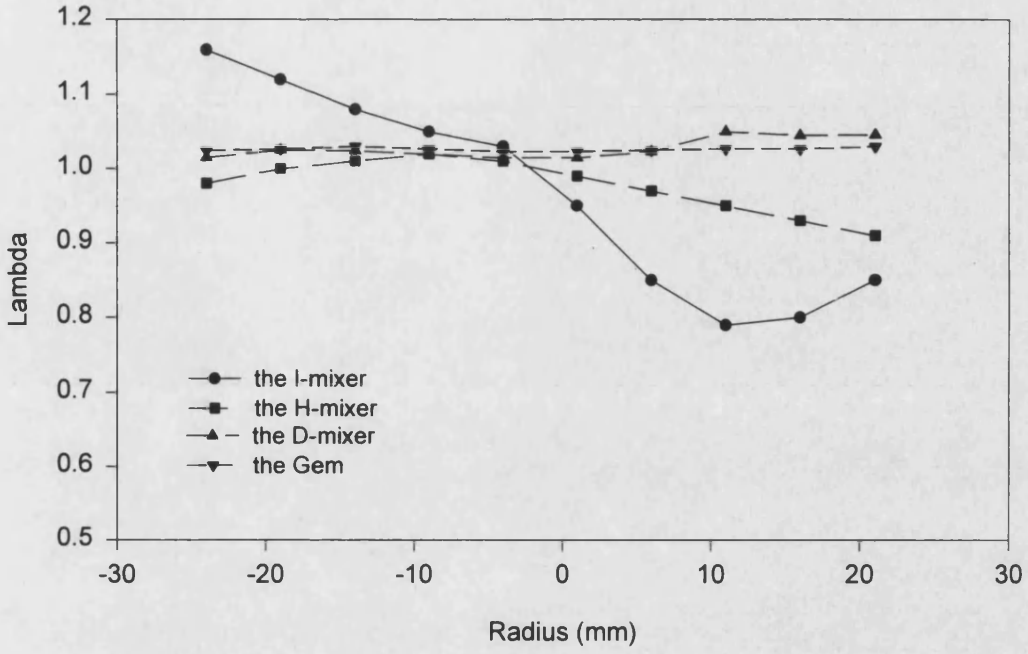

(A) Horizontal traverse

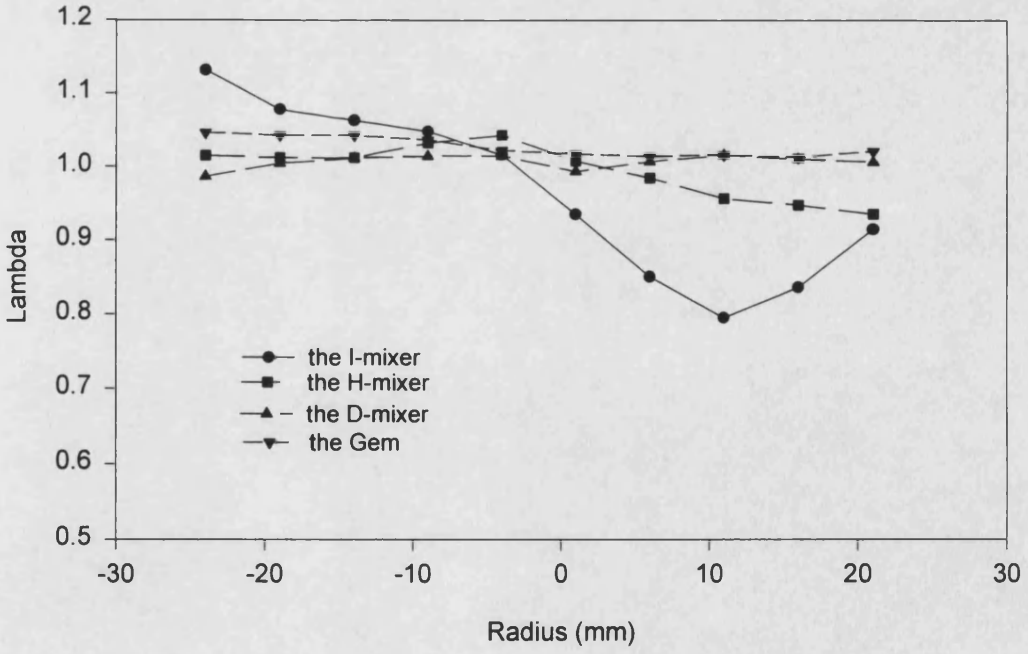

(B) Vertical traverse

Figure 4.26 Comparison of mixture distributions for the mixers at flow rate 100 m^3/hr

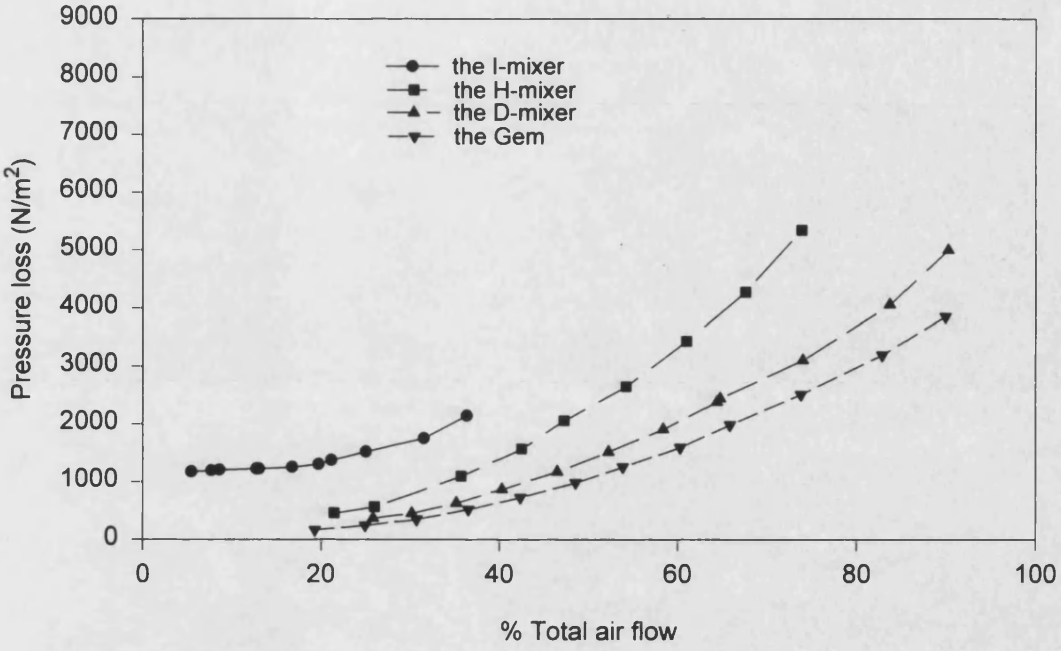

Figure 4.27 Comparison of pressure loss for the mixers with throttle valves

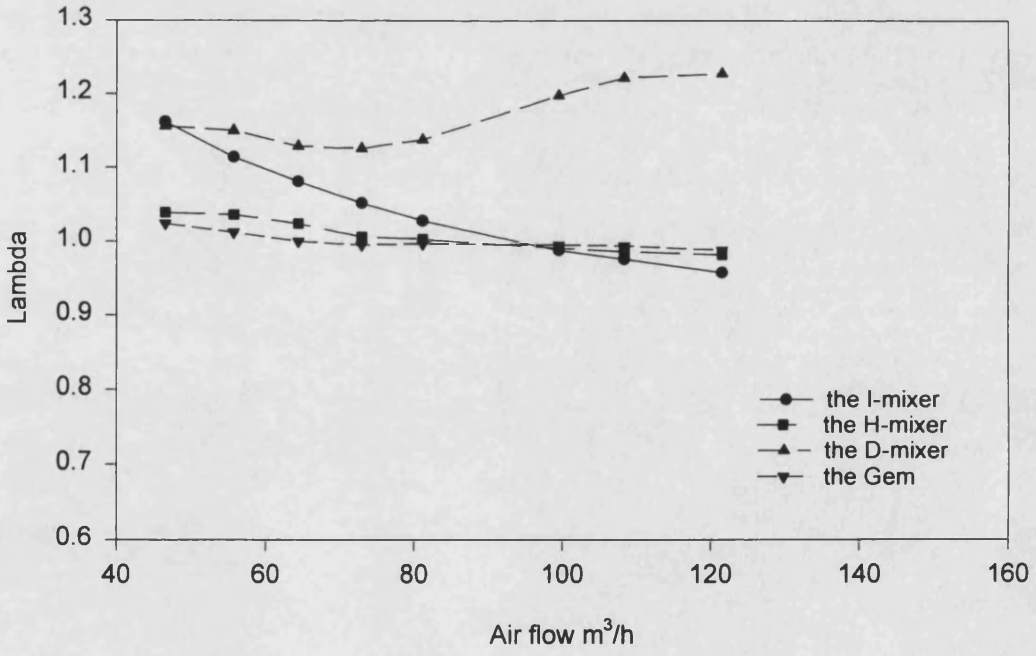

Figure 4.28 Comparison of mixture distributions for the mixers at zero gas pressure

5 Engine performance and emissions study

5.1 Introduction

The increasing interest in natural gas fuelled engines has resulted in considerable research activity on engine performance and emissions. Some of the test results indicated that the mixture preparation system of natural gas engines had a strong effect on the engine performance and emissions. For example, the variation of the mixture overall air fuel ratio control effected a dramatic difference in the engine performance and emissions. Apart from the mixture air fuel ratio control, the mixture concentration distribution was recognised to play a part in the gas engine performance and emissions. However there was no published report considering this influence. In the previous chapter, comparisons of different natural gas engine mixers were discussed. With respect to their main performance characteristics, the mixers examined exhibited quite different features in terms of mixture homogeneity and pressure loss. But the superiority does not necessarily mean that the Gem mixer will certainly result in a good engine performance and low emissions. For a throttle valve controlled spark ignition engine, the higher the pressure loss across the engine mixture preparation system, the lower the engine power output. A non-homogeneous mixture will certainly result in higher level of emissions and poorer engine performance when the engine is fuelled with gasoline or other liquid fuels. However, for a lower density gaseous fuel, it is likely that a gaseous fuel and air will continue to mix further downstream of the engine gas-air mixer and in the inlet manifold to give a reasonable homogeneous mixture before ignition. To clarify this theory, the engine performance and its emissions from the engine exhaust and from each of the individual cylinders with different mixers installed should be examined.

It is well known that the fuel and air flow into each cylinder of a multicylinder petrol engine is not identical when a carburettor produces a poor mixture distribution. That is one of the reasons why fuel injection is becoming popular in petrol engines. For the natural gas engine tested above, the mixture air fuel ratio variations out of each of the mixers were detected. But whether this variation continues to exist after the mixer and whether it affects the engine performance and emissions for the natural gas engine needs to be found out.

The objective of this study was to examine the influence of mixture quality on natural gas engine performance and emissions. Mixtures having good quality means that the mixtures have the right air fuel ratio required and a homogeneous mixture distribution. The approval and clarification of the relationship between mixture formation and engine performance would be very useful for guiding future natural gas engine mixers design and development.

5.2 Test facilities and test procedure

The test rig used was similar to that described in the previous chapter. A naturally aspirated 4 cylinder Power Torque Dovergas spark ignition natural gas engine was used. This had been converted from a Ford 2720 diesel engine and was derated for the stationary CHP application. The engine power output was absorbed and measured using a Heenan MK1 eddy current dynamometer. The speed was controlled by a Heinzmann electronic governor operating a throttle valve located downstream of the matched gas mixer. The dynamometer load exerted on the engine could be controlled independently of engine speed. Each gas mixer tested was mounted directly on the inlet manifold in turn. The arrangement of the test rig used in this research work is shown schematically in Figure 5.1.

Three mixers were tested in this comparative study. They were the venturi type D-mixer of fixed geometry, the non-symmetrical design variable restriction type I-mixer and the symmetrical geometry annular venturi type Gem mixer. Each of the three gas mixers tested was based on different operating principles. Here the term mixer is used instead of carburettor because the carburettor automatic control units for the D-mixer and Gem were disabled in order to focus on the comparison of the mixers themselves. The mixture strength was manually controlled to the values required for the D-mixer and Gem mixer under most of the engine loads and speeds. To control the mixture strength for the I-mixer, its pressure regulator and gas bleed valve which was designed to control the gas flow area were adjusted manually in addition to the inherent control valve which could not be disabled.

The gas flow rate consumed by the engine was measured by a positive displacement roots flow meter and the air flow rate by an orifice plate. In addition, a natural gas rotameter was inserted into the gas supply system, which made the engine operation much easier because of its direct reading. All the temperatures such as the gas, air and exhaust temperature were measured using K-type thermocouples and pressures were measured using water or mercury manometers according to their scales. Overall air fuel ratios were detected using a heated oxygen sensor placed in the exhaust manifold and the signals were fed into a Horiba Mexa-110 analyser which was specifically set with consideration of the composition of the natural gas supplied.

To evaluate the emissions status of the engine using different gas air mixers, the following regulated pollutants were measured: carbon monoxide (CO), unburned hydrocarbons (HC), carbon dioxide (CO_2) and nitrogen oxides (NOx) which included nitrogen monoxide (NO) and nitrogen dioxide (NO_2). Other pollutants, such as particulate matter, sulphur oxides and aldehydes, were not measured because they

were negligible for natural gas engines. In order to measure emissions both from the exhaust manifold and from the individual exhaust ports of each cylinder under the same engine operating conditions, a special sampling system was designed and installed in the engine exhaust system. The sampling tube at each of the exhaust ports was placed very near to its own exhaust valve in order to reduce the possibility of the interference of the exhaust from other ports. Thus the effect of the mixture homogeneity out of the mixers on emissions variations from each of the individual cylinders could be detected.

For the CO and CO_2 measurement, a non-dispersive infrared (NDIR) spectroscopic K 550 emission analyser was used. The NDIR used to be a standard instrument for the testing and legal certification of some automotive exhaust emissions. The instrument was originally designed for the measurement of CO and CO_2 concentrations from petrol engines. For natural gas engines, the chemical structures of the emissions of CO and CO_2 are identical to that from the petrol engines. Thus the measured results of CO and CO_2 by using the NDIR analyser were acceptable for natural gas engines. The NDIR analyser has become a common instrument for the measurement of CO and CO_2 from natural gas engines.

The unburned hydrocarbons in the exhaust of natural gas engines consisted of different compounds, each with different compositions and different number of carbon and hydrogen atoms. Although it was possible to measure each of these unburned hydrocarbon compounds separately by using gas chromatography, it was too expensive to purchase this kind of analyser specifically for the current comparative study. Therefore overall concentration of the unburned hydrocarbons from the engine using different gas air mixers was compared by measuring the equivalent concentration to one of the contents in the compounds. This kind of strategy has been used in conventional fuel engines for a long time. For example, in petrol engines the content of propane, C_3H_8, or hexane, C_6H_{14}, is often used as a reference substance and the HC concentration measured is the equivalent value to the reference content. Because the main content of HC emissions in natural gas engines is methane, CH_4, it would be more appropriate to use CH_4 as the reference substance. However, there was no commercial NDIR analyser available in which CH_4 was used as reference substance. Therefore the NDIR analyser using C_3H_8 as reference was used for the measurement of HC emissions. Though only C_3H_8 was used as reference substance, every hydrocarbon of the unburned hydrocarbons would contribute to the NDIR analyser signal output in a fixed proportion. Thus the measured value of C_3H_8 concentration could be taken as an equivalent value of the total HC concentration and the results were directly comparable between the engine exhaust HC emissions with different mixers. With a known conversion coefficient, the measured HC emissions results could be converted into the FID CH_4 equivalent values if needed. The correlation was achieved by measuring the same sample gas

simultaneously using the K550 NDIR analyser and the FID. The measured coefficient was about 12 between the NDIR C_6H_{14} and the FID CH_4 equivalent values of HC emissions. With the correlation result, the HC emissions could be presented either in NDIR C_6H_{14} equivalent value or in FID CH_4 equivalent value. For the K550 analyser used, a conversion coefficient was provided by the manufacturer between the propane and hexane, which was 0.5 and was internally set during the analyser calibration. Therefore the direct reading was in NDIR C_6H_{14} equivalent value. The reading could be easily converted into the NDIR C_3H_8 equivalent value. The measuring range and its resolution of the K550 NDIR analyser for each of the three contents are listed in Table 5.1.

Table 5.1 K550 analyser performance

Content	Range*	Resolution
CO	0-10% digital	0.01%
HC	0-4000 digital	2 ppm
CO_2	0-20% digital	0.02%

* The measuring range depends on each concentration value of the individual contents in the analyser calibration gas.

Oxides of nitrogen were measured with a Signal 4000 series chemiluminescent analyser. This type of analyser has become the standard instrument for NOx measurement in many countries. A heated sampling line was equipped during the test in order to reduce the influence of water condensation in the sample line. The NOx analyser was calibrated periodically against zero gas (dry air) and span gases of known NOx concentration which covered the measured NOx concentration range.

To compare the engine performance with different gas mixers, a set of engine performance parameters were determined. They were engine brake power output which was the product of the torque exerted by the dynamometer and the angular speed of the engine brake shaft; engine brake mean effective pressure which was obtained by dividing the work done per cycle by the cylinder volume displaced per cycle; engine brake specific energy consumption which was the fuel energy flow rate consumed per unit power output; volumetric efficiency which was derived by dividing the volume flow rate of air getting into the intake system by the flow rate at which the volume was displaced by the piston; and engine brake thermal efficiency which was also called the fuel conversion efficiency or enthalpy efficiency. To get an accurate power output measurement, the torque transducer was regularly calibrated by using known balance weight at the calibration position. The power output or the torque is a valuable measure of an engine's ability to do work, but it depends on the engine size. Therefore the brake mean effective pressure (BMEP) having a unit similar to that of the pressure was used

to assess the effectiveness of the engine performance. The BMEP is not only a parameter used in the engine performance assessment, but also a very important parameter used in initial engine design. To calculate the heat energy flow rate, the lower heating value of the fuel at constant pressure was used. The reason for using the brake specific energy consumption (BSEC) rather than the conventional brake specific fuel consumption (BSFC) was that the unusual density of the gaseous fuel. Besides, the energy consumption was readily comparable when fuels of the engine having different lower heating values. The volumetric efficiency, a parameter of measuring the effectiveness of an engine's induction system, was related to inlet air density which could be taken either as the atmospheric air density or the air density in inlet manifold. In order to evaluate the pumping performance of the entire inlet system, the atmospheric air density was used here. From the definition of the volumetric efficiency, it was apparent that gas engine volumetric efficiency was much lower than that of the conventional liquid fuel engine, because the gaseous fuels occupied a large percentage of the mixture in the intake system and they were not counted in the inlet air mass flow rate. Air mass flow rate was derived from the measured gas flow rate and the overall air fuel ratio, because the roots flow meter and the Horiba air fuel ratio analyser were more accurate than the orifice flow meter. Several other parameters, such as engine exhaust temperature, coolant temperature and oil temperature were measured in order to aid the analysis of the engine performance results. All data were taken after the engine was warmed and run steadily under measured operating conditions.

Due to the fact that the pressure, humidity, and temperature of ambient air induced into an engine affect the air mass flow rate and hence the power output, the measured engine performance varies from day to day because of changed weather conditions. In order to provide a more accurate basis for comparison amongst the performance data measured with different gas air mixers, the ambient conditions of pressure, temperature and relative humidity were first measured during each test by using the barometer, thermometer and whirling sling hygrometer respectively. All the ambient conditions were then corrected to standard conditions stated in BS 5514: Reciprocating Internal Combustion Engines: Performance.

In order to obtain a complete assessment of the engine performance for each mixer, the engine was tested at full load or wide open throttle (WOT) and part load over a wide range of engine operating speeds. The load conditions used for the part throttle test are listed in Table 5.2. Thus a full performance and emissions map was achieved for the engine with each of the three mixers over a wide range of air fuel ratios, which would enable the evaluation of the three gas mixers to be made including assessment of the emissions variations from each individual cylinder and from the whole engine. Throughout the test, engine ignition timing was kept unchanged for ease of comparison.

Throttle valve angular open positions of the engine were also measured through a rotating gauge to help the intake system performance analysis.

Measurement repeatability tests were made with each of the mixers at the beginning and end of the test series to check that the instruments remained in good condition and to ensure results comparability.

Table 5.2 Engine test conditions

SPEED (rpm)	Load (Nm)				
1200	50	100	150	200	235
1500	50	100	150	200	232
1800	50	100	150	200	224
2000	50	100	150	200	217
2300	50	100	150	203	-
2600	50	100	187	-	-

5.3 Test results for the Gem mixer

5.3.1 The engine performance at WOT

The engine brake power output with the Gem mixer under different operating speeds at wide open throttle is given in Figure 5.2. From 1200 rpm to 2000 rpm, the power output increased with the speed. At about 2000 rpm the power output exceeded the rated power output of 50 kW. Above 2000 rpm the power output decreased with increasing speed because of the reduced engine BMEP, as shown in Figure 5.3. The decreased BMEP resulted not only from the air flow limitation (or pumping loss) and increased mechanical friction loss at high piston speeds, but also from the gas supply restraint. The gas restraint came from two aspects. One was the gas main pressure. When the engine was run at high power outputs, the gas flow rate needed by the engine exceeded the supply ability of the gas main. As a result, the gas main pressure became very low. The monitored gas main pressure reduced from 7" to 5" water gauge at high speeds. Due to the cost and safety, it was not possible to increase the gas main pressure. Another restraint was the gas flow control valve. The air fuel ratio control unit used for the Gem mixer in this study was the one temporarily adopted from the D-mixer. For a 50 kW power output, the control valve was too small to supply adequate amount of gas demanded, especially at low gas main pressures. There was another possibility that the gas flow might have reached its choking condition between the gas flow control valve and the venturi throat because of the high gas signal used in the Gem mixer. If this had happened or only occurred during part of the intake process, then the gas flow rate would not be able to increase with engine speed. The intake mixture relative air fuel

ratio given in Figure 5.4 showed clearly that the mixture was weakened dramatically above 2000 rpm and it was not possible for the control system to enrich the mixture.

The engine brake energy consumption is shown in Figure 5.5 and its inverse dimensionless parameter, the engine brake thermal efficiency is given in Figure 5.6. At low speed, the engine mixture blow-by loss was high and the amount of heat transfer per cycle from working fluid to engine coolant was large. Thus the brake specific energy consumption was high or the thermal efficiency was low. Due to the heavily worn engine piston rings and cylinder liners, the blow-by loss accounted for a large proportion for the engine tested. When the engine speed exceeded 1800 rpm, the brake specific energy consumption increased with speed and the engine thermal efficiency decreased. This was attributed to several variables. Firstly, with the increasing engine speed the engine BMEP decreased, which tended to increase the energy consumption and reduce the thermal efficiency. Secondly, the mixture relative air fuel ratio exceeded its most economical value which was about λ=1~1.1. Fortunately the low heat transfer and low fresh charge blow-by loss appreciatively eased the increasing trend. As an overall effect from all these variables, the lowest energy consumption or the highest thermal efficiency occurred in the speed range of 1500 rpm to 1800 rpm. The variation of the fuel consumption and thermal efficiency within this range was mainly because of the changed relative air fuel ratios. If the mixture composition had been kept at its stoichiometric value, a single specific energy consumption trough and a single thermal efficiency crest would have appeared somewhere between the engine speed 1500 rpm and 1800 rpm.

Unlike liquid fuel, a gaseous fuel does not have the fresh charge cooling effect because there are no fuel droplets presented in the intake manifold wall or cylinders of the engine when gaseous fuels are used. This gave rise to a low engine volumetric efficiency, as shown in Figure 5.7. Another significant contribution to the low volumetric efficiency was the existence of natural gas in the mixture. This significantly reduced the partial pressure of the air in the intake manifold and hence the value of the volumetric efficiency. For naturally aspirated petrol engines, the typical maximum value of volumetric efficiency is in the range of 80% to 90%. But for the gas engine tested, the maximum volumetric efficiency was only 67%. In natural gas engines, the long charge heating time at low speeds was not as severe as that in petrol engines because there was no evaporation process in the gaseous fuel. Thus the maximum volumetric efficiency occurred in low speed range due to the low flow frictional loss. At high speeds, the lean mixture effected a strong influence on the volumetric efficiency and to a large extent compensated for the flow friction loss. That was why the curve did not go down dramatically with the increase of speed. Another reason for this was that the choke of the air flow did not occur, at least not in the mixer. This further proved that the designed

air flow ability of the Gem mixer was big enough for the engine power output required. If the gas flow ability can be improved. the engine power output will be increased at high speeds. To confirm this, the connecting passage between the mixer body and the mixture air fuel ratio control valve was enlarged and so was the connecting passage between the valve and the gas pressure regulator inserted in the gas supply system. The engine power at the speed of 2000 rpm to 2300 rpm was increased. Unfortunately, there was no bigger mixture air fuel ratio control valve available for the replacement of the existed one, which limited any further detailed test in this respect.

5.3.2 The engine emissions at WOT

Figure 5.8 shows the carbon monoxide emissions from the engine exhaust manifold with various engine speeds at WOT with the Gem mixer. At about 1200 rpm, the CO emission was about 0.3%, the highest value over the speed range tested. This resulted purely from the slightly rich mixture. It is well known that engine speed has no effect on CO concentration of which the oxidation is kinetically limited rather than mixing limited. Figure 5.4 shows that the mixture at this speed was the richest and its relative air fuel ratio was 0.98. From 1300 rpm to 1800 rpm, the mixture was controlled at about stoichiometric and hence the engine CO emissions were relatively constant at a value of 0.12%. When the speed was over 1800 rpm, the emission was further reduced because of the leaning-out mixture. The sensitivity of CO emission to the mixture relative air fuel ratio illustrated the importance of tight control of the air fuel ratio in order to obtain a very low emission level. For the multicylinder SI engine operating close to its stoichiometric mixture, the overall level of CO emission measured from the engine was very low compared with that from conventional petrol engines. This was attributed to the more homogeneous mixture prepared by the mixer.

The unburned hydrocarbon emissions in the exhaust are shown in Figure 5.9, where HC concentrations are expressed in parts per million NDIR C_6H_{14} equivalent value. Here the directly measured value is used without being converted into the FID CH_4 equivalent value, not as had been done in reference [155]. The result showed that the highest level of HC emissions occurred at the lowest engine speed and the level reduced with increasing speed. At low speeds, the amount of hydrocarbons trapped in the crevice volume was larger than that at high speeds because of the longer blow-by time and lower gas pressure. At low speeds, however, the incomplete combustion fraction, another source of the unburned hydrocarbons, tended to be small because of longer time available for mixing and combustion even though the tendency was substantially offset by the lower turbulence which could promote both the mixing and the flame propagation. By looking at the mixture air fuel ratio curve in Figure 5.4, it can be easily identified that the air fuel ratio change with the engine speed primarily dominated the

change of HC emissions. At about 1200 rpm the mixture was the richest over the speed range. Its relative air fuel ratio was about 0.98. From 1300 rpm to 1500 rpm, the amount of HC concentration remained nearly constant due to the constant mixture strength. At 1600 rpm, a slight λ value excursion to its rich side led to an increase of the HC emissions level. Above this speed the emissions decreased with the leaning-out mixture. The dependence of HC emissions on the mixture air fuel ratio indicated that the hydrocarbons stored in piston and ring crevices during the intake and compression processes, were the major contributor to HC emissions from the gas engine tested. As stated before, the engine was converted from a heavy duty diesel engine which normally has a higher top-land and hence a large crevice volume. The stored hydrocarbons were subsequently released during the expansion process, and it was quite difficult to completely oxidise them due to the reduced temperature in the cylinder at that time. Thus a portion of the trapped mass will contribute to the HC emissions. The richer the mixture, the higher the hydrocarbon concentration level in the exhaust. The larger the crevice volume, the higher the percentage accounted for in the contribution to the total HC emissions. Another contributor to the HC emissions was that the increasing engine speed improved the combustion process by increasing turbulence within the cylinder. This promoted after-oxidation of the HCs from the crevice volume while minimising the fraction of incomplete combustion. Nevertheless, the levels were quite low compared to the typical range from normally operated petrol engines without the after-treatment method. The relatively lower HC emissions in natural gas engines were believed to be the result of well prepared mixture homogeneity. Another reason was the oil layer storage effect which is the major source of HC emissions in petrol engines. Since methane and other fuel components of natural gas have a very low solubility in the oil layer, the contribution of this mechanism was believed to be negligible when the engine was fuelled with natural gas. The changed role of the oil layer as a source of HC emissions accounted for the largest part of the difference in HC emissions between the petrol and natural gas [17].

The concentration of nitrogen oxides emitted from the engine is given in Figure 5.10. It is a well accepted fact that NOx are mainly formed throughout the high temperature burned gases behind the flame where the compressed gases have a predominately high temperature. The higher the burned gas temperature, the higher the NOx emissions level. Because the formation of NOx is through chemical reactions involving nitrogen and oxygen atoms and molecules, not only the gas temperature but also the oxygen and nitrogen concentrations strongly affect the NOx formation. At the speed of 1200 rpm, the mixture λ value was about 0.98 which was slightly on its rich side. The gas temperature was high, but the oxygen concentration was low. Also the heat transferred to the engine coolant was high at the low speed. As a result of these three factors, NOx concentration at this speed was comparatively low. From 1300 rpm to 1800 rpm, the

concentrations increased with the speed because of the increased concentrations of oxygen and nitrogen. The enhanced turbulence flame propagation by the increased speed increased the fraction of the burned gas and its temperature during the early stage of the combustion process. This also contributed to the increased NOx curve over the speed range. Above 1800 rpm, increased oxygen concentrations offset the falling gas temperatures at first and then the low gas temperature brought down the NOx emissions level significantly. Another impact of the oxygen concentration on NOx came from the concentration of CO radical which split N_2 from NO. The higher the oxygen concentration, the lower the CO concentration and the lower the NO split. The excessive lean mixture also resulted in a low exhaust temperature, see Figure 5.11. The measured exhaust temperatures over the speed range were lower than typical natural gas engines, which was because of the extensively cooled exhaust manifold.

5.3.3 The engine performance and emissions at part loads

Results of the engine performance at part loads are given in Figures 5.12 to 5.19, where the engine load is represented by the engine BMEP. As the engine BMEP increased, the engine BSEC decreased and the thermal efficiency increased. This was attributed mainly to the sharp increase of the engine volumetric efficiency with the engine load or throttle opening position, see Figure 5.15. Other contributions to the result came from the engine mechanical efficiency, mixture air fuel ratio and importance of heat losses. At a small throttle setting, the engine pumping loss was very high, which gave a lower mechanical efficiency at lower engine loads. Fortunately, the mixture strength was able to be controlled close to its stoichiometric value throughout the loads tested, see Figure 5.16. At low loads, the percentage of heat losses per cycle was relative high, which also wasted a fraction of the input fuel energy. The engine speed did not significantly affect the engine BSEC, the thermal efficiency and the volumetric efficiency at part load. This was because the speed had an opposite effect on heat transfer and mechanical efficiency. But a trend was still distinguishable, which was that the highest thermal efficiency occurred at the middle of the speed range and the maximum speed gave the worst fuel economy due to the importance of friction losses and heat losses.

Because the mixture air fuel ratio, a primary factor that controls engine CO emission, was kept nearly unchanged over the engine loads tested, the concentration of carbon monoxide emissions did not change with different engine loads. The excursion at low loads at the speed of 1200 rpm was because the instrument interference by water vapour in the sampling line. The variations at high loads were due to the differences of mixture air fuel ratios supplied. The instrument interference and its resolution also contributed to the variations. The NDIR C_6H_{14} equivalent hydrocarbon concentration trends with load changes were speed dependent. At some speed the concentration value increased with

increasing loads and at other speeds it did not change. However, the trend with different engine speeds is clear, a higher speed leads to lower HC emissions at a given load. The reason for this is quite complicated because there are several HC formation mechanisms involved. Similar to the explanation given for the HC results at WOT, the engine thermal load status and the turbulence intensity in the engine cylinders and in the exhaust increased with the engine speed, which offset the effect of the reduced combustion time and after oxidation residence time. With the increase of engine load, a high thermal load status led to a high exhaust temperature, which aided the after-oxidation. On the other hand the increased exhaust volume flow rate reduced the residence time in the exhaust system, which offset the after-oxidation. Another contributor was the ignition timing which was fixed under all mixture air fuel ratios and engine speeds, especially over higher speeds range. This tended to deteriorate the combustion and cause higher HC emissions. The net trend was that HC emissions increased slightly with the increase of engine load at the higher speeds range. NOx emissions with various engine loads and speeds are given in Figure 5.19. The concentration of NOx increased with increasing load at a given speed. This was attributed to the increased inlet manifold pressure and reduced relative importance of heat transfer per cycle. The former contributed to the substantial residual gas fraction reduction and hence increased the temperature of both the burned and unburned gases. The latter also contributed significantly to the pressure and temperature increase in the cylinders and in the exhaust. NOx emissions results also showed that the increase of NOx concentrations was greater at lower loads than that at higher loads. This was because the two contributors were more significant at lower loads. The variation of NOx emissions with different engine speeds was subtle and unclear over all the part loads tested. The residual gas fraction fell with an increasing engine speed, which would increase NOx concentrations. A lower heat transfer per cycle would also contribute to an increase of NOx emissions. However, the fixed ignition timing which was set according to the maximum rated speed at wide open throttle for the stationary application tended to increase the maximum temperature and lengthen its residence time in cylinders. As a result of the three factors, NOx emissions at part loads did not change very much with engine speed at a given load. Another fact that should be pointed out here is that NOx emissions level from the natural gas engine was as high as that from typical petrol engines though there is very little nitrogen composition in natural gas. This was because the NOx emissions were mainly formed from atmospheric nitrogen, not the nitrogen of the fuel.

5.3.4 The engine performance and emissions with various λ values

The results shown so far are those variations of the engine performance and emissions from the exhaust manifold with changing speed and load. The emissions results have

shown that the pollutants emitted from the engine were very sensitive to the mixture air fuel ratio. Tiny differences in mixture relative air fuel ratio would give rise to substantial deviation of the concentration values for any of the three pollutants. Thus any clear differences in mixture homogeneity amongst cylinders caused by poor performance of the mixture preparation system will be demonstrated by different emissions results detected from different engine cylinders. The wider the deviation of the detected emissions amongst the engine cylinders, the worse the mixture homogeneity produced by the mixer installed. To correlate the mixer performance and the engine emissions from both the exhaust manifold and each of the individual cylinders, emissions of CO, HC and NOx were measured from each of the engine exhaust ports and exhaust manifold under different mixture air fuel ratios. The results could also demonstrate the performance of the mixer operating under different mixture strength schemes. To obtain a whole picture on the emissions of the engine with the Gem mixer, measurements were carried out at two different engine speeds and two different loads. Results are given in Figures 5.20 to 5.22.

CO emissions from the engine exhaust manifold and from the exhaust port with the Gem mixer at a speed 1500 rpm, BMEP 306 kPa are shown in Figure 5.20a. The graph underlined that the deviation of CO concentrations emitted from the four cylinders was so small that it was not detectable by the instrument used. The curves also showed that CO emissions were very sensitive to the mixture air fuel ratio when the engine was operating on the rich side of stoichiometric. Once the mixture λ value exceeded 1.1, CO concentrations did not decrease with the increasing mixture λ value and the value of CO concentration could not be zero no matter how lean the mixture was. Results obtained at a speed of 1500 rpm, BMEP 611 kPa and at a speed of 2000 rpm, BMEP 306 kPa led to the same conclusion on CO emissions from different cylinders and their sensitivity to the mixture strength. An exceptional point in Figure 5.20b for CO concentration from cylinder three was believed to be an odd point which resulted from the instrument malfunction. In order to achieve a very low level of CO emission, the mixture relative air fuel ratio control performance was critical when the engine was operated under stoichiometric conditions. The mixture homogeneity prepared by the Gem mixer was good enough to achieve a low level CO emission both from the individual cylinder and from the exhaust manifold as long as the mixture strength was accurately controlled.

Unburned hydrocarbon emissions from each individual cylinder and from the exhaust manifold with different mixture relative air fuel ratios are shown in Figure 5.21a. The variations of HC concentration from cylinder to cylinder were also quite small at constant mixture relative air fuel ratio. The biggest deviation came from the first cylinder where the temperature of the cylinder body was expected to be lower than the other cylinders because it was the nearest to engine coolant pump. The small HC

concentration variations from cylinder to cylinder indicated that the mixture delivered to all the cylinders was homogeneous enough to reduce HC emissions to a reasonable level as long as the mixture strength was accurately controlled at about λ=1.1~1.2. When the mixture was richer than λ=1.1~1.2, the HC concentration level went up even the mixture was still on the lean side of stoichiometric. When mixture λ value was shifted from 1.1 (or 1.2) to 1, the effect on the exhaust after oxidation was weakened because the oxygen content was reduced. As a result, HC concentrations increased moderately with mixtures from λ=1.1 (or 1.2) to λ=1. When the mixture was richer than stoichiometric, the fuel concentration in the crevice volume was high and no after oxidation existed due to the fact that there was no oxygen content in the exhaust. Another contribution to the HC emissions was incomplete combustion which became worse when the mixture became richer. Thus the richer the mixture, the higher the HC concentrations in the exhaust. When the mixture λ value was 0.9, i.e. the mixture was 10% richer than stoichiometric or 20% than the lowest HC emissions mixture strength, the average HC concentration value rose from the lowest 70 ppm to 130 ppm, nearly doubled the emissions level. When the mixture was leaner than that λ=1.1~1.2, the temperature of the exhaust was lower, which offset the effects of reduced fuel concentration in the crevice volume and higher oxygen content in the exhaust. As a result, HC concentration emitted from both individual cylinders and manifold increased with the increasing mixture λ value. When the mixture λ value exceeded 1.5, the lean operating limit of the engine was approached. So the combustion deteriorated significantly and HC emissions increased sharply. When the engine load was increased from 306 kPa BMEP to 611 kPa at a constant speed of 1500 rpm, the variations of HC concentration from different cylinders were still very small and the change of HC concentration with the mixture relative air fuel ratio followed the same trend and at the same level, see Figure 5.21b. But when the speed was increased to 2000 rpm at the load of 306 kPa, the HC emissions level, as shown in Figure 5.21c, was reduced by about 25% for the reasons explained before, for the part load engine emissions under various engine operating conditions.

The results for nitric oxides from each of the exhaust ports and from exhaust manifold at different engine operating speeds and loads with various mixture strengths are given in Figure 5.22. The results showed that NOx concentration variations from cylinder to cylinder were surprisingly small. The excursion of the concentration values from cylinder one was also believed to be the over cooling effect. The excursion in Figure 5.22b for the values from exhaust manifold with reference to those from cylinders was believed to be the effect of water condensation in the section before the heated sampling line. No matter what speed and what load the engine was operated at, there was a peak NOx concentration in the range of mixture relative air fuel ratio tested. For different engine speeds or loads, the λ values at which the maximum NOx concentration occurred

varied and the emissions levels changed. At a speed of 1500 rpm and BMEP 306 kPa, the maximum NOx concentration had a value of 2000 ppm which occurred at about λ=1.07 because the oxygen concentration was high and the burned gas temperature was just slightly lower than its maximum which occurred at λ=0.98 for the engine operating speed and load tested. When the mixture relative air fuel ratio changed from 1.07 to 0.98, the gas temperature increased to its maximum, but the oxygen concentration went down dramatically. The falling oxygen concentration offset the increasing temperature and resulted in a decrease in NOx concentrations for very rich mixtures. Below λ=0.98 both the gas temperature and oxygen concentration were going down and gave rise to lower NOx emissions. When the mixture was leaner than that λ=1.07, the low gas temperature offset the increased oxygen concentration. Thus NOx concentration was low for very lean mixtures as well. When the engine was operated at the same speed but a higher load, BMEP=611 kPa, the maximum NOx concentration increased from 2000 ppm to 3200 ppm and its corresponding λ value shifted from 1.07 to about 1.12. This was because the increased load reduced the inlet manifold vacuum and hence the mass of residual gases. As a result of less dilution at higher loads, the ignition delay was decreased, flame speed was increased and gas heat capacity was decreased. All of these resulted in an increase in gas temperature and its peak time in addition to the contribution made by the reduced importance of heat transfer, which produced higher NOx emissions and shifted the λ value further to its leaner side. When the engine was operated at the same load, BMEP=306 kPa, but a higher engine speed (2000 rpm), it had little effect on NOx emissions result. The increased engine speed resulted in an increased flame speed due to turbulence, and reduced heat losses, which tended to raise combustion temperature and pressure. But because the spark timing was unchanged, the high speed moved the main portion of the combustion into the late part of the expansion process, which tended to reduce the NOx formation rate.

5.4 Comparison of the engine performance and emissions

The engine was operated with the other two mixers installed in turn under identical conditions as presented in the previous section for the Gem mixer. Thus the engine performance and emissions between the newly designed Gem and other proprietary mixers can be compared.

5.4.1 Comparison of the engine performance for different mixers

The engine performance parameters of concern at wide open throttle for the three mixers are given in Figures 5.23 to 5.28. With respect to the engine brake power and the brake mean effective pressure the Gem gave the highest power output at speeds lower than 2000 rpm, the D-mixer the least with the I-mixer in between. This was due to the

relative sizes of the mixers, the pressure losses across them and the air fuel ratios supplied to the engine. Of the three mixers tested the Gem was the largest in size, gave the lowest pressure loss across it and supplied the richest mixture over most of the operating range for the gas pipeline pressure supplied. The D-mixer was the smallest and supplied a very lean mixture, consequently it produced significantly less power than the other two at higher engine speeds. Clearly even with the maximum regulated gas pressure the D-mixer still could not produce the maximum power required at the rated engine condition, because the peak flow rate is somewhat out of the manufacturer's specifications. In this study the Gem mixer adopted a step motor driven air fuel ratio control valve which was originally designed for the D-mixer. The small valve flow area for the main gas supply system caused a large gas pressure loss across the valve, which resulted in a leaner mixture produced from the Gem than that from the I-mixer when the engine was run at higher speeds at wide open throttle. This is clearly shown in Figure 5.25, where the variations of λ value with different engine speeds are presented. When the engine was run at high speed with the I-mixer, the variable geometry characteristic gave the mixer increased opening for both the air valve and the gas valve, which attributed to a significant reduction of the flow restriction. The pressure loss across the I-mixer is believed to be reduced dramatically at this condition and this is the reason why the engine installed with the I-mixer gave a higher power output at the extreme high speed at WOT. Of the three mixers tested the Gem gave the highest engine brake power output and mean effective pressure under most of the engine operation speeds. If a well designed air fuel control valve was used the power output and BMEP from the engine using the Gem mixer could be further increased.

Considering engine specific energy consumption and thermal efficiency, see Figures 5.26 and 5.27, the D-mixer at WOT gave the highest specific energy consumption and the lowest thermal efficiency of the three mixers tested when the engine was run at speeds above 1600 rpm. This was because the mixture strengths provided by the D-mixer at those speeds were well beyond the most economical mixture strength which was about λ=1.1 for the engine tested. The Gem gave a slightly lower specific energy consumption and higher thermal efficiency than the D-mixer above 1600 rpm. By comparing the mixture strengths produced by the two mixers over the speed range, it can be seen that the Gem produced a mixture close to its stoichiometric and much richer than that produced by the D-mixer except at speeds above 2200 rpm where the mixture relative air fuel ratio from the Gem was about 1.23 which was far leaner than stoichiometric, but still richer than that from the D-mixer. However, neither Gem nor the D-mixer produced a mixture as close to the most economical mixture strength as that produced by the I-mixer over the speed range from 1500 rpm to 2200 rpm. That was why the I-mixer gave the lowest specific energy consumption and highest thermal

efficiency over most of the operating range, but at around 1200 rpm and above 2200 rpm the Gem was slightly better.

The engine volumetric efficiency results for the three mixers are given in Figure 5.28. The comparison showed that there was little difference among the three mixers in this respect with the Gem showing the lowest value over most of the high speed range and the D-mixer the highest over most of the low speeds. This was because the Gem operating with the richest mixture strength of the three at high speeds and the D-mixer with the leanest mixture at all speeds. As explained before, mixture strength in a gaseous fuel engine had a strong effect on volumetric efficiency especially for natural gas in which CH_4 accounted for more than 92% in mass. But the D-mixer which had a smaller throat diameter could not cope with the air flow rate demanded over the engine speed of 2000 rpm even though the mixture air fuel ratio was extremely lean. The high flow restriction and probably the choking brought down the engine volumetric efficiency over speed 2000 rpm with the D-mixer. While with the Gem mixer, though the mixture was leaner than that with the I-mixer, the flow restriction offset the increase of mixture relative air fuel ratio. As a result, the engine volumetric efficiency with the Gem mixer was lower than that with the I-mixer over the speed of 2000 rpm. Because of its variable geometry characteristics for both the air flow and gas flow, the I-mixer gave a high volumetric efficiency when the engine speed exceeded 1600 rpm at WOT. But below that speed, the flow areas were small and flow restrictions were high for both the air and fuel. This, together with the lower relative air fuel ratio values, effected a very low volumetric efficiency for the I-mixer at lower speeds.

In order to confirm the effect of mixture air fuel ratio controllability on engine energy consumption with different mixers at WOT, the engine was run again with the I-mixer and Gem mixer installed in turn over a speed range from 1400 rpm to 2200 rpm at WOT. The mixture strengths were controlled closely in order to compare the two mixers, see Figure 5.29. For these nearly identical mixture strengths, the engine BSEC with the two mixers did not exhibit much difference to each other, see Figure 5.30. This indicated that to achieve the lowest energy consumption or the highest engine thermal efficiency, the mixture supplied to the engine should be controlled at its most economical mixture strength no matter which mixer was used and what kind of the operating principle it was based on. This requirement means firstly that the mixer itself should be able to produce a high enough gas signal and secondly the attached mixture air fuel ratio control unit should have good characteristics. The comparison of the engine fuel economy with the two mixers at nearly identical mixture strengths also showed that the effect of the pressure loss across the mixer had been over shadowed by the mixture strength over most of the operating speeds in this gaseous fuel case. The old

engine used had damped down the performance difference between the three mixers compared with what should have been shown.

At part loads the engine BSEC decreased and thermal efficiency increased with the increase of load for all the three mixers. It is interesting to notice that the specific energy consumption and the thermal efficiency were not very sensitive to the engine operating speed as long as the mixture air fuel ratio was kept to be the same. This further indicated the importance of a good mixture preparation system for natural gas engines. Because the mixture air fuel ratio supplied from each of the tested mixers was adjusted within a narrow λ range during the part load test, see Figure 5.31, the engine energy consumption and thermal efficiency exhibited no difference amongst the mixers used, except a tiny difference occurred at higher speeds between the I-mixer and Gem mixer, see Figures 5.32 and 5.33. But there was no clear difference between the D-mixer and Gem at any speed with the load tested. The causes for the difference were believed to be the difference in flow restriction. At the load tested the I-mixer had a smaller air and gas flow area and hence produced a higher flow restriction than that Gem mixer did. This tiny difference diminished with the increase of load, which had been proved by the test at a higher load, see Figures 5.34 to 5.36. At part loads, another influencing factor is the throttle opening position. For a required engine power output at a fixed engine operating speed, the throttle valve would have a different positions with different mixers should these mixers have different flow restriction characteristics. These throttle positions were automatically adjusted by a governor. A higher flow restriction activated a wider throttle opening and vice versa. Therefore the difference of the pressure losses amongst different mixers had been swamped by the throttle openings during the part load tests. However, the importance of lower flow restrictions were still demonstrated by the comparison.

5.4.2 Comparison of the engine emissions for different mixers

The emissions results are given in Figures 5.37 to 5.40 for the tests at WOT with the three mixers. The CO produced by the engine with the I-mixer and Gem mixer was slightly higher than that produced by the engine with the D-mixer fitted at lower speed range. This was entirely due to the lean mixture produced by the D-mixer which enabled the excess oxygen to fully oxidise the carbon monoxide to carbon dioxide. However at high speed the mixture produced by the D-mixer had become too lean to produce complete combustion. This is the reason for the relatively high value of unburned hydrocarbons formed under this condition. The I-mixer operated at approximately 1.1 λ value over a wide speed range, which is the condition that results in the highest NOx emissions for the reasons explained before. The extreme lean mixture produced from the D-mixer at the high speed range with the WOT test gave a very low

exhaust temperature and hence low NOx emissions. All the emissions results clearly showed that the mixture air fuel ratio significantly affected the engine emissions of the regulated gaseous pollutants at WOT under all the speeds irrespective of the mixers used.

The emissions results measured during the part load tests showed that there were no detectable differences for the engine with the three different mixers. When the engine was tested with the I-mixer and the D-mixer under various mixture strengths, the same as was performed with the Gem mixer, there was very little deviation between the values measured at each of the individual exhaust ports and at the engine exhaust manifold under the engine operating conditions tested, see Figures 5.20 to 5.22. This suggested that any uneven distribution of mixture strength emerging from the individual mixers, as shown in the previous chapter, had been damped, due to the mixing and turbulence in the inlet manifold, before the mixture entered the inlet valves to the individual cylinders.

The comparison given above was based on the results of the engine with different mixers tested at different times in a period of about three months. The comparisons can only be convincing should the engine operation and the instrumentation have a good repeatability. In order to show this, at the end of each test session the engine operating conditions used at the beginning were repeated for each of the mixers and the engine performance and emissions were measured. The repeatability results are shown in Figures 5.41 to 5.46, with the "A" standing for the result made at the beginning of its test session and "B" at the end. No matter what operating speed was tested and which mixer was used, the engine performance parameters measured had a very good repeatability. But for the emissions of the three main gaseous pollutants the repeatability was not as good as that of the performance parameters. Amongst the three, the CO emission results gave the best repeatability. As a comparative study the repeatability for the other two was certainly acceptable, especially when the percentage of their deviations was of the major concern.

5.5 Summary

An extensive engine performance and emissions comparison test for three different gas-air mixers had been carried out. The prototype Gem mixer exhibited very good characteristics with respect to load acceptance and to engine start up performance. It produced satisfactory air fuel mixtures over a wide range of engine steady operating conditions. In terms of the engine power output and BMEP, the engine with Gem produced the highest power and maximum BMEP over most of the engine operating speeds at WOT. With regard to engine brake specific energy consumption, brake

thermal efficiency and to engine emissions of CO, HC and NOx, there was not much difference amongst the three mixers when the air fuel ratio produced was the same irrespective of the engine operating speed and load. But the advantage of having a lower air flow restriction for the Gem and for the I-mixer at higher loads did demonstrated the superiority on the engine power output and BMEP. The I-mixer had showed its merit in mixture air fuel ratio control over all engine operating speeds and loads, especially when high engine outputs were required. However the D-mixer had showed that it was not rated for the engine power output demanded. It was more suitable for a smaller engine.

No matter which mixer was used, the most important features that a mixture preparation system should have are the mixture air fuel ratio controllability, the mixture homogeneity and the pressure loss across the mixer. The mixture air fuel ratio control should be given the first priority whenever it is possible because it is the most sensitive parameter which influences exhaust emissions and performance of natural gas engines. For the engine tested, mixture homogeneity variation from the mixers had neither a significant effect on the engine exhaust emissions, nor a significant effect on the emissions variation from engine cylinder to cylinder. The reason for this was believed to be the throttle valve and intake manifold which assisted further the mixing between the gas and air.

The results of the engine performance and emissions tests presented have shown the importance of the mixture air fuel ratio control. Integration design of the mixer and air fuel ratio control unit is necessary in order to improve the mixture strength control characteristics of the prototype Gem even for steady state engine operations. The engine emissions variation from cylinder to cylinder with the three gas mixers did not give the results which might have been expected from the mixture homogeneity obtained from the mixers.

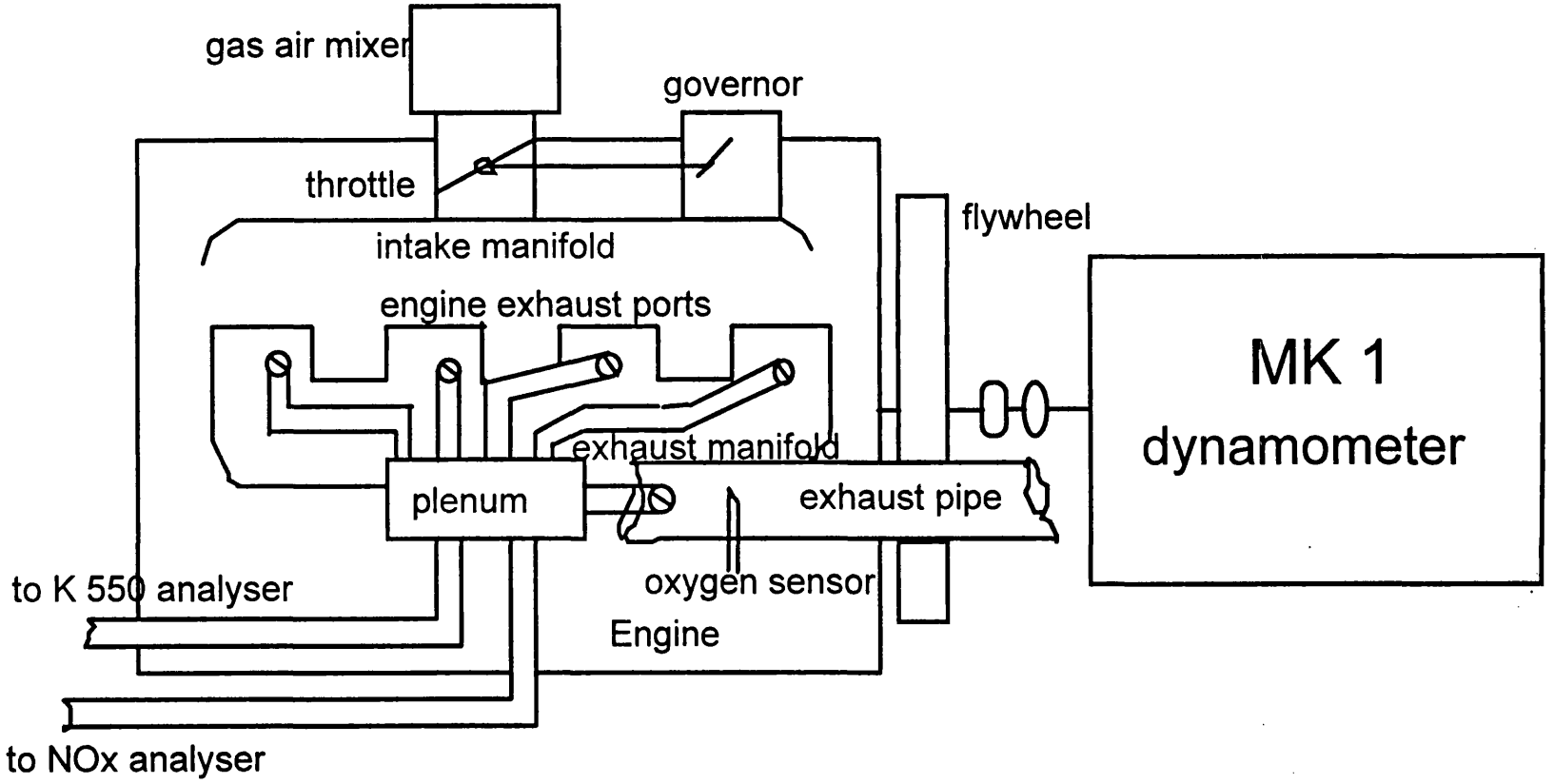

Figure 5.1 Engine performance test rig arrangement

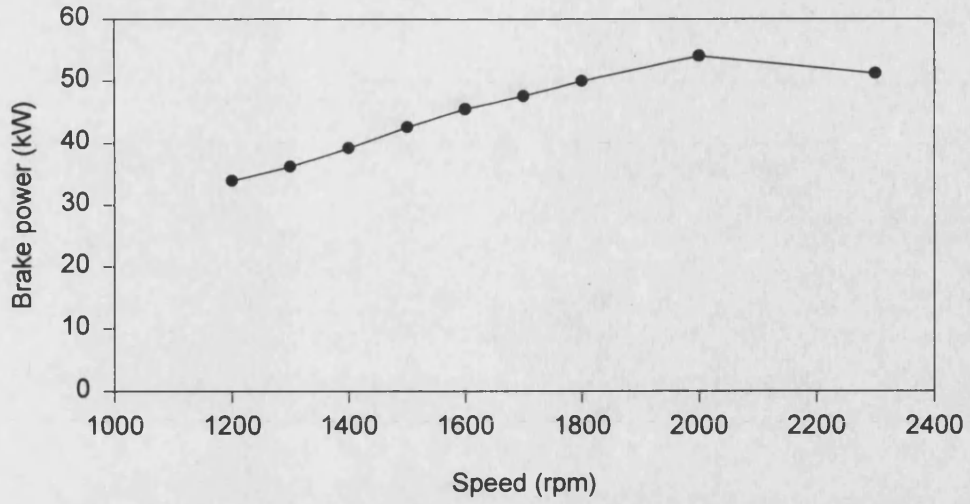

Figure 5.2 Engine brake power outputs for different engine speeds at WOT

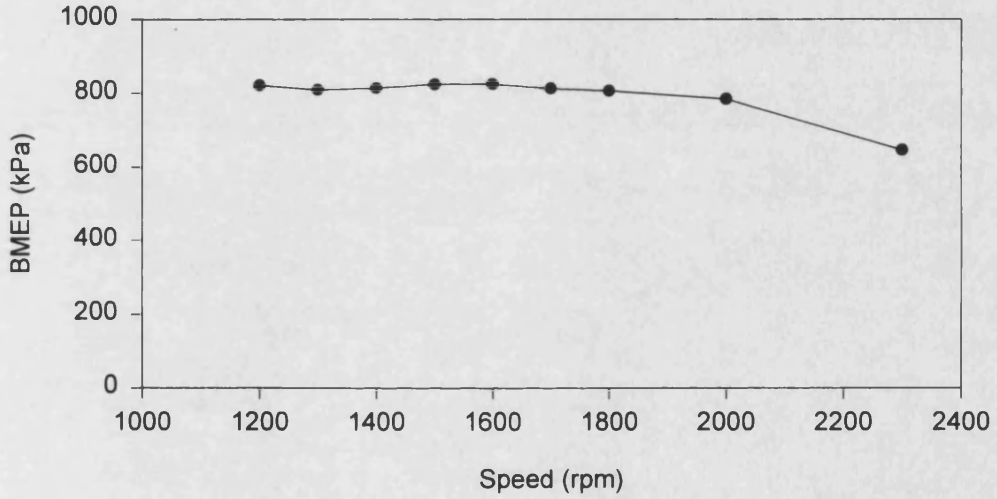

Figure 5.3 Engine brake mean effective pressures for different engine speeds at WOT

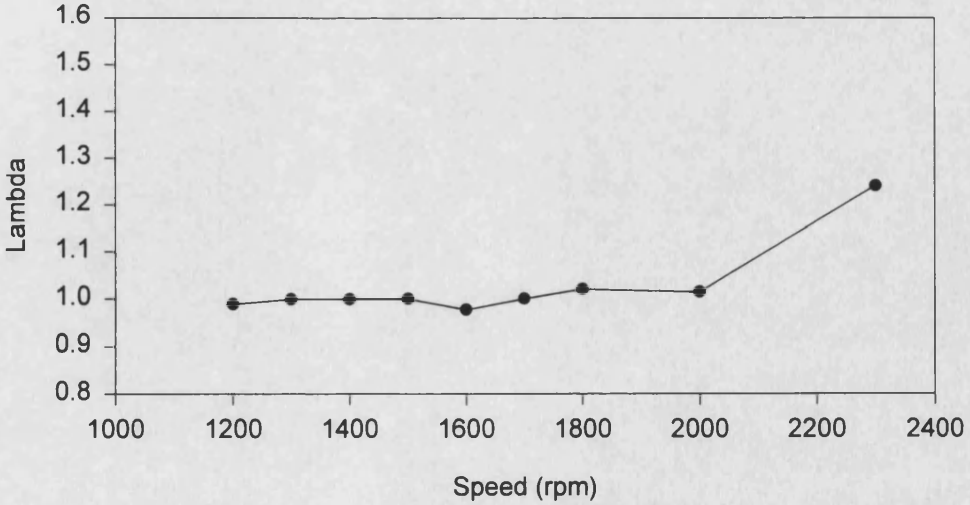

Figure 5.4 Mixture relative air fuel ratios for different engine speeds at WOT

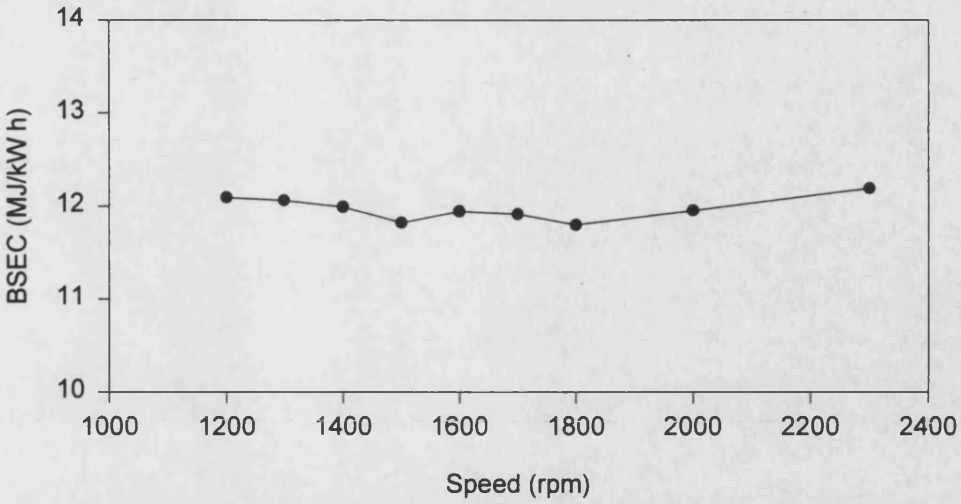

Figure 5.5 Brake specific energy consumptions for different engine speeds at WOT

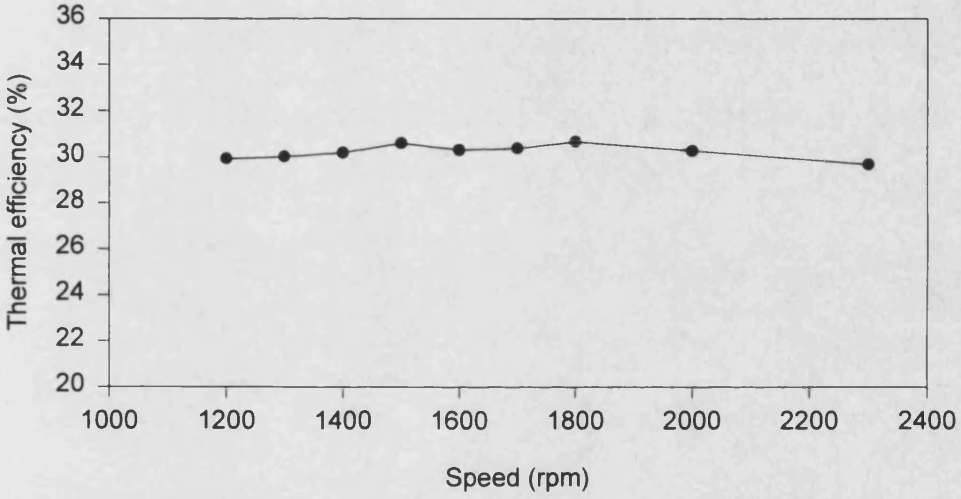

Figure 5.6 Engine thermal efficiencies for different engine speeds at WOT

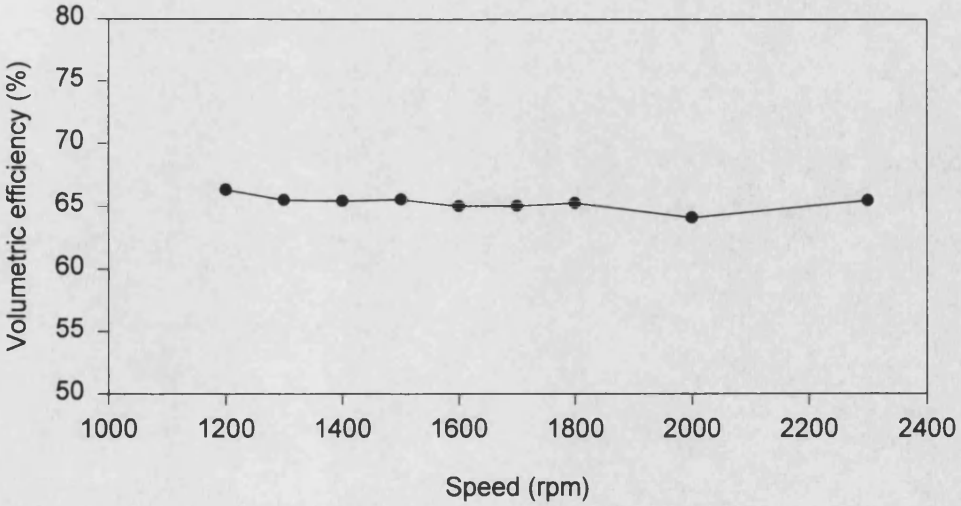

Figure 5.7 Engine volumetric efficiencies for different engine speeds at WOT

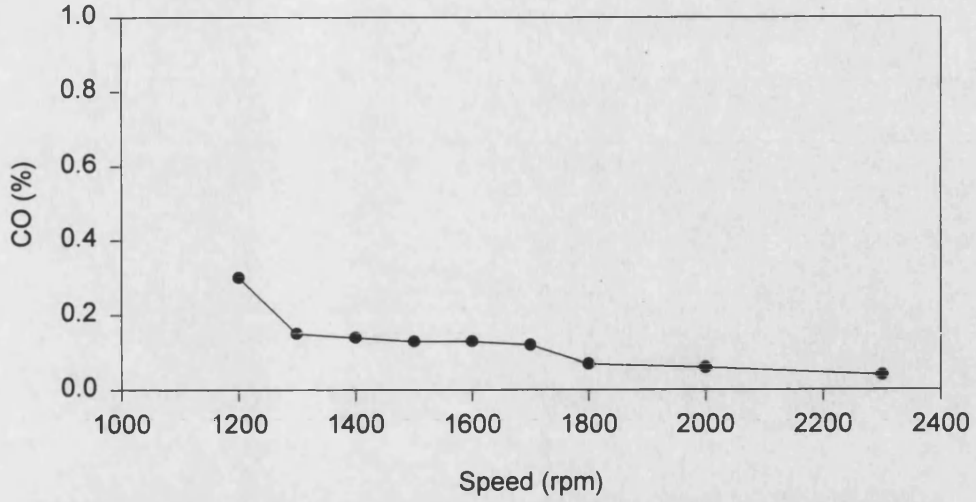

Figure 5.8 Exhaust manifold CO emissions for different engine speeds at WOT

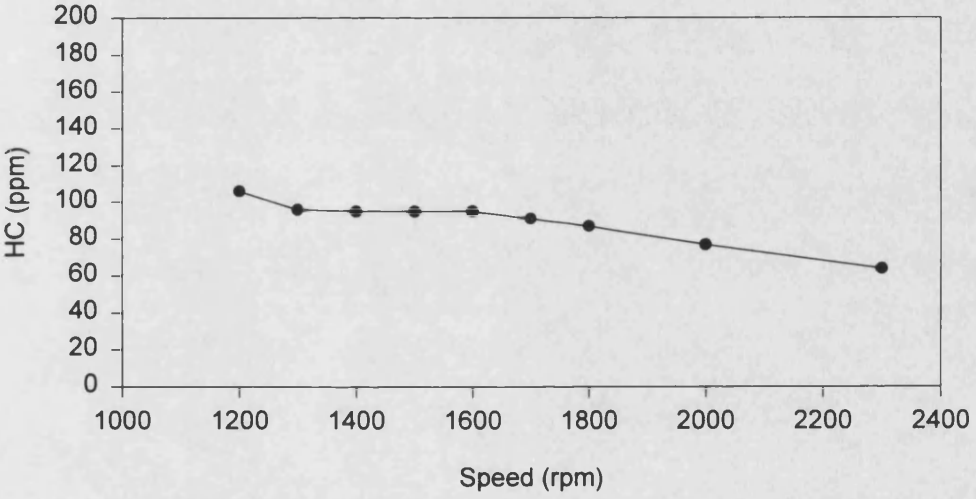

Figure 5.9 Exhaust manifold HC emissions for different engine speeds at WOT

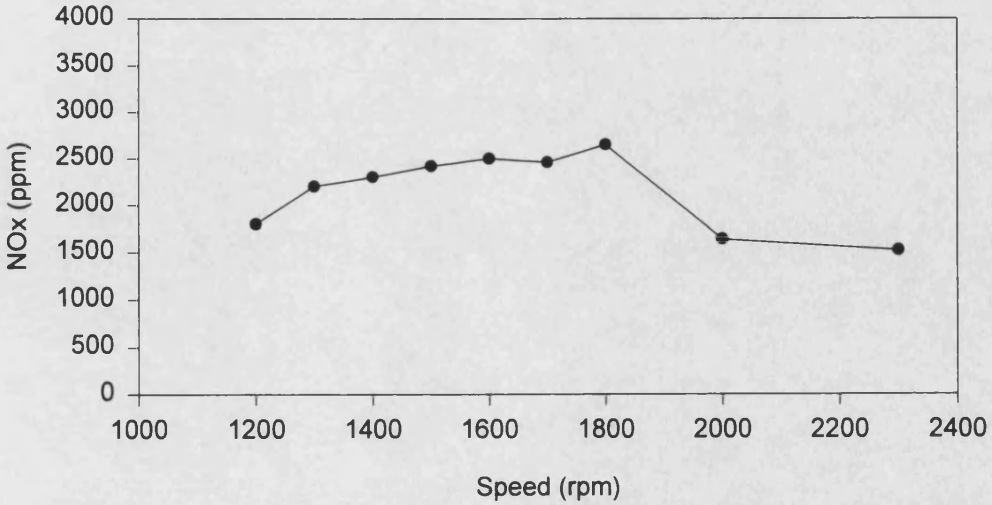

Figure 5.10 Exhaust manifold NOx emissions for different engine speeds at WOT

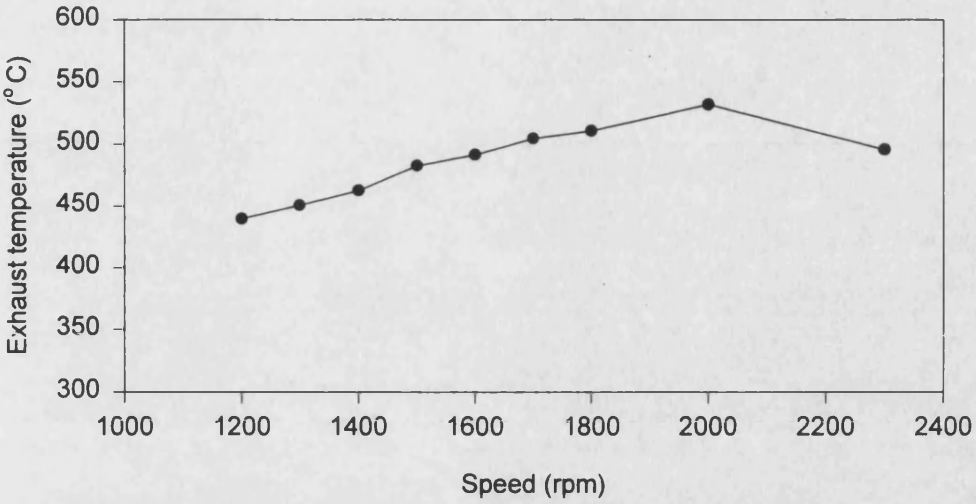

Figure 5.11 Engine exhaust temperatures for different engine speeds at WOT

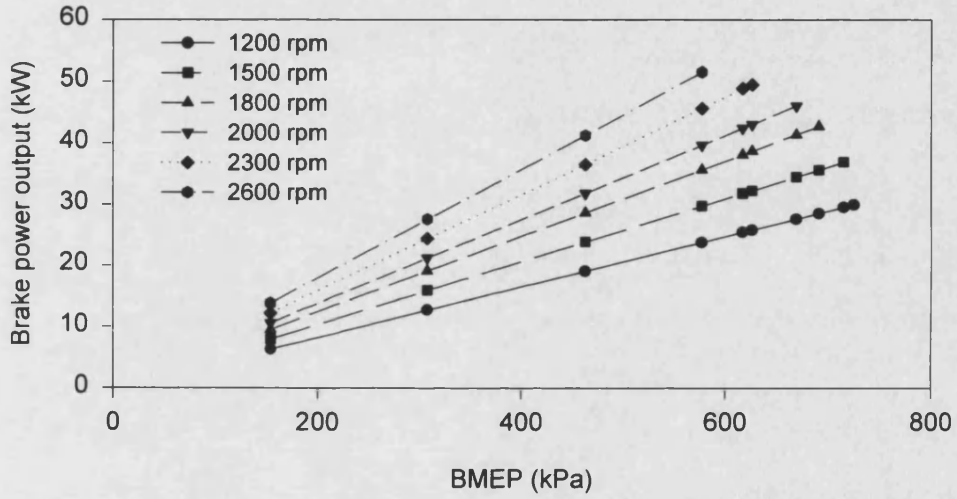

Figure 5.12 Engine brake power outputs at different engine loads and speeds

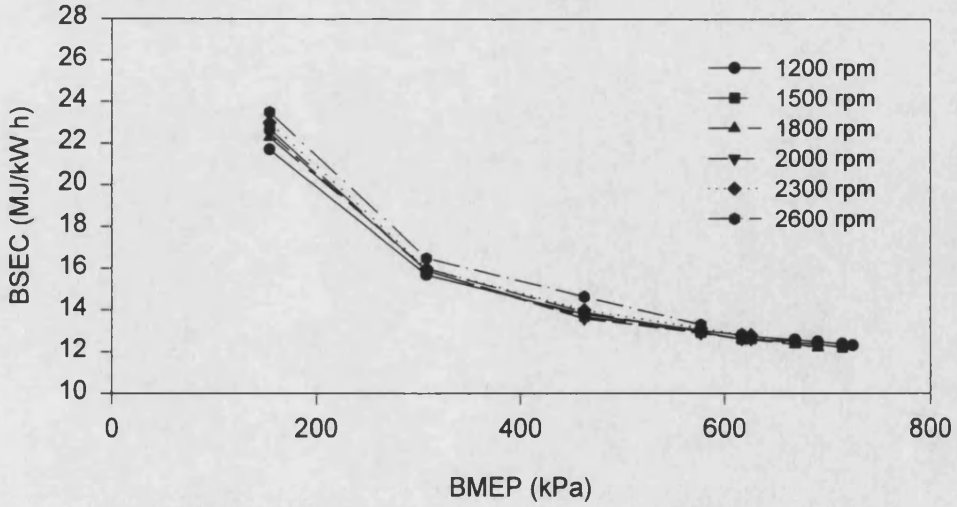

Figure 5.13 Brake specific energy consumptions at different engine loads and speeds

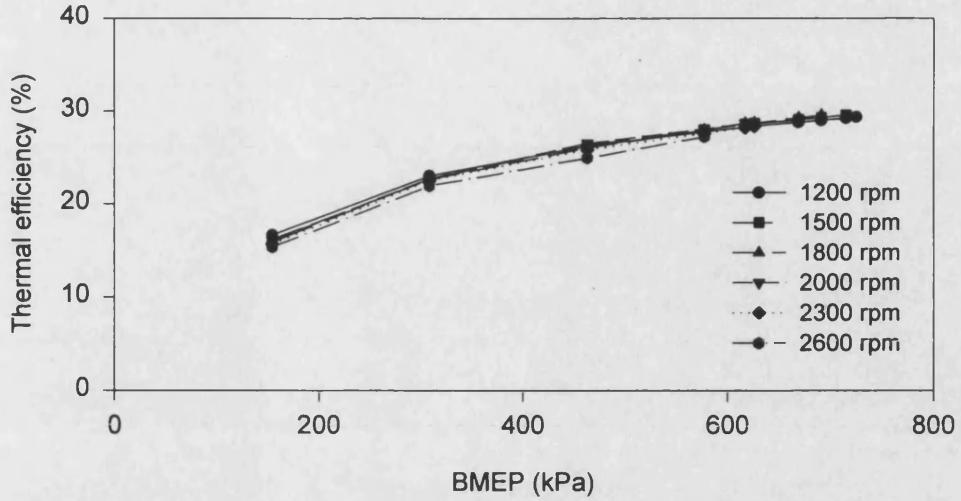

Figure 5.14 Engine thermal efficiencies at different engine loads and speeds

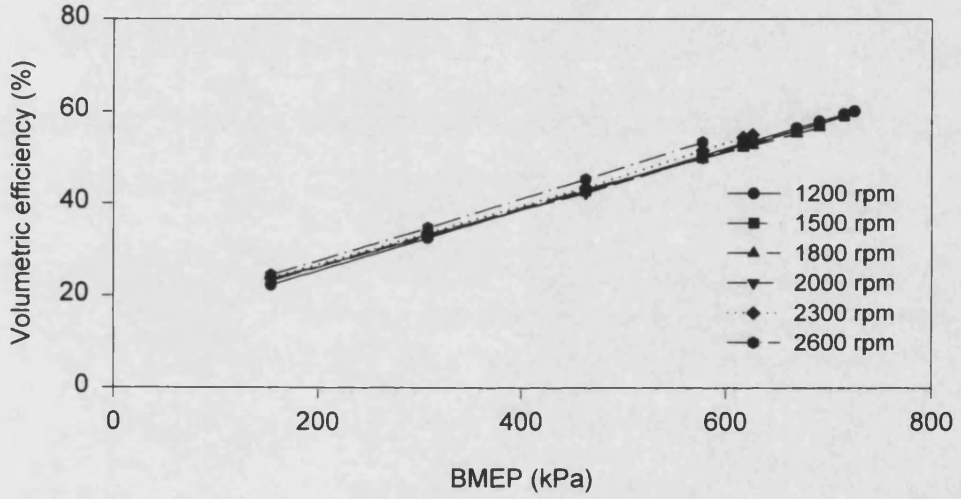

Figure 5.15 Engine volumetric efficiencies at different engine loads and speeds

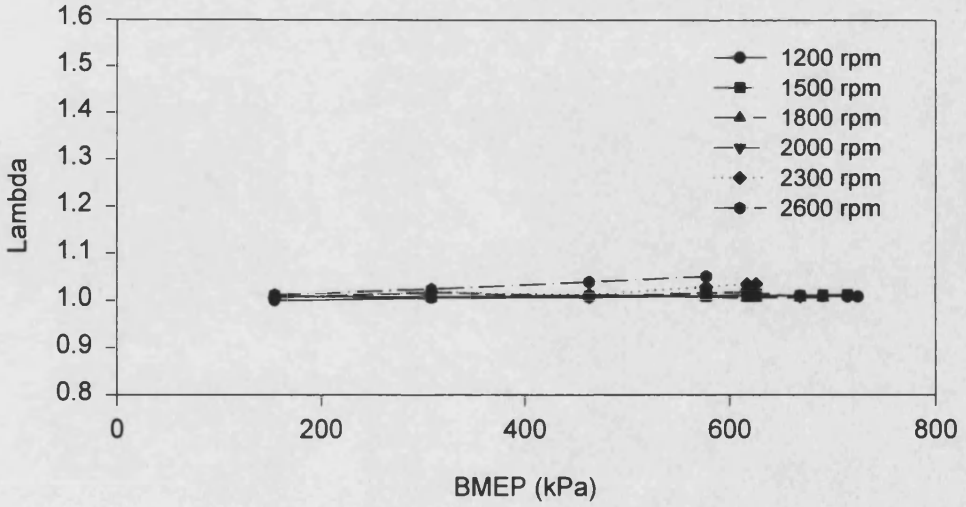

Figure 5.16 Mixture relative air fuel ratios at different engine loads and speeds

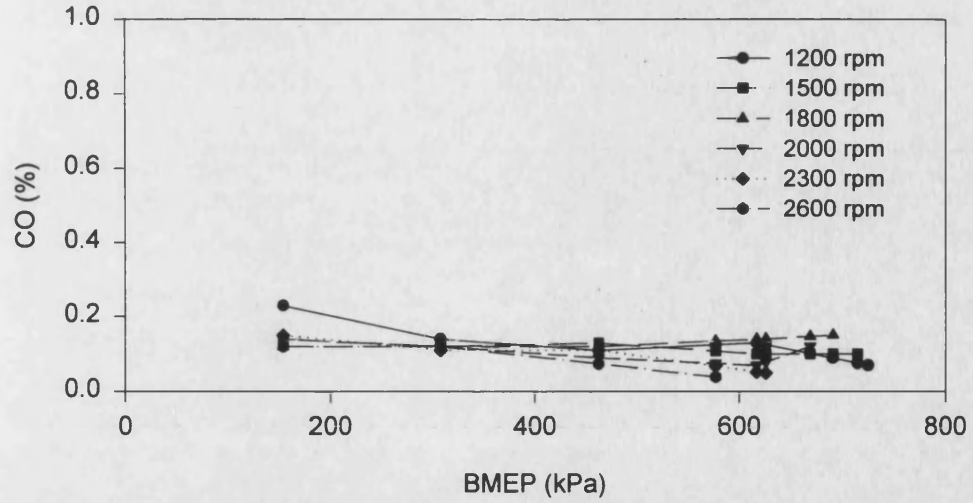

Figure 5.17 Exhaust manifold CO emissions at different engine loads and speeds

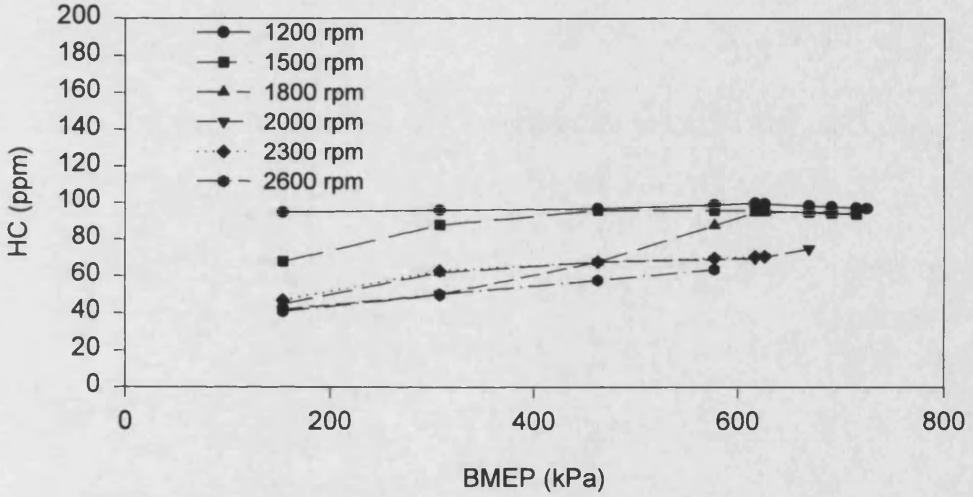

Figure 5.18 Exhaust manifold HC emissions at different engine loads and speeds

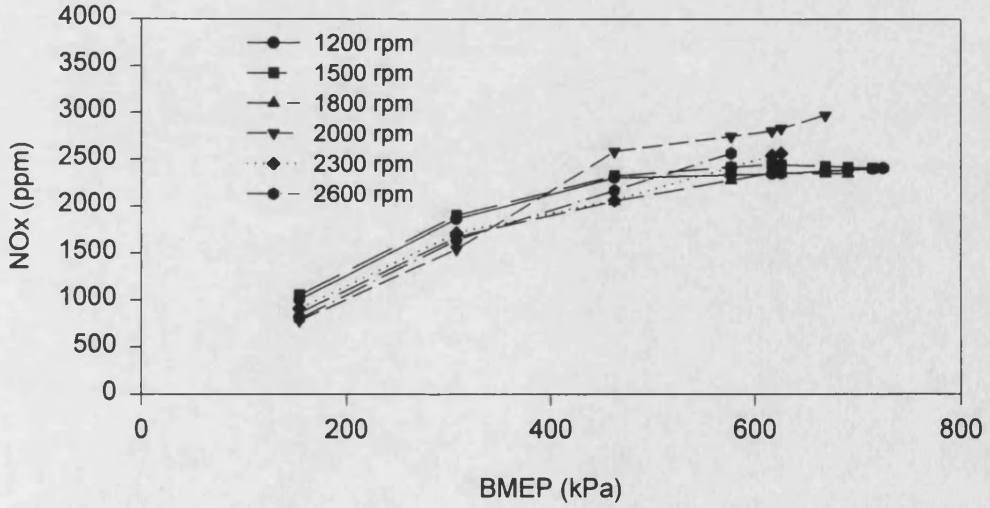

Figure 5.19 Exhaust manifold NOx emissions at different engine loads and speeds

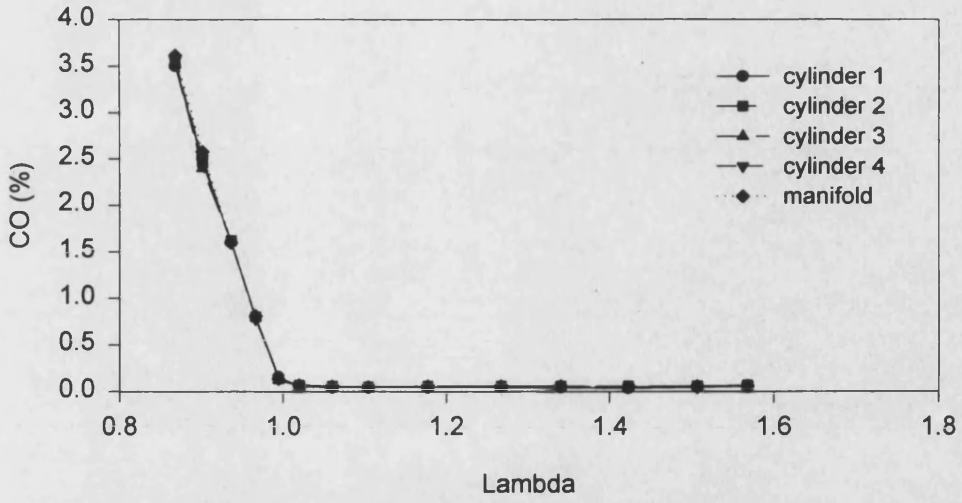

a) CO emissions at engine speed 1500 rpm and load 306 kPa

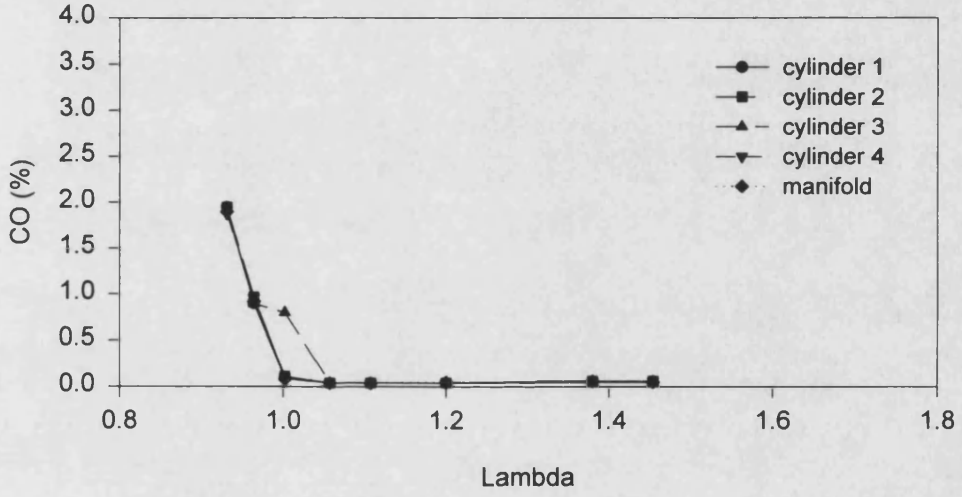

b) CO emissions at engine speed 1500 rpm and load 611 kPa

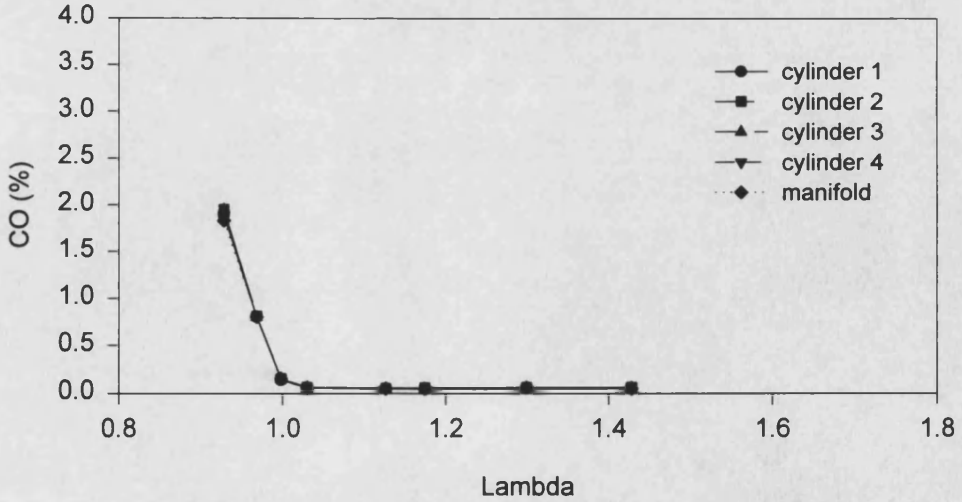

c) CO emissions at engine speed 2000 rpm and load 306 kPa

Figure 5.20 CO emissions from exhaust port and manifold at different engine speeds and loads

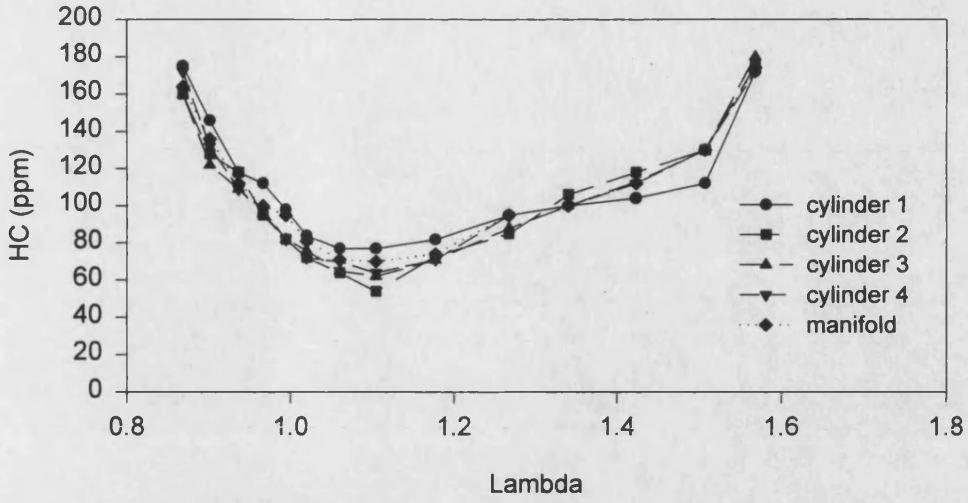

a) HC emissions at engine speed 1500 rpm and load 306 kPa

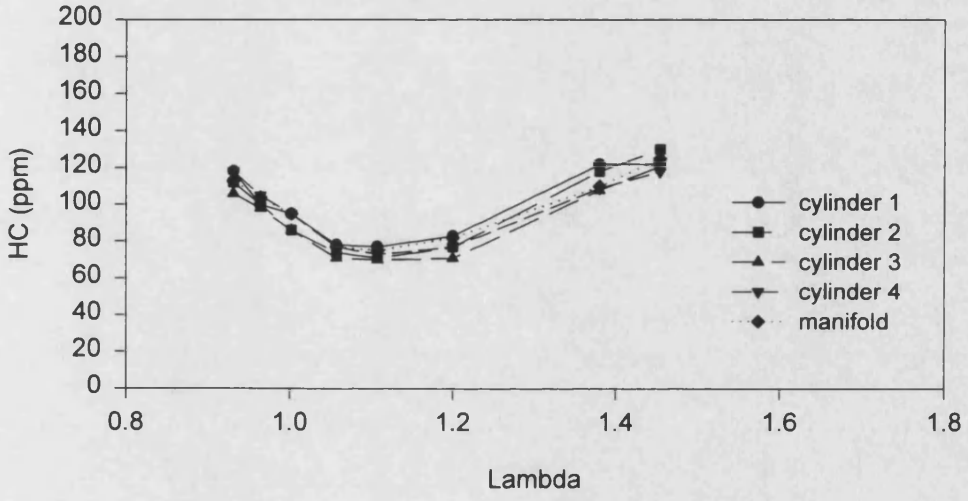

b) HC emissions at engine speed 1500 rpm and load 611 kPa

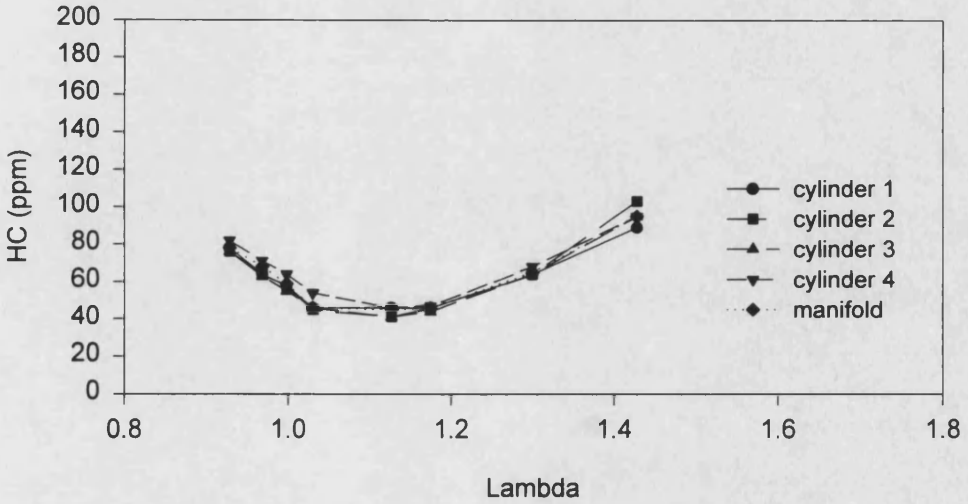

c) HC emissions at engine speed 2000 rpm and load 306 kPa

Figure 5.21 HC emissions from exhaust port and manifold at different engine speeds and loads

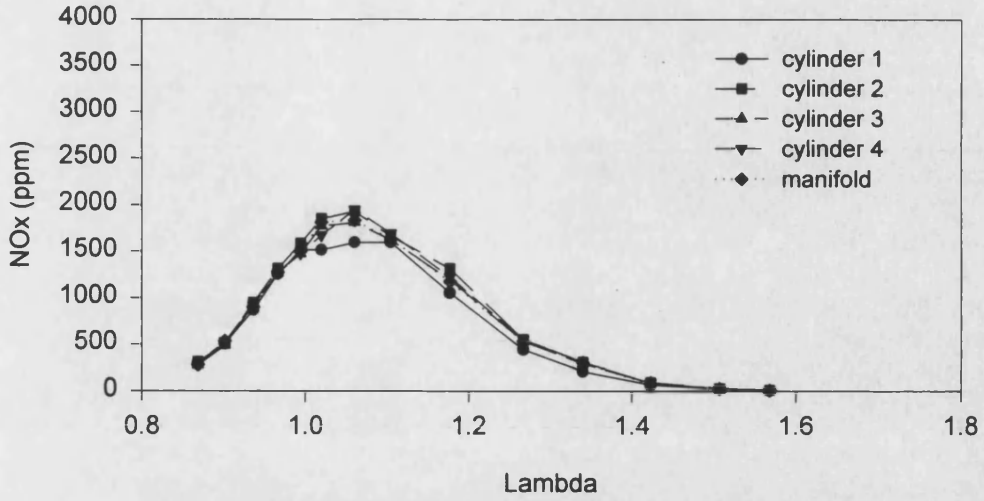

a) NOx emissions at engine speed 1500 rpm and load 306 kPa

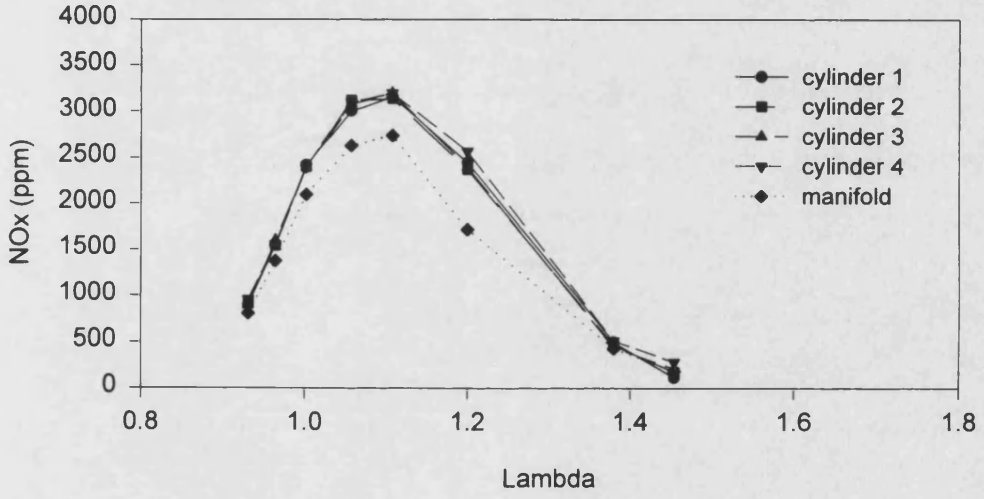

b) NOx emissions at engine speed 1500 rpm and load 611 kPa

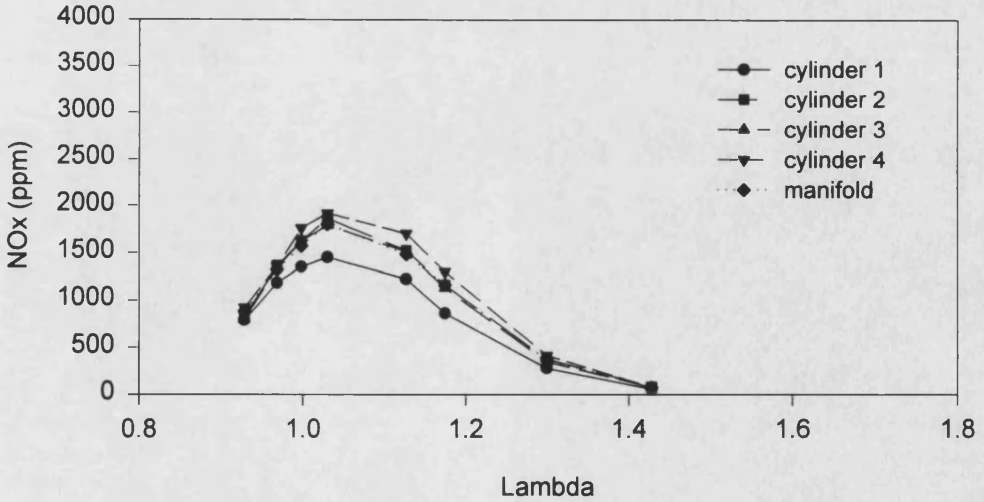

c) NOx emissions at engine speed 2000 rpm and load 306 kPa

Figure 5.22 NOx emissions from exhaust port and manifold at different engine speeds and loads

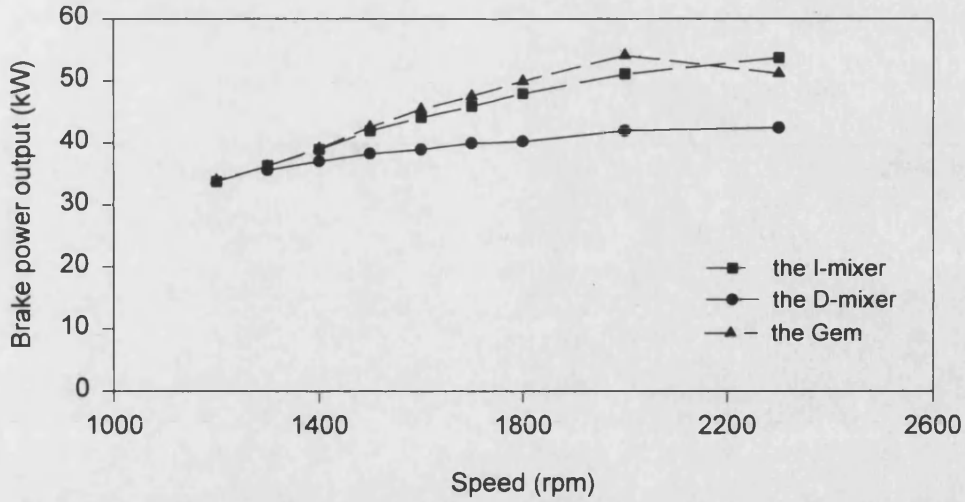

Figure 5.23 Comparison of engine brake power output for different mixers at WOT

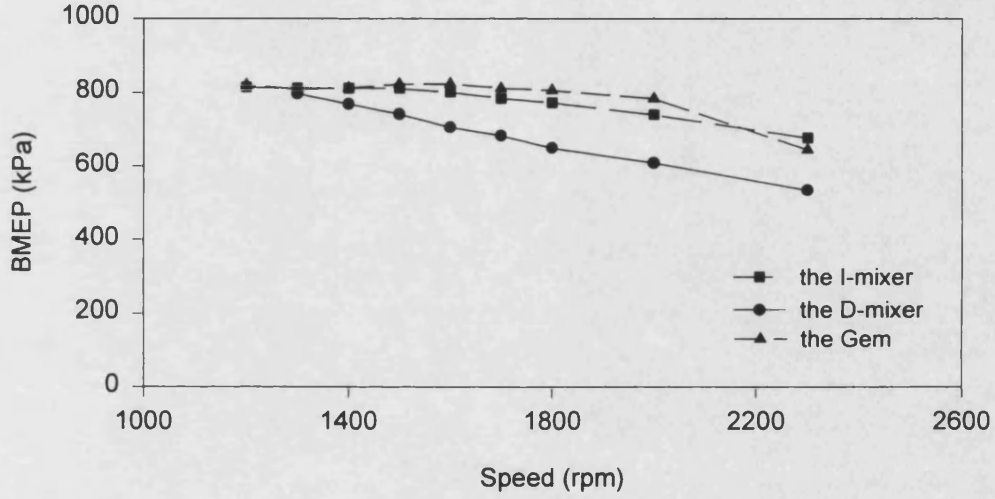

Figure 5.24 Comparison of engine brake mean effective pressure for different mixers at WOT

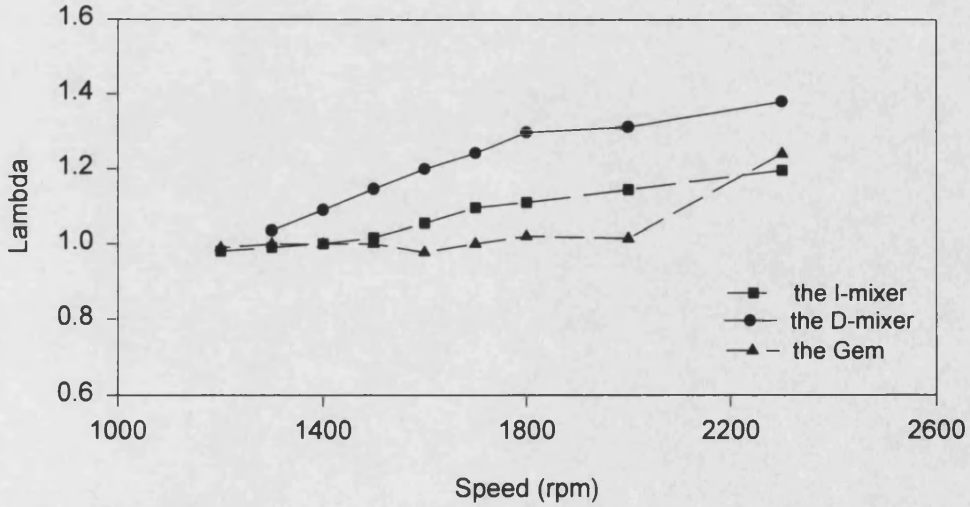

Figure 5.25 Comparison of mixture relative air fuel ratio for different mixers at WOT

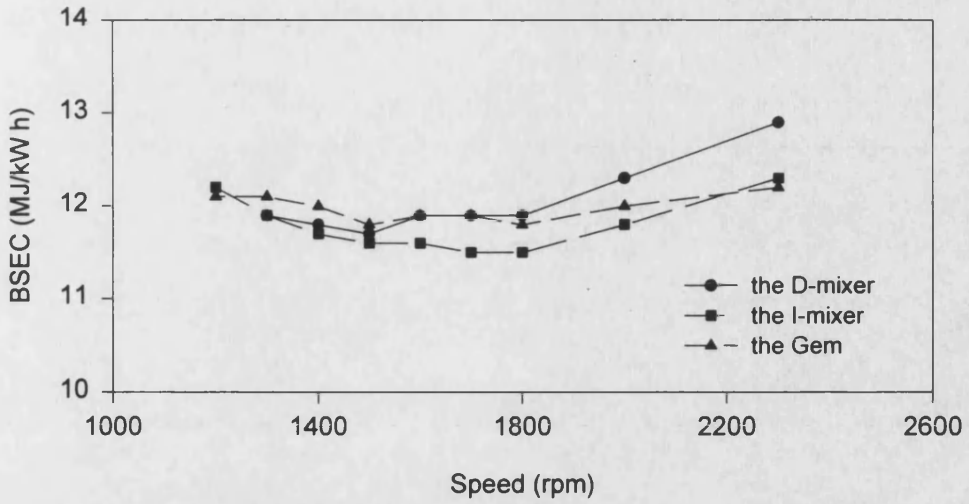

Figure 5.26 Comparison of brake specific energy consumption for different mixers at WOT

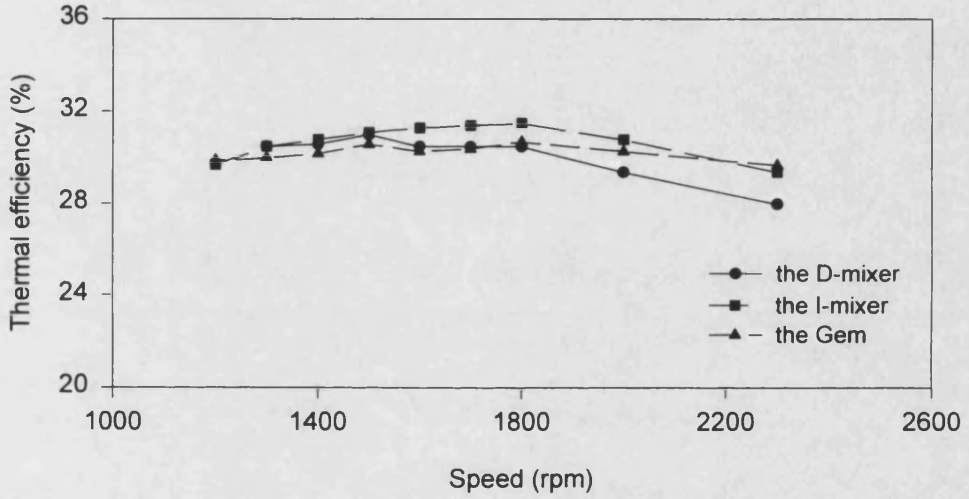

Figure 5.27 Comparison of engine thermal efficiency for different mixers at WOT

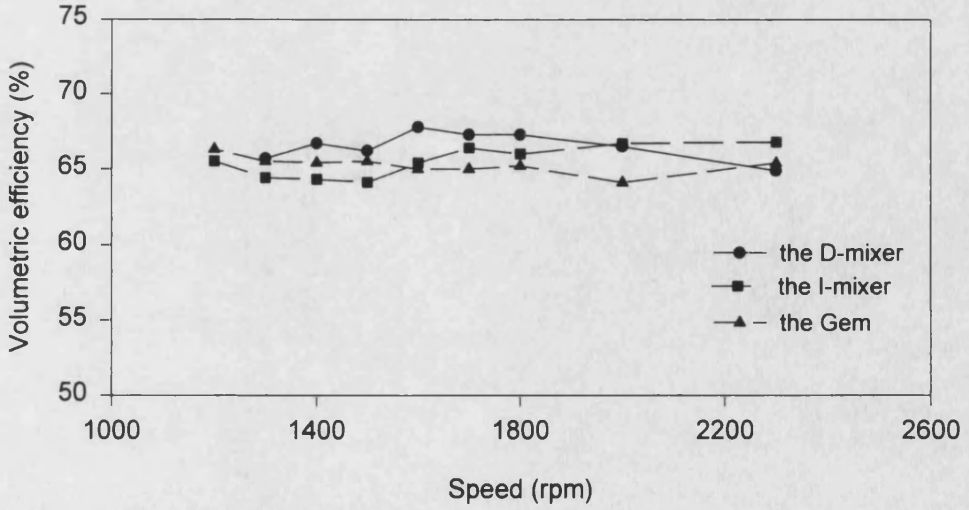

Figure 5.28 Comparison of engine volumetric efficiency for different mixers at WOT

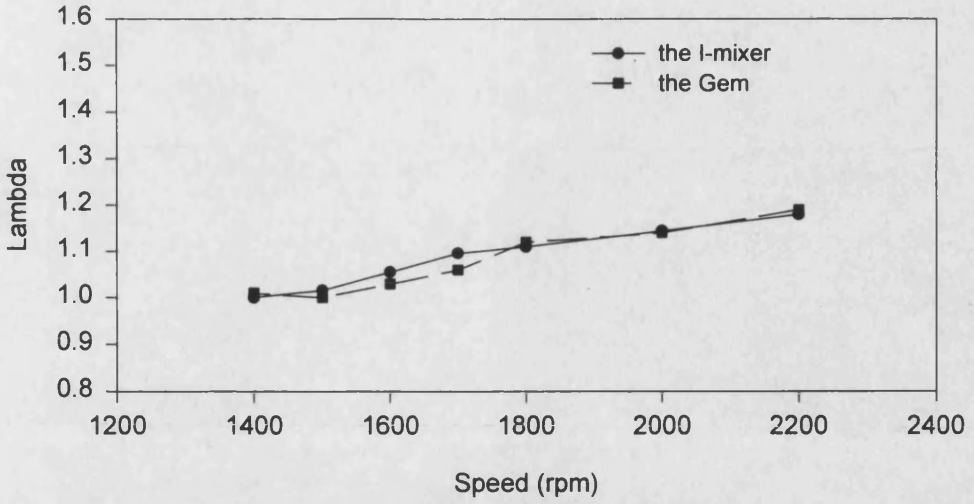

Figure 5.29 Comparison of mixture lambda value for the mixers at WOT

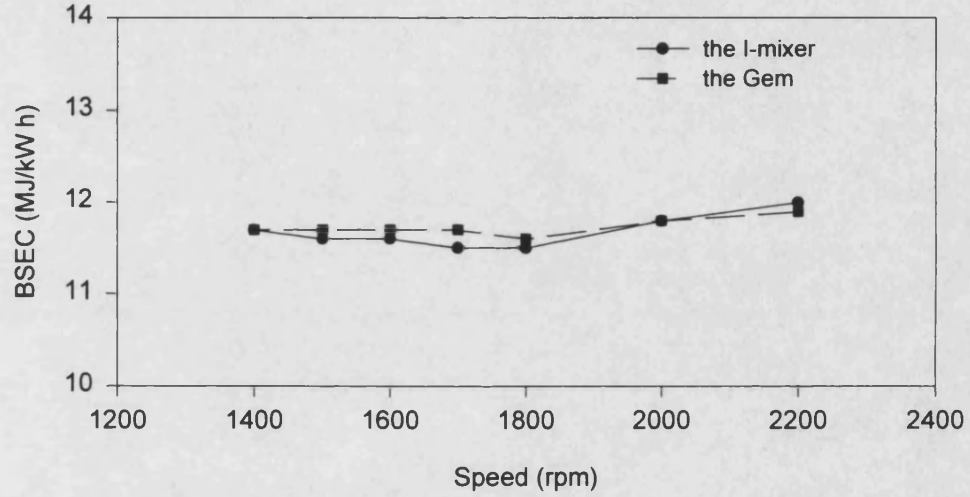

Figure 5.30 Comparison of brake specific energy consumption for the mixers at WOT

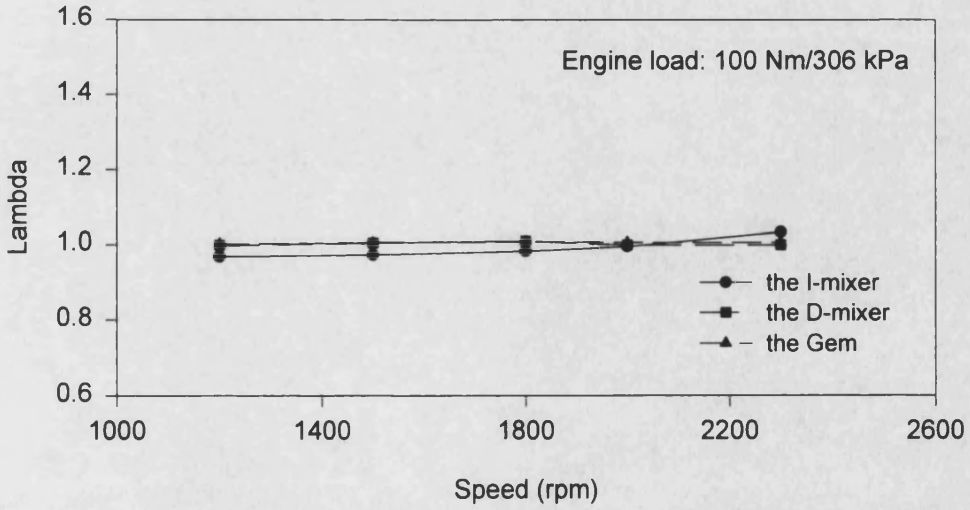

Figure 5.31 Comparison of mixture lambda value for the mixers at part load

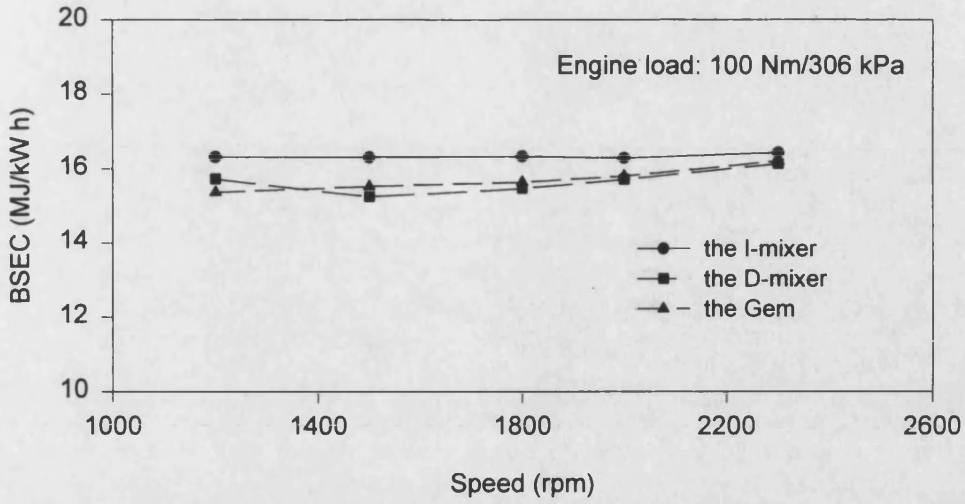

Figure 5.32 Comparison of brake specific energy consumption for the mixers at part load

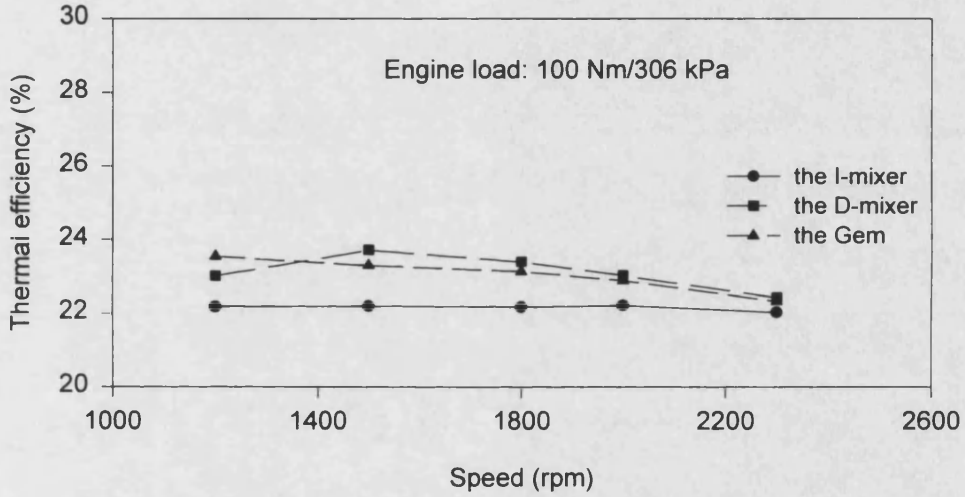

Figure 5.33 Comparison of engine thermal efficiency for the mixers at part load

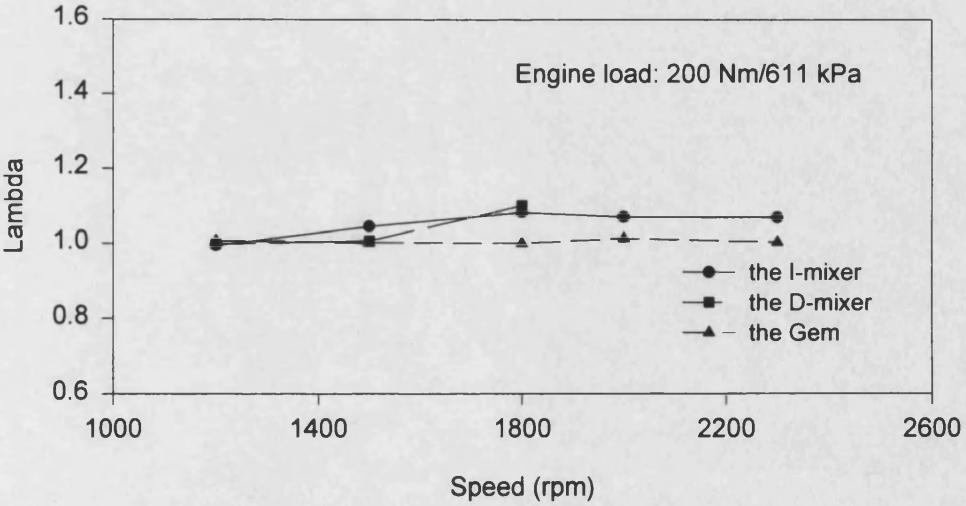

Figure 5.34 Comparison of mixture lambda value for the mixers at part load

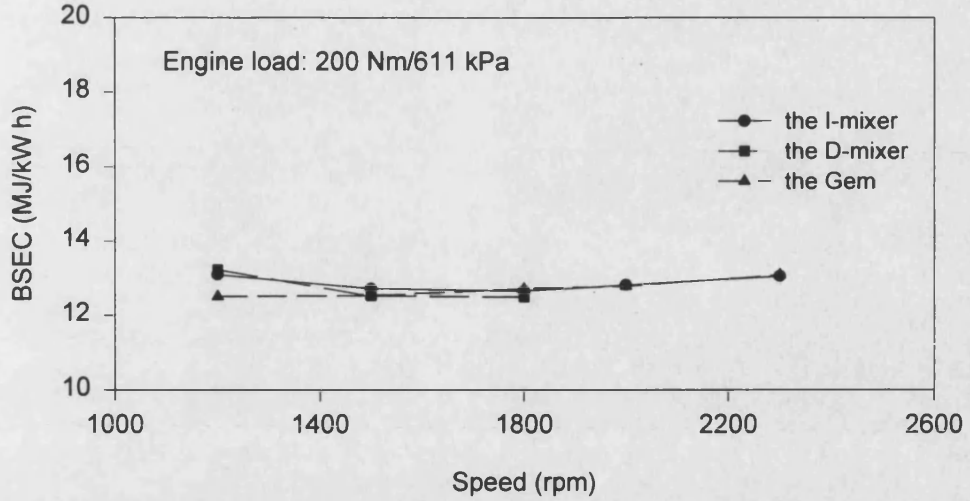

Figure 5.35 Comparison of brake specific energy consumption for the mixers at part load

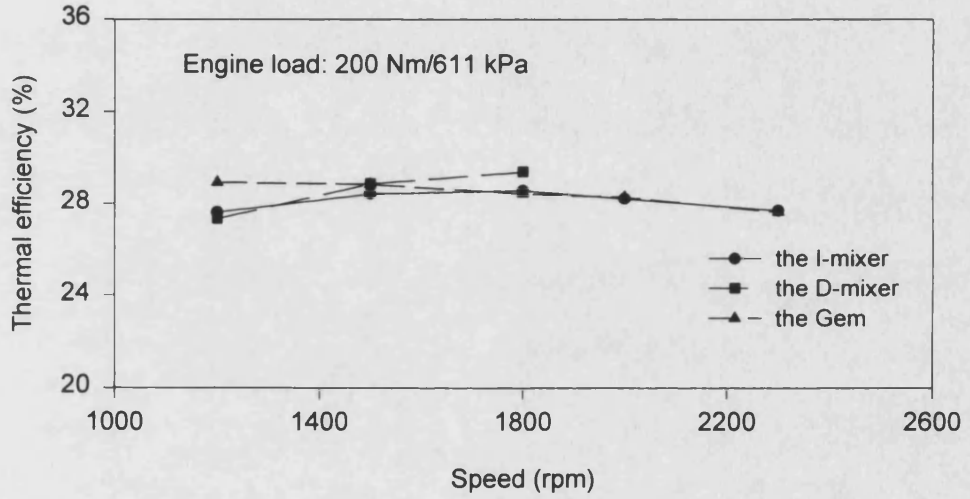

Figure 5.36 Comparison of engine thermal efficiency for the mixers at part load

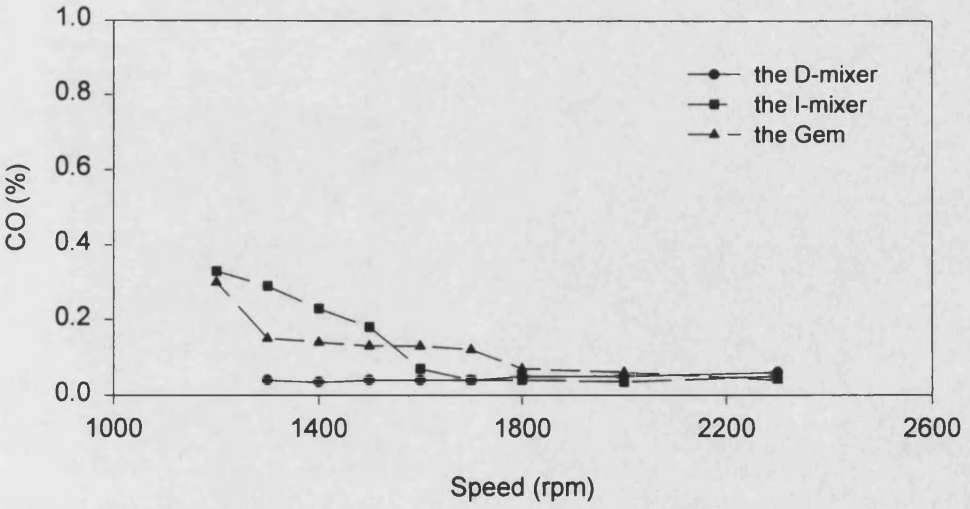

Figure 5.37 Comparison of exhaust manifold CO emission for the mixers at WOT

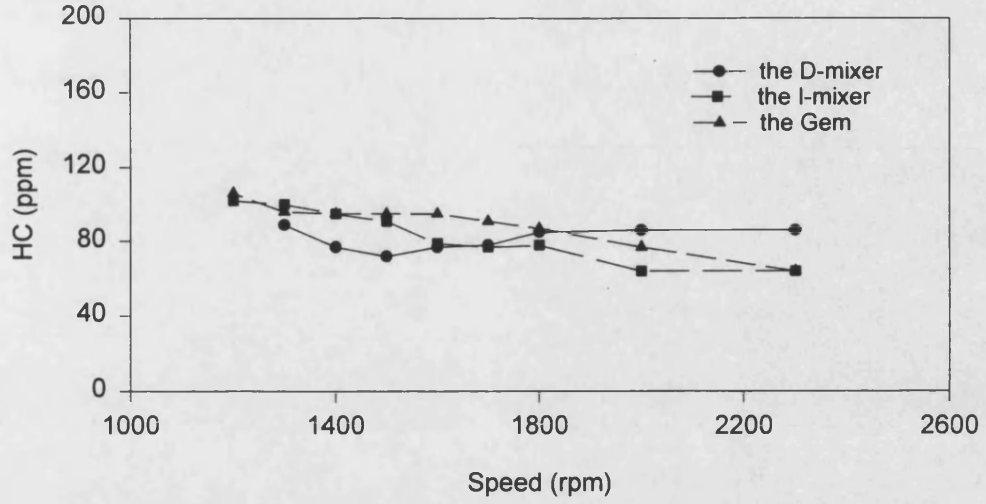

Figure 5.38 Comparison of exhaust manifold HC emissions for the mixers at WOT

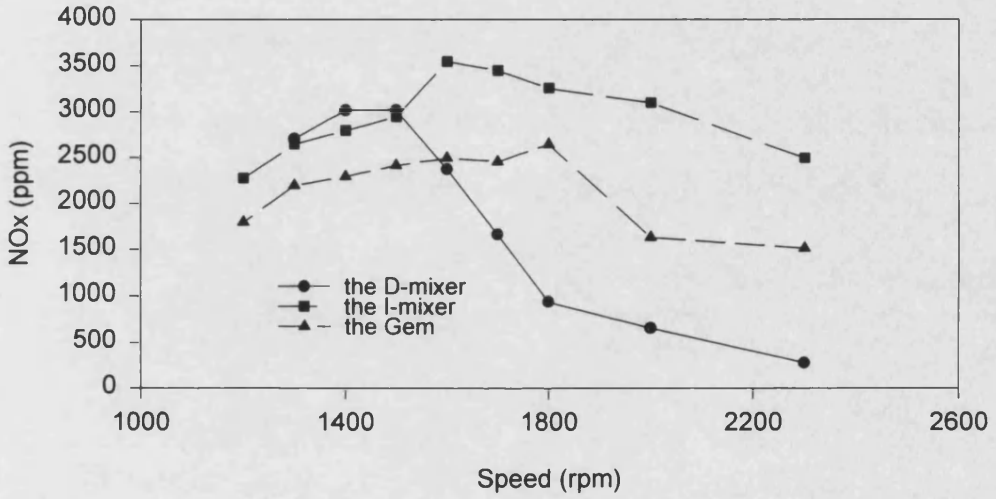

Figure 5.39 Comparison of exhaust manifold NOx emissions for the mixers at WOT

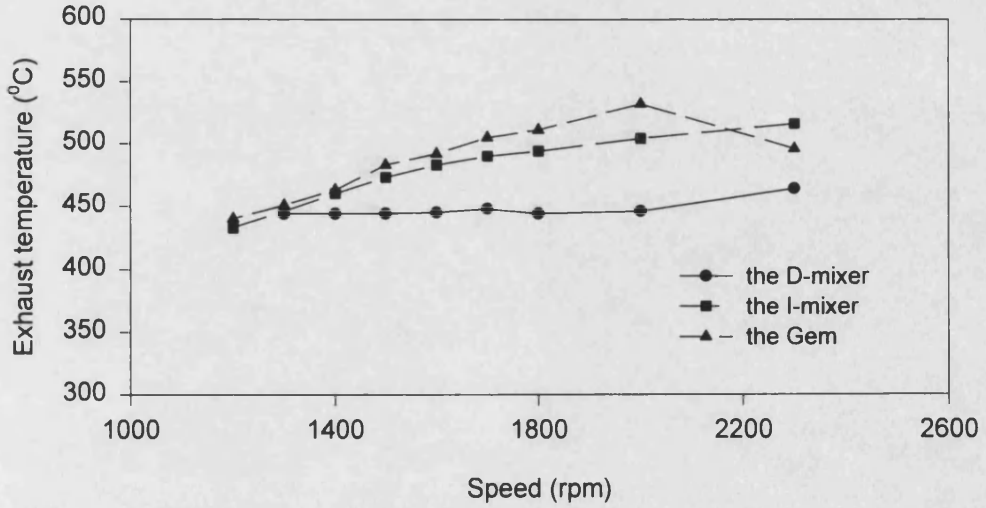

Figure 5.40 Comparison of engine exhaust temperature for the mixers at WOT

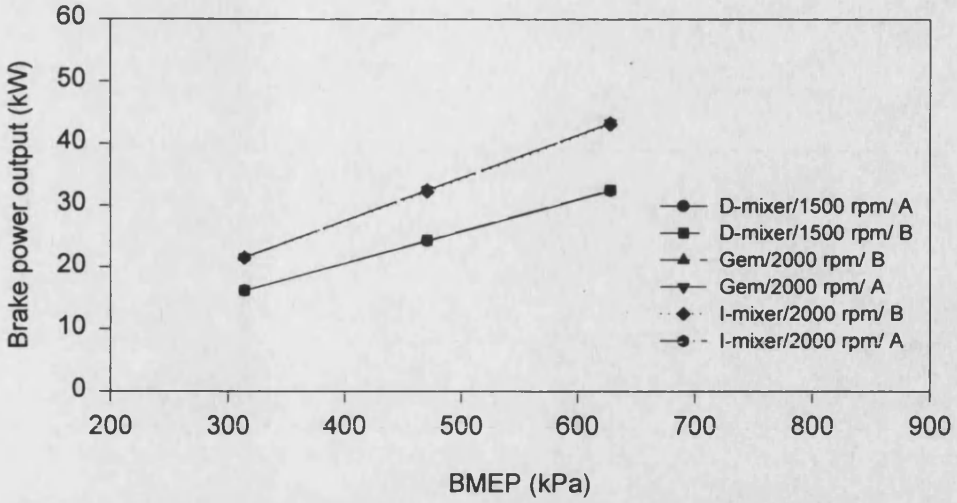

Figure 5.41 Repeatability of brake power output for the mixers at beginning and end of test

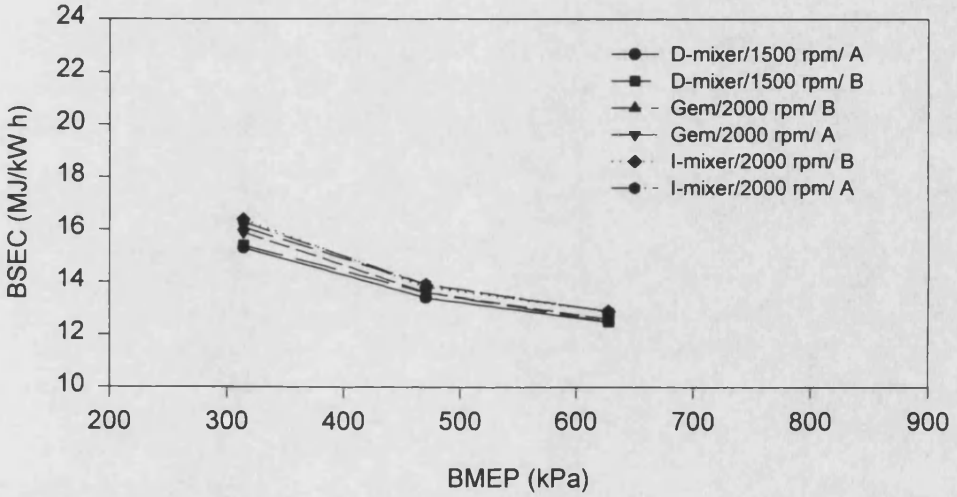

Figure 5.42 Repeatability of energy consumption for the mixers at beginning and end of test

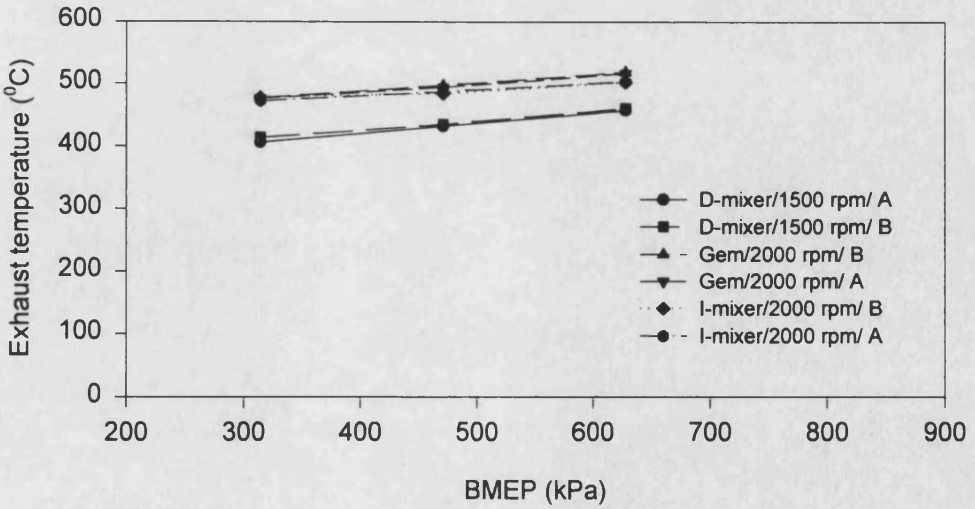

Figure 5.43 Repeatability of exhaust temperature for the mixers at beginning and end of test

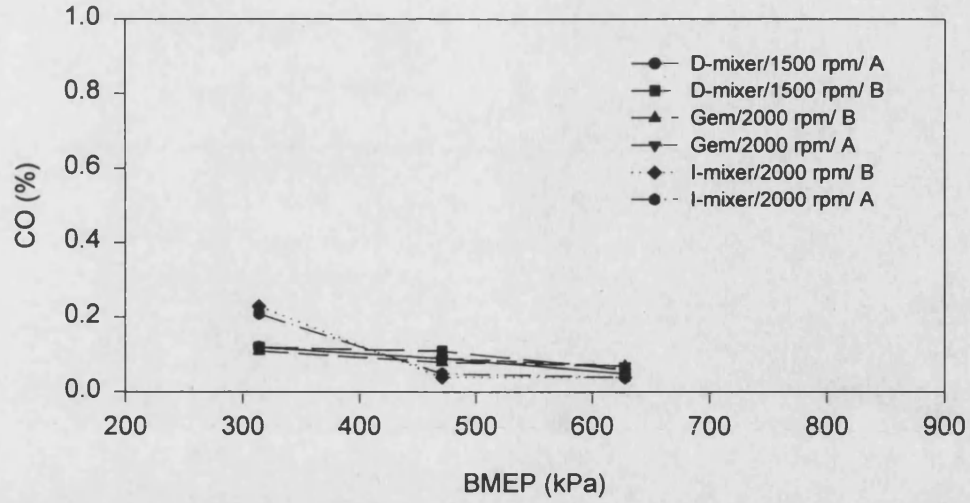

Figure 5.44 Repeatability of CO emission for the mixers at beginning and end of test

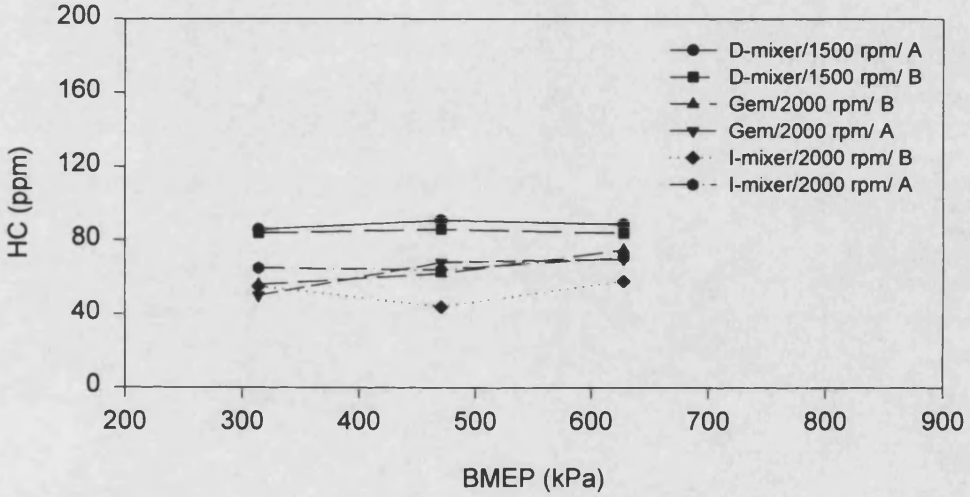

Figure 5.45 Repeatability of HC emissions for the mixers at beginning and end of test

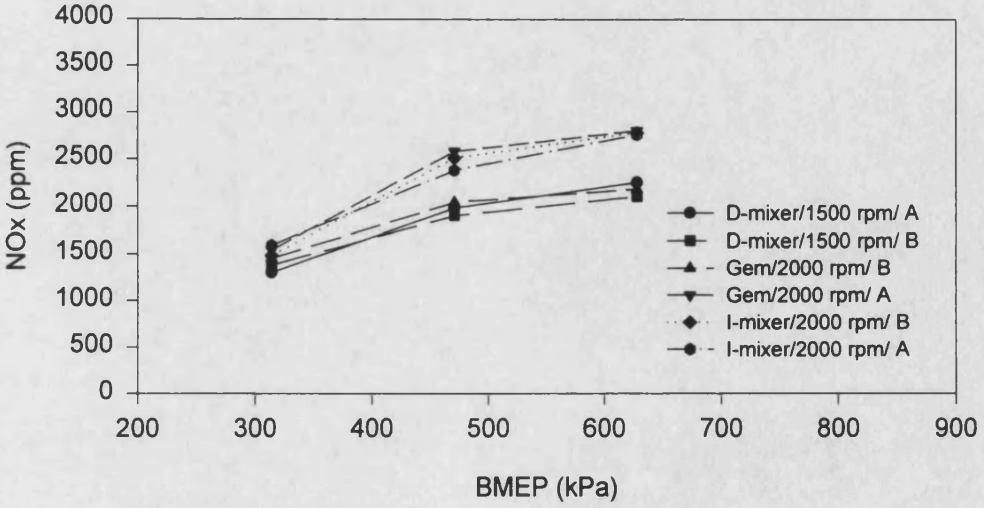

Figure 5.46 Repeatability of NOx emissions for the mixers at beginning and end of test

6. Study of mixture formation inside the intake manifold

6.1 Introduction

The engine performance and emissions study described in the previous chapter showed that there was not much difference between the emissions from each of the individual cylinders. The detected mixture concentration variations at the mixer outlet plane were believed to have been significantly reduced during the path over the throttle valve and intake manifold. It has been shown that the throttle valve had an influence on the mixing between the natural gas and air. Whether the intake manifold has a similar effect on the mixing of the two species remains to be examined. The purpose of this study was to examine the contribution made by the intake manifold towards the mixture formation. An attempt was also made on detecting the mixture formation variations within the intake manifold on a transient basis. The results were expected to lead to a better understanding of the mixture formation mechanism.

The FID was used to measure the mixture distributions in the manifold. This required the actual vacuum pressure levels inside the manifold to be measured under all the engine operating conditions in order to determine the FID pressure difference settings. Both the steady and the transient pressure inside the manifold were measured due to the possible pressure and flow pulsation in the manifold caused by each of the four engine working processes in each of the individual cylinders. The transient pressure measurement could also validate the assumption made on the pressure variations in a four cylinder four stroke engine during the CFD simulations. The results of the pressure variation of the engine and the effect of the variation on mixture preparation would be valuable for future transient study of the mixture formation in four stroke automobile engines.

6.2 Intake manifold pressure measurement

To measure the pressure within the engine intake manifold, as shown in Figure 6.1, two sections were chosen for placing the pressure transducers. The two sections were located on each side of the gas-air mixer and throttle block with the first one located just upstream of the intake ports of the cylinders one and two, and the second one just upstream of the intake ports of the cylinders three and four. Both the steady and transient pressures were measured at these two positions. To measure the steady pressure, a mercury manometer was used and two Druck pressure transducers PDCR 10/L were used for the transient pressure detection. The transient signals were conditioned by a DC instrumentation conditioning card and recorded by a GLOBAL LAB data acquisition and analysis system. The transient pressure measuring system was

firstly calibrated in order to interpret the measured signals into the actual pressure values. The calibration result is given in Figure 6.2. The transducers and their conditioning system had a very good linearity within the calibrated range which covered the pressure variation range needed to be measured. To monitor the pressure signals, an oscilloscope was used during the measurements and a digital multimeter was used to obtain the average values of the signals recorded. The average readings were compared with the recorded signal mean values as another means of monitoring. The values were also compared to the steady pressure values measured using the mercury manometer. Before the calibration, the engine was operated from idling to full throttle in order to obtain the pressure range. Based on the detected range, the conditioning card was set with an offset of 2.85 volt, which enabled the transducers to cover all the engine operating conditions. This is the reason that the calibration line given in Figure 6.2 does not go through the origin of the coodinate.

The steady and transient pressures were firstly measured under engine idling and full throttle conditions with the Gem mixer and then under different part throttle conditions. Because there was no difference between the results detected by the two transducers, only the results detected by one of them will be presented hereafter. The results are given in Figures 6.3 to 6.5 for the transient pressures measured. The mean values of these transient pressure signals agreed very well with the steady pressures measured by using the mercury manometer under the same engine operating conditions. These steady pressure results are listed in Table 6.1 together with some of the descriptive analysis of the transient pressures recorded.

Table 6.1 Descriptive analysis of the transient pressure signals

Operating conditions	idling	full throttle	1500/50	1500/100	1500/200
Throttle positions	0%	100%	4%	8%	22%
Mean (kPa)	24.02887	97.3658	36.22976	50.57783	81.8457
Standard Deviation(kPa)	1.509923	3.367254	1.949311	2.336075	3.173606
Deviation/Mean	6.28%	3.458%	5.38%	4.618%	3.8775%
Range (kPa)	5.67036	10.35633	7.32422	9.21434	11.18322
Minimum (kPa)	22.07819	93.23337	33.57643	46.61039	77.28547
Maximum (kPa)	27.74855	103.5897	40.90065	55.82473	88.46869
Count	1000	1000	1000	1000	1000
Operating conditions	1500/260	1500/100	1800/100	2000/100	2300/100
Throttle positions	68%	8%	10%	12%	17%
Mean (kPa)	97.40428	50.57783	51.90666	52.64711	52.57423
Standard Deviation(kPa)	3.349356	2.336075	2.343308	2.475165	2.432128
Deviation/Mean	3.438%	4.618%	4.5144%	4.7%	4.626%
Range (kPa)	10.2382	9.21434	10.04127	10.27754	11.57699
Minimum (kPa)	93.3515	46.61039	48.18548	48.93365	47.59482
Maximum (kPa)	103.5897	55.82473	58.22675	59.21119	59.17181
Count	1000	1000	1000	1000	1000

At idling operation, the steady pressure (absolute pressure) in the intake manifold was 24 kPa, which was much lower than the ambient pressure which was 100.26 kPa. This was because of the closed throttle valve which resulted in a high pressure loss when the engine cylinders were in operation. At full throttle position, the pressure in the intake manifold was 95.2 kPa, which was slightly lower than the ambient pressure. At part loads, the steady pressure in the intake manifold increased with the opening of the throttle valve. For example, when the engine load was increased from 50 Nm to 260 Nm at the engine speed of 1500 rpm, the throttle opening position was increased from 4% to 68%, the steady pressure in the intake manifold was increased from 36.22 kPa to 97.4 kPa. When the engine was run at a fixed load with an increasing speed, the pressure increased slightly because the throttle opening position had only changed slightly. It is interesting to notice that the flow restriction over the intake system depended on the system configuration, the throttle position and the engine operating condition. Both the engine speed and load influenced the flow restriction but with different scales. The pressure loss through the intake system was more sensitive to the engine load than to the engine speed. This was one of the reasons why the engine showed a very flat volumetric efficiency curve with various speeds at full throttle during the performance test, but had a sharp increase with the engine loads for all the speeds tested, see Figures 5.7 and 5.15.

To assess transient pressure variations over the steady pressure, 1000 consecutive samples were analysed for each of the engine operating conditions. The analysed samples covered more than one engine cycle under all the engine operating conditions, see Figures 6.3 and 6.4, where more than four waves are presented. It is believed that each of the waves was mainly contributed by the induction process of the engine cylinders. At the beginning of each inlet valve opening, the pressure in the intake manifold increased with time, which was resulted from the advanced inlet valve opening and the piston upwards movement. At about the piston top dead centre, the intake pressure reached its maximum level and then reduced with the piston downwards movement. At about the middle of the induction stroke, the piston had its maximum velocity which produced a maximum intake flow restriction. During the other half of the stroke, the intake pressure built up with the slowing down piston. Near the end of the process, another one of four inlet valves opened according to the engine firing order, which increased the intake pressure and repeated the same process as that carried out by its previous cylinder. In order to see the percentage of the intake pressure variations over the mean values of the pressure, a statistical parameter called standard deviation was calculated apart from the maximum, minimum and their difference (the Range). The standard deviation is a measure of how widely values are dispersed from the mean value, which uses the following formula:

$$\text{Standard deviation}=\sqrt{\frac{n\sum x^2-(\sum x)^2}{n(n-1)}} \qquad (6.1)$$

where n is the number of the samples used and x is the value of the sampled data, i.e. the deviate. Based on this statistical parameter, the pressure variations were assessed by using the ratio of the standard deviation of the sample set over the sample mean value, which is also listed in the Table. The results showed that the pressure variations only accounted for 3.458% at full open throttle and 6.28% at idling. During the part load running, the wider the throttle opening, the lower the pressure variations. No matter at which load and/or speed the engine was running, the pressure variations were relatively small. These results illustrated that the assumption made during the CFD simulation on the pressure boundary was reasonable and accurate enough for the comparative study.

Another pressure measurement was conducted with the aim of examining the pressure loss through the entire intake system when different gas-air mixers were used under the engine full throttle operation. The comparisons made in chapter four were under part throttle, which could not meet the requirement of engine performance comparison under full throttle operation. Two mixers were examined in the test. One of them was the I-mixer which exhibited the highest pressure loss across the mixer at the part loads tested. The other was the Gem which produced the lowest pressure loss at the part loads. With the same throttle valve at its wide open position and with the same intake manifold, the pressure within the intake manifold for the two mixers would provide direct information as to the performance comparison reported in chapter five under WOT conditions. The measured results are given in Figure 6.6, where the horizontal axis is the engine speed and the vertical one is the steady pressure losses across the mixers, the throttle valve and the manifold, i.e. the losses from the inlet of the mixers to the section of the intake manifold where the pressure transducer was placed.

The results given in Figure 6.6 showed that the pressure losses increased dramatically with the engine speed at WOT for both the mixers used. At the lower speeds, the pressure losses were nearly the same for the two mixers. At higher speeds, the pressure losses with the I-mixer were slightly lower than that with the Gem mixer. This result was quite different from what had been obtained during the part throttle test in which the pressure losses across the mixers alone were measured. The reason for this is believed to be the variable geometry character of the I-mixer. At wide open throttle and higher engine outputs, both the air and the gas flow restrictions in the I-mixer were dramatically reduced by the increased flow areas. While with the Gem, the fixed venturi could not change. The small gas flow area due to the connection constraint dragged down the pressure in the throat area which caused extra pressure losses across the mixer when the engine was run at higher outputs. The detected pressure loss difference

between the two mixers is believed to be one of the causes which gave the engine a slightly higher thermal efficiency with the I-mixer at WOT, as has been experienced during the performance test, see Figure 5.27. Therefore a higher priority should be given as to how to reduce the pressure loss across the mixer in future mixer design and development.

6.3 Mixture distributions inside the intake manifold

To examine the mixture homogeneity after the mixers, the throttle valve and the intake manifold, the mixture distribution inside the intake manifold was measured by using the Cambustion FID at the two sections where the pressure tappings were located. The same as that in the previous work, the pressures at the sections were also measured while measuring the mixture distributions in order to adjust the pressure of the span gas in order to achieve an accurate signal interpretation. The wall-to-wall distance at the sampling sections was about 58 mm. The sampling probes at each of the sections were traversed by two displacement mechanisms. Measurement was made at six sampling points with an evenly distributed traverse distance under all of the engine operating conditions. After both the engine and the FID were warmed up and running at steady operating status, the intake pressure was firstly measured and then the two sampling probes were traversed to the sampling positions. The pressures of the FID and the span gas were then adjusted to keep the pressure difference between the FID flame chamber and the CP chamber constant and to keep the span gas pressure at the same value as that of the pressure at the sampling source. After this the FID outputs were recorded at each of the sampling points for each of the engine operation conditions with the Gem mixer and also with the I-mixer independently.

The results for the Gem mixer are given in Figure 6.7, where the vertical axis is in relative air fuel ratio, the same unit as that used during the mixer performance study. The mixture distributions at the section upstream of the engine cylinders one and two were very homogeneous and as was the case at the sections upstream of the cylinders three and four. The variation of the mixture λ values was so small that it would not make any contribution to the cylinder-to-cylinder emissions variation of the engine. The tiny variation may also be attributed to the FID resolution. Experience showed that the FID output reading could only be accurate to three digits. When the signals were converted to the λ values, only the first three digits were meaningful and represented the concentration changes. Of course, within the first three digits reading, the FID worked very well and gave a steady reading. To confirm the FID had a reasonable resolution and its signal output did response with any mixture concentration change over certain threshold, the mixture supplied to the engine was deliberately changed while keeping the sampling probes at the same positions. The FID signal outputs increased with the

enriched mixture and decreased with the leaned off mixture whenever the change of the mixture air fuel ratio was over 0.2. This test indicated that the measured homogeneous mixture distribution was the actual mixture distribution, not false results produced by the instrument malfunction or by the poor resolution of the FID.

The results for the I-mixer are given in Figure 6.8 where the vertical axis has the same unit and range as that used for the Gem mixer. Clearly the mixture distributions were not as homogeneous as that with the Gem mixer because the λ value variation at certain engine operating conditions was higher and changed randomly. But the mixture distributions for all the measurements were still quite homogeneous if the instrument resolution was taken into account, because the largest λ variation was only about 0.06. Another factor that needs to be pointed out is that after the sections where the measurements were taken, the mixture will have been further mixed in the due course from the sampling places to each of the individual cylinders before the start of ignition. So that even with the I-mixer, the mixture homogeneity will not cause any deterioration to the engine performance and emissions or the performance and emissions difference is too little to be detected if there is any. These results further confirmed the conclusions drawn in which the overall air fuel ratio control and the pressure losses across the mixer are the most important features needed to pay attention to during the design and development of natural gas engine carburettors. The results given in the two figures also showed that the mixture distributions were not sensitive to the engine operating conditions, a phenomenon that had been identified during the CFD simulations and the mixer performance experiments.

After these steady mixture distribution measurements, attempts were also made on measuring the transient mixture distribution inside the intake manifold on a cycle-by-cycle basis and on a basis of sudden throttle operation. In order to do this, the plenum originally used during the steady measurement, see Figure 4.3, was removed and the transfer tube was replaced by a tube which had a length of 100 mm and a diameter of 1 mm. The connecting tube had a diameter of 0.012 in (0.03 mm). The FID signal was directly recorded by the GLOBLE LAB data acquisition and analysis system. As a reference to the FID signal, the transient pressure was also measured at the same time and at the same place as that of the sampling probe. The results of the transient mixture distributions inside the intake manifold are given in Figure 6.9 together with the transient pressure signals. Unfortunately, with the construction of the FID sampling system used the sample flow rate was strongly affected by the pressure change at the sampling point. The transient mixture concentration failed to be detected on a cycle-by-cycle basis. Similar tests were also carried out for other engine operating conditions. None of them could give the information about the transient mixture distributions in the intake manifold. To monitor the transient mixture concentrations in the intake system,

the sampling system needs to be further modified in order to eliminate the pressure interference. A sample tube having a much lower capacity and a two T-pieces design used by the researchers in reference [144] may help. This remains to be tested if the engine of interest is for automobile application. A similar attempt was also made on measuring the transient exhaust HC emissions of the engine, the same conclusion was drawn. With the arrangement of the sample system for the model of the FID used, the signals detected were the signals of the pressure, rather than the signals of the mixture concentrations. The FID acted as an expensive transient pressure measuring system. Another difficulty of measuring the transient mixture concentrations in the intake system came from the low pressure at the sampling source. There was only a small margin for adjusting the pressure difference between the CP chamber and the flame chamber. Under certain engine operating conditions, the pressure pulsation in the intake manifold even caused an oscillation of the flow within the transfer tube or connecting tube and hence an oscillation of sampling flow rate. An adaptive flow rate control system which can control the pressure in the CP chamber accordingly with the pressure at the sampling source remains to be devised.

6.4 Summary

The steady and transient pressures inside the engine intake system under different engine operating conditions were measured with the Gem mixer in place. The pressure variations caused by the engine induction process only accounted for 3.48% at wide open throttle and 6.28% at the idling condition with that at part throttle positions in between. This indicated that the assumption made on the pressure changes during the CFD simulations was correct and this kind of assumption is suitable for the intake system simulations of all kind of four stroke engines under steady operating conditions. By measuring the pressure losses across the entire intake system using both the Gem and the I-mixer at WOT, the queries about the flow restriction with the variable geometry I-mixer at WOT were resolved and the results explained the engine performance comparisons made in chapter five.

The mixture distributions inside the intake manifold proved that further mixing existed downstream of the mixer. The measured mixture λ value variations in the intake manifold for the Gem mixer was within 2.4% and it was within 6% for the I-mixer. The actual mixture in the cylinders before ignition will be much more homogeneous than these. In future natural gas engine gas-air mixer design, higher priority should be given to the pressure loss across the mixer, rather than the mixture homogeneity.

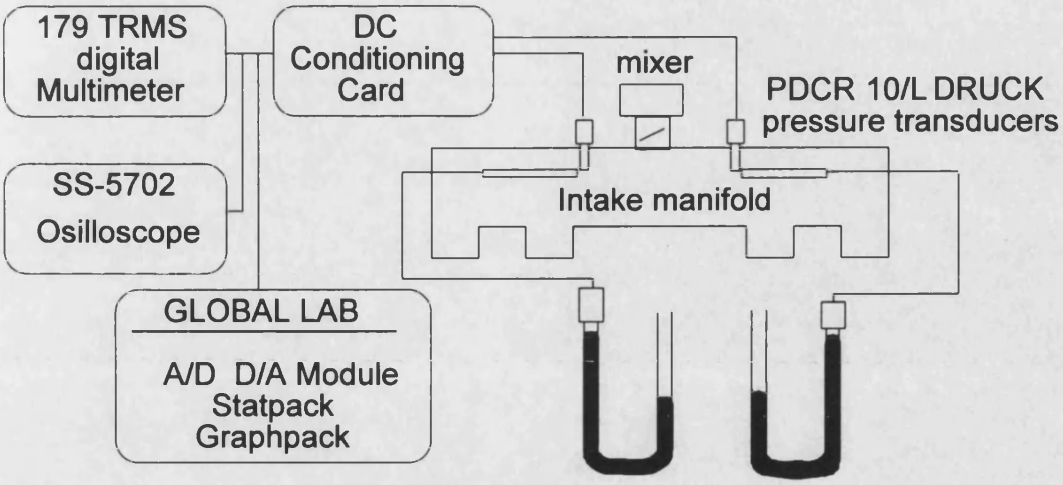

Figure 6.1 Lay out of the intake pressure measurement

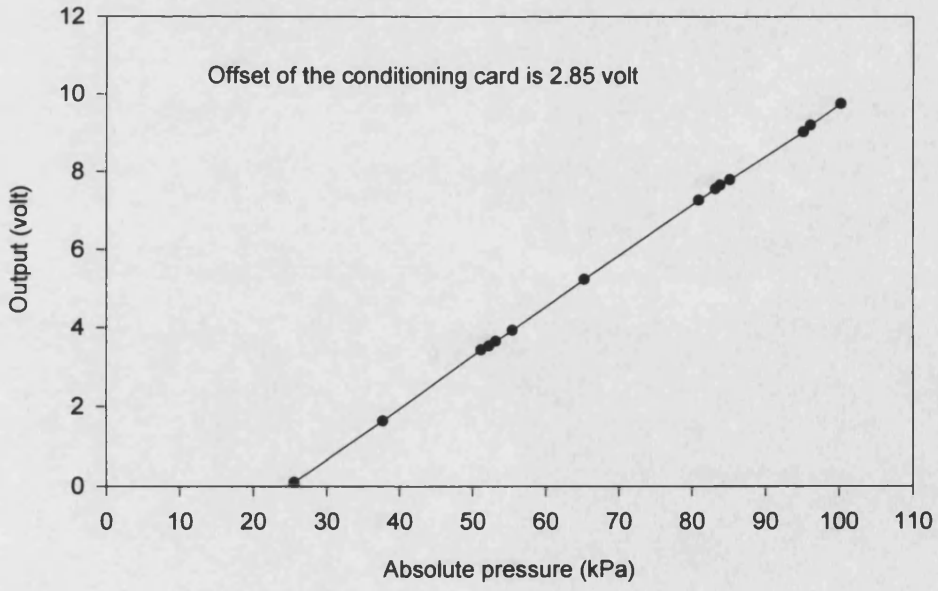

Figure 6.2 Calibration of the pressure transducers

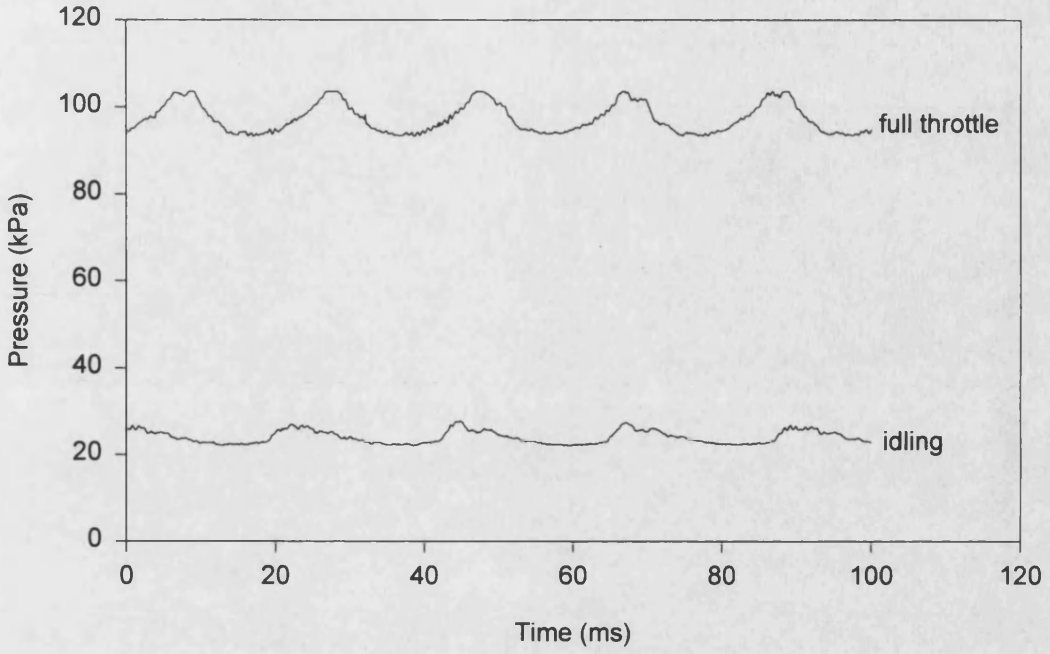

Figure 6.3 Transient pressures of the intake manifold at idling and full throttle

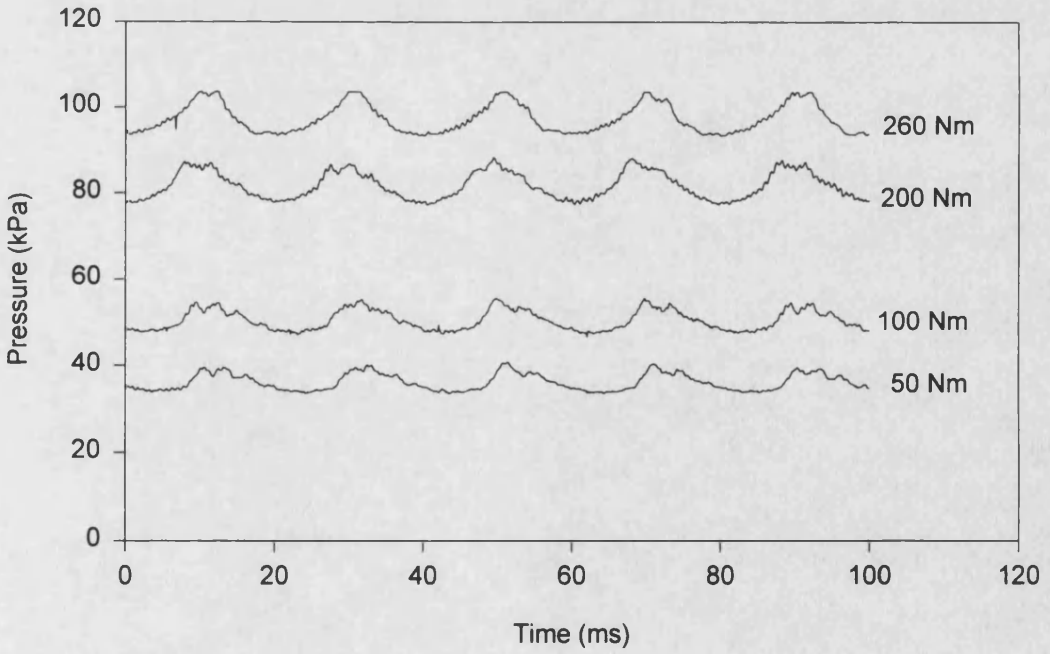

Figure 6.4 Transient pressures of the intake manifold for various loads at 1500 rpm

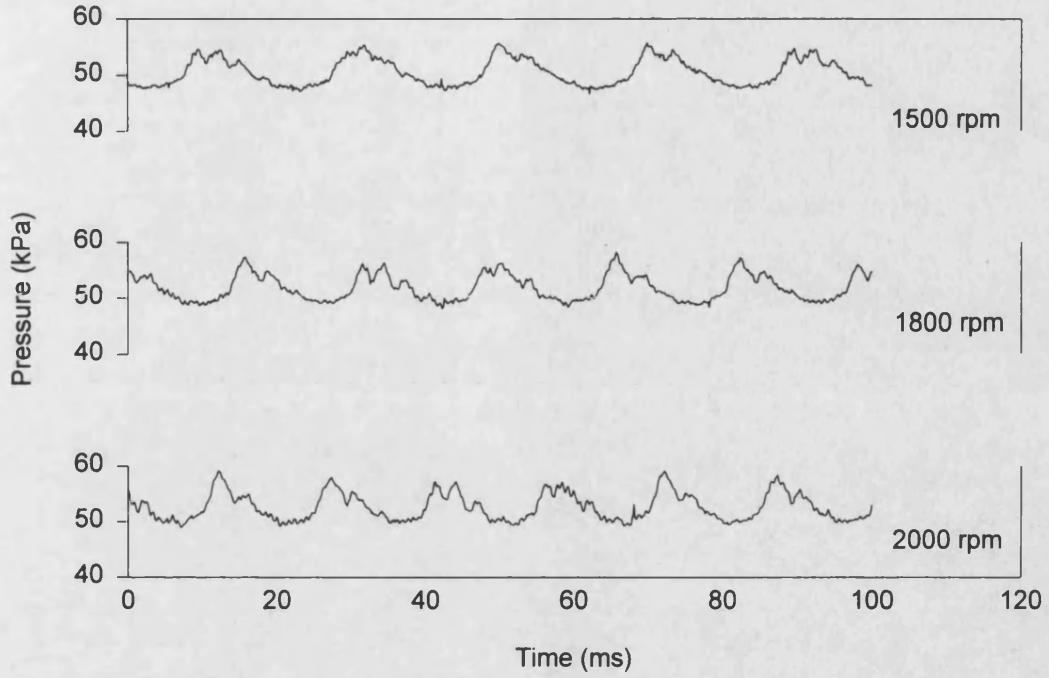

Figure 6.5 Transient pressures of the intake manifold for various speeds at 100 Nm

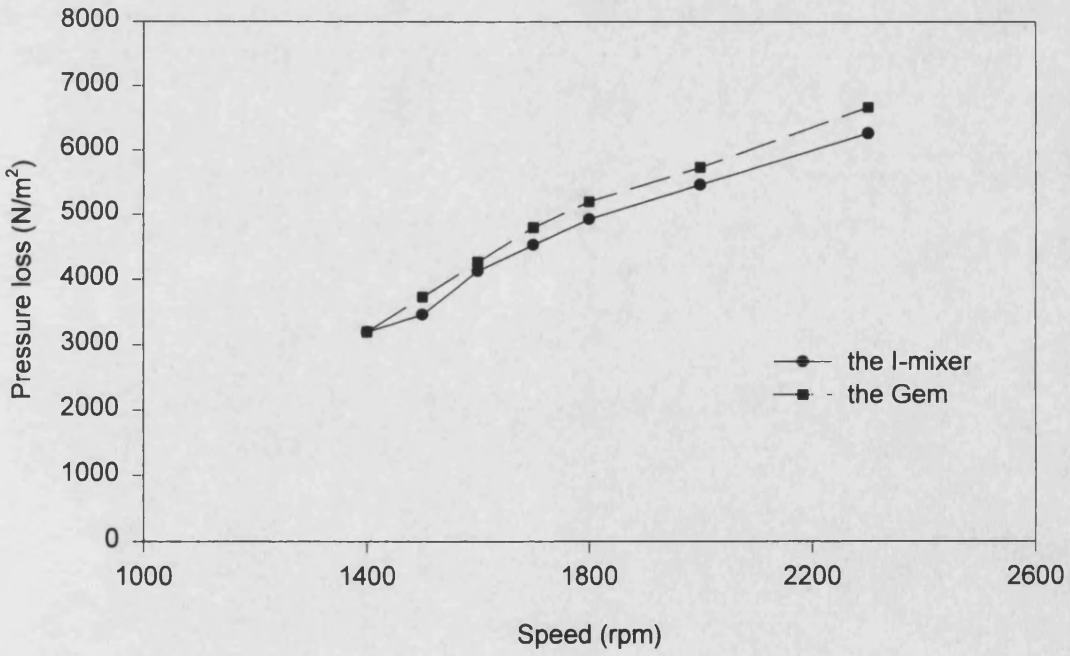

Figure 6.6 Pressure losses of the mixture via the mixers, throttle and manifold at WOT

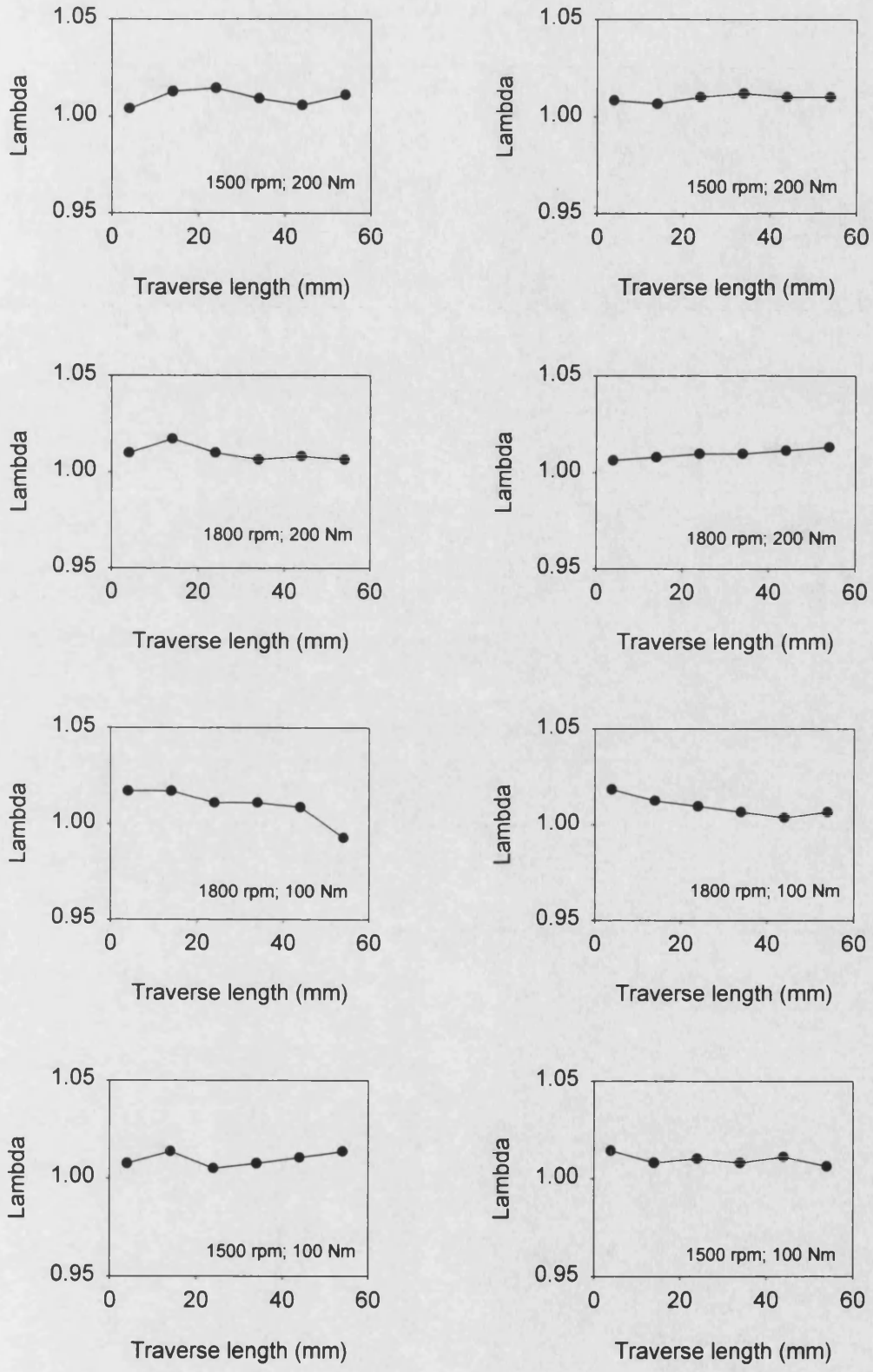

a) For cylinders 1&2

b) For cylinders 3&4

Figure 6.7 Mixture distributions at the intake manifold with the Gem mixer

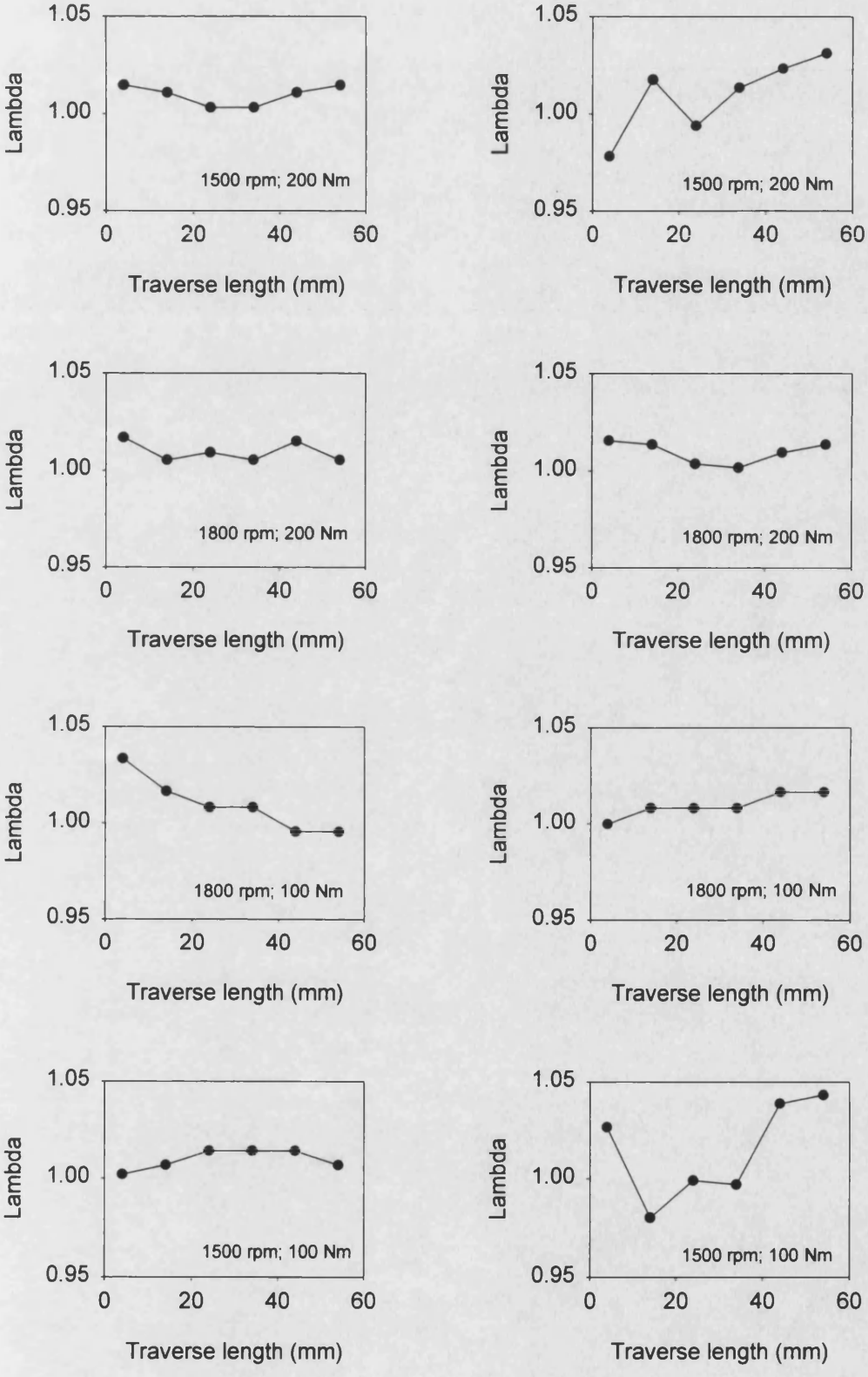

a) For cylinders 1&2

b) For cylinders 3&4

Figure 6.8 Mixture distributions at the intake manifold with the I-mixer

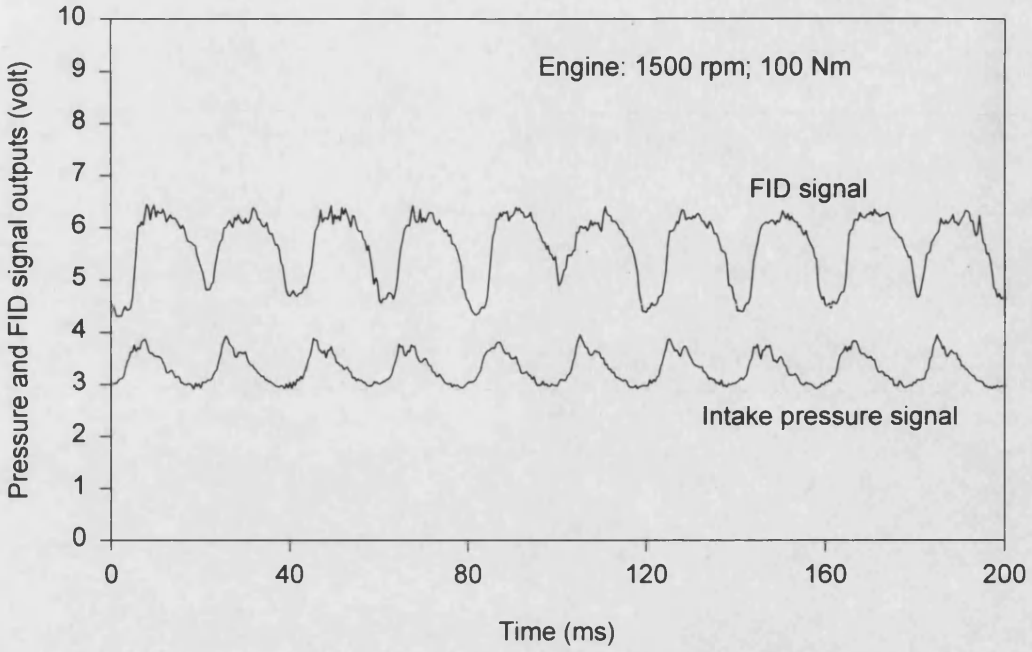

Figure 6.9 Transient measurement of the mixture concentration in the intake system

7. CFD aided gas-air mixer design

7.1 Introduction

With the aid of an extensive experimental and computational study, a prototype natural gas engine gas-air mixer was designed and developed for a 50 kW power output stationary natural gas engine. As described in the previous chapters, CFD simulations have played a very important role in understanding the mixing mechanism of the venturi type mixers and in correlating the mixer performance governing factors with design parameters during the prototype mixer design. However, the CFD technique only acted as a rough guide to the design and development of the mixer due to the awareness of the immaturity of the technique and the difficulty of the simulation of the mixing process. The final design decisions and mixer performance evaluations were actually made based on the engine experimental test results in which the mixer performance characteristics were measured by using the flame ionisation detection technique and other associated techniques. The procedure performed during the prototype mixer design and development can be summarised into the following processes.

- Concept generation; in which different operating principles were firstly considered and then basic configurations and essential dimensions were decided based on the measurement and analysis made on proprietary mixers.
- CFD simulation; in which basic mixer configurations and major dimensions were geometrically modelled. With selected turbulence models and specified boundary conditions related to the engine operating conditions and the properties of the fuel used, flow behaviours including the mixing phenomena between two different species within the mixer flow domain were simulated using a general purpose CFD package. A parametric study was made on the mixer main dimensions and the results were assessed by using two of the important fluid dynamic variables as criteria.
- Detailed design; in which an optimised mixer configuration and a set of dimensions were decided and detailed component drawings were produced. In this process the flexibility of the prototype was considered together with the available materials, the standard seals and the possible machining cost.
- Machining and assembly; in which all the components were machined and assembled.
- Test rig evaluation; in which a particular engine test rig was constructed and various kinds of instruments were facilitated. The prototype mixer was tested on various performance parameters. By comparing the computational and experimental results obtained under identical conditions, the CFD simulations were validated. Some of

the alternatives which were suggested by the simulation results were also tested after they were machined and assembled.

- Modification; in which the first version of the Gem mixer was modified based on the results of both simulations and experiments. At this point a virtual cycle had been achieved for the design and development. The idea of the modification was firstly simulated using the CFD technique. Only those modifications proved by the simulation results were machined, assembled and experimentally evaluated. The application of the CFD technique in the design process reduced the mixer design and development time as well as cost, especially when some of the processes proceeded concurrently.

Mixer bench tests and engine performance tests with the final version of the prototype Gem mixer as well as the three proprietary mixers installed showed that the new Gem mixer exhibited similar or superior performance to the proprietary mixers. Based on the prototype Gem 50 mixer, the manufacturing cost was studied by manufacturing experts who considered the material cost, bought in cost, overheads and direct labour cost (including administration). At an estimated batch size of 200 units per annum, the unit cost was only £27.64 based on typical quotations for complete subcontract manufacturers. Estimation was also made on the same basis for the competing carburettors and the result showed that the Gem had a definite cost advantage over all of its competitors. The potential low manufacturing cost of the new mixer makes the new mixer an attractive marketable product. The feature will certainly enhance its market competitiveness when the Gem is launched on to the market. However, as a new product to squeeze into the market and to survive fierce competition, superiority in functionality and low price are not enough. The desirability of early participation in a growing market is another factor for a late entrant to consider in order to capture a large share of new customers. Certainly the wider the range of applications the product can cover, the bigger the market the product can poach.

The objective of this study was to scale-up the previous prototype design with the aim of widening the product operating range and enlarging its potential market. In order to introduce the new products into fiercely competitive market on time and on budget, a short design and development lead time at low cost with minimum risk is very important. This can only be achieved by using the right tools for the right job with the right method. During the prototype mixer design, CFD simulations were used as an analysis tool to obtain an insight into the flow domain and to get a better understanding on the mixer parametric influences. With the experiences acquired through the package validation and through actual mixing problem analysis, the CFD technique was resorted to as a main design tool in this study to reduce the lead times and costs of the design and development spending on the paperwork, machining, test rig and instruments. With the

aid of the CFD technique the detail engineering drawings, the components machining and assembling, and the engine test rig evaluation processes were replaced by flow domain sketches, geometrical models creation and computational execution. Through this efficient track, the mixer scaling-up design cost was significantly reduced. The study of the CFD aided gas-air mixer design will be described in the following sections.

7.2 Requirements of the new mixer

Before undertaking any design activity, a comprehensive product specification needed to be well defined. To effect a right first time result, a market oriented design target based upon competition analysis, literature searching, patent extracting and technology status review was made. With the philosophy of customer focus and the awareness of existing features and market positions of the competitors products, a market study was carried out by a group of final year research students to determine the actual market size and potential share of gas-air mixers. As environmental issues are becoming more and more important and government incentives are favouring clean fuels, natural gas engines have a growing domestic and world-wide market. In the United Kingdom, the result of their market research showed that 150 kW power output stationary gas engines appeared to have a big demand in addition to the one having 50 kW power output. Even though the market had already been penetrated by the I-mixer and the D-mixer, this power output range should be covered by Gem in order to poach a big slice of market from these two main suppliers. Therefore a scaling-up design was conducted for the 150 kW power output natural gas engine first. The parameters would then be scaled up further to suit higher power output requirements when the first scaling up design had been shown to be successful. As a development design or evolutionary design, where a similar design had already existed, much of the original design content was retained while providing substantial improvements in areas such as flow rate capability, size and some aspects of the pitfalls illustrated during the mixer performance tests and engine tests.

Concerning the working environment of the mixer, normal room temperature, atmospheric pressure and humidity range was assumed for the air. But for the fuel, natural gas, its main pressure changes had to be considered. Both the air and fuel have a corrosive feature which requires a corrosion resistant material for the mixer. Maintenance-free operation of the mixer was desirable throughout its service life which must overlast the engine and withstand continuous and/or intermittent use due to its low wear feature. Under all operation conditions of the engine, the mixer should operate reliably at its best performance characteristics. There was no definite restrictions on size and weight of the product. But the upstream end of the mixer should be compatible with

hoses which connect the mixer to an air filter and the downstream end should be in concordance with the size of its matched throttle valve. When necessary, a special flange at each end is allowed provided that they do not change the performance and increase the cost very much. Due to the fact that the mixer weight is directly linked to the cost of the final product, a lighter weight was desired.

To make the product competitive and avoid legal problems, the proposed product must not clash with any existing patented products. Where applicable, current International and/or British Standards should be used. The target product cost should be much less than the market prices of competitor's products in order to gain a wider profitable margin under fierce competition. Concerning the cost of the product, the manufacturing facilities required were based on conventional machines.

In the process of the design, all the requirements were considered. To evaluate each of the design concepts, three characteristics were used as main evaluation criteria during the concept screening procedure. They were the mixture homogeneity, pressure loss and manufacturing cost.

7.3 Conceptual design and CFD evaluations

At this stage, the first activity was to generate alternative design concepts to comply with the requirements of the product discussed above. To get the essential concept right first time, previous experience was very important. The prototype mixer for 50 kW engine output was a venturi type and so was the D-mixer, because of the favourable characteristics of the venturi in gas signal production and flow restriction. While the project was proceeding, the I-mixer had been modified by its original manufacturer. The modified I-mixer was still a variable geometry type, but its gas signal was produced by using the venturi principle. Therefore the basic operating principle of the mixer of concern ought to be the venturi principle.

7.3.1 Comparison of different gas admission arrangements

Using the venturi principle, the air inlet configuration would be fixed. A systematic search for possible design concepts generated several gas admission arrangements in response to the product requirements. Each of the concepts featured its own advantages and disadvantages. Careful evaluation and screening of these concepts needed to be performed in order to obtain an optimum design and satisfy the target specifications.

7.3.1.1 Comparison between slit and multihole design concepts

During the Gem 50 design and development, the concept of a single inner gas admission slit was firstly considered to draw the gas into the mixer for reasons of simplicity and potentially low manufacturing cost. It was then found that the single gas admission slit design could not produce a satisfactory mixture homogeneity. The prediction given by the CFD modelling showed that two gas admission slits could produce a more homogeneous mixture and this was verified by later experimental results.

Instead of the gas admission slit, there is another way to draw the gas into the mixer, which is through a number of small holes, as that used in the D-mixer. To find out which of the two methods gives a more homogeneous mixture at lower flow restriction and lower potential manufacturing cost, the two methods were computationally compared. When the multiholes were used, 3D geometrical models had to be created instead of a single layer 2D models in order to describe the physical problem correctly, especially when some of the holes were located in the side wall or cross bridge, as it was with the D-mixer. To reduce the computing time, only a quadrant of the cylindrical mixer was simulated owing to the geometrical symmetry. For the venturi air flow domain, a base geometrical model was firstly created, see Figure 7.1, which had a total number of 25500 cells. The reason for this high mesh density was that some of the key parameters of interest such as concentration distribution were affected by the mesh density. For an acceptable computational cost, the higher the mesh density, the higher the computational resolution which could be expected.

With the same base geometrical model, different gas admission boundaries were then defined. Natural gas was firstly drawn into the mixer through two slits located in both the inner and outer walls, see Figure 7.2(a), which was the method retained directly from the Gem 50 mixer. Both slits here had a width of 1 mm. Then another case study was conducted where the gas was admitted into the mixer through 14 small holes located in both the outer and inner walls of the quadrant while keeping all of the boundary settings identical to those used in the slits arrangement simulation, see Figure 7.2(b). This was inspired by the gas admission method used in the D-mixer. Next, another model was created in which natural gas was not only admitted into the mixer through the 14 holes located in the inner and outer walls, but also through 4 additional holes located in each of the two side walls. All the holes were positioned at the same section which was upstream of the mixing chamber, see Figure 7.2(c). The model was to show the effect of the quadrant division on the mixture formation. After this, different positions of the holes along the mixing chamber or the throat part of the mixer were simulated in order to see their effect on the mixture formation, see Figure 7.2(d) and (e).

Table 7.1 Key parameters of the mixer with different gas admission methods

Parameters	Natural gas admission method					
	Base	A	B	C	D	E
Av. static pressure loss (N/m^2)	715	1210	1589	1716	1287	1748
Max. velocity in x direction (m/s)	75.02	79.76	80.92	79.72	78.7	79.26
Max. velocity in y direction (m/s)	25.07	29.16	36.4	30.6	30.64	30.6
Max. velocity in z direction (m/s)	19.99	19.89	20.98	20.43	19.61	20.79
Max. turb. kinetic energy (m^2/s^2)	224.8	230.8	247.8	300.7	300.7	300.7
Max. dissipation rate (m^2/s^3)	7.964 E+5	3.968 E+6	3.8 E+6	4.285 E+6	4.285 E+6	4.285 E+6

The computational results of some key parameters for different gas admission methods under the same simulation conditions are listed in Table 7.1. To make the evaluation of the mixture distribution easier, the mixture concentration on the central layer of the mixer outlet plane are plotted in Figure 7.3. Clearly the mixture homogeneity was not very satisfactory because of the small inlet to throat area ratio and the long cross distance that the gas streams need to penetrate. But the comparison between the different gas admission methods are valid and the results showed that the multihole arrangement produced a slightly more homogeneous mixture than that produced by the double-slit design but with an increased pressure loss. This was because the small locally distributed air streams and gas streams could be easily broken through by the gas plumes. which increased the contact area between the air and gas downstream of the mixer. The curved characteristics of the concentration trajectory further enhanced the mixing, see Figure 7.4. It is believed that a more homogeneous mixture can be produced from a carefully arranged multihole gas admission design with a similar flow restriction. The potential manufacturing cost may, however, be increased. Thus the three conflicting variables, the mixture homogeneity, the flow restriction and the manufacturing cost have to be weighed carefully by taking the associated factors into account in order to make an appropriate compromise. It is interesting to notice that the mixture prepared was different when the admission holes were moved upstream or downstream of the mixing chamber. In the model (d), the outer and inner row of holes were located downstream of the chamber. The mixing feature in the mixer was worse than that in the mixers represented by models (c) and (e), but the pressure loss across the mixer was lower. The reason for this is believed to be that in the mixer represented by

model (d), soon after the gas stream was admitted into the mixing chamber at its downstream part it flowed quickly out of the chamber. There was little time for the air and gas to mix with each other in this area. Once the gas stream ran into the divergent part of the mixer, it was difficult for the gas to fully mix with the main air stream. But this kind of hole location was more favourable to pressure recovery. It can therefore be concluded that a certain length of the mixing chamber is necessary to obtain a homogeneous mixture.

7.3.1.2 Comparison between different gas admission passage angles

In the previous five models, the gas was admitted into the mixer in a direction perpendicular to the cylindrical mixer axis which was the direction of the main air flow stream. The research work on blade film cooling in the turbine industry showed that the hole or the slit angle toward the main flow stream had a profound effect on the secondary flow stream penetration. Similar kind of research had also been conducted on fuel injection in diesel and petrol engines. Their conclusions indicate that different gas induction angles may result in different penetration lengths and trajectories of the gas stream. The mixture distribution and the flow restriction will then be quite different for different passage angles. To verify this, simulation models were created as in Figures 7.5 and 7.6, and computations were carried out using these models. To save the cost of the comparative study, 2-D models instead of 3-D were created with a total number of 3554 cells. An acceptable computation time of about 16 hours was achieved for the boundary setting combination used. This can be further shortened by proper setting of the initial conditions. For the air flow rate and gas flow rate simulated, the inlet boundary settings were used for both air and gas boundary specifications. The settings for the models were identical. The pressure and concentration distributions at the mixer outlet plane are give in Figures 7.7 and 7.8. The results showed that the gas admission passage angle influenced the mixture preparation. The vertical design resulted in a deeper gas penetration into the main air stream and a better mixture homogeneity, but with a higher flow restriction. Because the flow restriction was the most important aspect of the mixer characteristics, the downwards inclined gas admission passage with a angle of about 45 degrees was a more favourable design, which was an appropriate compromise between the two mixer performance characteristics.

7.3.2 Comparison of different venturi tube numbers

A mixer designed for a higher power output engine will apparently have a bigger venturi diameter in order to provide an adequate amount of air and gas flow. To increase the interacting surface area between the two mixing species and to reduce the distance which the gas stream has to penetrate to produce a homogeneous mixture, the double

venturi principle was used in the studies carried out above. The double venturi configuration design is likely to increase the difficulty of the mixer manufacture and lead to a higher price. This will be a disadvantage in market competition unless the mixture prepared is better than that out of the single venturi mixer with a similar flow restriction.

To compare the two design concepts, the criterion of having similar pressure loss between the different designs was used. Thus another geometrical model which has a similar area ratio of the air inlet to throat was created, see Figures 7.9 to 7.11 and simulations were pursued using these models for the single venturi tube mixer. The results for these three different gas inlet arrangements are given in Figures 7.12 and 7.13 on the pressure losses across the mixers and the mixture concentrations at the outlet plane of the mixers. Of the three arrangements, the upward 45 degree inclined passage angle gave the most homogeneous mixture and the highest pressure loss across the mixer. The downward 45 degree inclined one gave the lowest pressure loss but the worst mixture homogeneity of the three. The same conclusion was drawn for the double venturi design with different gas admission passage angles.

To compare the effect of different venturi numbers on the mixture formation and flow restriction, the results discussed above are re-produced, see Figures 7.14 and 7.15. These graphs showed that the double venturi design produced a more homogeneous mixture than that produced by the single venturi mixer. It is interesting to notice that the pressure loss or flow restriction is more sensitive to the gas admission passage arrangement for the single venturi design. For the single venturi design the gas was drawn into the mixer through two admission slits while it was three for the double venturi design. The interacting surface area between the gas and air streams for the single venturi design was less than that for the double. Thus the pressure loss across the mixer was higher for the double venturi design. The single venturi inclined gas admission passage design resulted in a very low flow restriction. It can be concluded that the double venturi design is superior to the single venturi in term of the mixture homogeneity under conditions of similar flow restriction.

7.3.3 Comparison of different inner surface curvatures

There are many conflicting parameters which play very important roles on the mixer performance. Investigations have been made so far on the role played by the inner bullet diameter, gas admission method and its arrangement. There is another one, the flow domain profile, which should have an effect on the flow restriction and on the mixture homogeneity. Between the two evaluating parameters, flow restriction and mixture homogeneity, the former one is more important because the low inertia gas can be

further mixed with the air during the path of the flow through the throttle valve, the intake manifold, the inlet port, the inlet valve and finally the cylinder. There is plenty of time for the gas and air streams to mix before the ignition started.

There are different means to reduce the flow restriction. One is to reduce inner surface roughness of the solid wall and velocity gradient between the wall and the fluid in the vicinity in order to reduce the Newtonian shear stress. But this will result in a poor mixture homogeneity. Another one is to reduce the interacting surface area between the solid wall and the flow stream, especially the area before the gas is admitted into the flow domain. This will not cause the mixture homogeneity to deteriorate while reducing the flow restriction effectively. Of course a smooth flow field will contribute a great deal to the flow restriction reduction.

To find out the effect of the surface curvature on flow restriction, three geometrical models were created with each having a different interacting surface area, as shown in Figures 7.16 to 7.18. To eliminate the influence of the gas blocking effect on the assessment, gas was not introduced into the mixer. This made the comparison much easier. The simulations were made with these three models under the identical boundary condition settings. The results given in Figure 7.19 showed that the one having a minimum interacting surface area produced the lowest pressure loss and the one having a maximum interact surface area produced the highest pressure loss. Apart from the minimum surface area, the results were also attributed to the smooth flow field and the area where higher velocities interacted with the surface. Because of the smooth flow area change in the convergent and divergent section, the velocity in the area of the throat was lower for the minimum surface area curvature while the pressure depression or gas signal was the same as that of the other two. The simulations on different outer wall interacting surface areas were made for the double venturi design as well and the same conclusions drawn.

The minimum area curvature modelled above was the minimum one of the three. In order to achieve the smallest intersurface area of all the possible options, a mathematical tool was resorted to and the proof is as follows.

The gas air mixer inlet and outlet will inevitably be of circular geometry and the mixer should be symmetrical about the rotation axis. Thus the surface must be symmetrical about the axis and is bounded by two rings perpendicular to the axis, see Figure 7.20. Considering an element of the length of the surface ds in the x-y plane, the area of surface contained between the two planes perpendicular to the axis at x and $x+dx$ is

$$dA = 2\pi y ds \tag{7.1}$$

The element length ds in Cartesian co-ordinates can be expressed as:

$$ds = \left[(dx)^2 + (dy)^2\right]^{\frac{1}{2}} = \left[1 + \left(\frac{dy}{dx}\right)^2\right]^{\frac{1}{2}} dx \qquad (7.2)$$

assuming that the y(x) is a continuous function of the independent variable x and satisfies the boundary conditions of the joining fixed points (x_1, y_1) and (x_2, y_2) where the mixer inlet and outlet circles are located. Therefore

$$dA = 2\pi y\left(1 + y_x^{\,2}\right)^{\frac{1}{2}} dx \quad \text{where } y_x = \frac{dy}{dx} \qquad (7.3)$$

The total area of the surface is

$$A = \int_{x_1}^{x_2} 2\pi y\left(1 + y_x^{\,2}\right)^{\frac{1}{2}} dx = \int_{x_1}^{x_2} f(x, y, y_x) dx \qquad (7.4)$$

where the $f(x, y(x), y_x(x))$ is assumed to be a real valued continuous function in its closure set $x_1 \le x \le x_2; y(x) \ge 0$. The minimum of the functional A=A(y) in the class of all admissible paths (trajectories) y(x) with both end points fixed is a typical Langrangian problem of the calculus of variations. Thus the Euler necessary condition (or Euler's equation) should be resorted which is

$$\frac{d}{dx}\left(\frac{\partial f}{\partial y_x}\right) - \frac{\partial f}{\partial y} = 0 \qquad (7.5)$$

or in another expression

$$\frac{d}{dx}\left(f - y_x \frac{\partial f}{\partial y_x}\right) = 0 \qquad (7.6)$$

When the Euler's equation is satisfied, the function y(x) lying in its constraints with the boundary conditions is the extreme path for all admissible trajectories, i.e. the surface has the minimum surface area.

Integrating Eq. 7.6,

$$f - y_x \frac{\partial f}{\partial y_x} = c, \qquad (7.7)$$

where c is a constant. Substituting for f from Eq. 7.4,

$$y\left(1 + y_x^{\,2}\right)^{\frac{1}{2}} - y_x \frac{\partial}{\partial y_x}\left[y\left(1 + y_x^{\,2}\right)^{\frac{1}{2}}\right] = \frac{c}{2\pi} = c_1 \qquad (7.8)$$

Performing the partial differentiation in Eq. 7.8,

$$\frac{\partial}{\partial y_x}\left[y\left(1 + y_x^{\,2}\right)^{\frac{1}{2}}\right] = \frac{1}{2} y\left(1 + y_x^{\,2}\right)^{-\frac{1}{2}} 2y_x = y\left(1 + y_x^{\,2}\right)^{-\frac{1}{2}} y_x \qquad (7.9)$$

Substituting this to Eq. 7.8,

$$y\left(1+y_x^{\,2}\right)^{\frac{1}{2}} - y_x^{\,2}y\left(1+y_x^{\,2}\right)^{-\frac{1}{2}} = y\left(1+y_x^{\,2}\right)^{\frac{1}{2}}\left[1-y_x^{\,2}\left(1+y_x^{\,2}\right)^{-1}\right] = c_1 \tag{7.10}$$

Simplifying Eq. 7.10,

$$y\left(1+y_x^{\,2}\right)^{-\frac{1}{2}} = c_1 \tag{7.11}$$

This gives

$$\frac{dy}{dx} = \left(\frac{y^2}{c_1^{\,2}} - 1\right)^{\frac{1}{2}} = \left(\frac{y^2 - c_1^{\,2}}{c_1^{\,2}}\right)^{\frac{1}{2}} \tag{7.12}$$

Integrating,

$$y = c_1 \cosh\left(\frac{x - c_2}{c_1}\right) \tag{7.13}$$

where c_2 is the integration constant and is zero for a symmetry surface. The trajectory is a catenary of revolution about the x-axis, or catenoid, bounded by the two rings. The area formed by the catenoid is the minimum surface area of all the possible curvatures bounded by two coaxial rings perpendicular to the axis. Apparently, the mixer of design should follow this minimum surface area principle of having a solid wall inner surface profile of catenoid.

7.4 Detail design of the Gem 150 gas-air mixer

During the intensive computational studies, the concepts generated have been systematically evaluated. Through the CFD evaluation process, a greater understanding of the potential solutions has been achieved. As a complete mechanical engineering product design, a set of instructions for manufacturing should be provided, not just relying on the CFD geometrical models and their simulation results. To engineer these models into a product is of equal importance as is the concepts generation and evaluation, because it is the detailed final design which determines whether the best ideas have been realised and whether the requirements of the product have been complied with. To convert the design concepts into detailed engineering drawings, configuration and dimensions of both flow domain and non-flow domain parts were determined. This process will dictate the manufacturing tools needed, the machining process used and the ultimate cost of the product.

The evaluations discussed above resulted in a clear picture about the new mixer. A fixed double coaxial venturi principle with downwards inclined gas admission slits should be

used for this larger flow capacity mixer. The solid outer body should have an inner surface profile which gives a minimum surface area upstream of the mixing chamber in order to reduce the pressure loss across the mixer. The convergent and divergent part of the mixer should be changed gradually to ensure a smooth flow field within the entire flow domain. The inner body should accommodate a large gas volume flow and have a small outer surface area. The shape of the inner body should have a head which produces a low flow restriction and have a tail which is designed to give a smooth flow and to enhance further mixing between the gas and air streams. The gas should be drawn into the mixer through the slits placed in the outer and inner body separately and holes if necessary in the wings which should have aerofoil cross sections in volume production and function as a locator as well as gas passages to the inner body. To aid the homogeneous mixture preparation and to ease the manufacturing difficulty, the mixer should be geometrically symmetrical. The length or the height of the mixer should be designed to give a size as small as the mixture homogeneity can tolerate in order to reduce the engine overall dimension. The implementation of the design was based upon these principles. As an initial design the dimensions of the Gem 150 were taken from the Gem 50 mixer based on the comparable gas and air flow rates calculated. The air inlet diameter was decided in such a way that the air velocity at the boundary was lower than that of the Gem 50 mixer in order to produce a lower flow resistance. A dimension of 94 mm in diameter was used. The area ratio of the air inlet to the throat was taken from the Gem 50 mixer first and then was modified based on the simulation results to produce a reasonable gas signal without high throat velocities. The basic calculations are given below for the Gem 150 mixer.

The air inlet area is:

$$\frac{\pi}{4}\times 94^2 = 6936.26 \text{ mm}^2 \qquad (7.14)$$

The throat area is about:

$$\frac{\pi}{4}\times 74^2 - \frac{\pi}{4}\times 60^2 - 16\times 7\times 4 + \frac{\pi}{4}\times 8^2 = 1074.9 \text{ mm}^2 \qquad (7.15)$$

The gas admission area is:

$$\pi\times 60\times 2 + \pi\times 74\times 2 - 16\times 2\times 4\times 2 + \pi\times 8\times 2 = 635.76 \text{ mm}^2 \qquad (7.16)$$

Thus the area ratio of the air inlet to the throat is 6.45 which is larger than 4.34 of the Gem 50 mixer. This bigger area ratio will result in higher velocities in the area of the throat and higher turbulence intensities which will aid the mixing between the air and fuel. The area ratio of the air inlet to the gas inlet is 10.91 which is slightly larger than

9.77 for the Gem 50 mixer. The mixture outlet area is the same as the air inlet and is expected to give a very good pressure recovery.

To cope with the gas admission area in the inner venturi body, the total inner area of the four wings was designed to be:

$$\frac{\pi}{4} \times 12^2 \times 4 = 452.16 \text{ mm}^2 \qquad (7.17)$$

This is greater than the gas admission area in the inner body. The area of the two hoses which connect the main gas supply to the mixer is:

$$\frac{\pi}{4} \times 23^2 \times 2 = 830.53 \text{ mm}^2 \qquad (7.18)$$

which is greater than the total gas admission area of 635.76 mm^2. At this point it was the time to decide the configurations of the detailed inner body of the Gem 150 mixer. In order to design the shape and dimensions of the mixer inner body, simulations were conducted using the models given in Figure 7.21(a)~(d). The simulated average pressure loss across the mixer out of the model A was 2036.24 N/m^2 and the concentration distribution at the outlet plane is given in Figure 7.22. When the mixer axial length was elongated in the section downstream of the mixer, see model B, the flow field within the flow domain was improved and became more uniform than the previous one, which resulted in a lower shear friction and hence a lower pressure loss. The simulated average pressure loss was 2013.6 N/m^2, which is similar to that of the model A. The concentration distribution was improved too because the extra axial length gave an extra distance and time for the two species to mix and for the pressure to further recover. However, the mixture homogeneity was still not satisfactory. To improve the mixture homogeneity prepared, the length of the mixing chamber was increased. The flow diversion, after the gas stream was admitted into the mixer, was constrained. These modifications were embedded in the simulation model C. The results showed that the pressure loss was 2042.16 N/m^2, which is similar to that of the models A and B. The concentration distribution given in Figure 7.22 showed that the mixture was quite homogeneous. But the flow field within the flow domain showed that local configuration modifications were still necessary to get a more uniform flow field and to position the maximum turbulence in the area of the mixing chamber. The simulation using the model D gave a satisfactory result on all parameters of interest. The mixer designed according to this model was the prototype of the Gem 150 natural gas-air mixer for the stationary natural gas engine having a power output 150 kW. The simulation results showed that the new mixer had relatively lower throat velocities and a lower pressure loss across the mixer, see Figure 7.23, while having the same mixture homogeneity.

According to the venturi air inlet and throat dimensions, the curvature of the outer body inner surface was formed using the following catenoid equation in Cartesian co-ordinates:

$$y = 37 \times \cosh(\frac{x-32}{37}) \text{ mm} \qquad (7.19)$$

where $6 \le x \le 59$. The nose of the inner body had an elliptic section which was governed by the following ellipse equation:

$$\frac{(x-32)^2}{18^2} + \frac{(y-17)^2}{13^2} = 1 \qquad (7.20)$$

where $14 \le x \le 32$ and $4 \le y \le 30$ for the upper axis part of the section. The tail of the inner body was composed of two symmetrical arcs whose centres were located at the points (40,45.115384) and (40,-11.115384) respectively and had the same radius of 41.115384, where $40 \le x \le 70$ and $4 \le y \le 30$ for the upper axis part of the section. The whole mixer was an axisymmetrical unit. The scheme assembly drawing of the mixer is given in Figure 7.24.

The computed variation of the mixture concentration distribution at the outlet plane of the mixer was mainly because of the underestimation of the turbulence generation and turbulent species transportation. This was also encountered during the Gem 50 experimental validations and performance tests. In the simulations carried out above, the four gas conduits which acted as bridges for the gas to flow into the inner body were not considered in the models for the sake of the computation cost. The mixture homogeneity will be further improved in the actual mixer with the conduits placed in, especially when gas admission holes are designed into the middle of each conduit. Thus the actual mixture distribution out of the new mixer was expected to be better than that predicted by the CFD simulations.

Materials of which the mixer is to be made was another important issue. To select right materials for the mixer, both the mixer working environment and the manufacturing processes should be considered. Because the mixer is to work at about room temperature within a corrosive environment, non-ferrous materials were preferred. From the basic configuration of the mixer, rigidity of the material should be high enough to remain each of the components in the right location and dimension. Thus amongst those feasible materials, aluminium alloy was the most suitable which also met the product requirements of light weight and low cost. Compared to copper based alloys, aluminium alloys are cheaper and have wide spread availability. Unlike thermoplastics, aluminium alloys do not require special manufacturing equipment. A market analysis resulted in a preliminary estimated annual production volume of 500 set of mixers. Therefore only two manufacturing processes are suitable for such a small quantity of production

requiring complicated curvatures. One is CNC machining and the other is investment casting (lost wax casting). Of course the former is the only viable choice for the prototype machining. Thus wrought aluminium alloy is very suitable.

7.5 Summary

With the replacement of the test rig evaluations by the CFD technique, many comparisons were made on gas admission methods, gas admission passage arrangements, number of venturi barrels and the profiles of the solid wall interacting surface. These simulations dramatically reduced the lead times and the cost of the mixer scaling up design and development. The computed results clearly revealed the comprehensive relationship between these influencing factors. To get the lowest flow restriction which is overwhelmingly important for the high performance gas-air mixer, a double venturi main body and downstream inclined gas admission passage arrangement were used in this scaled up design. To meet the requirements of high mixture homogeneity, multi-slits were used to draw the natural gas into the mixer. Optimisation was made not only on the outer body, but also on the inner body and the total length of the mixer. The simulation results of the final version of the Gem 150 gas-air mixer showed that the Gem 150 mixer had very encouraging characteristics on all of the evaluation respects. The performance of the new mixer is expected to be superior to the prototype of the Gem 50 mixer.

With the guidance of the CFD simulations, the design of the Gem 150 mixer was conducted with confidence. The study showed that the CFD analysis not only predicted the mixture distributions at the outlet plane of the mixer, as well as an experimental approach could achieve, but also provided highly detailed information within the entire mixer flow domain. This wealth of information resulted in a fundamental insight into the mixing behaviour of each of the design options. The active and successful application of the CFD technique to engine component design will certainly contribute to the promotion of this technique and speed up its usage in the engine community.

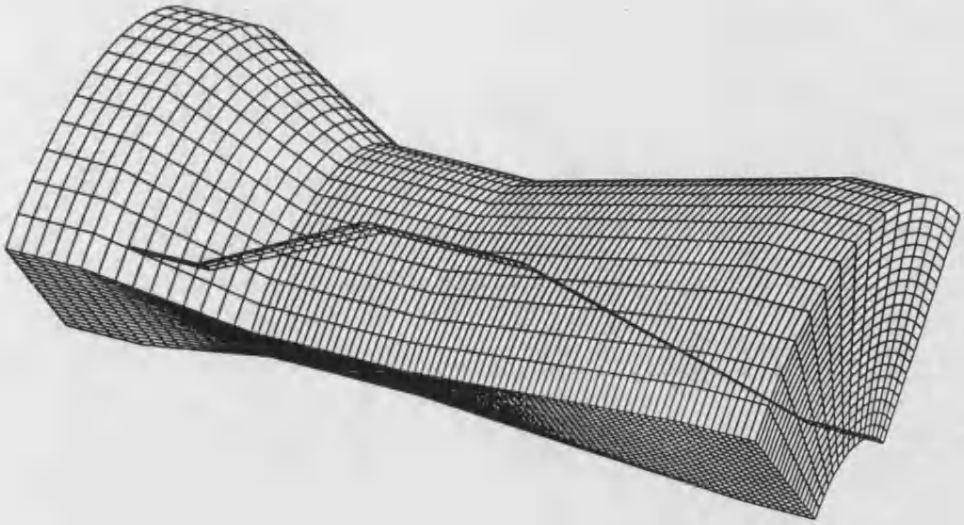

Figure 7.1 Base CFD model for gas admission methods comparison

(a)

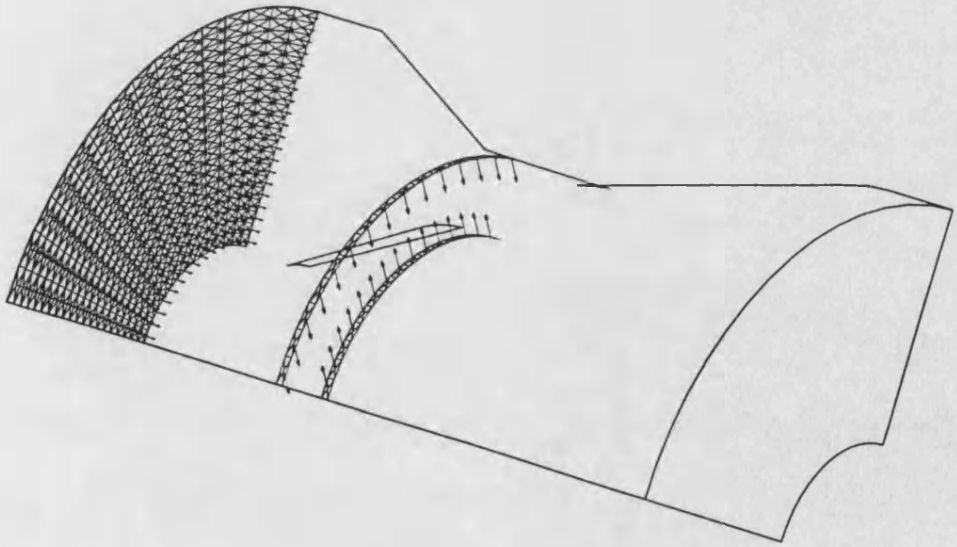

Figure 7.2a CFD model for slits gas admission simulation

(b)

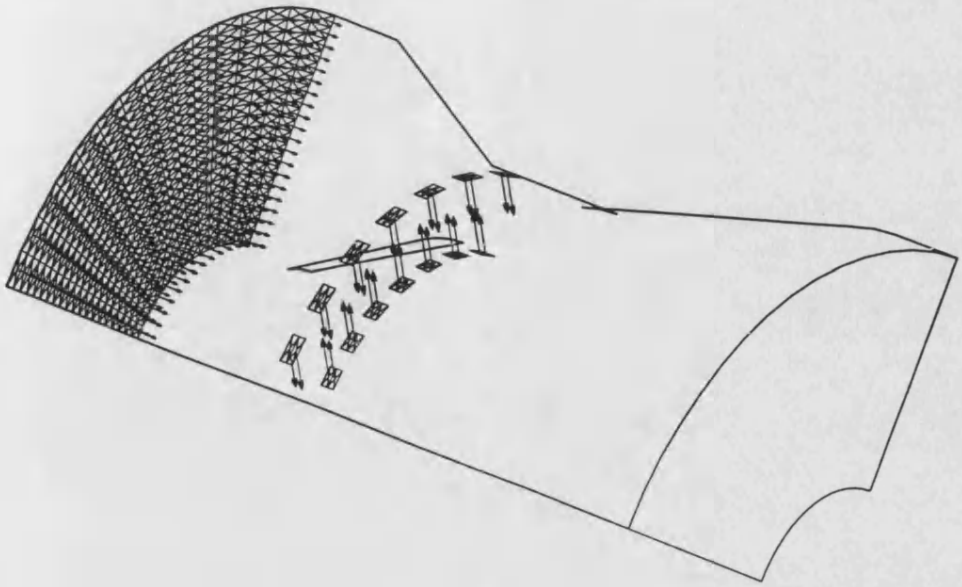

(c)

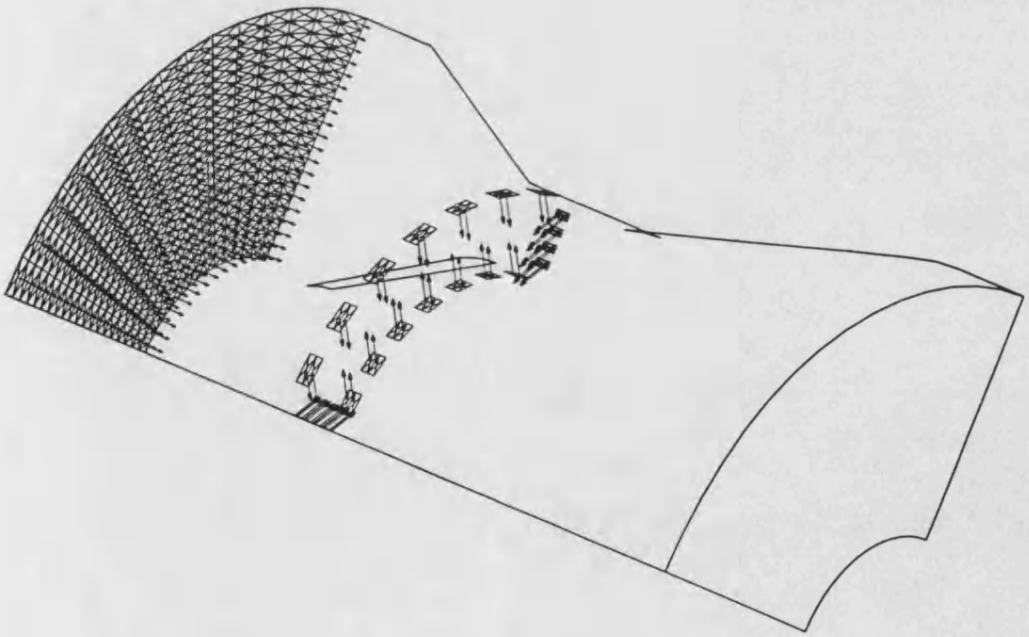

Figure 7.2b&c CFD models for multihole gas admission simulations

(d)

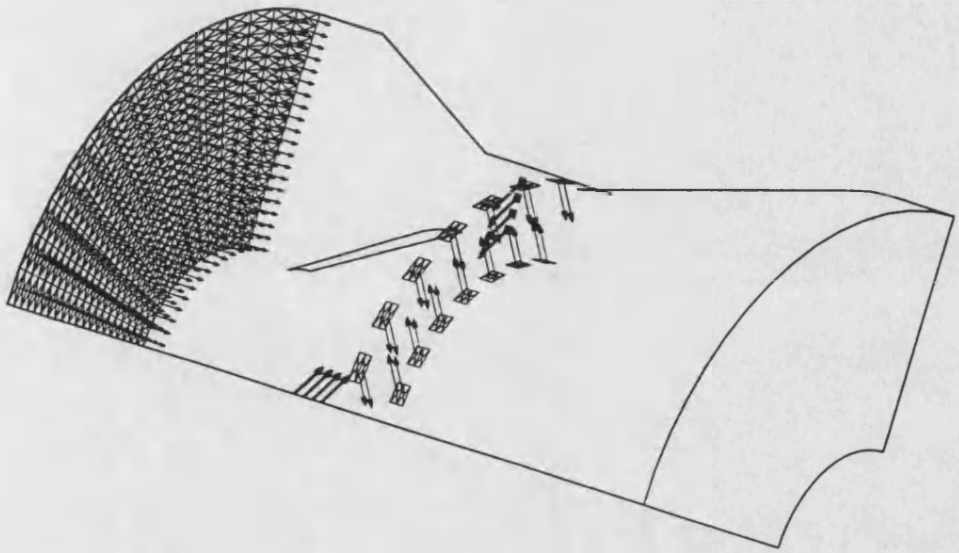

(e)

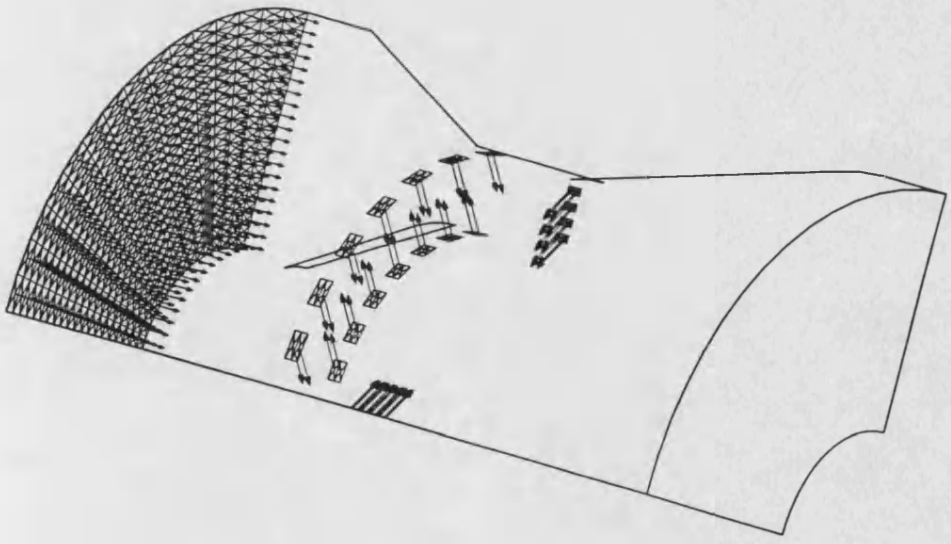

Figure 7.2d&e CFD models for multihole gas admission simulations

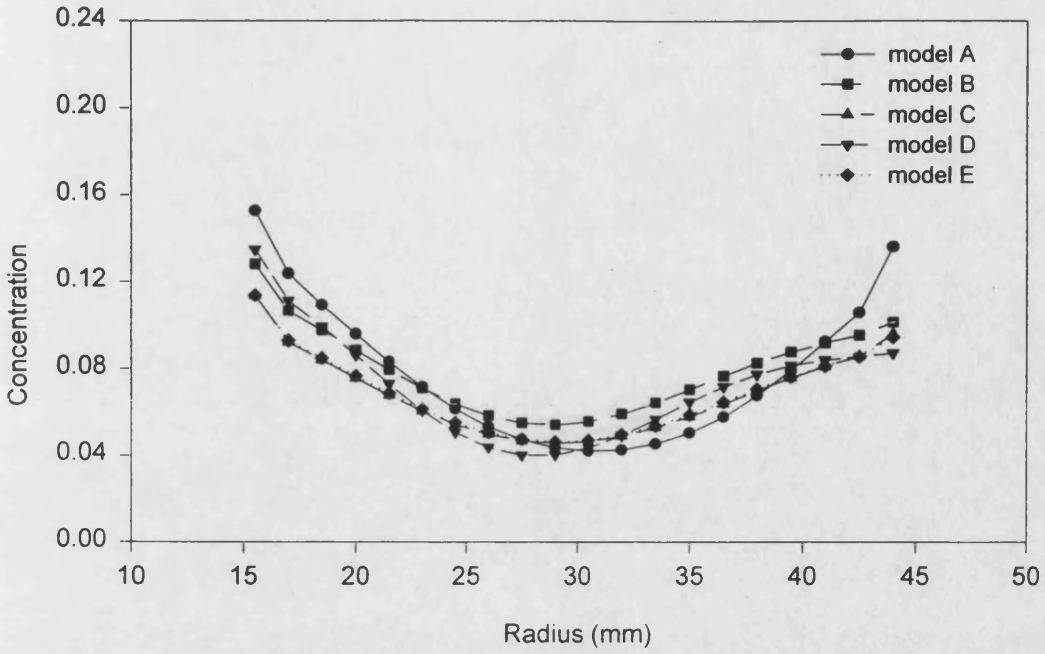

Figure 7.3 Mixture concentration distributions on the center layer of the mixer outlet plane with different gas admission methods

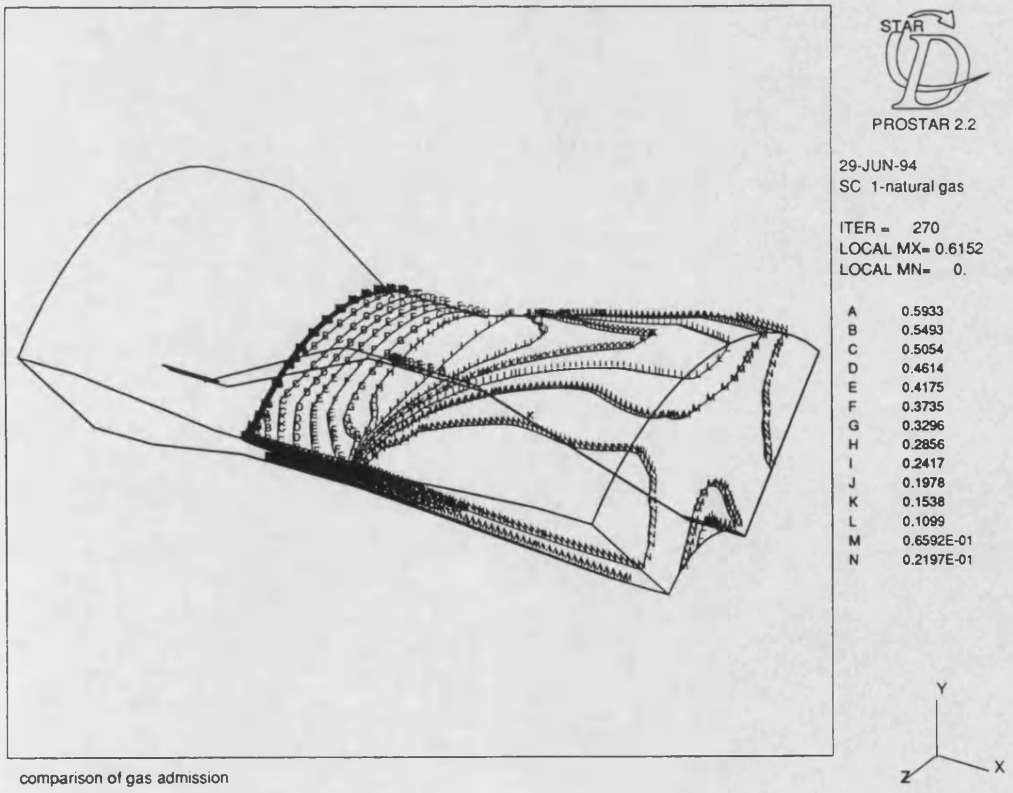

Figure 7.4a Comparison of gas stream trajectory within the flow domain of the mixer with slits gas admission method

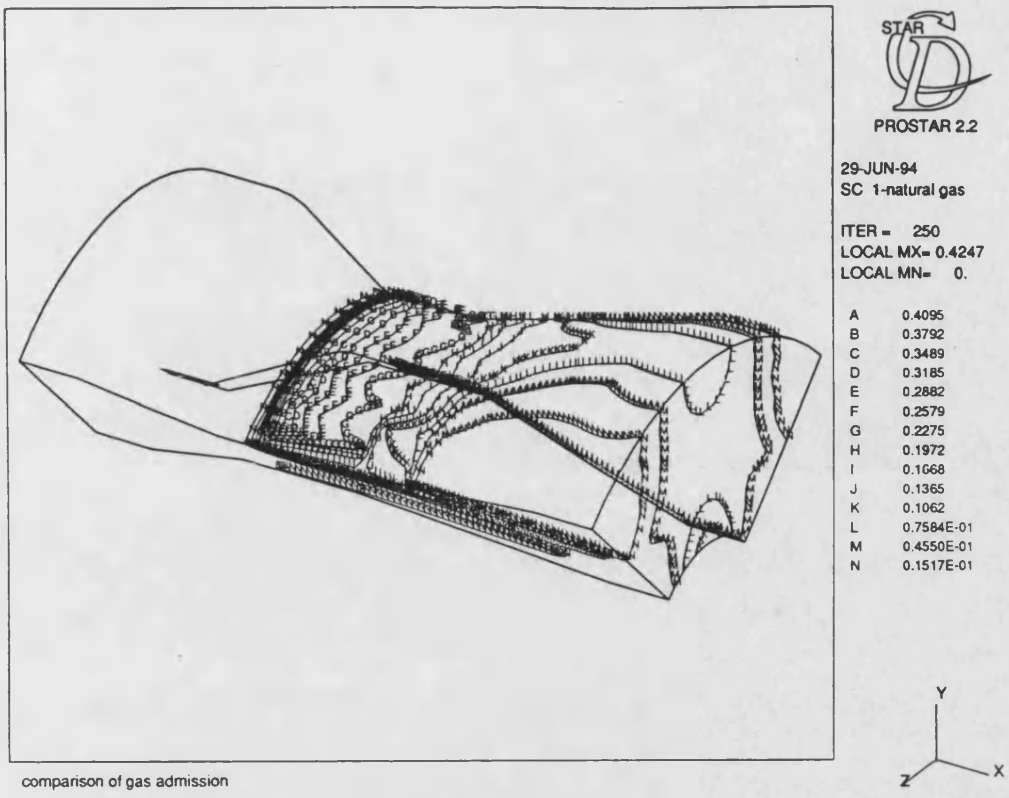

Figure 7.4b Comparison of gas stream trajectory within the flow domain of the mixer with multiholes gas admission method

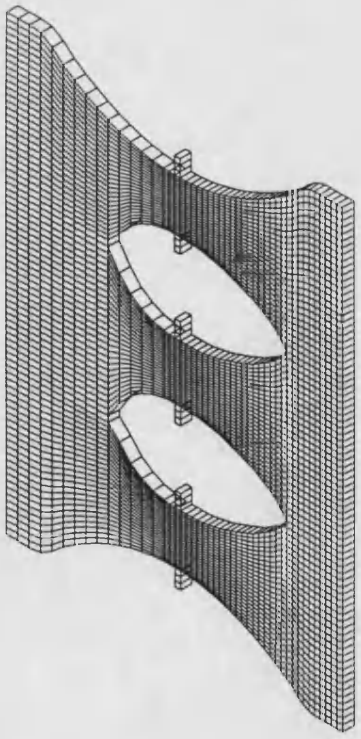

Figure 7.5 CFD model for the mixer with vertical gas admission passage

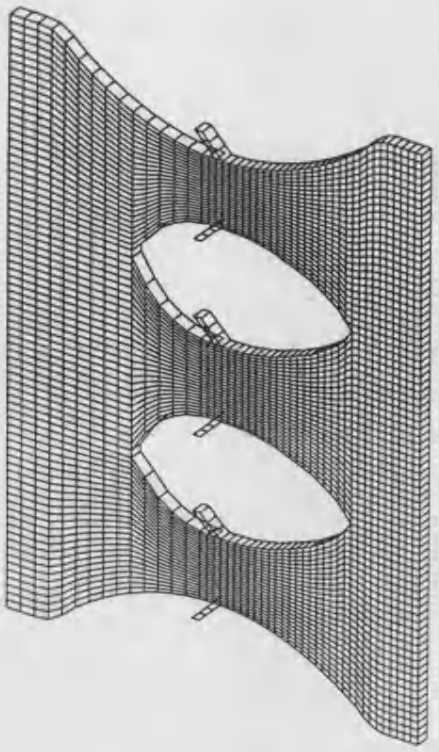

Figure 7.6 CFD model for the mixer with inclined gas admission passage

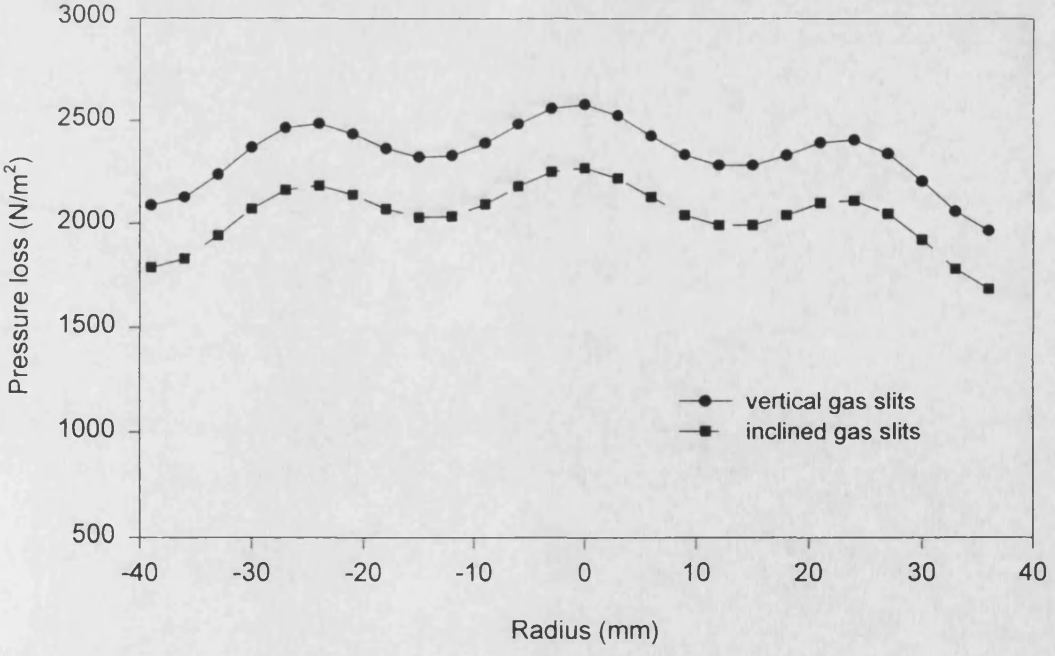

Figure 7.7 Pressure distributions at the outlet plane of the mixer with different gas admission passage angles towards the main air stream

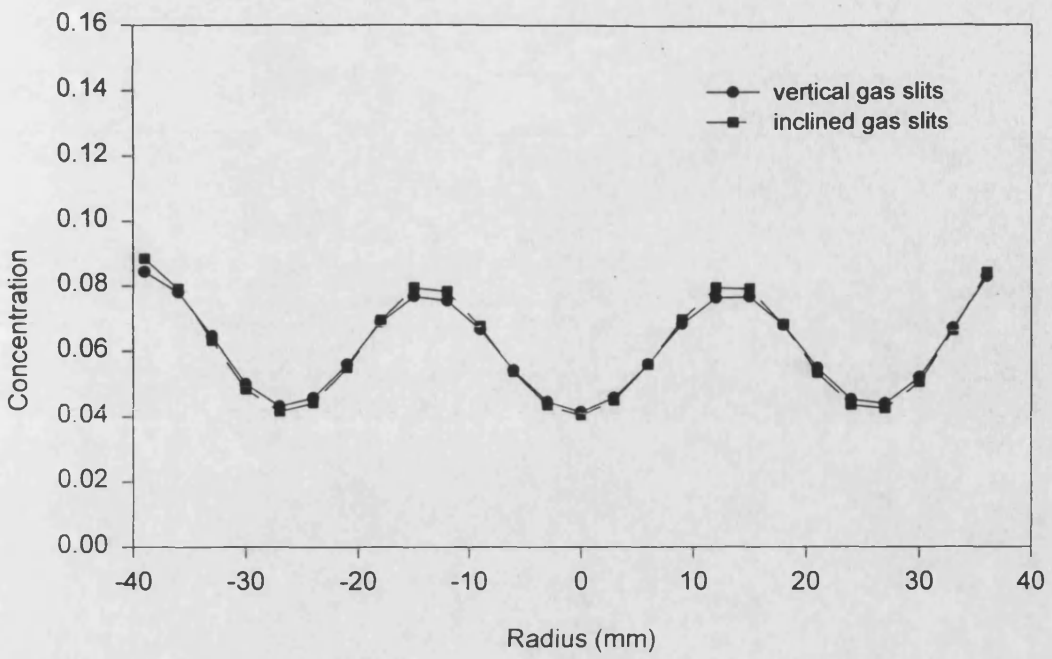

Figure 7.8 Mixture concentration distributions at the outlet plane of the mixer with different gas admission passage angles towards the main air stream

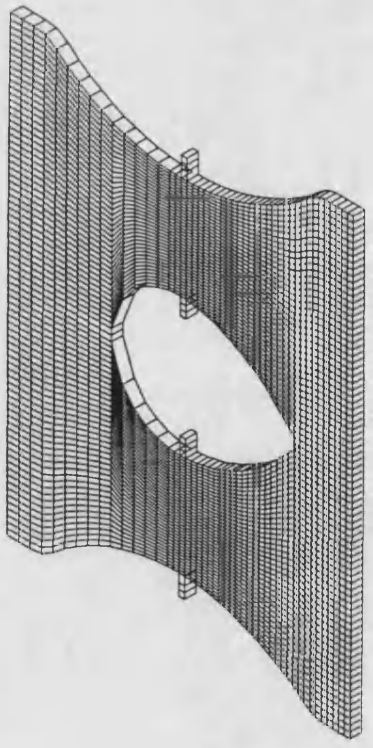

Figure 7.9 CFD model of the single venturi mixer with vertical gas admission passage towards the main air stream

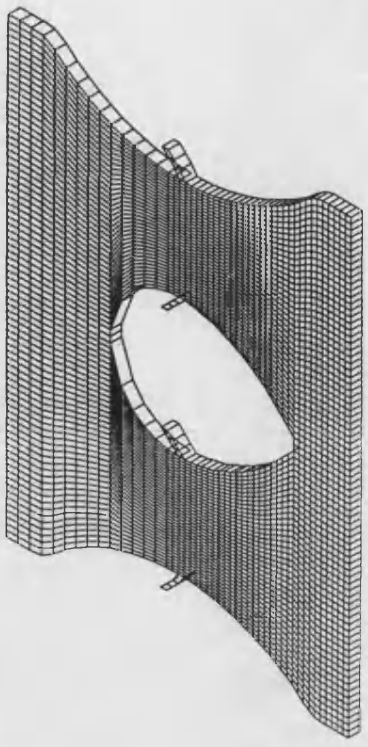

Figure 7.10 CFD model of the single venturi mixer with downwards inclined gas admission passage towards the main air stream

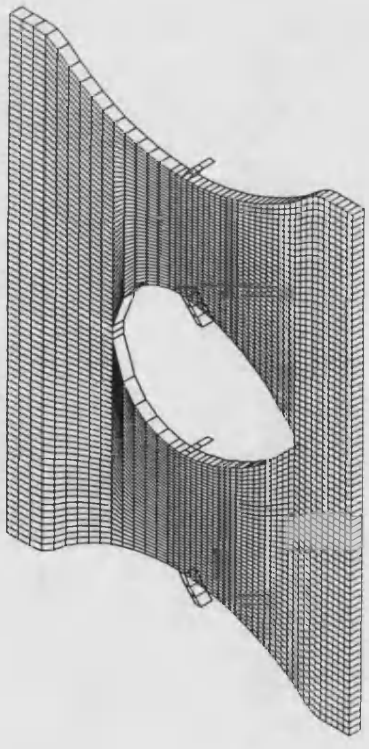

Figure 7.11 CFD model of the single venturi mixer with upwards inclined gas admission passage towards the main air stream

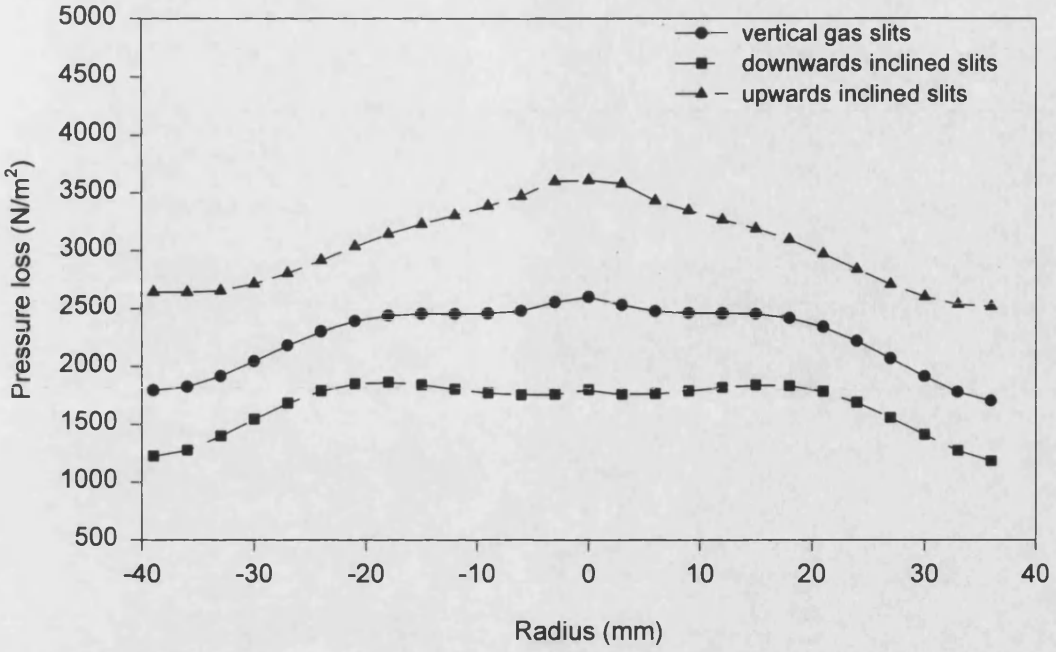

Figure 7.12 Pressure distributions at the outlet plane of the single venturi mixer with different gas admission passage angles towards the air stream

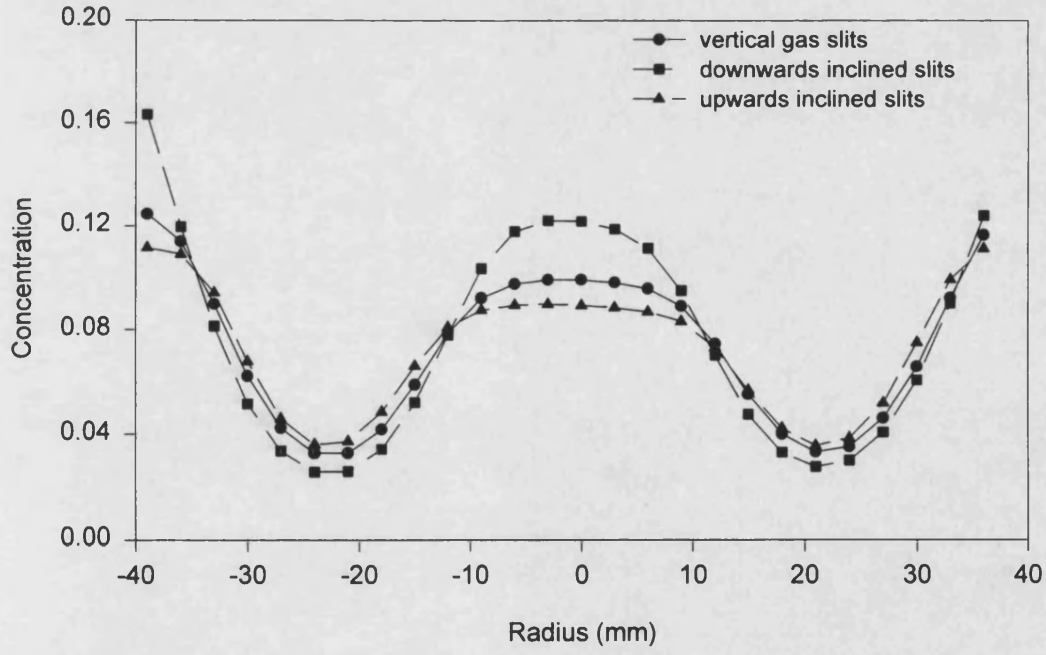

Figure 7.13 Mixture concentration distributions at the outlet plane of the single venturi mixer with different gas admission passage angles

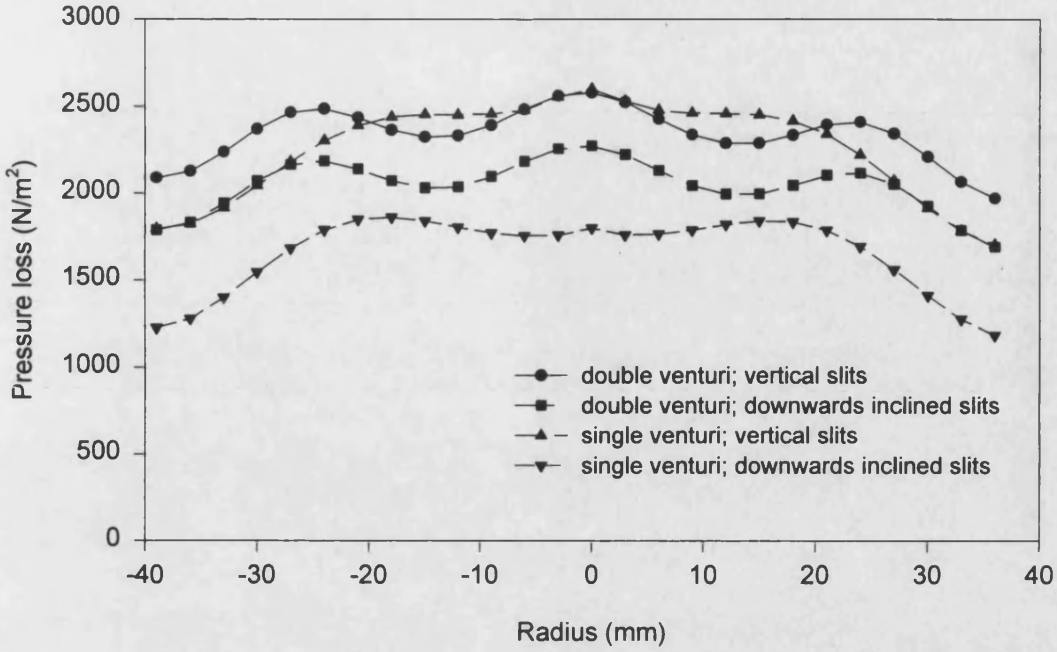

Figure 7.14 Comparison of pressure distributions at the outlet plane of the mixer with different venturi numbers and different gas admission passage angles

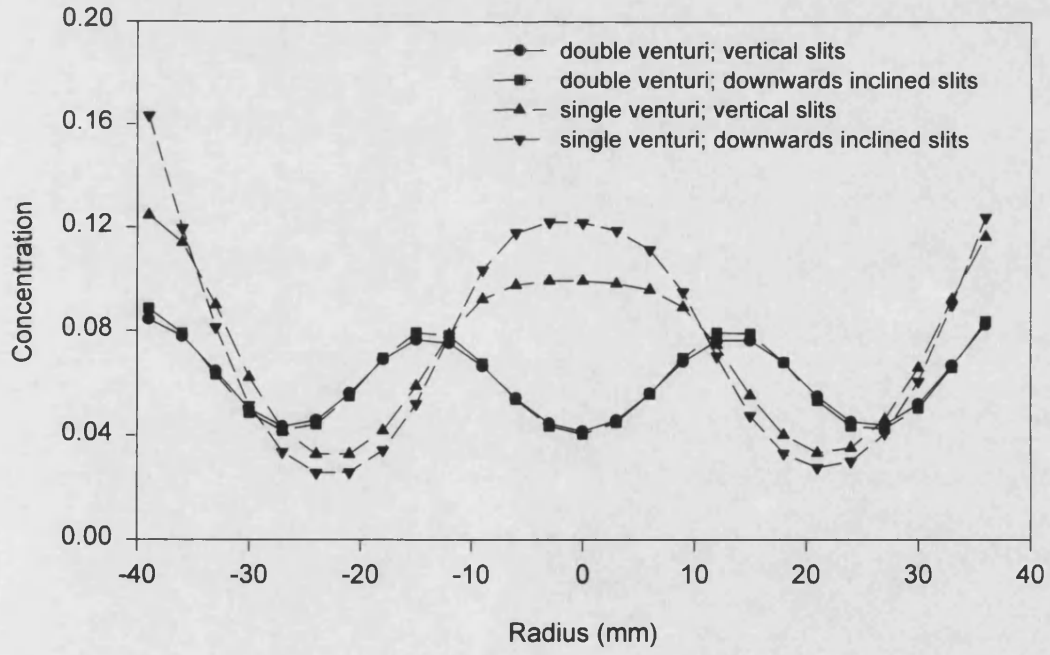

Figure 7.15 Comparison of mixture concentration distributions at the outlet plane of the mixer with different venturi numbers and different gas admission passage angles

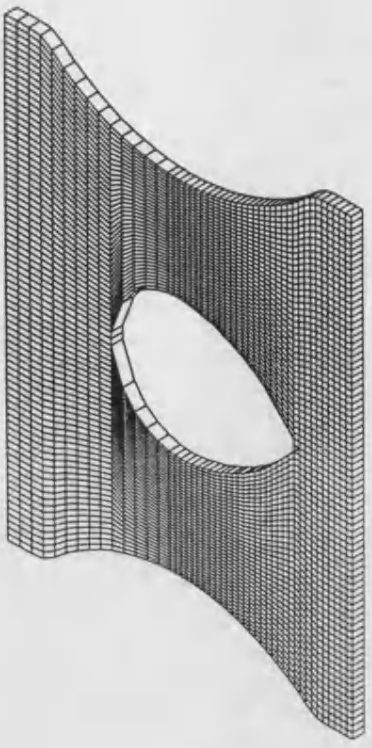

Figure 7.16 CFD model of the single venturi mixer with a minimum outer body interacting surface area

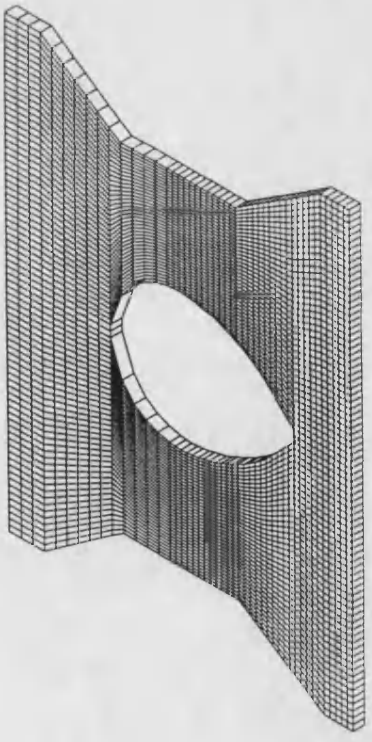

Figure 7.17 CFD model of the single venturi mixer with a intermediate outer body interacting surface area

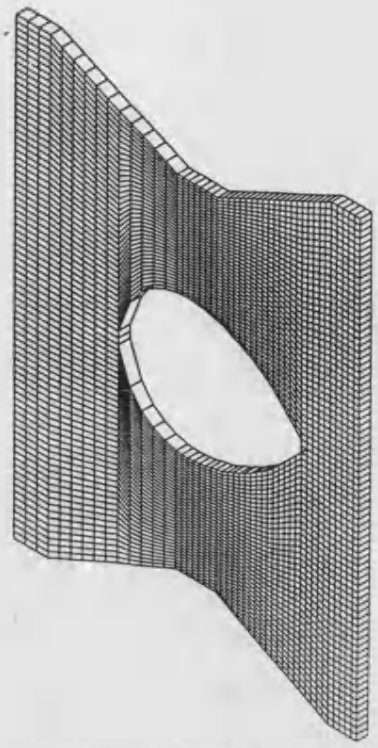

Figure 7.18 CFD model of single venturi mixer with a maximum outer body interacting surface area

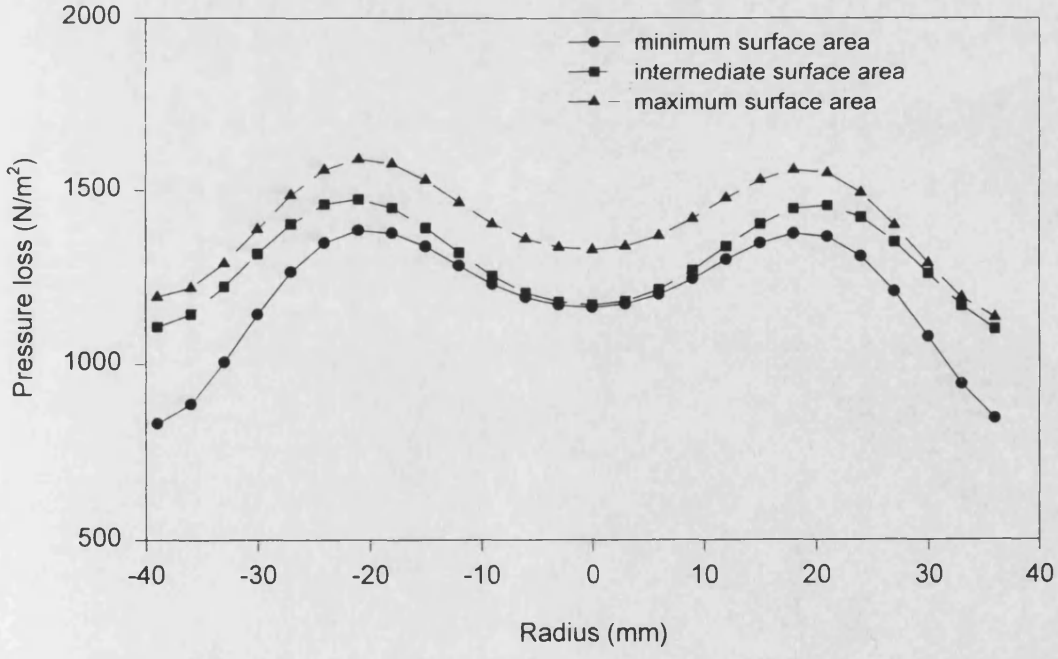

Figure 7.19 Comparison of pressure loss for different outer body surface areas

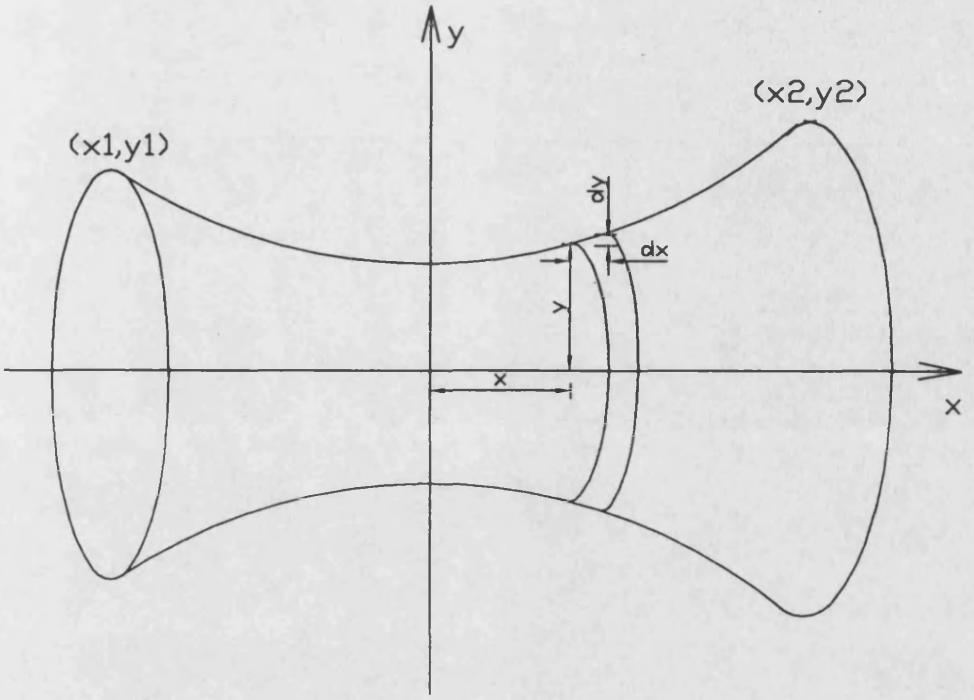

Figure 7.20 Axially symmetrical surface joining two coaxial rings perpendicular to their common axis

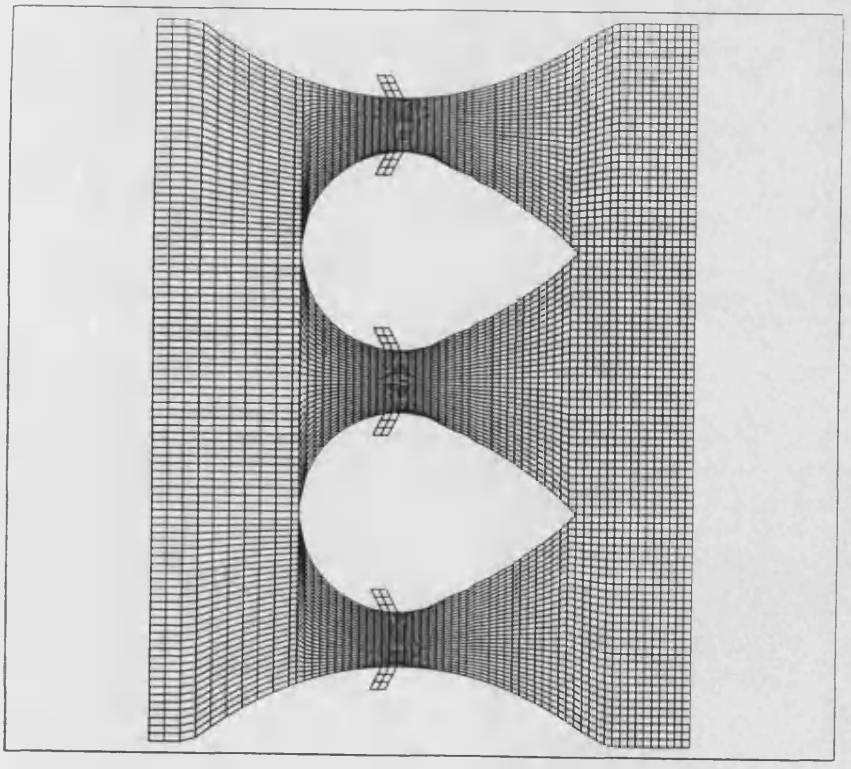

Figure 7.21a CFD model of the Gem 150 mixer

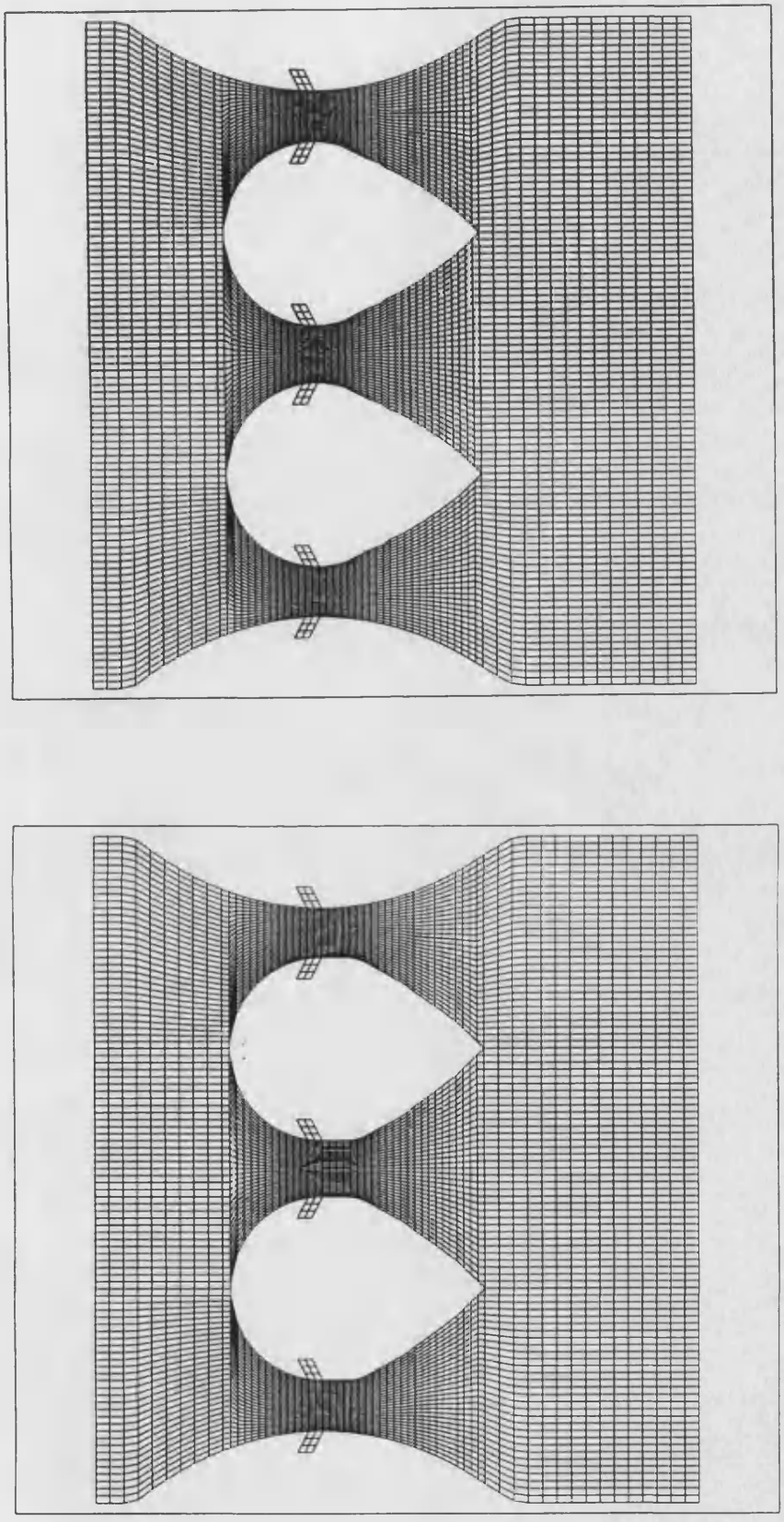

Figure 7.21b&c CFD models of the Gem 150 mixer with different inner body configurations and dimensions

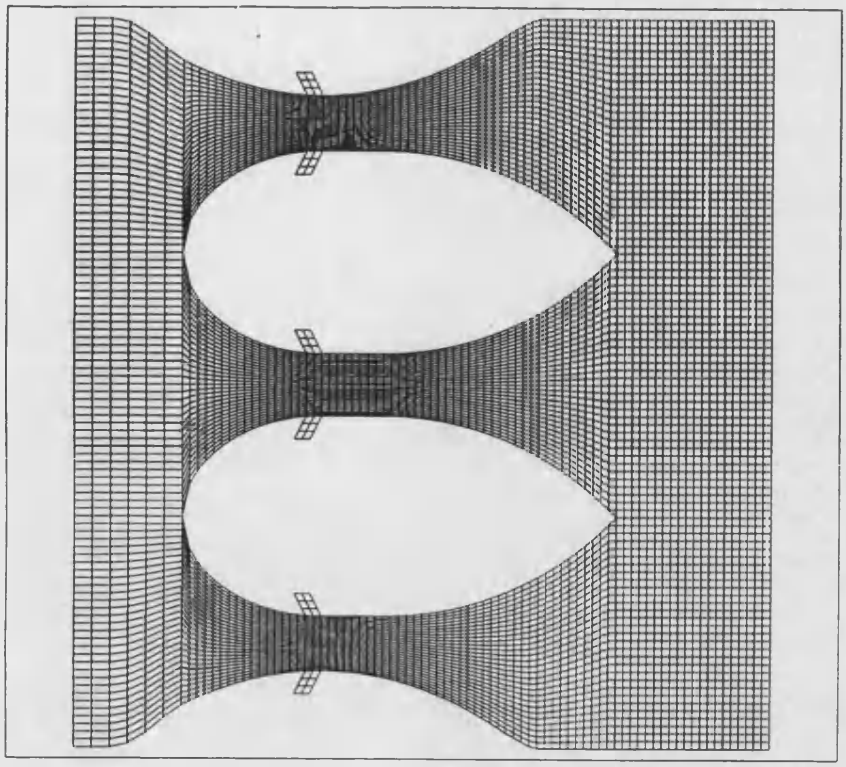

Figure 7.21d CFD model of the Gem 150 mixer

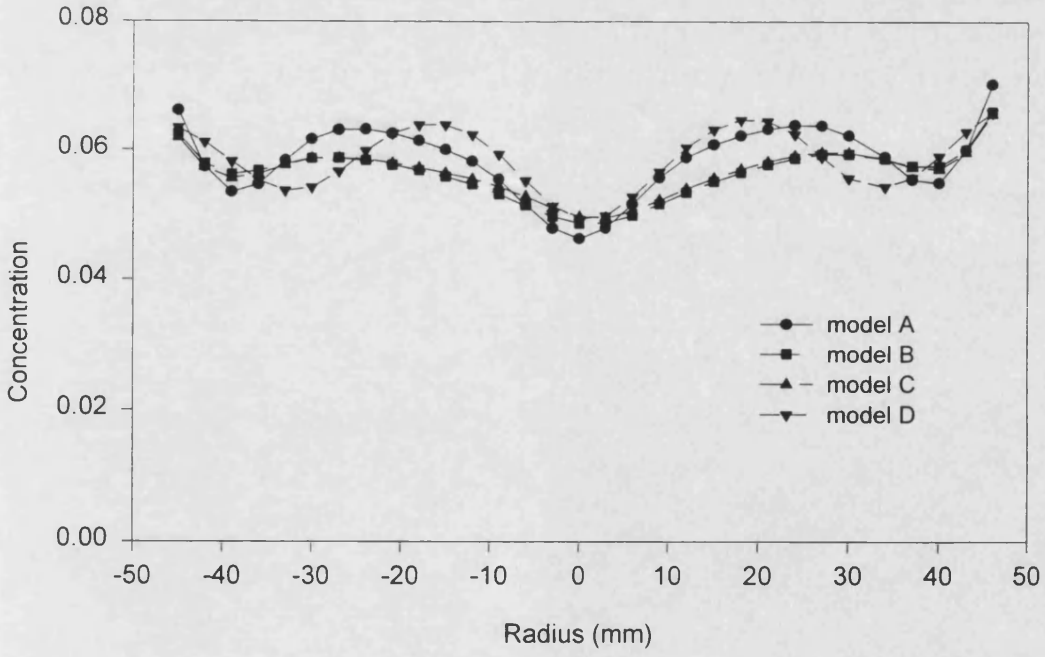

Figure 7.22 Comparison of the mixture concentration distributions of the mixer with different inner body configurations and dimensions

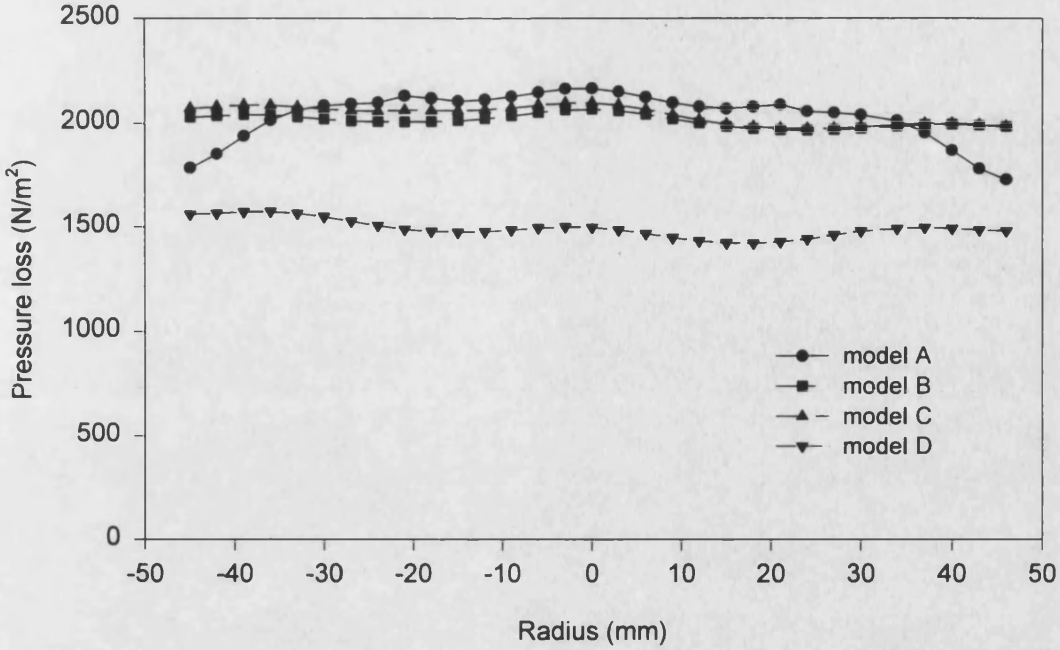

Figure 7.23 Comparison of the pressure losses across the mixer with different inner body configurations and dimensions

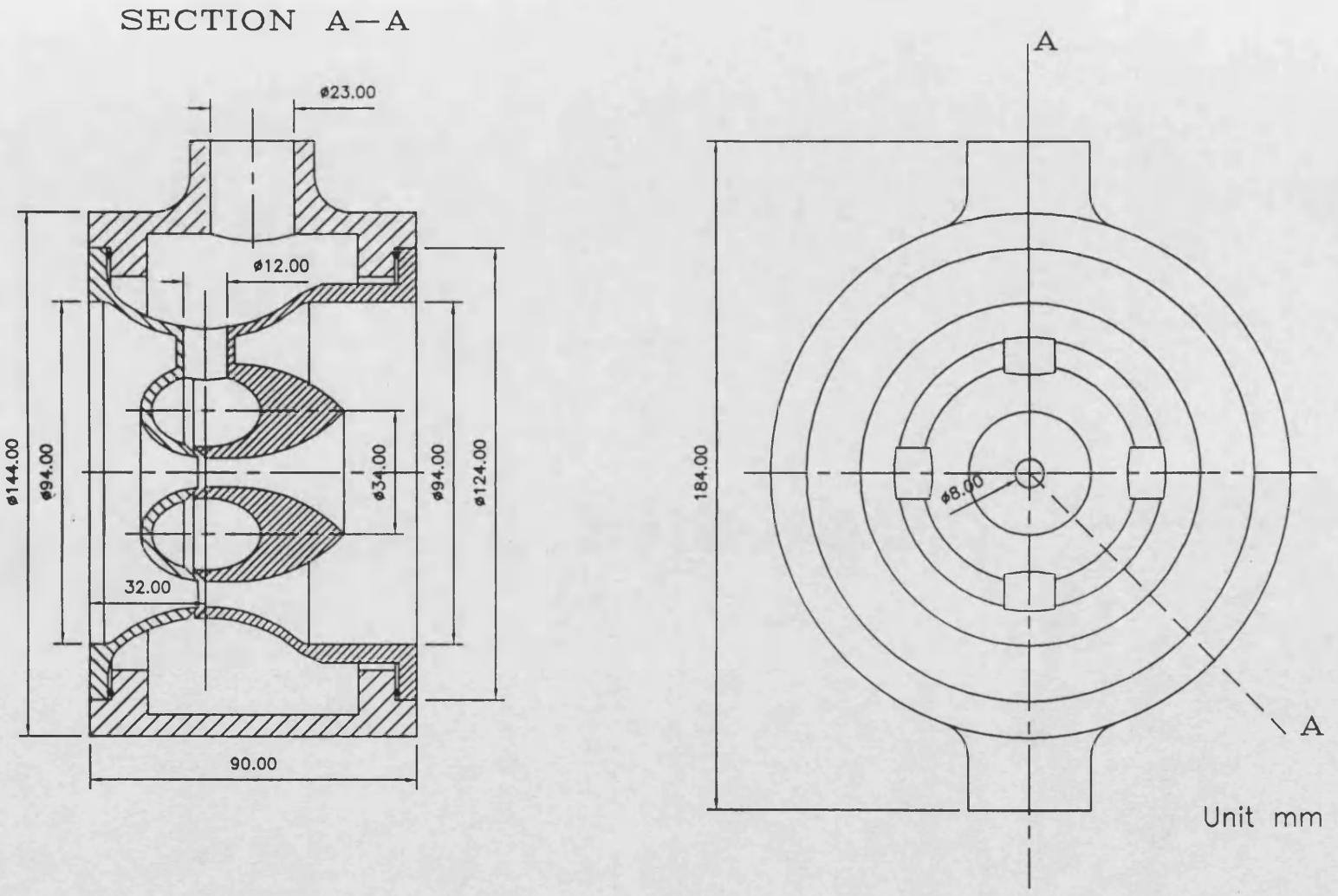

Figure 7.24 Scheme assembly of the Gem 150 gas-air mixer

8. Conclusions and recommendations for future work

8.1 Conclusions of this project

An intensive investigation into the mixture preparation for natural gas engines has been conducted by using two newly emerged techniques, computational fluid dynamics and the flame ionisation detector. From the series of in-depth computational and experimental studies, the following main conclusions were drawn.

With the aid of CFD simulations, a greater understanding of the mixing processes taking place within venturi type natural gas engine mixers was achieved. In the venturi type gas-air mixer, the mixture homogeneity was governed by the flow momentum flux ratio of the gas stream over the air stream. Due to the low gas momentum flux, it was very difficult for the gas stream to penetrate into the air stream which had a higher momentum flux. Increase of the intersurface area, the contact time and the turbulence between the two flow streams were essential to achieve a homogeneous mixture. An asymmetrical air flow pattern would cause a non-homogeneous mixture distribution and the non-homogeneous concentration distribution would impair the flow symmetry downstream of the mixer. For annular venturi type mixers, the dimensions, positions and numbers of the gas admission slits affected the mixture formation. Different inner bullet nose and venturi outer body configurations could also effect the flow restriction and the mixture homogeneity of the mixers. With respect to the mixture homogeneity, the single gas admission slit concept was unacceptable and the two gas admission slits design gave favourable results no matter what width of gas slit was used. The inner bullet diameter affected both the mixture homogeneity and the pressure loss across the mixer. A compromise had to be made between good mixture quality and a low pressure loss.

The FID indirect sample flow rate control technique used during the measurement of the mixture concentration distributions was successful. In order to interpret the FID signal into the mixture concentration, calibrations by using the right span gas at the right pressure with a constant pressure difference between the flame chamber and the CP chamber were essential. Comparisons between the CFD computational results and the FID experimental results illustrated that the geometrical models created, the boundary regions defined, the fluid properties specified, and the control parameters posed were successful. Of the three variables compared, all of them gave excellent agreement between the predicted and the measured results. The CFD simulations well represented the actual mixing behaviour which occurred in the mixer. The predictions not only gave information about the variables of interest on the outlet plane of the mixer, as the experiments did, but also gave more detailed fluid dynamics information within the

whole mixer on every variable involved. For simulations of a multi-cylinder engine under steady operation, a steady intake pressure assumption was reasonable, because the pressure variations caused by the engine induction process only accounted for 3.48% at WOT and 6.28% at idling with that at part throttle positions in between.

The Gem mixer exhibited similar or superior performance to the three proprietary mixers tested. The variation in λ value across the outlet plane was about 3% for the Gem, compared to approximately 4% for the D-mixer, the best of the three. The simplicity of the Gem design can result in potentially lower manufacturing costs. In terms of engine performance and emissions with different mixers, the engine with the Gem produced the highest power and maximum BMEP over most of the engine operating speeds at WOT. With regard to the engine brake specific energy consumption, brake thermal efficiency and to the engine emissions of CO, HC and NOx, there was not much difference amongst the three mixers when the air fuel ratio produced was the same irrespective of the engine operating speed and load. The advantage of having a lower air flow restriction for the Gem at part loads and for the I-mixer at higher loads demonstrated the superiority on the engine power output and BMEP. No matter which mixer was used, the most important features that a mixture preparation system should have were the mixture air fuel ratio controllability, the mixture homogeneity and the pressure loss across the mixer. Of the three, the mixture air fuel ratio control was the most sensitive parameter which influenced exhaust emissions and the performance of natural gas engines, because the mixture homogeneity could be improved down stream of the mixer when the mixture passed through the throttle valve, the intake manifold and the cylinders.

The experience of the project showed that the CFD technique had been developed to such a stage that it could replace some of the costly and time consuming experimental evaluations for different design options of the mixer and reduce the mixer design and development lead time dramatically. This conclusion can be extended to some other engine component design activities where the relative evaluation of the superiority or inferiority of the flow behaviour related design proposals are required. It is only through consideration of individual applications where the CFD models are compared with experimental results, that the weakness of the numerical solutions embedded in existing CFD packages can be exposed and the solutions improved.

8.2 Recommendations for future work

In this study, the Gem series have been designed for both the 50 and 150 kW engine output. The former one was tested on an engine test bench, but not the latter. A comparative experimental study should be made between this new Gem 150 mixer and

other proprietary mixers for the same power output gas engine. The results should be compared to those of the Gem 50 mixer as well. When all of this has been completed and the predictions verified, then it would be appropriate to extend different designs to meet the demand for different engine power outputs.

The mixture preparation system investigated in this project was for stationary natural gas engines. The findings and conclusions of the study can be extended to automobile applications in order to meet the demands from the increasing natural gas vehicle market. Another area of interest which needs to be looked at is the natural gas injection system. The experience and knowledge acquired in this project has laid a sound foundation for facing the challenge in the design and development of a new series of natural gas injection systems. For example, a CFD aided natural gas engine injection nozzle design will not be too difficult to conduct.

For dynamically controlled species transportation process, turbulence is one of the key parameters which have a profound effect on species concentration distribution. The turbulence models embedded in any of the general purpose CFD packages were derived from particular experiments and are only suitable to the flow behaviours which fall into the same category as that of the experiments. Even so empirical tuning of coefficients within the model is still needed in order to produce a good agreement between the predictive and experimental data. In this study, the basic k-ε model was used because the curvature of the flow domain was simple and smooth, and there was no rotational flow within the flow domain. However, the comparison presented in chapter four between the CFD predicted and the FID measured mixture concentration distribution results showed that there existed a difference between them, even with the boundary specifications made after the sensitivity tests. This indicated that a better agreement required better tuned empirical coefficients within the turbulence models and some other associated models, in addition to the choice of differencing schemes and mesh densities. This demanded an accurate measurement of the turbulence. Based on the turbulence and mixture formation measurement, a new turbulence model could be formulated which would particularly suit flows involving species transformation. The work will not only contribute to the predictions of mixture formation, but also contribute to other species transformation behaviours often encountered in chemical, civil and environmental engineering. The turbulence measurement can also create correlation between the turbulent wall roughness number and mechanical surface roughness, which will, to a large extent, reduce the arbitrary boundary condition definitions.

Though the input file editing technique was used during the modification of different design concepts in this study, it was not always possible just by editing some of the

modified dimensions or boundary conditions of a basic model. Occasionally, a complete geometrical model had to be re-created and all other input data had to be specified when a different configuration was proposed. The ease and speed of the modelling process and simulation conditions specific to the changing design or simple design modification profoundly affect the effectiveness of the CFD technique as a design tool. An integrated facility between the CAD and CFD will greatly ease the problem. It is recommended that an attempt on this area should be made in the future. An integrated tool will release designers or CFD practitioners from the tedious repeated work in order to spend most of their activities on creative design.

Appendix I New and proposed engine emissions standards

1. For light duty vehicles

US federal emissions standards for light duty vehicles (FTP-75) [156]

Federal	HC/NMHC(g/mile)	CO (g/mile)	NOx (g/mile)
1983-1993	0.41	3.40	1.0
1994(Tier 1)	0.25	3.40	0.4*
2004(Tier 2)	0.125	1.7	0.2

* It is 1.0 g/mile for diesel fuel

California emissions standards for light duty vehicles [156]

California	NMHC/NMOG(g/mile)	CO (g/mile)	NOx (g/mile)
1993	0.25	3.40	0.4
TLEV	0.125	3.40	0.4*
LEV(1997)	0.075	1.7	0.2
ULEV(2003)	0.04	1.7	0.2

European emissions legislation for light duty vehicles [156]-[158]

Standard and Introduction	Fuel	CO (g/km)	HC+NOx (g/km)	Particulates (g/km)
Dir. 91/441/EEC; 1992	Gasoline	2.72	0.97	-
	Diesel	2.72	0.97 (1.36 for DI)	0.14 (0.19 for DI)
EC Stage 2 1995	Gasoline	2.2	0.5	-
	Diesel	1.0	0.7 (0.9 for DI)	0.08 (0.10 for DI)
EC Stage 3 1999	Gasoline	1.5	0.2	-
	Diesel	0.5	0.2-0.5	0.04

NB: 1). The values given here are for passenger cars and light duty commercial vehicles having reference weight less than 1700 kg.

2). The durability quoted for the US federal and Californian standards is 80,000 km, rather than 160,000 km [157].

2. For stationary engines

The German TA-Luft emissions standard is used as the current European standard for stationary natural gas engines [29]

Standard	NOx g/m^3 (5% O_2)	NMHC g/m^3	CO g/m^3 (5% O_2)
TA-Luft	0.50	0.15	0.65

Appendix II Governing equations

1. The mass conservation equation for general incompressible and compressible fluid flows and a moving coordinate frame in Cartesian tensor notation:

$$\frac{1}{\sqrt{g}}\frac{\partial}{\partial t}(\sqrt{g}\rho)+\frac{\partial}{\partial x_j}(\rho\tilde{u}_j)=s_m \qquad \text{(A-II.1)}$$

where $\frac{\partial}{\partial x_j}(\rho\tilde{u}_j)$ denote summation of the repeated subscripts j,

For example: $\frac{\partial}{\partial x_j}(\rho\tilde{u}_j)=\frac{\partial(\rho\tilde{u}_1)}{\partial x_1}+\frac{\partial(\rho\tilde{u}_2)}{\partial x_2}+\frac{\partial(\rho\tilde{u}_3)}{\partial x_3}$

2. The momentum conservation equation for general incompressible and compressible fluid flows and a moving coordinate frame in Cartesian tensor notation:

$$\frac{1}{\sqrt{g}}\frac{\partial}{\partial t}(\sqrt{g}\rho u_i)+\frac{\partial}{\partial x_j}(\rho\tilde{u}_j u_i-\tau_{ij})=-\frac{\partial p}{\partial x_i}+s_i \qquad \text{(A-II.2)}$$

1) For Newtonian laminar flows, the components of the stress tensor and velocities are related via the constitutive relations of strain deformation rates

$$\tau_{ij}=2\mu s_{ij}-\frac{2}{3}\mu\frac{\partial u_k}{\partial x_k}\delta_{ij} \qquad \text{(A-II.3)}$$

Where $s_{ij}\equiv\frac{1}{2}(\frac{\partial u_i}{\partial x_j}+\frac{\partial u_j}{\partial x_i})$ is the rate of strain tensor

2) For Newtonian turbulent flows, the ensemble average values are used for all variables. Thus the relations become

$$\tau_{ij} = 2\mu s_{ij} - \frac{2}{3}\mu \frac{\partial u_k}{\partial x_k}\delta_{ij} - \bar{\rho}\overline{u_i' u_j'} \qquad \text{(A-II.4)}$$

The rightmost term represents the additional Reynolds stresses due to the turbulent motion and they are linked to the ensemble average flow properties in an analogous fashion to their laminar flow counterparts via the following constitutive relations.

$$-\bar{\rho}\overline{u_i' u_j'} = 2\mu_t s_{ij} - \frac{2}{3}(\mu_t \frac{\partial u_k}{\partial x_k} + \rho k)\delta_{ij} \qquad \text{(A-II.5)}$$

where $k \equiv \frac{\overline{u_i' u_i'}}{2}$ is the turbulent kinetic energy; ε is its dissipation rate and μ_t the turbulent viscosity which is related to the κ and ε by the relation: $\mu_t = f_\mu \frac{C_\mu \rho k^2}{\varepsilon}$; the κ and l are linked via $\mu_t = f_\mu C_\mu^{1/4} \rho k^{1/2} l$. the κ and ε are to be determined from the modelled turbulence transport equations.

3) The source term s_i can be specified by users according to the problem considered. For example, the term will be expressed as $s_i = g_i \times \rho$ when the body force buoyancy is considered; where g_i is the gravitational acceleration component in direction x_i.

3. The energy conservation equation for a general fluid mixture at all Mach numbers in Cartesian tensor notation:

$$\frac{1}{\sqrt{g}}\frac{\partial}{\partial t}(\sqrt{g}\rho h) + \frac{\partial}{\partial x_j}(\rho \tilde{u}_j h - F_{h,j}) = \frac{1}{\sqrt{g}}\frac{\partial}{\partial t}(\sqrt{g}p) + u_j \frac{\partial p}{\partial x_j} + \tau_{ij}\frac{\partial u_i}{\partial x_j} + s_h \qquad \text{(A-II.6)}$$

Here the static enthalpy is defined by:

$$h = \bar{c}_p T - c_p^0 T_0 + \sum m_m H_m \qquad \text{(A-II.7)}$$

In some special cases, it is the internal energy e rather than the enthalpy h used for the energy conservation equation. The equation is similar in form to equation (A-II.6), but does not contain the pressure related terms and the mean constant pressure specific heat $\bar{c}_p$ at temperature T will be replaced by the mean constant volume specific heat $\bar{c}_v$.

1) For laminar flow, the molecular diffusional energy fluxes of heat are assumed to obey Fourier's law. Accordingly:

$$F_{h,j} = \psi \frac{\partial T}{\partial x_j} + \sum_m h_m \rho D_m \frac{\partial m_m}{\partial x_j} \qquad \text{(A-II.8)}$$

where the ψ is the thermal conductivity, D_m is the molecular diffusivity of constituent m, and h_m is its enthalpy.

2) For turbulent flow, the diffusional energy fluxes (time averaged)

$$F_{h,j} = \psi \frac{\partial T}{\partial x_j} - \bar{\rho}\overline{u_j' h'} + \sum_m h_m \rho D_m \frac{\partial m_m}{\partial x_j} \qquad \text{(A-II.9)}$$

where the turbulent diffusional flux of energy is represented using the following constitutive relations:

$$\bar{\rho}\overline{u_j' h'} = -\frac{\mu_t}{\sigma_{h,t}} \frac{\partial h}{\partial x_j} \qquad \text{(A-II.10)}$$

4. The species conservation equation for each constituent c of a fluid mixture in Cartesian tensor notation:

$$\frac{1}{\sqrt{g}} \frac{\partial}{\partial t}(\sqrt{g}\rho m_c) + \frac{\partial}{\partial x_j}(\rho \tilde{u}_j m_c - F_{c,j}) = s_c \qquad \text{(A-II.11)}$$

The molecular diffusional species fluxes of mass are assumed to obey Fick's law. Thus the diffusional species fluxes of the constituent c are related to their local concentrations or mass fractions m_c through the molecular diffusivity of the component D_c. By analogy with the energy equation:

1) For laminar flow

$$F_{c,j} = \rho D_c \frac{\partial m_c}{\partial x_j} \qquad \text{(A-II.12)}$$

2) For turbulent flow (time averaged)

$$F_{c,j} = \rho D_c \frac{\partial m_c}{\partial x_j} - \bar{\rho}\overline{u_j' m_c'} \qquad \text{(A-II.13)}$$

$$\bar{\rho}\overline{u_j' m_c'} = -\frac{\mu_t}{\sigma_{c,t}} \frac{\partial m_c}{\partial x_j} \qquad \text{(A-II.14)}$$

5. Thermophysical properties

1)Equations of state (density)

a) For incompressible liquids or gases

$$\rho = \rho_0 \; ; \qquad \text{(A-II.15)}$$

where ρ_0 is the density at the reference state T_0 and is a constant

b) For mixtures of incompressible components

$$\rho = \left[\sum_c \left(\frac{m_c}{\rho_c} \right) \right]^{-1} \qquad \text{(A-II.16)}$$

c) For isobaric density variation

$$\rho = \frac{\rho_0}{1+\beta(T-T_0)} \qquad \text{(A-II.17)}$$

d) Isobaric variation for multicomponent mixtures

$$\rho = \frac{\rho_0}{\left[1+\beta\ (T-T_0) + \sum_c \beta_c \left(m_c - m_c^0 \right) \right]} \qquad \text{(A-II.18)}$$

e) For ideal gases or mixtures

$$\rho = \frac{p}{RT(\sum \frac{m_k}{M_k})} \qquad \text{(A-II.19)}$$

where the summation is over all constituents and R the universal gas constant

2) Mixture properties

For multicomponent mixtures of constituent(s) 'c' in a background fluid 'bg', the mixture properties such as the local mixture viscosity, thermal conductivity and specific heat capacity are calculated as mass weighted averages of the component values, i.e.

$$\phi = \sum_{c \neq bg} m_c \phi_c + \left(1 - \sum_{c \neq bg} m_c \right) \phi_{bg} \qquad \text{(A-II.20)}$$

here ϕ is the mixture value of any of the properties, ϕ_c and m_c are the property value and mass fraction of constituent c, respectively, and ϕ_{bg} is the property value of the background fluid.

6. Turbulence model equations

1) The k-ε model equations

a) Turbulence energy:

$$\frac{1}{\sqrt{g}}\frac{\partial}{\partial t}(\sqrt{g}\rho k)+\frac{\partial}{\partial x_j}(\rho\tilde{u}_j k-\frac{\mu_{eff}}{\sigma_k}\frac{\partial k}{\partial x_j})$$
$$=\mu_t(P+P_B)-\rho\varepsilon-\frac{2}{3}(\mu_t\frac{\partial u_i}{\partial x_i}+\rho k)\frac{\partial u_i}{\partial x_i} \quad \text{(A-II.21)}$$

where $P=2s_{ij}\frac{\partial u_i}{\partial x_j}$; $P_B\equiv-\frac{g_i}{\sigma_{h,t}}\frac{1}{\rho}\frac{\partial\rho}{\partial x_i}$ and $\mu_{eff}=\mu+\mu_t$

b) Turbulence dissipation rate

$$\frac{1}{\sqrt{g}}\frac{\partial}{\partial t}(\sqrt{g}\rho\varepsilon)+\frac{\partial}{\partial x_j}(\rho\tilde{u}_j\varepsilon-\frac{\mu_{eff}}{\sigma_\varepsilon}\frac{\partial\varepsilon}{\partial x_j})$$
$$=C_{\varepsilon1}\frac{\varepsilon}{k}\left[\mu_t\left(P+C_{\varepsilon3}P_B\right)-\frac{2}{3}\left(\mu_t\frac{\partial u_i}{\partial x_i}+\rho k\right)\frac{\partial u_i}{\partial x_i}\right]-C_{\varepsilon2}\rho\frac{\varepsilon^2}{k}-C_{\varepsilon4}\rho\varepsilon\frac{\partial u_i}{\partial x_i} \quad \text{(A-II.22)}$$

2) The RNG k-ε model equations

a) Turbulence energy

$$\frac{1}{\sqrt{g}}\frac{\partial}{\partial t}(\sqrt{g}\rho k)+\frac{\partial}{\partial x_j}\left(\rho\tilde{u}_j k-\frac{\mu_{eff}}{\sigma_k}\frac{\partial k}{\partial x_j}\right)=\mu_t P-\rho\varepsilon \quad \text{(A-II.23)}$$

b) Turbulence dissipation rate

$$\frac{1}{\sqrt{g}}\frac{\partial}{\partial t}\left(\sqrt{g}\rho\varepsilon\right)+\frac{\partial}{\partial x_j}\left(\rho\tilde{u}_j\varepsilon-\frac{\mu_{eff}}{\sigma_\varepsilon}\frac{\partial\varepsilon}{\partial x_j}\right)$$
$$=C_{\varepsilon1}\frac{\varepsilon}{k}\mu_t P-C_{\varepsilon2}\rho\frac{\varepsilon^2}{k}-\frac{C_\mu\eta^3(1-\eta/\eta_0)}{1+\beta\eta^3}\frac{\rho\varepsilon^2}{k} \quad \text{(A-II.24)}$$

where $\eta=S\frac{k}{\varepsilon}$; $S=\left(2s_{ij}s_{ij}\right)^{\frac{1}{2}}$ and η_0 and β are empirical coefficients.

3) Equations of the two layer models

a) Norris and Reynolds model

i) Turbulence dissipation rate function

$$\varepsilon = \frac{k^{\frac{3}{2}}}{l}\left(1+\frac{C_\varepsilon}{\mathrm{Re}_y}\right) \qquad \text{(A-II.25)}$$

here $\mathrm{Re}_y = \frac{\sqrt{k}y}{v}$, $l = kC_\mu^{-0.75}y$ and C_ε=5.3

ii) f_μ function

$f_\mu = 1-\exp\left(-\frac{1}{A_\mu}\mathrm{Re}_y\right)$; here Re_y is the same as above and A_μ=50.5

b) Wolfshtein model

i) Turbulence dissipation rate function

$$\varepsilon = \frac{k^{\frac{3}{2}}}{l}\frac{1}{1-\exp\left(-\frac{1}{A_\varepsilon}\mathrm{Re}_y\right)} \qquad \text{(A-II.26)}$$

here $\mathrm{Re}_y = \frac{\sqrt{k}y}{v}$, $l = kC_\mu^{-0.75}y$ and A_ε=5.1

ii) f_μ function

$f_\mu = 1-\exp\left(-\frac{1}{A_\mu}\mathrm{Re}_y\right)$; here Re_y is the same as above and A_μ=70.0

c) Hassid and Porch model

i) Turbulence dissipation rate function

$$\varepsilon = \frac{k^{\frac{3}{2}}}{l}\left(C_{D1}f_\mu+\frac{C_{D2}}{\mathrm{Re}_l}\right) \qquad \text{(A-II.27)}$$

here $\mathrm{Re}_l = \frac{\sqrt{k}l}{v}$, l=ky, C_{D1}=0.164 and C_{D2}=0.336

ii) f_μ function

$f_\mu = 1-\exp\left(-\frac{1}{A_\mu}\mathrm{Re}_l\right)$; here Re_l is the same as above and A_μ=34.48

Appendix III Typical composition of UK mains natural gas [93]

Composition	Symbol	% vol.	% mass
Methane	CH_4	92.7	85.64
Ethane	C_2H_6	4.34+	7.52
Propane	C_3H_8	0.93	2.36
Butane	C_4H_{10}	0.29	0.97
Pentane	C_5H_{12}	0.08	0.33
Nitrogen	N_2	1.12	1.81
Carbon Dioxide	CO_2	0.54	1.37

Appendix IV An example of the CFD commands used

```
title
Simulation of mixture preparation
v 1 0 0
v 7 14 0
vfil 1 7 5 2 1
v 63 70 0
v 83 90 0
vfil 7 63 55 8 1
vfil 63 83 19 64 1
v 1601 0 16
v 1607 14 16
vfil 1601 1607 5 1602 1
v 1608 15 12.7273
v 1609 16 11.0444
v 1610 17 9.814
v 1611 18 8.829
v 1612 19 8.0084
v 1613 20 7.3104
v 1614 21 6.71
v 1615 22 6.2
v 1616 23 5.7417
v 1617 24 5.355
v 1618 25 5.0233
v 1619 26 4.7435
v 1620 27 4.5117
v 1621 28 4.3251
v 1622 29 4.182
v 1623 30 4.0805
v 1624 31 4.0201
v 1625 32 4
v 1633 40 4
vfil 1625 1633 7 1626 1
v 1634 41 4.01216
v 1635 42 4.048672
v 1636 43 4.109594
v 1637 44 4.195
v 1638 45 4.30515
v 1639 46 4.44
v 1640 47 4.6
v 1641 48 4.7858
v 1642 49 4.99712
v 1643 50 5.2346
v 1644 51 5.49878
v 1645 52 5.79
v 1646 53 6.1093
v 1647 54 6.45694
v 1648 55 6.83386
v 1649 56 7.24092
v 1650 57 7.6791
v 1651 58 8.149524
v 1652 59 8.6534
v 1653 60 9.1922
v 1654 61 9.76747
v 1655 62 10.381
v 1656 63 11.03496
v 1657 64 11.73163
v 1658 65 12.47377
v 1659 66 13.2645
v 1660 67 14.1077
v 1661 68 15
v 1662 69 15.9696
v 1663 70 16
v 1683 90 16
vfil 1663 1683 19 1664 1
v 1701 0 17
v 1707 14 17
vfil 1701 1707 5 1702 1
v 1763 70 17
v 1783 90 17
vfil 1763 1783 19 1764 1
v 90 29.5 5
v 91 30.5 5
v 92 31.5 5
v 93 29 6
v 94 30 6
v 95 31 6
v 96 28.5 7
v 97 29.5 7
```

```
v 98 30.5 7
vloc 11 cart 1701 x 1763 y 1
vref 11 2 200 1601 1683 1
vref 11 2 100 90 98 1
csys 1
v 4701 0 47
v 4702 2.333 47
v 4703 4.666 47
v 4704 6.999 46.5173
v 4705 9.332 45.0606
v 4706 11.665 43.1212
v 4707 14 41.4654
v 4708 15 40.9746
v 4709 16 40.5137
v 4710 17 40.0824
v 4711 18 39.6804
v 4712 19 39.3074
v 4713 20 38.9631
v 4714 21 38.6472
v 4715 22 38.3596
v 4716 23 38.1
v 4717 24 37.8682
v 4718 25 37.6641
v 4719 26 37.4876
v 4720 27 37.3384
v 4721 28 37.2164
v 4722 29 37.1217
v 4723 30 37.0541
v 4724 31 37.0135
v 4725 32 37
v 4726 33 37.0135
v 4727 34 37.0541
v 4728 35 37.1217
v 4729 36 37.2164
v 4730 37 37.3384
v 4731 38 37.4876
v 4732 39 37.6641
v 4733 40 37.8682
v 4734 41 38.1
v 4735 42 38.3596
v 4736 43 38.6472
v 4737 44 38.9631
v 4738 45 39.3074
v 4739 46 39.6804
v 4740 47 40.0824
v 4741 48 40.5137
v 4742 49 40.9746
v 4743 50 41.4654
v 4744 51 41.9865
v 4745 52 42.5383
v 4746 53 43.1212
v 4747 54 43.7355
v 4748 55 44.3818
v 4749 56 45.0606
v 4750 57 45.6
v 4751 58 46.2
v 4752 59 46.7
v 4753 60 47
v 4763 70 47
v 4783 90 47
vfil 4753 4763 9 4754 1
vfil 4763 4783 19 4764 1
vset all
vfil 1 1601 15 101 100 83 1
vfil 1801 4701 28 1901 100 83 1
v 390 29.5 38
v 391 30.5 38
v 392 31.5 38
v 393 29 39
v 394 30 39
v 395 31 39
v 396 28.5 40
v 397 29.5 40
v 398 30.5 40
vset all
vset dele vran 1 83 1
vref 1 2 5000 vset
vset all
vgen 2 10000 vset 0 0 0 0 2
vset all
vscal 1 30000 1 0.001 0.001 0.001
vset all
c 10001 10002 2 1 10101 10102 102 101
cgen 16 100 1 1 1
cgen 82 1 1 16 1
c 11601 11602 1602 1601 11701 11702 1702 1701
cgen 6 1 1313 1313 1
c 11663 11664 1664 1663 11763 11764 1764 1763
cgen 20 1 1319 1319 1
cgen 2 100 1313 1338 1
cset all
c 11801 11802 1802 1801 11901 11902 1902 1901
cgen 29 100 1365 1365 1
cgen 82 1 1365 1393 1
c 1662 1663 1763 1763 11662 11663 11763 11763
c 1763 1863 1862 1862 11763 11863 11862 11862
c 1607 1608 1707 1707 11607 11608 11707 11707
c 1707 1808 1807 1807 11707 11808 11807 11807
cset all
c 15101 15102 5102 5101 10001 10002 2 1
cgen 82 1 3747 3747 1
c 15201 15202 5202 5201 15101 15102 5102 5101
cgen 15 100 3829 3829 1
cgen 82 1 3829 3843 1
c 16701 16702 6702 6701 16601 16602 6602 6601
cgen 6 1 5059 5059 1
c 16763 16764 6764 6763 16663 16664 6664 6663
cgen 20 1 5065 5065 1
cgen 2 100 5059 5084 1
c 16901 16902 6902 6901 16801 16802 6802 6801
cgen 29 100 5111 5111 1
cgen 82 1 5111 5139 1
c 6862 6863 6763 6763 16862 16863 16763 16763
c 6763 6663 6662 6662 16763 16663 16662 16662
c 6807 6808 6707 6707 16807 16808 16707 16707
c 6707 6608 6607 6607 16707 16608 16607 16607
cset all
c 11623 11624 1624 1623 10090 10091 91 90
cgen 2 1 7493 7493 1
c 10090 10091 91 90 10093 10094 94 93
cgen 2 1 7495 7495 1
cgen 2 3 7495 7496 1
cset all
c 10196 10197 197 196 10193 10194 194 193
```

```
cgen 2 1 7499 7499 1
c 10193 10194 194 193 10190 10191 191 190
cgen 2 1 7501 7501 1
c 10190 10191 191 190 11823 11824 1824 1823
cgen 2 1 7503 7503 1
cset all
c 14723 14724 4724 4723 10390 10391 391 390
cgen 2 1 7505 7505 1
c 10390 10391 391 390 10393 10394 394 393
cgen 2 1 7507 7507 1
cgen 2 3 7507 7508 1
cset all
c 15096 15097 5097 5096 15093 15094 5094 5093
cgen 2 1 7511 7511 1
c 15093 15094 5094 5093 15090 15091 5091 5090
cgen 2 1 7513 7513 1
c 15090 15091 5091 5090 16623 16624 6624 6623
cgen 2 1 7515 7515 1
c 16823 16824 6824 6823 15190 15191 5191 5190
cgen 2 1 7517 7517 1
c 15190 15191 5191 5190 15193 15194 5194 5193
cgen 2 1 7519 7519 1
cgen 2 3 7519 7520 1
c 15396 15397 5397 5396 15393 15394 5394 5393
cgen 2 1 7523 7523 1
c 15393 15394 5394 5393 15390 15391 5391 5390
cgen 2 1 7525 7525 1
c 15390 15391 5391 5390 19723 19724 9724 9723
cgen 2 1 7527 7527 1
cset all
bound
bdef 1 101 10101 10001 1
bgen 47 100 1 1 1
bdef 1 1 10001 15101 5101
bdef 1 5101 15101 15201 5201
bgen 46 100 49 49 1
bset all
bdef 2 83 183 10183 10083
bgen 47 100 95 95 1
bdef 2 5183 83 10083 15183
bdef 2 5283 5183 15183 15283
bgen 46 100 143 143 1
bdef 3 10096 10097 97 96
bgen 2 1 189 189 1
bdef 4 10196 10197 197 196
bgen 2 1 191 191 1
bdef 5 10396 10397 397 396
bgen 2 1 193 193 1
bset all
bdef 6 15096 15097 5097 5096
bgen 2 1 195 195 1
bdef 7 15196 15197 5197 5196
bgen 2 1 197 197 1
bdef 8 15396 15397 5397 5396
bgen 2 1 199 199 1
bset all
plty qhid
view 0 0 1
cset all
cplo
view 0 0 1
bzon 9 all
view 0 0 -1
repl
bzon 10 all
view 0 0 1
bset all
cset all
prop
turb ke 0.094
dens multi 1.2
solv lt y
solv lw n
scal
sc 1 on
natural gas
1.0 100 0.05
n n n n
trans
0 const 3.004E-5 0.9 38.7E06 16
0.68 1.175E-5 0.038 2230 n
rturb inlet mixl
rturb press mixl
rdef 1 inlet
16.3265 0 0 1 0 0.4 0.0094 293 1.2
rdef 2 outlet
split 1.0
rdef 3 inlet
6.839 -13.678 0 1 0 0.4 0.0002 293 0.68
rdef 4 inlet
 6.839 13.6780 1 0 0.4 0.0002 293 0.68
rdef 5 inlet
6.839 -13.678 0 1 0 0.4 0.0002 293 0.68
rdef 6 inlet
6.839 13.678 0 1 0 0.4 0.0002 293 0.68
rdef 7 inlet
6.839 -13.678 0 1 0 0.4 0.0002 293 0.68
rdef 8 inlet
6.839 13.678 0 1 0 0.4 0.0002 293 0.68
rdef 9 symp
rdef 10 symp
scrm 1 3
1.0
scrm 1 4
1.0
scrm 1 5
1.0
scrm 1 6
1.0
scrm 1 7
1.0
scrm 1 8
1.0
init
stand 20 0 0 150 6000 293
moni 3310
iter 500 0.05
wdat post 100
cset all
bset all
geom 8
prob 10
quit
y
```

Reference

1. Duggal, V. K., (1992), " The natural gas L10 urban bus engine--an alternative fuel option ", Proceedings of the Institute of Mechanical Engineers, Conference: Bus'92 The Expanding Role of Buses Towards the Twenty-first Century, C437/026, pp. 15-28, UK.
2. Wallace, J. S., (1989), " Assessment of 'first generation' propane conversion equipment ", SAE paper 892144.
3. Nichols, R. J., (1993), " The challenges of change in the auto industry : Why alternative fuels? ", ASME Conference: Alternative fuels, engine performance and emissions, ICE-Vol. 20. pp. 3-10, Morgantown, West Virginia, USA.
4. Koyanagi, K., Hiruma, M., Yamane, K. and Furuhama, S., (1993), " Effect of hydrogen jet on mixture formation in a high-pressure injection hydrogen fuelled engine with spark ignition ", SAE Paper No. 931811; SP-982: SAE future transportation technology conference, pp. 123-132, San Antonio, Texas, USA.
5. Peschka, W. and Escher, W. J. D., (1993), " Germany's contribution to the demonstrated technical feasibility of the liquid-hydrogen fuelled passenger automobile ", SAE Paper No. 931812; SP-982: SAE future transportation technology conference, pp. 133-150, San Antonio, Texas, USA.
6. Larsen, J. F. and Wallace, J. S., (1995), " Comparison of emissions and efficiency of a turbocharged lean-burn natural gas and Hythane fuelled engine ", ASME spring engine technology conference, ICE-Vol. 24, natural gas and alternative fuels for engines, pp. 31-40, Marietta, Ohio, USA.
7. Meyers, D. P. and Kubesh, J. T., (1995), " The hybrid rich-burn/lean-burn engine ", ASME spring engine technology conference, ICE-Vol. 24, natural gas and alternative fuels for engines, pp. 91-98, Marietta, Ohio, USA.
8. DeLuchi, M. A., Johnston, R. A. and Sperling, D., (1988), " Methanol vs. natural gas vehicles: a comparison of resource supply, performance, emissions, fuel storage, safety, costs and transitions ", SAE paper 881656.
9. Wang, W., Gautam, M., Sun, X., Bata, R., Clark, N., Palmer, G. M. and Lyons, D., (1993), " Emissions comparisons of twenty-six heavy-duty vehicles operated on conventional and alternative fuels ", SAE Paper 932952.
10. Conti, L., Ferrera, M., Garlaseo, R., Volpi, E. and Cornetti, G. M., (1993), " Rationale of dedicated low emitting CNG cars ", SAE Paper 932763.
11. Zelenka, P., Kapus, P. and Mikulic, L. A., (1991), " Development and optimisation of methanol fuel compression ignition engines for passenger cars and light duty trucks ", SAE paper 910851.
12. Black, F., (1991), " An overview of the technical implications of methanol and ethanol as highway motor vehicle fuels ", SAE paper 912413.
13. Weaver, C. S., (1989), " Natural gas vehicles -- a review of the state of the art " , SAE paper 892133.

14. Cornetti, G. M., Filippi, F. and Signer, M., (1992), " CNG low emission city buses ", Proceedings of the Institute of Mechanical Engineers, Conference: Bus'92 The Expanding Role of Buses Towards the Twenty-first Century, C437/030, pp. 29-38, UK.
15. Turner, J. E. and Topaloglu, T., (1994), " Experience with compressed natural gas in the Ontario transit bus industry ", ASME The Energy Sources Technology Conference : Natural gas and alternative fuels for engines, ICE -Vol. 21, pp. 87-97, New Orleans, Louisiana, USA.
16. Stone, C. R. and Ladommatos, N., (1991), " Design and evaluation of a fast-burn spark-ignition combustion system for gaseous fuels at high compression ratios ", Journal of the Institute of Energy, Vol. 64, pp. 202-211.
17. Jaaskelainen, H. E. and Wallace, J. S., (1993), " Performance and emissions of a natural gas-fuelled 16 valve DOHC four-cylinder engine ", SAE paper 930380.
18. Roberts, G. R., Thuston, R. R. and Broomhall, D. J., (1990), " Oxygen control for gas engines with catalytic converters: a reliable low cost development ", IMechE Seminar : Gas Engines and Co-generation, pp. 89-96, Solihull, UK.
19. Shiells, W., Garcia, P., Chanchaona, S., Mcfeaters, J. S. and Raine, R. R., (1989), " Performance and cyclic variability of natural gas fuelled heavy duty engines ", SAE paper 892137.
20. Raine, R. R., McFeaters, J. S., Elder, S. T. and Stephenson, J., (1989), " New Zealand experience with natural gas fuelling of heavy transport engines ", SAE paper 892136.
21. Goulburn, J. R. and McCluney, P., (1993), " A natural gas fuel two-stroke engine with low pressure fuel injection ", IMechE Seminar: Gas Engines for Co-generation, pp. 39-46, London, UK.
22. Goulburn, J. R., Blain, G. P. and Donohoe, M, (1990), " A natural gas fired two stroke engine designed for high thermal efficiency and low environmental impact ", IMechE Seminar : Gas Engines and Co-generation, pp. 83-88, Solihull, UK.
23. Winterbotham, A. W., Eiermann, D. and Nuber, R., (1990), " Wankel rotary gas engines", IMechE Seminar : Gas Engines and Co-generation, pp. 57-67, Solihull, UK.
24. Linnell, C. J., (1990), " The first 10 years on the UK market for packaged Co-generation plant -- a review ", IMechE Seminar : Gas Engines and Co-generation, pp. 5-17, Solihull, UK.
25. Walker, W. J. N. and Hellman, J. O., (1990), " The slow speed dual fuel engine for power generation ", IMechE Seminar : Gas Engines and Co-generation, pp. 43-55, Solihull, UK.
26. Fritz, S. G. and Egbuonu, R. I., (1993), " Emissions from heavy-duty trucks converted to compressed natural gas ", SAE Paper 932950.
27. Hundleby, G. E., (1989), " Low emissions approaches for heavy duty gas powered urban vehicles ", SAE paper 892134.

28. Beaty, K. D., (1992), " Development of a low emission Volvo 9.6 litre natural gas fuelled bus engine ", SAE paper 921554.
29. Chmela, F. G. and Kapus, P., (1993), " The new AVL high turbulence lean burn natural gas engine ", IMechE Seminar: Gas Engines for Co-generation, pp. 11-18, London, UK.
30. Gupta, M. and Bell, S. R, (1994), " An investigation of lean combustion in a natural gas fuelled spark ignited engine ", ASME The Energy Sources Technology Conference : Natural gas and alternative fuels for engines, ICE -Vol. 21, pp. 37-46, New Orleans, Louisiana, USA.
31. Al-Shemmeri, T. T. and Zhuo, B., (1993), " Experimental and computational study of a spark ignition engine fuelled with petrol or natural gas ", Proceedings of the Institution of Mechanical Engineers, International Conference : Experimental and predictive methods in engine research and development, No. C465/015/93, pp. 79-86, Birmingham, UK.
32. Jager, D. J., (1992), " A study of mixing and combustion in a divided chamber turbocharged natural gas engine ", Ph.D. Thesis, University of Bath, UK.
33. Jager, D. J., Charlton, S. J. and Tawfig, M. E., (1991), " In-cylinder measurement of mixture strength on a turbocharged natural gas engine ", IMechE Seminar : Experimental methods in engine research and development '91, pp. 1-6, London, UK.
34. Moore, D. S., (1987), " Design of a single cylinder research engine and development of a computer model for lean burn combustion studies ", Ph.D. Thesis, University of Bath, UK.
35. Ladommatos, N. and Stone, R., (1991), " Conversion of a diesel engine for gaseous fuel operation at high compression ratio ", SAE paper 910849.
36. Charlton, S. J., Jager, D. J. and Shooshtarian, A., (1990), " An investigation of mixing and combustion in a lean burn natural gas engine ", IMechE Seminar : Gas Engines and Co-generation, pp. 77-82, Solihull, UK.
37. Klimstra, J., (1990), " Performance of lean-burn natural-gas-fuelled engines -- on specific fuel consumption, power capacity and emissions ", SAE paper 901495.
38. Clarke, D. P., Such, C. H., Overington, M. T. and Das, P. K., (1992), " A lean burn turbocharged, natural gas engine for the US medium duty automotive market ", SAE paper 921552.
39. Siewert, R. M., Mitchell, P. J. and Mulawa, P. A., (1993), " Environmental potential of natural gas fuel for light-duty vehicles: an engine-dynamometer study of exhaust-emission-control strategies and fuel consumption ", SAE Paper 932744.
40. Mendis, K. J. S., Stone, C. R., Ladommatos, N. and Daragheh, M., (1993), " An lean burn low emissions gas engine ", IMechE Seminar: Gas Engines for Co-generation, pp. 1-10, London, UK.
41. Mendis, K. J. S., Stone, C. R., Ladommatos, N. and Weller, G., (1993), " Modelling and measurements from a natural gas fuelled engine ", SAE Paper 930927.

42. Evans, R. L. and Blaszczyk, J., (1993), " The effect of combustion chamber design on exhaust emissions from spark-ignition engines ", IMechE Seminar: World Engine Emission Standards and How to Meet Them ", pp. 25-29, London, UK.
43. Gambino, M., Corbo, P., Iannaccone, S., Unich, A. and Bata, R., (1993), " High turbulence combustion chamber for lean-burn heavy-duty CNG engines ", ASME Conference: Alternative fuels, engine performance and emissions, ICE-Vol. 20. pp. 11-14, Morgantown, West Virginia, USA.
44. Kapus, P. E. and Chmela, F. G., (1993), " The new AVL gas engine combustion system ", ASME Conference: Alternative fuels, engine performance and emissions, ICE-Vol. 20. pp. 15-21, Morgantown, West Virginia, USA.
45. Clarke, D. P., Penny, I. J. and Wise, D. A., (1994), " Understanding the potential of the non-after cooled Navistar 7.3T CNG engine ", SAE Paper 940549.
46. Whattam, M. and Sinha, S. K., (1990), " RK270 spark ignited engine ", IMechE Seminar : Gas Engines and Co-generation, pp. 33-42, Solihull, UK.
47. Whattam, M., Sinha, S. K. and Johnson, D., (1993), " Operating experience and design process cooperate in the RK270 spark ignition engine development ", IMechE Seminar : Gas Engines for Co-generation, pp. 29-37, London, UK.
48. Sinha, S. K., Bretton, A. S. and Clough, E., (1992), " In-cylinder sampling technique used in the development of the Ruston RK270 lean burn gas engine ", Proceedings of the Institution of Mechanical Engineers, International Conference : Combustion in Engines-- Technology, applications and the environment, No. C448/068, pp. 107-116, London, UK.
49. Blumrich, S., Engler, B., Honnen, W. and Koberstein, E., (1990), " Catalytic exhaust gas cleaning for engines used in co-generation ", IMechE Seminar : Gas Engines and Co-generation, pp. 117-127, Solihull, UK.
50. Engler, B. H., Gluck, K. H., Lox, E. and Schafer-Sindlinger, A., (1993), " Catalyst development for stoichiometric and lean burn natural gas engines ", IMechE Seminar : Gas Engines for Co-generation, pp. 19-28, London, UK.
51. Klimstra, J., (1987), " Catalytic converters for natural gas fuelled engines ----- a measurement and control problem ", SAE paper 872165.
52. Thiagarajan, S., Midkiff, K. C., Bell, S. R. and Green, M. N., (1995), " Investigation of fuel composition effects on a natural gas fuelled spark-ignited engine ", ASME spring engine technology conference, ICE-Vol. 24, natural gas and alternative fuels for engines, pp. 41-51, Marietta, Ohio, USA.
53. Tiedema, P. and Wolters, L., (1990), " Recent developments in gas-air mixers and in microprocessor air-fuel ratio control systems ", IMechE Seminar : Gas Engines and Co-generation, pp. 97-105, Solihull, UK.
54. Parker, J. K. and Hopko, S. N., (1994), " Computer controlled natural gas carburettor ", ASME The Energy Sources Technology Conference : Natural gas and alternative fuels for engines, ICE -Vol. 21, pp. 47-53, New Orleans, Louisiana, USA.

55. Sakai, T., Choi, B., Osuga, R., Ko, Y. and Kim, Z., (1992), " Unburned fuel and formaldehyde purification characteristics of catalytic converters for natural gas fuelled automotive engine ", SAE paper 920596.
56. Ko, Y., Kurihara, K., Sakai, T., Osuga, R., Choi, B-C., Ayusawa, T. and Kim, E., (1992), " Research and development of LNG vehicle for practical use ", SAE paper No. 920594.
57. Morsing, P. and Sϕndergaard, K., (1990), " Use of selective catalytic reduction for reduction of NOx in gas engine exhaust ", IMechE Seminar : Gas Engines and Co-generation, pp. 129-138, Solihull, UK.
58. Bloomfield, G. W. and Guntrum, R., (1990), " Emission control for gas engines. Reduction of nitrogen oxides, hydrocarbon, and carbon monoxide levels ", IMechE Seminar : Gas Engines and Co-generation, pp. 139-143, Solihull, UK.
59. Poole, C. J., Hancock, R. J. and Cairns, D. C., (1992), " Cosworth MBA engine ", SAE paper 920849.
60. Gardiner, D. P., Bardon, M. F. and Rao, V. K., (1991), " Effects of prompt EGR on warm-up and steady state fuel consumption and emissions ", SAE paper 912374.
61. Gardiner, D. P., Rao, V. K., Bardon, M. F. and Battista, V., (1991), " Improving the cold start combustion in methanol fuelled spark ignition engines by means of prompt EGR ", SAE paper 910377.
62. Gambino, M., Corbo, P., Iannaccone, S. and Unich, A., (1995), " Low emission stoichiometric CNG engine with EGR ", ASME spring engine technology conference, ICE-Vol. 24, natural gas and alternative fuels for engines, pp. 53-58, Marietta, Ohio, USA.
63. Raine, R. R. and Jones, G. M., (1990), " Comparison of temperatures measured in natural gas and gasoline fuelled engines ", SAE paper 901503.
64. Klimstra, J. and Overmars, F., (1991), " Monitoring the spark plug gap of natural gas fuelled stationary engines ", SAE paper 912361.
65. Ask, T. ϕ., Almas, T., Hansen, T. and Valland, H., (1991), " Study of ignition in spark ignition engines with a specially designed schlieren system and digital image processing ", IMechE Seminar : Experimental methods in engine research and development '91, pp. 29-39, London, UK.
66. Ask, T. ϕ., Almas, T., Valland, H. and Paulsen, H., (1994), " Study of the initial flame growth in a spark ignition engine " IMchE Seminar : Measurement and observation analysis of combustion in engines, pp. 69-83, London, UK.
67. Unich, A., Bata, R. M. and Lyons, D. W., (1993), " Natural gas: a promising fuel for IC. engines ", SAE Paper 930929.
68. Green, C. J. and Wallace, J. S., (1989), " Electrically actuated injectors for gaseous fuels ", SAE paper 892143.

69. Sierens, R. and Rosseel, E., (1995), " Development of a multi-point timed injection SI natural gas engine ", ASME spring engine technology conference, ICE-Vol. 24, natural gas and alternative fuels for engines, pp. 99-104, Marietta, Ohio, USA.
70. Bell, S. R., Parker, J. K., Newman, F. L. and Dinh, H., (1995), " Performance and emissions of natural gas conversion equipment ", ASME spring engine technology conference, ICE-Vol. 24, natural gas and alternative fuels for engines, pp. 59-68, Marietta, Ohio, USA.
71. Blazek, C. F., Grimes, J. W., Freeman, P., Bailey, B. K. and Calucci, C., (1994), " Natural gas vehicle conversion system testing ", ASME The Energy Sources Technology Conference : Natural gas and alternative fuels for engines, ICE -Vol. 21, pp. 55-66, New Orleans, Louisiana, USA.
72. Franklin, M. L., Kittelson, D. B., Leuer, R. H. and Pipho, R. H., (1994), " A PC-based fuel and ignition control system used to map the 3-D surfaces of torque and emissions versus air-fuel ratio and ignition timing ", SAE Paper 940546.
73. Franklin, M. L., Kittelson, D. B., Leuer, R. H. and Pipho, R. H., (1994), " Synchronous, simultaneous optimisation of ignition timing and air-fuel ratio in a gas fuelled spark ignition engine ", SAE Paper 940547.
74. Gros, S. and Vestergen, R., (1991), " High pressure gas technology and emission control for modern four-stroke diesel engines ", Wartsila Diesel Technology Report.
75. Hodgins, K. B., Gunawan, H. and Hill, P. G., (1992), " Intensifier-injector for natural gas fuelling of diesel engines ", SAE paper 921553.
76. Fraser, R. A., Siebers, D. L. and Edwards, C. F., (1991)," Autoignition of methane and natural gas in a simulated diesel environment ", SAE paper 910227.
77. Jensen, S. P., (1994), " A retrofit system to convert a locomotive to natural gas operation ", ASME The Energy Sources Technology Conference : Natural gas and alternative fuels for engines, ICE -Vol. 21, pp. 1-5, New Orleans, Louisiana, USA.
78. Weaver, C. S. and Turner, S. H, (1994), " Dual fuel natural gas/diesel engines : technology, performance, and emissions ", SAE Paper 940548.
79. Hodgins, K. B., Gunawan, H. and Hill, P. G., (1992), " Intensifier-injector for natural gas fuelling of diesel engines ", SAE Paper No. 921553/ SP-927, pp. 29-39.
80. Hsu, B. D., Confer, G. L. and McDowell, R. E., (1995), " The H-process dual fuel diesel engine ", ASME spring engine technology conference, ICE-Vol. 24, natural gas and alternative fuels for engines, pp. 25-30, Marietta, Ohio, USA.
81. Carter, S. A., Williamson, B. C., Kozole, K. H. and Knappers, M. A., (1990), " Gaseous fuel injection (GFI) of natural gas&propane: An update ", 1990 Windsor workshop on alternate fuels, pp. 52-61, Toronto, Ontario, Canada.
82. Geiss, R. O., Burkmyre, W. M. and Lanigan, J. W., (1992), " Technical highlights of the Dodge compressed natural gas ram van/wagon ", SAE Paper No. 921551/ SP-927, pp. 9-20.

83. Hong, H., Krepec, T. and Cheng, R. M. H., (1993), " Optimisation of electronically controlled injections for direct injection of natural gas in diesel engines ", SAE Paper No. 930928.
84. Jennings, M. J. and Jeske, F. R., (1993), " Analysis of the injection process in direct injected natural gas engines- Part I: Study of unconfined and in-cylinder plume behaviour ", ASME Conference: Alternative fuels, engine performance and emissions, ICE-Vol. 20. pp. 23-30, Morgantown, West Virginia, USA.
85. Jennings, M. J. and Jeske, F. R., (1993), " Analysis of the injection process in direct injected natural gas engines----Part II: Effects of injector and combustion chamber design ", ASME Conference: Alternative fuels, engine performance and emissions, ICE-Vol. 20. pp. 31-39, Morgantown, West Virginia, USA.
86. Zhang, J., Fraser, R. A. and Strong, A. B, (1994), " Modelling diesel engine natural gas injection : injector/cylinder boundary conditions ", SAE Paper 940329.
87. Klimstra, J., (1989), " Carburettors for gaseous fuels--on air-to-fuel ratio, homogeneity and flow restriction ", SAE paper 892141.
88. Dinh, H. T.,(1994), " Operating, performance and emission characteristics of compressed natural gas vehicles ", ASME The Energy Sources Technology Conference: Natural gas and alternative fuels for engines, ICE -Vol. 21, pp. 7-15, New Orleans, Louisiana, USA.
89. King, S. R., (1992), " The impact of natural gas compositions on fuel metering and engine operational characteristics ", SAE paper 920593.
90. Kittelson, D. B., Pipho, M. J. and Franklin, M. L., (1989), " Dynamic optimisation of spark advance and air-fuel ratio for a natural gas engine ", SAE paper 892142.
91. Wadman, B., (1993), " Electronic alternative fuel management ", High Speed Diesels and Drives, Volume XII, No. 7, pp. 22-23.
92. Smith, D. H. and Gettel, L. E., (1993), " A compressed natural gas mass flow driven heavy duty electronic engine management system ", SAE Paper No. 931822; SP-982: SAE future transportation technology conference, pp. 201-223, San Antonio, Texas, USA.
93. Charlton, S. J., Tawfig, M. E. and Shooshtarian, A., (1993), " The response of an open-chamber natural gas engine to gas composition ", IMechE Seminar : Gas Engines for Cogeneration, pp. 61-77, London, UK.
94. Ryan III, T. W. and Callaghan, T. J., (1992), " The effects of natural gas composition on engine combustion, performance, and emissions ", XXIV FISITA congress : The vehicle and the environment, London, No. C389/403 or FISITA paper No. 925012.
95. Kubesh, J., King, S. R. and Liss, W. E., (1992), " Effect of gas composition on octane number of natural gas fuels ", SAE paper 922359.
96. Schiffgens, H.-J., Endres, H., Wackertapp, H. and Schrey, E.,(1993), " Concepts for the adaptation of SI gas engines to changing methane number ", ASME Conference:

Alternative fuels, engine performance and emissions, ICE-Vol. 20. pp. 41-50, Morgantown, West Virginia, USA.
97. Gillispie, M. J. and Jensen, M. A., (1994), " Effects of fuel gas mixtures on power limits in a dual-fuel engine ", ASME The Energy Sources Technology Conference : Natural gas and alternative fuels for engines, ICE -Vol. 21, pp. 31-36, New Orleans, Louisiana, USA.
98. Durst, F., Jovanovic, J. and Sender, J., (1993), " Detailed measurements of the near wall region of turbulent pipe flow ", ASME conference: Data for validation of CFD codes; FED-Vol. 146, pp. 79-87, Washington, DC., USA.
99. Papst, F., (1993), " Low emission natural gas engines for commercial vehicles ", IMechE International Conference : AUTOTECH'93---Automobile emissions and combustion, pp. 195-201, Birmingham, UK.
100. Tiller, D. B., Cederberg, A. R. and Schimenti, J. D., (1993), " Toughness testing of an all-composite fuel container for natural gas vehicles ", SAE Paper No. 931785 or SP-982: SAE future transportation technology conference, pp. 49-55, San Antonio, Texas, USA.
101. Liss, W. E., Okazaki, S., Acker, Jr. G. H. and Moulton, S., (1992) " Fuel issues for liquefied natural gas vehicles ", SAE Paper 922360.
102. Tummala, M., Krepec, T. and Ahmed, A. K. W., (1993), " Simulation, testing and optimisation of natural gas on-board storage system for automotive applications ", SAE Paper No. 931820 or SP-982: SAE future transportation technology conference, pp. 181-188, San Antonio, Texas, USA.
103. Quinn, D., (1990), " Carbon adsorbents for natural gas ", Gas utilisation research forum (GURF) on Adsorbed Natural Gas (ANG), London, UK.
104. Malling, J. and Kjær, J., (1990), " Low pressure temperature controlled storage of natural gas ", Gas utilisation research forum (GURF) on Adsorbed Natural Gas (ANG), London, UK.
105. Lin, Y. C. and Huff, G. A., (1993), " Adsorbed natural gas (ANG): Fuel of the future ", SAE Paper No. 931821; SP-982: SAE future transportation technology conference, pp. 189-199, San Antonio, Texas, USA.
106. Gosman, A. D., Hill, C., Marooney, C. J. and Sarantinos, M., (1991), " Interactive computational fluid dynamics tools for engine design ", Proceedings of the Institution of Mechanical Engineers, International Conference : Computers in engine technology, No. C430/023, pp. 1-6, Cambridge, UK.
107. Gosman, A. D., Kralj, C., Marooney, C. J. and Theodossopoulos, P., (1992), " Development strategies for diesel combustion simulation using the SPEED code ", Proceedings of the Institution of Mechanical Engineers, International Conference : Combustion in Engines-- Technology, applications and the environment, No. C448/035, pp. 21-27, London, UK.

108. Boretti, A. A., Nebuloni, P., Lisbona, M. G. and Milazzo, P., (1992), " Diesel engine combustion chamber design with three-dimensional flow computations ", Proceedings of the Institution of Mechanical Engineers, International Conference : Combustion in Engines-- Technology, applications and the environment, No. C448/005, pp. 1-8, London, UK.
109. Kobayashi, T. and Kitoh, K., (1992), " A review of CFD methods and their application to automobile aerodynamics ", SAE Paper 920338.
110. Kuriyama, T., (1993), " Automobile design and visual computational fluid dynamics ", JSAE Review Vol. 14, No. 4, pp. 68-70.
111. Chen, J. X., (1991), " The numerical solution of complex fluid flow phenomena ", Ph.D. Thesis, University of Leeds, UK.
112. STAR-CD Version 2.2 Manuals, (1991), Computational Dynamics Ltd, London, UK.
113. Johns, R. J. R. and Jones, P. M., (1991), " Computer modelling of the flow in a lean burn natural gas engine ", Proceedings of the Institution of Mechanical Engineers, International Conference : Computers in engine technology, No. C430/058, pp. 21-25, Cambridge, UK.
114. Mendonca, F. G. and Bretton, A. S., (1993), " Simulation of in-cylinder fuel mixing in a large spark ignition lean burn engine ", Proceedings of the Institution of Mechanical Engineers, International Conference : Experimental and predictive methods in engine research and development, No. C465/010/93, pp. 67-77, Birmingham, UK.
115. Whelan, S. and Needham, J., (1993), " Meeting the challenge of low emissions and fuel economy with the Ricardo 4-valve HSDI ", IMechE International Conference : AUTOTECH'93-Automobile emissions and combustion, pp. 161-171, Birmingham, UK.
116. Charlton, S. J., Cox, A., Somerville, B. J., Watts, M. J. and Horrocks, R. W., (1992), " An investigation of the emission characteristics of the passenger car IDI diesel engine ", Proceedings of the Institution of Mechanical Engineers, International Conference : Combustion in Engines-- Technology, applications and the environment, No. C448/025, pp. 9-20, London, UK.
117. Somerville, B. J., Charlton, S. J. and Nasseri, B., (1993), " CFD study of air motion in a passenger car IDI diesel engine ", Proceedings of the Institution of Mechanical Engineers, European Conference : Engineering applications of computational fluid dynamics, No. C461/023/93, pp. 69-75, London, UK.
118. Seeley, W. A., Baker, P., Girgis, N. S., and Benjamin, S. F., (1994), " An experimental and predictive study of the tumbling generating characteristics of four-valve cylinder heads under steady flow conditions ", IMechE Seminar : The validation of computational techniques in vehicle design--CFD; London, UK.
119. Barraclough, S., Shaw, C. T. and Arcoumanis, C., (1994), " Comparison of CFD and experimental results for the flow field through a 4-valve inlet port under steady state

conditions ", IMechE Seminar : The validation of computational techniques in vehicle design--CFD; London, UK.
120. Shaw, C. T., Graysmith, J. L. and Richardson, S. H., (1993), " Influencing engine design using computational fluid dynamics ", SAE Paper 930877; SP-972, pp. 127-136.
121. Saad, M. T., Afify, E. M. and Klett, D. E., (1993), " Multidimensional modelling of combustion and NO emission of the Ricardo Hydra direct injection diesel engine: KIVA-II versus experiment ", ASME Conference: Alternative fuels, engine performance and emissions, ICE-Vol. 20. pp. 89-98, Morgantown, West Virginia, USA.
122. Dillies, B., Marx, K., Dec, J. and Espey, C., (1993), " Diesel engine combustion modelling using the coherent flame model in KIVA-II ", SAE Paper 930074.
123. Liu, A. B., Mather, D. and Reitz, R. D., (1993), " Modelling the effects of drop drag and break-up on fuel sprays ", SAE Paper 930072.
124. Robinson, S., Blunsdon, C. A., Dent, J. C. and Garner, C. P., (1991), " Charge coupled device camera/computer analysis of flame propagation in a spark ignition engine, and some comparisons with a computational fluid dynamic model ", Proceedings of the Institution of Mechanical Engineers, International Conference : Computers in engine technology, No. C430/066, pp. 69-77, Cambridge, UK.
125. Griffiths, J. F., Rose, D. J., Schreiber, M., Meyer, J. and Knoche, K. F., (1992), " Application of CFD to the modelling of autoignition at high pressure in a cylinder ", Proceedings of the Institution of Mechanical Engineers, International Conference : Combustion in Engines-- Technology, applications and the environment, No. C448/030, pp. 29-35, London, UK.
126. Amato, U., Belardini, P., Bertoli, C. and Giacomo, N. DEL., (1991), " The joint use of multi-dimensional modelling and field experiments in order to design diesel combustion systems ", Proceedings of the Institution of Mechanical Engineers, International Conference : Computers in engine technology, No. C430/045, pp. 57-61, Cambridge, UK.
127. Kenny, R. G., McKinley, N. R. and Raghunathan, B. D., (1994), " Experimental and theoretical studies of two-stroke loop scavenging ", IMechE Seminar : The validation of computational techniques in vehicle design--CFD; London, UK.
128. Jeske, F. R., Jennings, M. J. and Welch, A. B., (1992), " Modelling of the natural gas injection process in a two-stroke diesel engine ", SAE Paper 920192.
129. Huh, K. Y., Kim, K. K., Choi, C. R., Park, S. C., Moon, S. and Lee, Y., (1993), " Scavenging flow simulation of a four-poppet-valved two-stroke engine ", SAE Paper No. 930500.
130. Baxendale, A. J., (1993), " Computational fluid dynamics applied to exhaust systems design and development ", IMechE International Conference : AUTOTECH'93-Automobile emissions and combustion, pp. 71-78, Birmingham, UK.
131. Clarkson, R. J., Benjamin, S. F., Girgis, N. S. and Richardson, S., (1994), " Theoretical and experimental investigation of the flow in catalytic converters ", IMechE

Seminar : The validation of computational techniques in vehicle design--CFD; London, UK.
132. Shih, L. K. and Assanis, N., (1993), " Effect of ring dynamics and crevice flows on unburned hydrocarbon emissions ", ASME Conference: Alternative fuels, engine performance and emissions, ICE-Vol. 20. pp. 195-206, Morgantown, West Virginia, USA.
133. Jones, I. P., (1994), " Experience on the validation of Computational Fluid Dynamics ", IMechE Seminar : The validation of computational techniques in vehicle design--CFD; London, UK.
134. Graysmith, J. L., Baxendale, A. J. and Haynes, T., (1994), " Validating two CFD codes for external flow ", IMechE Seminar : The validation of computational techniques in vehicle design--CFD; London, UK.
135. McDonell, V. G. and Samuelsen, S., (1993), " An experimental data base for the computational fluid dynamics of reacting and non-reacting methanol sprays ", ASME conference: Data for validation of CFD codes; FED-Vol. 146, pp. 1-12, Washington, DC., USA.
136. Durst, F., Jovanovic, J. and Sender, J., (1993), " Detailed measurements of the near wall region of turbulent pipe flow ", ASME conference: Data for validation of CFD codes; FED-Vol. 146, pp. 79-87, Washington, DC., USA.
137. Buckle, U. and Durst, F., (1993), " Investigations of laminar flow in a pipe with sudden contraction of cross sectional area ", ASME conference: Data for validation of CFD codes; FED-Vol. 146, pp. 61-78, Washington, DC., USA.
138. Slowley, J., Jager, D. J., Charlton, S. J., Tang, W. and Roberts, G., (1995), " An investigation into gas engine carburation and the development of a novel high performance gas carburettor ", ASME spring engine technology conference, ICE-Vol. 24, natural gas and alternative fuels for engines, pp. 69-79, Marietta, Ohio, USA.
139. Patterson D. J. and Henein, N. A., (1973), " Emissions from combustion engines and their control ", Ann Arbor science publishers inc., Michigan, USA.
140. Collings, N., (1988), " A new technique for measuring HC concentration in real time in a running engine ", SAE Paper 880517.
141. Cheng, W. K., Galliot, F. and Collings, N., (1989), " On the time delay in continuous in-cylinder sampling from IC engines ", SAE Paper 890579.
142. Sleightholme, G. R., (1990), " In-cylinder measurements of charge inhomogeneity in a spark-ignition engine ", SAE Paper 900484.
143. Galliot, F., Cheng, W. K., Cheng, C-O., Sztenderowicz, M., Heywood, B. and Collings, N., (1990), " In-cylinder measurements of residual gas concentration in a spark ignition engine ", SAE Paper 900485.
144. Ladommatos, N., (1992), " Cyclically resolved measurements of hydrocarbons in the cylinders of internal combustion engines, by means of a fast flame ionisation detector ", Journal of the Institute of Energy, Vol. 65, No. 463, pp. 94-101.

145. Ladommatos, N. and Rose, D., (1994), " Measurement of in-cylinder air-fuel ratio excursions during fast throttle opening using a fast flame ionisation detector ", IMechE Seminar: Fast response flame ionisation detector--measuring hydrocarbon emissions from IC engines, London, UK.
146. Collings, N. and Willey, J., (1987), " Cyclically resolved HC emissions from a spark ignition engine ", SAE Paper 871691.
147. Collings, N. and Eade, D., (1988), " An improved technique for measuring cyclic variations in the hydrocarbon concentration in an engine exhaust ", SAE Paper 880316.
148. Collings, N. and Hands, T., (1990), " Response of three-way catalysts to transient hydrocarbon emissions ", IMechE Seminar: Engine transient performance, pp. 1-3, London, UK.
149. Collings, N. and Hands, T., (1990), " A new technique to study the response of catalysts to transient conditions ", JSAE COMODIA Conference, Japan.
150. Boam, D. J., (1994), " The interpretation of fast response flame ionisation signals in exhaust ports ", IMechE Seminar: Fast response flame ionisation detector--measuring hydrocarbon emissions from IC engines, London, UK.
151. Rouveirolles, P. and Roy, J. P., (1994), " Cyclically resolved HC emissions in the exhaust port of a firing SI engine ", IMechE Seminar: Fast response flame ionisation detector--measuring hydrocarbon emissions from IC engines, London, UK.
152. Lucas, G. G., Emtage, A. L. and Mason, A., (1994), " A study of the signals from a fast response flame ionisation detector unit fitted in the exhaust port of No 4 cylinder of a 2 litre spark ignition engine ", IMechE Seminar: Fast response flame ionisation detector--measuring hydrocarbon emissions from IC engines, London, UK.
153. Brown, P. G. and Woods, W. A., (1994), " A direct comparison of hydrocarbon measurements taken with a fast response flame ionisation detector and a sampling valve ", IMechE Seminar: Fast response flame ionisation detector--measuring hydrocarbon emissions from IC engines, London, UK.
154. Heywood, J. B., (1989), " Internal combustion engine fundamentals ", McGraw-Hill book company, New York, USA.
155. Slowley, J., Tang, W. and Roberts, G., (1995), " A comparative study on natural gas engine performance and emissions with different gas carburettors ", ASME spring engine technology conference, ICE-Vol. 24, natural gas and alternative fuels for engines, pp. 81-89, Marietta, Ohio, USA.
156. Hadded, O., Stokes, J. and Grigg, D. W., (1993), " Low emission vehicle technology for ULEV and European Stage 3 emission standards ", IMechE International Conference : AUTOTECH'93--Automobile emissions and combustion, pp. 59-69, Birmingham, UK
157. Horrocks, R. W., (1993), " Light duty diesels --an update on the emissions challenge " IMechE Seminar : World-wide engine emission standards and how to meet them, pp. 155-169, London, UK

158. Dunne, J. M. and Greening, P. J., (1993), " European emission standards to the year 2000 ", IMechE Seminar : World-wide engine emission standards and how to meet them, pp. 1-8, London, UK
159. Nylund, N. and Riikonen, A., (1991), " Low-polluting gas fuelled heavy-duty vehicles ", SAE paper 912365.